Ph.D. Program in Civil, Chemical and Environmental Engineering

Curriculum in Chemical, Materials and Process Engineering

Department of Civil, Chemical and Environmental Engineering

Polytechnic School, University of Genoa, Italy.

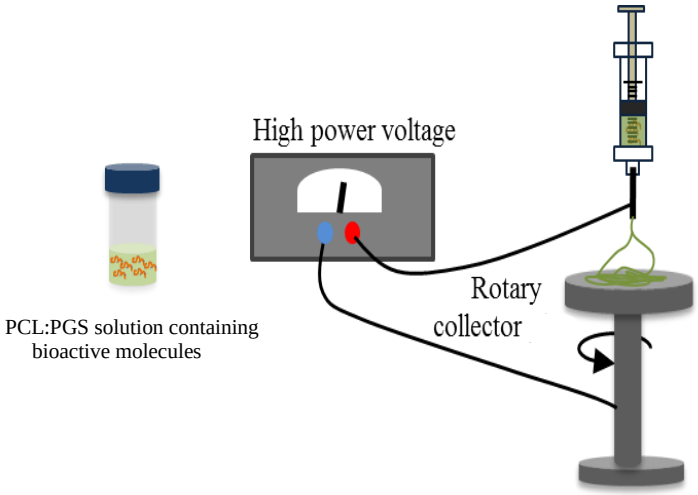

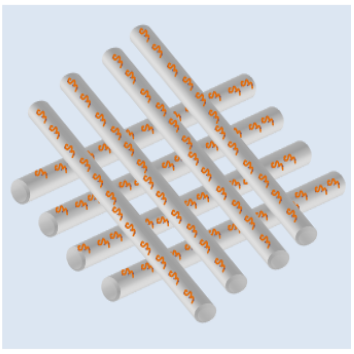

Functionalized biodegradable electrospun scaffold

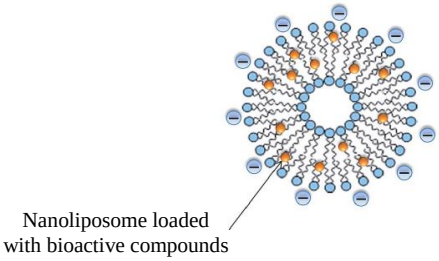

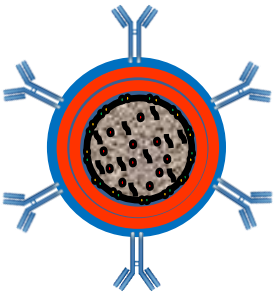

Engineered $CaCO_3$ nanoparticle with targeting activity encapsulating bioactive compounds

Functionalized biodegradable electrospun scaffolds and nanoengineered particles as innovative tools for vascular medicine

Pier Francesco Ferrari

FUNCTIONALIZED BIODEGRADABLE ELECTROSPUN SCAFFOLDS AND NANOENGINEERED PARTICLES AS INNOVATIVE TOOLS FOR VASCULAR MEDICINE

BY

PIER FRANCESCO FERRARI

Dissertation discussed in partial fulfillment of
the requirements for the Degree of

DOCTOR OF PHILOSOPHY

Civil, Chemical and Environmental Engineering
curriculum in Chemical, Materials and Process Engineering,
Department of Civil, Chemical and Environmental Engineering, University of Genoa, Italy

May, 2018

Adviser:
Prof. Patrizia Perego – Department of Civil, Chemical and Environmental Engineering, University of Genoa

External Reviewers:
Prof. Huabing Yin – College of Science and Engineering, Division of Biomedical Engineering, University of Glasgow
Prof. Nabil Chakfé – Department of Vascular Surgery and Kidney Transplantation, University Hospital of Strasbourg, University of Strasbourg

Ph.D. program in Civil, Chemical and Environmental Engineering

Curriculum in Chemical, Materials and Process Engineering

Cycle XXX

INDEX

ABBREVIATIONS

$^{\cdot}O_2$	superoxide radical
$^{\cdot}OH$	hydroxyl radical
$^1O_2$	singlet oxygen
3D	Three Dimensional
AAMI	Association for the Advancement of Medical Instruments
AFM	Atomic Force Microscopy
ANOVA	ANalysis Of Variance
ANSI	American National Standard Institute
ATR	Attenuated Total Reflectance
BCA	Bicinchoninic Acid Assay
BSA	Bovine Serum Albumin
$CaCl_2$	Calcium Chloride
$CaCO_3$	Calcium Carbonate
CAE	Caffeic Acid Equivalent
CHI	CHItosan
CM	Conditioned Media
CO_2	Carbon Dioxide
CTL	Control
DEX	DEXtran sulfate
DLS	Dynamic Light Scattering
DMEM	Dulbecco's Modified Eagle Medium
DNA	DeossiriboNucleic Acid
DPBS	Dulbecco's Phosphate-Buffered Saline
DTGS	Deuterated TriGlycine Sulfate
E	Ethanol
e.g.	exemplum given
ECM	ExtraCellular Matrix
EDTA	EthyleneDiamineTetraacetic Acid
EL	Empty Liposomes
ELISA	Enzyme-Linked ImmunoSorbent Assay
ePTFE	expanded PolyTetraFluoroEthylene

FTIR	Fourier Transform Infrared spectroscopy
GCS	Gelatin Coated Scaffolds
GIMP	GNU Image Manipulation Program
GPC	Gel Permeation Chromatography
H_2O_2	hydrogen peroxide
hMSC	human Mesenchymal Stem Cell
HPLC	High Pressure Liquid Chromatography
HRP	Horse Radish Peroxidase
IgG	ImmunoGlobulin G
IL-6	InterLeukin-6
LbL	Layer-by-Layer
LDH	Lactate DeHydrogenase
LDL	Low-Density Lipoprotein
MMP-9	Matrix MetalloProteinase-9
Mn	Mean molecular weight
Mw	Molecular weight
Na_2CO_3	Sodium Carbonate
NaCl	Sodium Chloride
NaOH	Sodium Hydroxide
NPS	NanoParticles
NS	Nanoparticles-functionalized Scaffolds
NT	Not-Treated
NTA	Nanoparticles Tracking Analysis
PAANa	Poly (Acrylic Acid) sodium salt
PBS	Phospate-Buffered Saline
PCL	Poly (ε-CaproLactone)
PDI	PolyDispersity Index
PET	PolyEthylene Terephthalate
PGA	Poly (Glycolic Acid)
PGS	Poly (Glycerol Sebacate)
PLA	Poly (Lactic Acid)
PPS	Pure Polymeric Scaffolds
PUFA	Poly-Unsaturated Fatty Acids
Q	Quercetin

QCM-D	Quartz Crystal Microbalance with Dissipation monitoring
QGCS	Quercetin-functionalized and Gelatin Coated Scaffolds
QL	Quercetin-loaded Liposomes
QS	Quercetin-functionalized Scaffolds
RL	Rapeseed Lecithin
RLS	Rapeseed Lecithin-functionalized Scaffolds
RNS	Reactive Nitrogen Species
$RO_2^{\cdot}$	peroxyl radicals
ROS	Reactive Oxygen Species
rpm	revolutions per minute
SD	Standard Deviation
SEM	Scanning Electron Microscopy
SL	Salmon Lecithin
SLE	Solid-Liquid Extraction
SLS	Salmon Lecithin-functionalized Scaffolds
sp.	species
TE	Tissue Engineering
TEM	Transmission Electron Miscroscopy
THF	Tetrahydrofuran
TNF-α	Tumor Necrosis Factor-α
TPC	Total Phenolic Concentration
UV	UltraViolet
v/v	volume/volume
w/v	weight/volume
WJ	Wharton's Jelly

INDEX OF FIGURES

INDEX OF TABLES

ABSTRACT

In the Western World, atherosclerosis-related diseases, including coronary and peripheral arterial pathologies, are one of the most common cause of morbidity and mortality. In some cases, in order to restore the blood flow, preserving all the functions of the downstream tissue, is necessary to introduce an arterial bypass or substitute in the patient. If autologous veins or artery are not available for different reasons (previous harvest, anatomical defects and anomalies, disease progression, other vascular problems etc.), artificial vascular constructs are required. During the last decade, different type of vascular grafts have been used to bypass or replace stenosed blood vessels. Non-degradable synthetic grafts (e.g. poly (ethylene terephthalate fibers and expanded poly (tetrafluoroethylene), commercially known as Dacron® and Teflon®, respectively) have been successfully used as vascular grafts for aortic and iliac reconstruction. These materials are poorly used as substitutes for small-caliber vessels (inner diameter < 6 mm) in the clinical practice for many reasons: high frequency of infection, absence of endothelialization after the implantation, a possible short-term thrombosis and myointimal hyperplasia, presence of dystrophic calcification and aneurysm, compliance mismatch between the native tissue and the artificial material, and related inflammatory response to the foreign materials. Until today, different approaches have been studied to fabricate high-performing small-caliber blood vessel grafts, including cell-seeded collagen gels, cell seeded or not, biodegradable polymers through 3D printing, electrospinning, film casting, self-assembling methodologies, and decellularized matrices from animals. The ideal vascular prosthesis could be biodegradable, acting as a structural framework in order to reproduce a native artery. It should hopefully exhibit resistance to thrombosis, infections, aneurysmal dilatation and ectopic calcification showing good suture retention, ease of handling, flexibility with kink resistance, bio- and hemocompatibility and predictable degradation kinetic. Considering this background, the aim of this Ph.D. thesis was at first to fabricate small-caliber vascular prostheses made of biodegradable and bioadsorbable polymers through electrospinning and then to functionalize them with bioactive compounds. Electrospinning has been considered in the last decade one of the most promising technique in the field of vascular tissue engineering since a microstructure very similar to extracellular matrix is formed during the whole process. During electrospinning the solvents evaporate quickly and a high electrical field charges the polymeric solution that is deposed onto a roto-translating collector. The two studied polymers were poly (ε-caprolactone) (PCL) and poly (glycerol sebacate) (PGS), alone or in a mixture with different ratios. In details, it was possible to obtain electrospun vascular grafts working with PCL:PGS (both 20 %, w/v) at ratios of 1:0, 1:1, 2:1, and 3:1. As a result, the first part was addressed to elect, after an adequate physico-chemical and mechanical characterization and biological validation, the best performing PCL:PGS blend. PCL:PGS (1:1, v/v) was considered the construct showing the best properties but its water permeability was too

high even at low pressure. For this reason, it was coated with gelatin. The presence of gelatin significantly reduced the permeability of water make the scaffold potentially implantable in animal models.

Nowadays the classical concept of tissue engineering, according to which the scaffold is described as a simple extracellular matrix-inspired framework, is overcome. The new concept is to fabricate constructs able to actively interact with cells during the regeneration process, releasing growth factors and chemoattractant proteins. Despite the majority of tissue engineering research is focused on the fabrication of the perfect vascular scaffold mimicking biochemical, physiological, biomechanical and architectural characteristics of the native tissues, the counteracting of the surgical-related inflammation represents today a new challenge. In fact, the post-surgical inflammation is able to affect negatively the cellular attachment and cellular growth on the bioprostheses, inducing many damages to the microstructure of the biomaterials, compromising its physico-chemical and mechanical properties, leading, in the worst case, to the rejection of the graft. For this reason, PCL:PGS (1:1, v/v), the best performing scaffold, was functionalized with the direct addition of an antioxidant in the spinning solution. Among antioxidants, there is a class of compounds, known as polyphenols, that show anti-inflammatory activity both *in vitro* and *in vivo*.

Quercetin (3, 3', 4', 5, 7-pentahydroxyflavone) is one of the most prominent dietary antioxidant present in different kinds of fruit (apples, grapes, berries), vegetables (red onions, celery, broccoli) and beverages (tea, wine). It plays various beneficial health effect, not only acting as scavenger towards peroxynitrites and hydroxyl radicals, but even protecting against osteoporosis, cancer, cardiovascular diseases and inflammation. The presence of free quercetin in the polymeric scaffold did not induce negative changes in morphology, physicochemical, mechanical properties and it was bio- and hemocompatible. In addition, the presence of quercetin counteracted the activity of TNF-α inducing a decrease in MMP-9 expression level, showing a general anti-inflammatory activity.

To have protein in the scaffolds, PCL:PGS (1:1, v/v), was functionalized with the addition of calcium carbonate ($CaCO_3$) nanoparticles encapsulating bovine serum albumin (BSA), as a model protein. The addition of $CaCO_3$ nanoparticles directly inside the biomaterial architecture did not modify its properties and, as a consequence, a more sustained release of the protein during time was obtained.

To develop a biocompatible surface, one approach is that of mimicking the erythrocyte and endothelial cellular membranes. Lecithin is made of phospholipids that are one of the main component of the plasmatic membrane. Phospholipids are amphiphilic molecules, with a hydrophilic head and a

hydrophobic tail. Because of their chemical structure, they organize into a bilayer matrix and serve as a good building block of cell membranes. For all these reasons, PCL:PGS (1:1, v/v) was functionalized employing three different concentrations of rapeseed and salmon lecithin.
The novelty of this part of the work was to fabricate a general model of biodegradable small diameter vascular scaffold that was prone to be easily functionalized with bioactive compounds with different chemical properties, without negatively influencing all the characteristics of the material itself.

The second part of this Ph.D. research thesis is focused on the synthesis and biological validation of two different nanosystems for drug delivery. These nanodelivery systems were thought to be potentially applied as innovative therapy for vascular pathologies. In particular, for atherosclerotic pre-lesions, when the blood flow is not compromised, the use of vascular scaffolds is not required. It is preferable to have a particles-based system able to inhibit with specific drugs the progression of the atherosclerotic lesion. Despite of different positive effects on the human health, the majority of polyphenols show only a limited application in the pharmaceutical sector, due to their low solubility in water and, similarly to the proteins, a low stability when they are exposed to environmental conditions (temperature, light, presence of oxygen etc.). With the aim of overcoming all these drawbacks, two different synthesis protocol were established to synthetize $CaCO_3$ nanoparticles and nanoliposomes.

In this work, $CaCO_3$ nanoparticles were synthetized through a two-step protocol which consisting in complex coacervation and mineralization. They were loaded with different antioxidants and with BSA, as a model protein. The second step was to engineered the nanoparticles in order to prevent a burst release of the embedded compounds, deposing onto their surface different polysaccharidic layers. This multi-shell architecture allowed the immobilization at the level of the last layer of an antibody. When this functionalized nanoparticles were put in contact with human endothelial cells EA. hy 926, their phagocytosis occurred.

The second nanoencapsulation system was studied at the Laboratoire d'Ingénierie des Biomoleculès (LIBio), at the University of Nancy, under the supervision of Professor Elmira Arab-Tehrany. Here, it was optimized the encapsulation of quercetin, one of the most common and promising polyphenolic compound, and BSA, a model protein, in rapeseed lecithin nanoliposomes. Liposomes were prepared mixing quercetin and rapeseed lecithin in water and nanoparticles were obtained after the sonication process. Morphology, size, ζ-potential, stability at three different temperatures, entrapment efficiency, release studies in different environmental conditions, FTIR, rheological properties of the water-based nano-formulation and biocompatibility with human stem cells and fibroblasts were assessed.

This part of the work represents a promising therapeutic approach for the treatment of the early stages of

one of the most widespread cardiovascular disease, atherosclerosis. The main advantage of this research was to take into account the possibility of developing two drug delivery systems to counteract atherosclerosis with a targeted therapy.

AIM OF THE THESIS

Cardiovascular diseases that result in the occlusion of vessels are one of the leading cause of death in the Western world. They are provoked as a consequence of an unhealthy lifestyle, genetic susceptibility, and other concomitant disorders. Nowadays, with the aim of counteracting such pathologies different strategies are commonly used. First of all, it has to be cited the use of different drugs that are able to interfere with the metabolism of cholesterol (e.g. statin). Another possibility to avoid the complete occlusion of vessel, with dramatic consequences depending on the site it will occur, is vascular surgery. The use of synthetic prostheses is a widespread surgery practice in all over the world. The occurrence of thrombosis in the case of implanting synthetic small dimeter vascular grafts has stimulated the vascular research in the developing of small diameter biodegradable prostheses. They are good candidate in vascular tissue engineering to substitute occluded vessel or to be implanted as bypass. Their play a pivotal role in patients in which the diameter of the lumen is already compromised. On the other hand, vascular medicine is forcing to the prevention of the complete occlusion of vessel and different protocol of therapy will be approved to counteract the early stages of the occlusion. This Ph.D. thesis present two different innovative tools to counteract the occlusion of vessel during in early (nanodelivery systems) or late (biodegradable scaffolds) stages.

The first part is addressed to the synthesis of small diameter vascular prostheses made of biodegradable polymers and their coating/functionalization with different bioactive molecules: gelatin, quercetin, proteins, and lecithin from rapeseed and salmon. Gelatin was used to reduce the permeability of the scaffolds, quercetin was used because of its anti-inflammatory activity that will be useful in the early period after the implantation to prevent the rejection of the graft, proteins encapsulated in nanoparticles because of their prolonged release will be able to recruit cells, induce their growth, and in some cases, their differentiation, and lecithin will prevent oxidative stress and will serve as a building block for cellular membranes. The choice to synthetize specifically small diameter substitutes (2 and 5 mm in diameter) derived from the lack of synthetic materials showing good performances when implanted in upper and lower limbs.

The second part of the thesis was dedicated to the synthesis of two different nanodelivery systems for the treatment of the early stages pre-lesions of occluding pathologies, when the prostheses are not yet required because of the vessel is not completely occluded. Their role is the encapsulation and the delivery in site of bioactive compounds (polyphenols and proteins) with the aim of decreasing their potentially side effects and to reduce the concentration used in the common therapy. The proposed nanosystems are nanoparticles made of calcium carbonate and poly (acrylic acid) and rapeseed lecithin nanoliposomes. The first nanosystem was engineered through Layer-by-Layer self-assembling technique to allow the attachment of a specific antibody on the nanoparticle surface. The antibody acted as a driving molecule,

allowing the nanoparticles to reach exclusively the pathologic tissue, where they are able to release a specific drug.

The thesis consists of:

- chapter I: it is a brief introduction to the main topics of the thesis, focusing on vascular tissue engineering and nanotechnologies for drug delivery systems;
- chapter II: this chapter concerns the synthesis, the functionalization, and the characterization of electrospun small diameter scaffolds;
- chapter III: this chapter describes the synthesis, the engineering and the biological validation of calcium carbonate nanoparticles encapsulating proteins and polyphenols,
- chapter IV: this chapter is focused on the development and characterization of rapeseed nanoliposomes entrapping proteins and quercetin

CHAPTER I

1. BACKGROUND

The lost or irreversible damages to a tissue or to a whole organ is one of the most common, disabling and costly problem in the modern medicine. The replacement of failed organs represents today the only solution to this problem (Langer and Vacanti, 1993). The problems regarding an autogenic transplantation derive from the difficulties we have nowadays to generate a new organ starting from cells isolated from patients. A possibility to overcome this kind of problem is taking into consideration an allogenic transplantation instead of the autogenic ones. Here, the insufficient number of donors, the risk of pathogen (viral and bacterial) transmission and the possibility of a rejection by immune system have limited the allogenic transplantation of donor organs (Lanza et al., 2000; Fuchs et al., 2001). As a consequence, patients have to wait for an organ for many years and if they will receive one in time, they have to get immunosuppressive drugs for a long period. In the worst cases, their situation do not change because of the transplanted organ is completely rejected by their immune system.

Tissue engineering (TE) is defined as an interdisciplinary and multidisciplinary field that applies the principles of engineering, material, life, and clinical science to study and develop substitutes to restore, maintain or improve tissue functions (Langer and Vacanti, 1993). One of the aim of TE is to obtain a valid substitute that could temporarily replace the damaged organ, better known as scaffold, that could potentially generate a new well-functioning organ. A good knowledge of the involved tissues is required before starting to develop new substitutes for them. Under a biological point of view, tissues consist of cells, signaling pathways and extracellular matrix (ECM) (Lanza et al., 2000). Cells secrete the ECM in which they are completely immersed and in which they communicate through signaling molecules. The ECM could be considered as a framework responsible of supporting cells during their growth and for their entire life (Badylak, 2007).

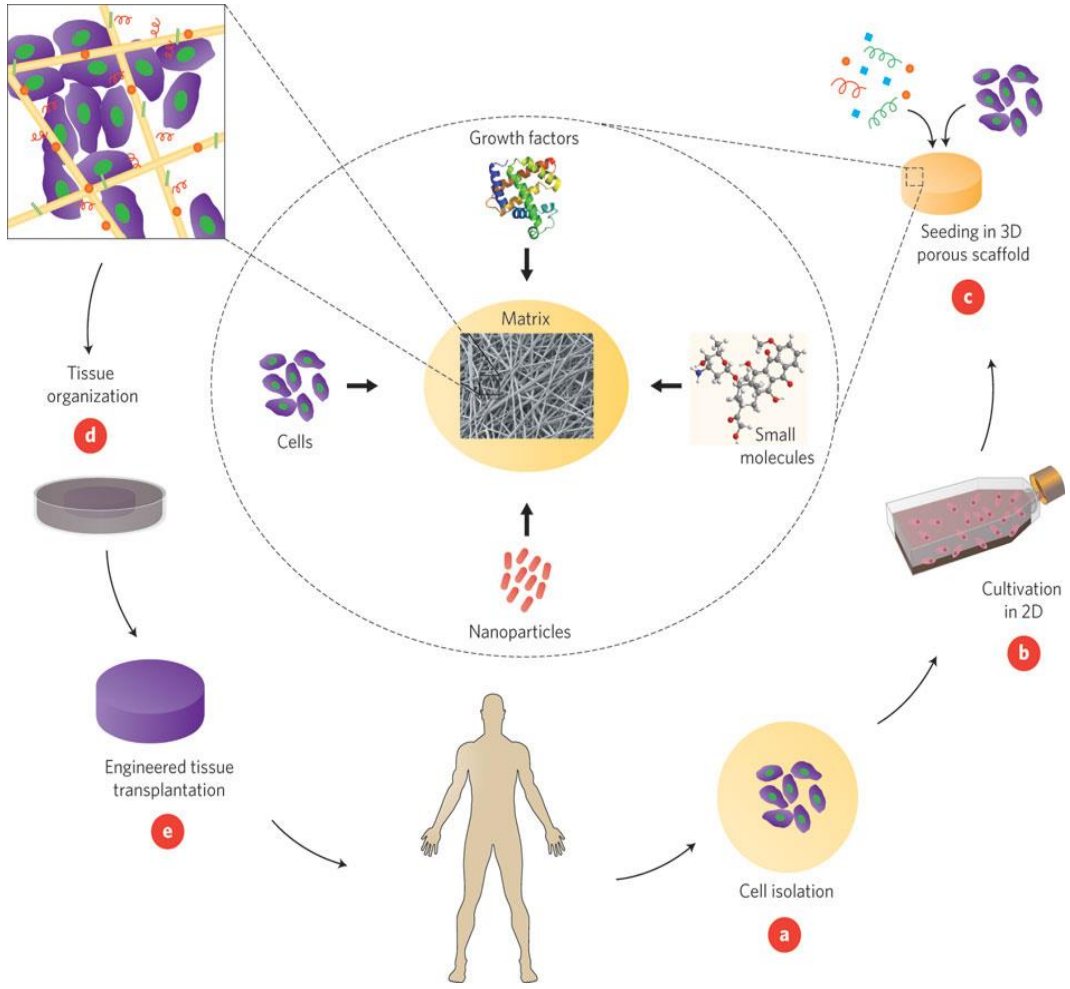

Figure 1.1: an example of TE concept involving cell seeding on porous scaffolds. (a) Cells are isolated from the patient, (b) cells are *in vitro* cultivated and expanded, (c) cells are seeded within the porous scaffold together with growth factors and free or encapsulated bioactive molecules, (d) the construct is cultivated in bioreactors, (e) the construct is implanted in the patient to restore the lost function (adapted from Dvir et al., 2011).

Figure 1.1 depicts the classical principles of TE. The first step is represented by isolating cells from the patient. Then, they are expanded *in vitro* and introduced into a biodegradable scaffold. Finally, the scaffold is implanted *in vivo*. The modern concept of TE consists of the development of biodegradable scaffolds that could be functionalized with free or micro- and nanoencapsulated bioactive compounds (proteins, drugs, natural molecules etc.) and then they are directly implanted, bypassing the cell seeding step, *in vivo*. Once it is in the patient, the presence of biomolecules within the scaffold induces a cell recruitment and their attachment and proliferation on the implanted scaffold. Furthermore, the presence of synthetic or natural compounds with anti-inflammatory activity could counteract the post-surgical inflammation process. The design of a good substitute need optimization of several aspects. Each tissue requires different materials and porosity of the scaffold. In general, the scaffold should allow three dimensional tissue regeneration,

providing a good support for cells, enabling nutrient and waste exchange (Takezawa, 2003; Hollister, 2005).

The term regenerative medicine is often used as synonym of TE but it has to be considered as a broader field which includes tissue engineering. The basic principle of regenerative medicine is that the body, with the help of biomaterial, uses its own system to recreate and rebuild tissues and organs. Regenerative medicine is based on the use of stem cells.

1.1.Biomaterials

Biomaterials are materials able to interact with cells in living tissues/organs. Biomaterials are generally polymers and they can be synthetic or natural. Poly (ε-caprolactone) (PCL), poly (glycerol sebacate) (PGS), poly (lactic acid) (PLA), and poly (glycolic acid) (PGA) are well-known examples of synthetic biomaterials while gelatin, chitosan, hyaluronic acid, and dextran are examples of natural ones. Synthetic materials show good mechanical properties while the natural ones are less toxic and induce a limited inflammatory reaction. All these materials find application as tissue engineering scaffolds. Biocompatibility is the most important and desirable property they have to show. The first definition of "biocompatibility" was provided by the European Society for Biomaterials in 1986 as: "the ability of a material to perform with an appropriate host response in a specific application" (Williams, 1986). Therefore, the biomaterials have to induce an adequate biological response without causing negative effects in the surrounding tissues and in the whole body. Another peculiarity of scaffolds is that they have to be biodegradable at the same time as the tissue regeneration. 3D scaffolds have to provide mechanical and adhesive support for cells, allowing vascularization and shape maintenance during the regeneration process. Initially enough mechanical strength and stiffness is required to counteract wound contraction forces and later to ensure a perfect rebuilding of the tissue, physically supporting the growing cells (Hutmacher, 2000). Scaffolds should present high porosity, high surface area, fully interconnected geometry and a well-defined 3D shape. Finally, scaffolds should be manufactured in a reproducible, controlled and, if it is possible, cost-effective process. During their synthesis is desirable to include bioactive compounds inside their matrices to make them "active scaffolds", able to participate actively to the regeneration of the damaged tissue.

Biomaterials are often divided into two groups: synthetic or natural, depending from their origin.

1.1.1. Synthetic polymers

Different polymers are used in TE because of their good versatility, stable properties and high workability. Working with synthetic polymers, presents the advantage of obtaining scaffolds with predictable properties. As examples, it is reported that the degradation and fluid uptake rate can be adapted to specific applications

by changing the composition of the scaffolds in terms of polymers, copolymers or blends. However, a disadvantage of synthetic polymers is their low biocompatibility. This property could be overcome working with blends of polymers with natural materials or reducing their hydrophobicity. In this section, a brief description of the polymers used during the Ph.D. research activity are presented.

Poly (ε-caprolactone)

Poly (ε-caprolactone) (PCL) is an aliphatic biodegradable polyester. It is well-known for its good biocompatibility and bioresorbability. It is synthetized by a ring-opening polymerization of ε-caprolactone, employing stannous octanoate as catalyst (Figure 1.2). It has been reported that it is degraded by hydrolytic mechanism (Sun et al., 2006; . It is suitable for long-term implantable substitutes because its hydrolytic degradation is slower in comparison with hydrophilic biomaterials.

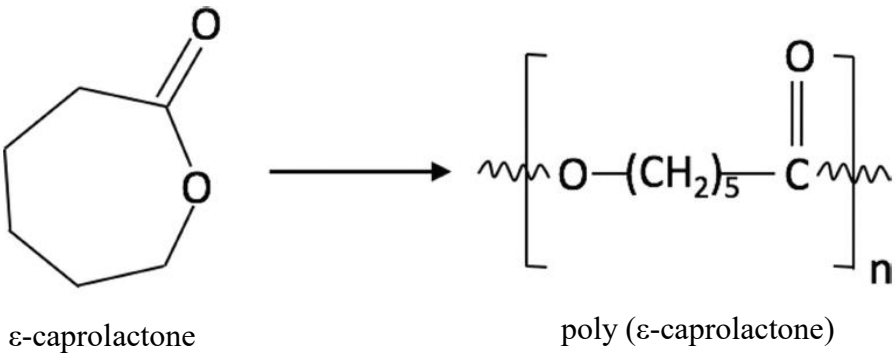

Figure 1.2: synthesis of PCL (adapted from Osathanon et al., 2017).

Poly (glycerol sebacate)

Poly (glycerol sebacate) (PGS) is a transparent, almost colorless biodegradable polymer. Chemically, it is a polyester prepared by the polycondensation of glycerol and sebacic acid (Figure 1.3). Since its high hydrophilicity, it shows a good biocompatibility with different kind of cells and a good biodegradability. Controlling curing time, curing temperature and the reagents concentration, is possible to modulate the degradation kinetic and mechanical properties of the resulting polymer. Due its mechanical properties, it is generally used for soft tissues as cardiac muscle, vessels, nerve, cartilage and retina (Rai et al., 2012).

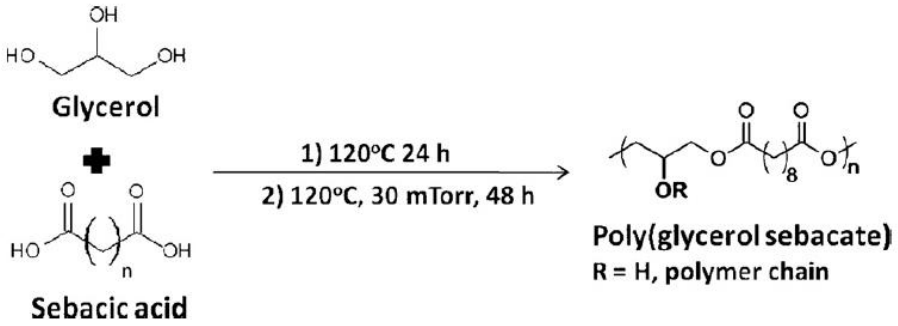

Figure 1.3: synthesis of PGS (adapted from Wang et al., 2002).

Poly-L-arginine

Poly-L-arginine is a positively charged synthetic polyamino acid (Figure 1.4). It appears as a crystalline solid soluble in water. It is widely used for the layer-by-layer deposition technique in combination with dextran sulfate (De Geest et al., 2006; De Koker et al., 2009).

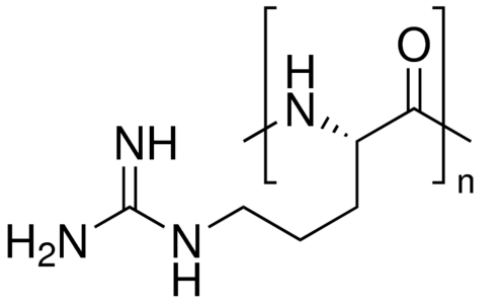

Figure 1.4 chemical structure of poly-L-arginine (adapted from Sigma-Aldrich website).

1.1.2. Natural polymers

Natural polymers are generally extracted form plants, animals or human tissues. Usually, chemical modifications are useful to enhance their properties, like mechanical and surface properties. The chemical modifications are able to modulate both the degradation and fluid uptake rate of the polymer. In this section, the natural polymers used during the Ph.D. research activity are briefly described.

Gelatin

Gelatin derives from the hydrolysis of collagen, the most abundant protein in the connective tissue (K. Y. Lee & Mooney, 2001) (Figure 1.5). Gelatin solubilizes in water at 60°C and it forms gels at room temperature (Young et al., 2005). Gelatin is widely used for pharmaceutical and medical applications. In fact, it is easy to be manipulated, extremely biodegradable and cheap (Zandi et al., 2007).

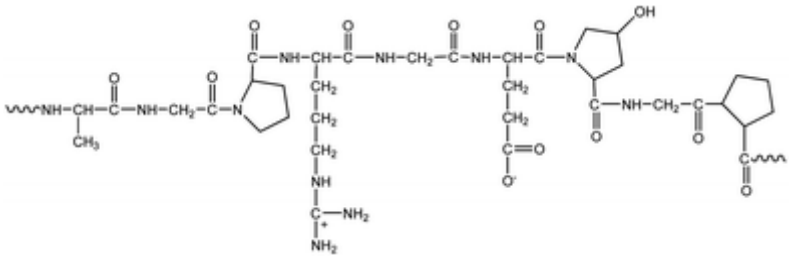

Figure 1.5: chemical structure of gelatin (adapted from Ge et al., 2012).

Chitosan

Chitosan is an amino polysaccharide synthetized by partial N-deacetylation of chitin (Figure 1.6). In nature it is the structural element of the exoskeleton of crustaceans (shrimp, crabs etc.) and cell walls of fungi.

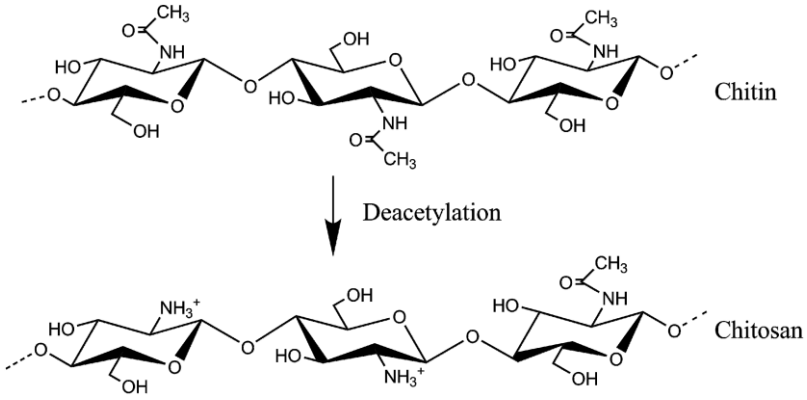

Figure 1.6: deacetylation of chitin and formation of chitosan (adapted from Nilsen-Nygaard et al., 2015).

Chitosan shows many applications in the biomedical sector because of its low cytotoxicity, structural similarity to natural glycosaminoglycans, and good biodegradability (Singh & Ray, 2000). It is widely employed as polycation in layer-by-layer self- assembling protocols (Zhou et al., 2010).

Dextran

Dextran is a complex branched homopolysaccharide made of many glucose molecules (Figure 1.7). The straight chain consists of α-1,6 glycosidic linkages between glucose molecules. Branches start from α-1,3 linkages. Some acid bacteria, like *Leuconostoc* sp. are able to produce dextran starting from sucrose. It is

used as an antithrombotic to reduce blood viscosity and as polyanion in drug delivery applications (Serizawa et al., 2002).

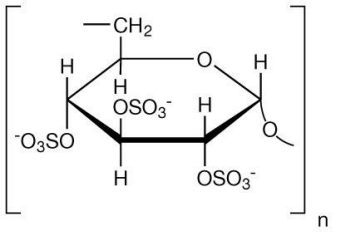

Figure 1.7: chemical structure of dextran sulfate (adapted from De Clercq, 2013).

1.2. Vascular tissue engineering

Vascular diseases are the leading cause of morbidity and mortality in the Western World (Ravi & Chaikof, 2010). The fabrication of prosthetic vascular conduits began necessary in the last decades because of a limited availability of healthy autologous vessels. To overcome this problem, different strategies were proposed over the time and to date in vascular surgery only artificial non-degradable prostheses are used. Nevertheless, the current synthetic polymers used (e.g. polyethylene terephthalate and expanded polytetrafluoroethylene) show many important drawbacks.

1.2.1. Vessel structure

Vessels are conduits of the cardiovascular system able to transport blood from heart to tissues and from the tissues to the heart again. There are three different kind of vessels: arteries, veins and capillaries (Figure 1.8). Arteries are responsible of carrying the oxygenated blood from the hearth. They consist of three different layers: the tunica intima, made up of endothelial cells, tunica media, made up of smooth muscle cells and elastic tissue, and tunica externa, made up of connective tissue. Veins are responsible of transporting the deoxygenated blood from the periphery to the heart. Structurally, they are similar to arteries but they present thinner walls and valves. Each layer that contributes to the formation of a vessel has a defined role and contributes to its function. In particular, endothelial cells constitute the inner surface of the vessel and they, being aligned, show anti-thrombotic properties. Smooth muscle cells and elastin are responsible of the elasticity of the vessel. Collagen makes viscoelastic the vessel, inducing a higher

elasticity at low pressure and a higher rigidity at high pressure (Baguneid et al., 2006; (Isenberg, Williams, & Tranquillo, 2006).

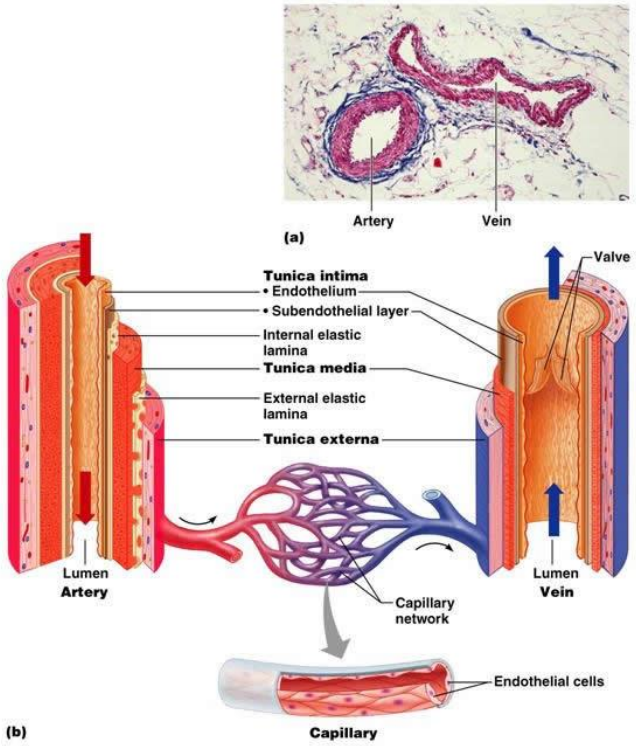

Figure 1.8: anatomic structure of (a) arteries, veins, and (b) capillaries (adapted from Anatomy and Physiology, a learning initiative).

1.2.2. Pathologies related to vessel obstruction

In general, a vessel has to be considered occluded when there is a significant reduction of its lumen. This phenomenon can happen because of many reasons. The widest pathology related to vessel obstruction is atherosclerosis. The typical lesion of this pathology is the atherosclerotic plaque characterized by the thickening of tunica intima due to the accumulation of lipids and a consequent recruitment of leukocyres from blood, fibroblasts proliferation, and macrophages proliferation. Generally, this pathology is characterized by two steps: first, endothelial damages and oxidation of low-density-lipoprotein (LDL) in the tunica intima, and second, the inflammation-related process. At this time, macrophages try to phagocytize oxidized LDL, becoming foam cells. These cells secrete molecular factors that play a pivotal role in recruiting blood leukocytes and in inducing the synthesis of ECM by smooth muscle cells (Figure 1.9). In the worst cases, the atherosclerotic plaque can evolve to a thrombus with a full occlusion of the

blood vessel.

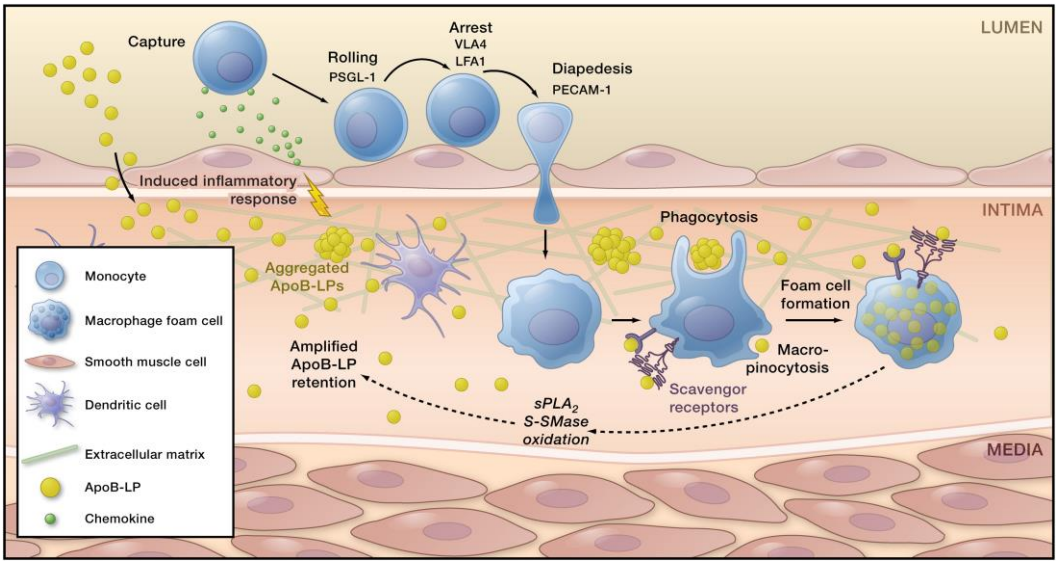

Figure 1.9: molecular and cellular mechanism involved in the atherosclerotic plaque formation (adapted from Moore & Tabas, 2011).

1.2.3. Treatment of small-caliber blood vessel occlusion

Angioplasty, atheroectomy and use of bypass are current surgery strategies performed to remove the occlusion of small-diameter blood vessel

Angioplasty

Balloon angioplasty or percutaneous transluminal angioplasty, is a low invasive endovascular procedure to widen narrowed or occluded blood vessels and typically is used to treat arterial atherosclerosis. It is usually performed when the occlusion of the blood vessel is less than 70 %. A deflated balloon attached to a catheter is passed over a guide-wire into the narrowed vessel and then inflated to a fixed size. The balloon forces an expansion of the blood vessel and the surrounding muscular wall, allowing an improved blood flow (Figure 1.10). A stent may be inserted at the time of using the balloon to ensure the complete reopening of the vessel (Tatterton et al., 2012).

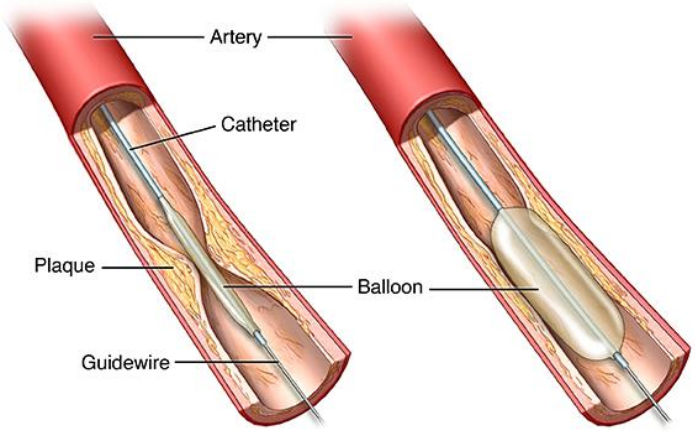

Figure 1.10: angioplasty (adapted from John Hopkins Medicine website).

Atherectomy

Atherectomy is a minimally invasive endovascular surgery technique addressed to remove atherosclerotic plaque from blood vessel (Figure 1.11). It is suitable for the treatment of peripheral and coronary artery diseases (Ambler et al., 2014).

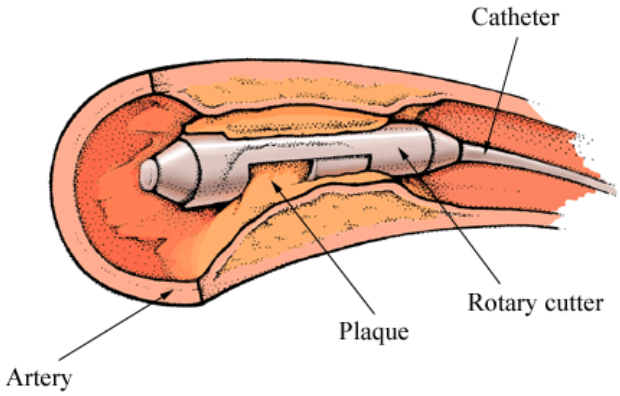

Figure 1.11: atherectomy with rotary cutter (adapted from Keck School of Medicine of USC).

Use of bypass

Bypass technique consists of overcoming a partially or completely obstructed blood vessel. Briefly, an autologous blood vessel is removed from another region of the body and it is used to do a bypass closed to the occluded vessel. Unfortunately, not always is possible, for many reasons, to do a by-pass with autologous vessel. A valid solution to this problem is the use of synthetic grafts (Figure 1.12), that are the main topic of this Ph.D. thesis.

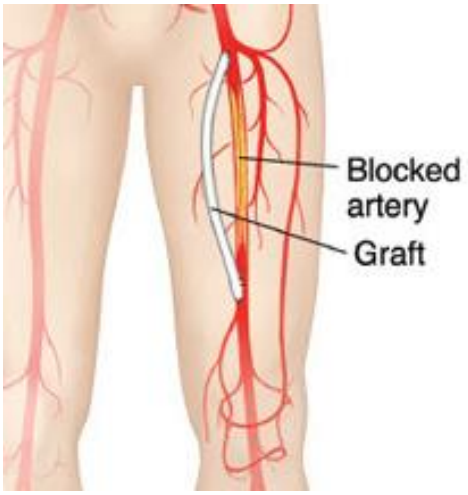

Figure 1.12: bypass procedure (adapted from Medtronic website).

1.2.4. Vascular substitutes

According to a recent statistical study of the American Health Association, cardiovascular diseases are responsible of 34 % of deaths in United States of America. Another report states that 36 thousands babies per year is affected by congenital diseases of the cardiovascular system (Nuti et al., 2010). The treatment to such pathologies needs vascular substitutes. The treatment of cardiovascular diseases with autologous substitutes still remains a valid option. To this purpose, the vena saphena magna, the internal mammary artery or the radial artery are employed. Although vascular bypass grafting remains the most common revascularization treatment for ischemic heart and peripheral vascular diseases, the majority of patients do not have healthy vessels suitable to be harvested. In addition, the population undergoing repeated coronary revascularization is augmenting. Therefore, there is an increased need for alternative, synthetic vascular substitutes. It has been well accepted that the formation of neointima, endothelialization at the graft walls and the absence of thrombogenicity are the goals of graft healing. Materials that are currently used in the vascular surgery are polyethylene terephthalate (PET, Dacron®) and expanded polytetrafluoroethylene (ePTFE, Teflon®) (Figure 1.13).

Figure 1.13: synthetic vascular prosthesis made of poly (ethylene terephthalate) (left) and expanded poly (tetrafluoroethylene) (right).

Poly (ethylene terephthalate) is a thermo-elastic polymer belonging to the polyesters family. Poly (ethylene terephthalate) is a resistant, biostable and stretchy polymer. It is commonly used in vascular surgery as a substitute only in the case of large diameter vessel.

Expanded poly (tetrafluoroethylene) is one of the most inert polymers known, and its electronegative surface has been supposed to be non-thrombogenic, even in the case of small diameter grafts (Campbell et al., 1975). Its matrix is highly porous and permits the formation of neointima lining the lumen of the graft. Cellular infiltration and endothelialization of implanted expanded poly (tetrafluoroethylene) grafts was observed in animal models (Sauvage et al., 1974). On the contrary, several authors demonstrated that the endothelialization of expanded poly (tetrafluoroethylene) grafts in human was rare except the short segment next to the anastomosis site, even after five years. In fact, other clinical studies highlighted that the tissue ingrowth and the development of a well-organized neointima was extremely poor in expanded poly (tetrafluoroethylene) small diameter grafts implanted in human (Camilleri et al., 1985; Guidon et al., 1993; Formichi et al., 1998). As a consequence, the use of these two synthetic materials is limited to the dimension of the graft. These synthetic prostheses are good candidates when the required diameter is higher than 5-6 mm. For the opposite, as mentioned before, the majority of small diameter vascular graft fails within 5 years and the frequency of thrombogenic event is high. For all these reasons, the use of vascular substitutes fabricated with these two materials is limited to cases where there is a substantial blood flow and in conditions of low resistance.

The properties to be improved developing a synthetic graft are:

1. poor elasticity and compliance to the hematic flow;
2. thrombogenicity of the surfaces;

3. impossibility to accept and sustain the growth of cells for a long period.

Requisites of a vascular substitute

The properties of a blood vessel are rather complex, starting from its multilayered structure. In particular, a small caliber blood vessel substitute have to possess:

1. a smooth internal surface with the lowest possible friction coefficient;
2. size and properties similar to the vessel to be substituted;
3. avoid platelet aggregation and thrombogenic phenomena;
4. minimize blood flow interferences,
5. show optimal transfer of pulsatile energy.

Moreover, a vascular substitute should resist bending, be simple to be sutured and handle, and require short production time and low production cost. At the moment being, the scaffold used in the new generation vascular tissue engineering scenario can essentially be divided into two categories:

- polymeric scaffolds, including electrospun ones;
- biological, like decellularized scaffolds.

1.2.5. Electrospun scaffolds

Among polymeric scaffolds, electrospun scaffolds are playing a primary role in the vascular surgery field. Fibrous structures are raising a great interest, due to the fact that they are structurally closed to the ECM architecture. Electrostatic spinning (electrospinning) is one of the most emerging techniques to fabricate fibrous scaffold. The numerous process parameters that characterize this technique offer a wide range of possibilities to modulate the properties of the resulting electrospun scaffolds. Different type of polymers can be used during the electrospinning process: synthetic, natural or mixtures of them. For TE applications, the most promising bioresorbable polymers, as previously reported, are PCL, PGS and PLA.

1.2.5.1. Electrospinning technique

Electrospinning has established a significant role in the field of TE over the last fifteen years. Indeed, this technique allows to obtain polymeric scaffolds with ultrathin micro- or nanofibers (Cui et al., 2010). Electrospinning can be considered a particular case of electrospraying. It is indeed a method for atomization of fluids with application in mass spectrometry and in the industrial field of surface coating. If the fluid

employed for electrospinning presents a low molecular weight, the stream becomes unstable before it reaches the collector and transfroms just into a spray of electrostatically charged small drops. By using fluid polymers instead, the viscoelastic forces stabilize the stream, allowing the formation of thin charged filaments that deposit into a twist of fibers. The diameter are far smaller that those of extruded or mechanically stretched fibers (wet, dry, and melt spinning).The electrospinning technique is able to produce micro- or nanofibers through an uniaxial stretching of a viscoelastic solution. Unlike dry-spinning and melt-spinning, electrospinning uses electrostatic forces to stretch the polymeric solution as it is extruded from the needle. The instrumentation is composed by (Figure 1.14):

- a syringe (usually in glass), containing the polymeric solution to be electrospun;
- a pump, feeding the polymeric solution that is extruded from the syringe;
- a high voltage DC generator that is connected to the needle by means of an electrical contact (the set-up could be either in positive or negative modality (Lingaiah et al., 2007);
- a metallic collector, on the ground, that has the role to collect the fibers. There are many collectors that differ in terms of size, shape (cylinder, flat etc.), and material.

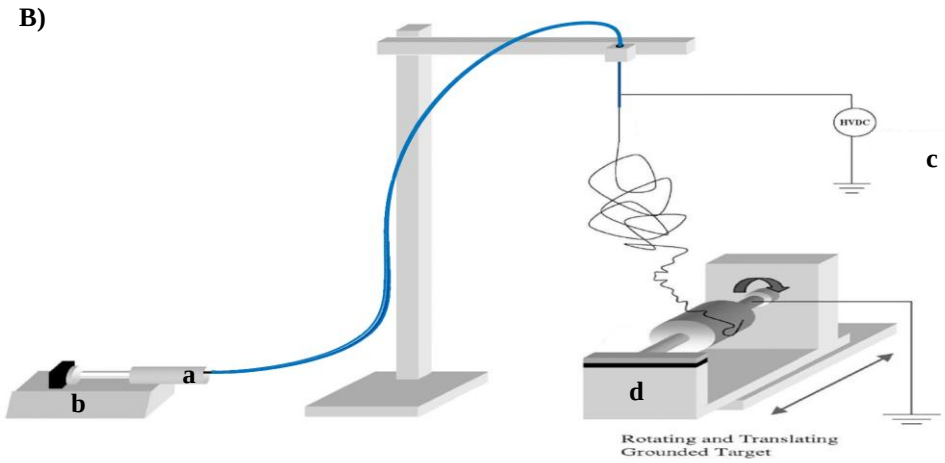

Figure 1.14: (A) picture and (B) schematic representation of a common electrospinning apparatus set-up: (a) syringe, (b) peristaltic pump, (c) high-voltage DC supply, (d) rotating and translating grounded collector.

The advantage of electrospinning system can be summarized in:

- the fiber structure, with tunable fiber diameter, that mimics that of ECM (ECM presents protein fibers ranging between 50 and 500 nm);
- high surface/volume ratio of the ultrathin fibers, which allows a significant cell attachment. In particular, it seems that micrometric structures are better accepted by cells than sub-micrometer structures (Del Gaudio et al., 2009);
- control over fiber orientation (aligned or random distribution);
- wide range of electrospun materials.

The electrospinning process and the fiber morphology could be influenced by many parameters. These parameters can be divided into three categories: properties of the polymeric solution, electrospinning set-up, and environmental conditions. The type of collector employed influenced the properties of the final constructs, especially the shape and consequently the application. Solution properties depend on its viscosity, electrical conductivity, and surface tension. They are clearly tied to both the characteristics of the polymer and of the solvent or mixture of solvents used.

- Viscosity: it is one of the parameters with a greater influence over the diameter and morphology of the fibers. Viscoelastic forces are deeply correlated to the polymer structure (linear or reticulated) and to its molecular weight. Hence, for any considered system there is a range of concentration. Below a prefixed concentration, the chain entanglements are too limited to support the spinning process and drops are formed; above it the drop of solution dries before the stream starts to carry

the fibers accelerated by electric field towards the collector. To increase the viscosity of the solution, one can increase the molecular weight or the concentration of the polymer. However, increasing viscosity also increases the fiber diameter because the solution becomes more resistant to be stretched because of the electric field, and consequently the stream stabilizes and runs over a shorter path.

- Electrical conductivity: the increase of a solution conductivity causes a greater repulsion of the flow's jet, and therefore a greater stretch of the fibers, which decrease in diameter (Bosworth and Downes, 2009). Possible approaches to increase conductivity are the addition of salts (Deitzel et al., 2001), and the use of more conductive solvent (Beachley & Wen, 2009).
- Surface tension: with the aim of fabricating nanofibers, the electric charge should overcome the solution surface tension. During the electrospinning process, the surface tension opposes the jet stretch, causing the formation of drops or fibers with drops. To avoid this phenomenon, a solution with low surface tension is preferable.

Set-up parameters are related to the fibers production and they comprise the voltage, the flow rate, the distance between the collector and the needle and roto-translating movement of the collector.

- Voltage: an increase in voltage induces a higher electrostatic repulsion of the flow. Therefore, thinner fibers will be obtained. With large potential differences, fiber diameters become larger due to the difficulty of the solvent to evaporate (Venugopal et al., 2007).
- Pumping flow rate: high flow rate cause an increase in fiber mean size. Indeed, these do not have sufficient time to permit the solvent evaporation (Bosworth and Downes, 2009). However, this parameter is less influent than the others.
- Distance between the needle and the collector: this distance influences the time that the fiber has to reach the collector. Reducing the distance, the flow has a minimal time to dry before be deposed on the collector.
- Diameter of the needle: a needle with smaller internal diameter reduces the number of drops and consequently the fiber diameter. A drop at the end of the needle will have smaller size and greater surface tension. For the same voltage, a greater Coulomb friction is therefore needed to form the flow, with a consequent decrease in flow acceleration (Buruaga et al., 2009).

Even environmental parameters influence the morphology of the fibers and the external electrical field.

- Humidity: an increase in humidity increases the size, number and distribution of pores on the fiber surface (Bosworth and Downes, 2009). At the same time, depending on the polymer, the increase in humidity causes an increase or a decrease in fiber diameter.

- Temperature: the increase in the temperature of the solution has two opposed effects on the electrospinning process. Indeed, it increases solvent evaporation, increasing fiber size as a consequence. However, it could also decreases the viscosity with an opposite effect (Mo et al., 2004).

1.3.Drug delivery

Bioactive compounds often show undesired pharmacological properties (Langer, 1998). In the field of nanotechnology, pivotal challenges are represented by overcoming the insufficient drug doses reaching the pathological site, by increasing the short half-life and/or by prolonging the shelf-life of drugs. In order to achieve these objectives, scientists have been developing innovative drug delivery systems. Another aim of drug delivery is to have the release of drugs in a control and localized way. In drug delivery different materials are used. They derive from natural or synthetic sources and, in any case, they have to be extremely biocompatible. As shown in Figure 1.15, all these materials can be rearranged in such a manner that they are considered as micro- or nanosized particles (polymeric, nanoparticles, liposomes, polymeric micelles etc.) (Rampino et al., 2013). Controlled and localized delivery of drugs is related to the concept of concentrating the therapeutic treatment only at a level of the pathological tissue (Bhatt & Addepalli, 2010). As a consequence of that, an improved bioavailability of the drug occurs. The control of the release of a determined drug at a specific site could be very difficult and it is obtain modifying the surface of the carriers (e.g. layer-by-layer technology). Often when the drug delivery system enter in our body, an inflammatory reaction is provoked (Farra et al., 2012). For that reason, it is fundamental to assess if the studied drug delivery system is able to evoke inflammation. The list of advantages that derives from drug delivery is quite extensive (Wu & Grainger, 2006; Zilberman et al., 2010). First, by concentrating the drug only to the target tissue, it reduces the quantity of drug, often expensive, that is necessary to have a therapeutic effect (Uhrich et al., 1999). Second, by carrying the drugs to site where they are necessary, the side effects are drastically reduced. Third, by delivering the drugs to the site where they are needed, it allows to increase the bioavailability of the drug (Ndesendo et al., 2011; Wong et al., 2010).

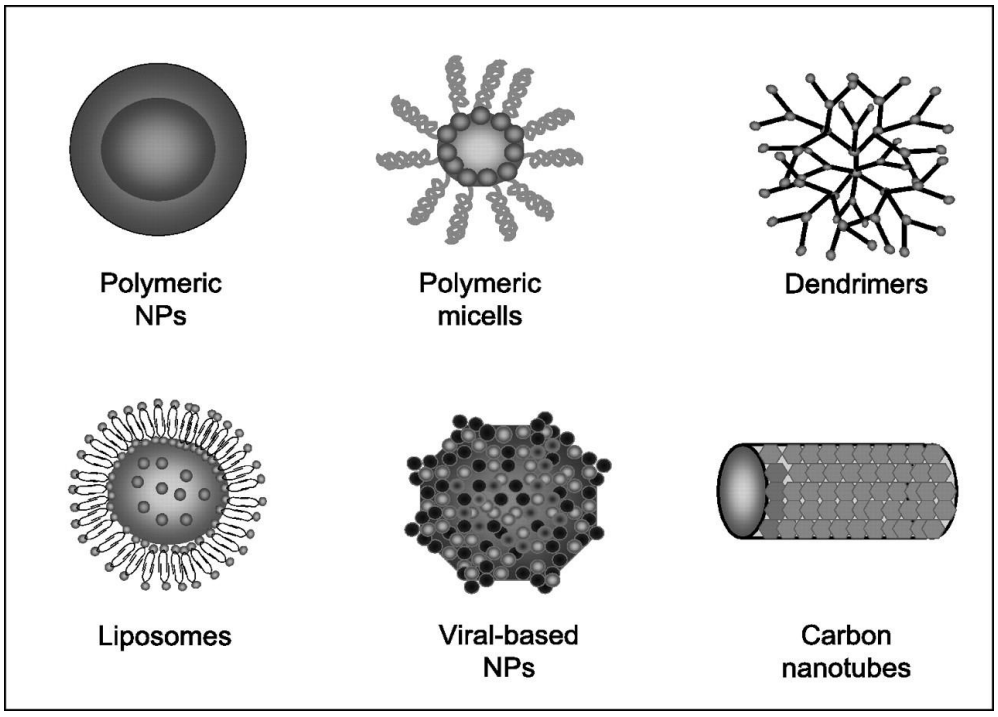

Figure 1.15: different carriers commonly studied in drug delivery (adapted from Cho et al., 2008). NPs: nanoparticles.

1.3.1. Calcium carbonate nanoparticles

Calcium carbonate ($CaCO_3$) is one of the most abundant inorganic biominerals. The worldwide availability of $CaCO_3$ (as limestone), and its non-toxicity towards the human body makes the synthesis of this material an interesting and attractive topic for scientists and researchers to delve into. Therefore, countless studies dealt with the task of using $CaCO_3$ particles in drug delivery procols. Its biocompatibility, its biodegradability, its low toxicity and its low cost make it a perfect candidate as a micro/nanocarrier of a wide range of biomolecules.

Thanks to these properties, $CaCO_3$ is becoming an usual material for the encapsulation and delivery of biomolecules. $CaCO_3$ exists as three anhydrous crystalline polymorphs (calcite, vaterite, aragonite); two hydrated metastable forms (monohydrocalcite and $CaCO_3$ hexahydrate), and an unstable amorphous phase. Calcite, vaterite and aragonite have typical morphologies (shapes) which are rhombohedral, spherical and needle-like, respectively (Boyjoo et al., 2014). Calcite is the most thermodynamically stable phase among the six forms of $CaCO_3$. Vaterite has better water solubility, higher

porosity, and is more easily dissolved than calcite or aragonite. The thermodynamic instability of vaterite, however, makes its natural occurrence rare, requiring kinetic stabilization even for laboratory production (Nagaraja et al., 2014). Aragonite has needle-like crystals that are used as fillers for the improvement of mechanical properties of paper and polymeric materials, and is also a good biomedical material, because it is denser than calcite and can be easily replaced by bone (Wang et al., 1999). Amorphous calcium carbonate is the least stable phase and transforms rapidly into one of the crystalline polymorphs unless it is stabilized by specific additives. Thus, it has the highest solubility in water and is the only form that has isotropic property and does not diffract X-rays (Huang et al., 2007). There are three main techniques to encapsulate biomolecules in $CaCO_3$ particles: direct crystallization, co-precipitation, and complex coacervation followed by mineralization (Lauth et al., 2014).

Briefly:

- direct crystallization: the encapsualtion of drugs is a consequence of the physical adsorption onto synthetized crystals (Sukhorukov et al., 2004). The main characteristic of the produced carriers regards their large size (1-5 μm), crystalline polymorphism and highly porous structure. Some disadvantages come from this technique, such as the crystalline structure that is subject to recrystallization in water, which could induce changes in the shape (Petrov et al., 2005).
- Co-precipitation method: the precipitation of $CaCO_3$ is initiated in a solution that contains the drug to be encapsulated. The morphology of products obtained via co-precipitation is extremely heterogeneous, ranging from macrosized to nanosized particles. Working with a co-precipitation method ensure to obtain high encapsulation efficiency values (Wang et al., 2014).
- Complex coacervation followed by mineralization: the coacervation is considered the separation into two liquid phases (Eghbal & Choudhary, 2018). During complex coacervation two molecules with oppositely charge are mixed together in a single solvent (e.g. water) (Figure 1.16). The dispersed core material is suspended in an aqueous phase containing the active agent (Onder et al., 2007). The resulting product of this process are coacervates that are miscible in the solvent. After the formation of these coacervates, it is possible to increase their stability using inorganic salts, like sodium carbonate, obtaining fully mineralized amorphous $CaCO_3$ particles.

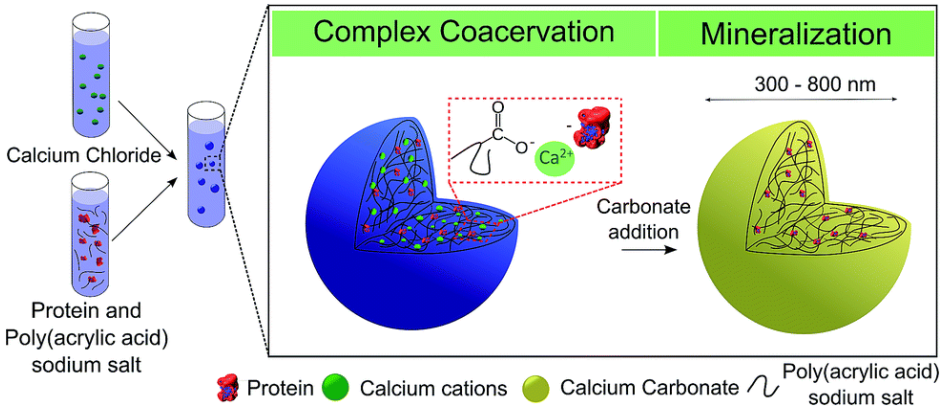

Figure 1.16: complex coacervation and mineralization for $CaCO_3$ particles synthesis (adapted from Lauth et al., 2014).

1.3.2. Layer-by-Layer self-assembling technique

Layer-by-Layer (LbL) is a quite simple technique based on the alternated deposition of polycations and polyanions onto the surfaces of inorganic or organic substrates (De Cock et al., 2010) (Figure 1.17). For its good versatility, low cost, and possibility to control the thickness of each single layer, it is a wide technique to functionalize particles having a diameter ranging from 50 nm up to 10 μm (Pastorino et al., 2011). The presence of different layers surrounding particles is aimed to: first, to obtain a fully controlled release of the entrapped molecules, changing the number and the thickness of the layers, second, to attach at the level of the last layer guidance molecules, such as antibodies.

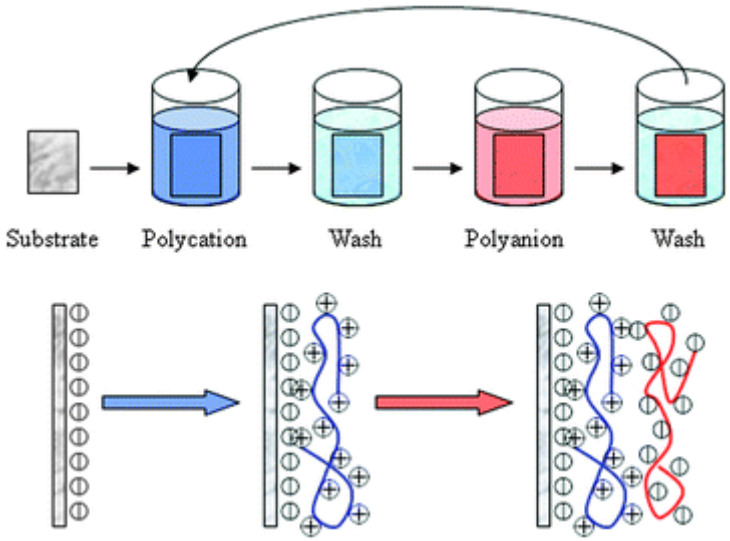

Figure 1.17: schematic protocol for LbL self-assembling technique (adapted from Xiang et al., 2012).

1.3.3. Encapsulation in liposomes

Liposomes were described for the first time by Bangham et al., (1965) as colloidal particles formed by one or more phospholipids bilayers separated by water compartments (Figure 1.18). In the last decades, they were used for the entrapment, delivery and release of a wide spectrum of molecules, both hydrophilic and hydrophobic (Fang & Bhandari, 2010). Important advantages of the encapsulation of bioactive compounds in liposomes are the possibility to carry them exactly to the tissue where they are needed, in complete agreement with the definition of drug delivery system, and to protect the entrapped substances during the transport from the injection site to the pathological tissue. In literature several technique to synthetize liposomes were reported, such as lipid film hydration, reverse phase evaporation, solvent injection or freeze thawing, sonication, French press and extrusion (Mozafari et al., 2008; Fathi et al., 2012; Patil & Jadhav, 2014).

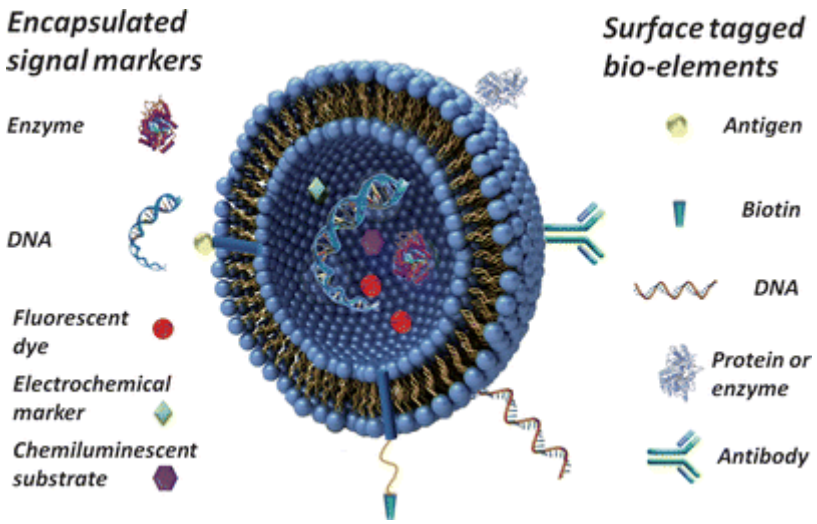

Figure 1.18: encapsulation of different bioactive molecules in liposomes and functionalization of their surface (adapted from Liu & Boyd, 2013).

1.4. Polyphenols

Polyphenols are a large family of secondary metabolites produced by plants via shikimate pathway (Tsao, 2010). They are characterized by the presence of one or more aromatic rings, with one or more hydroxyl group as substitutes. They are well-known for their antioxidant activity. This property consists in counteracting the activity of reactive oxygen species (ROS), such as such as superoxide radical ($^{\cdot}O2$), hydrogen peroxide (H_2O_2), hydroxyl radical ($^{\cdot}OH$), singlet oxygen ($^1O_2$) or peroxyl radicals ($RO_2^{\cdot}$) and

reactive nitrogen species (RNS). These reactive species are produced both by exogenous chemicals or by endogenous metabolic activity (Georgetti et al., 2008). Their antioxidant activity is due to two different activities: the radical scavenging activity and the interactions with proteins and ions (Munin & Edwards-Lévy, 2011). They exhibit antioxidant activity trought two different mechanisms: donation of a hydrogen atom or donation of an electron (Leopoldini et al., 2011; Rice-Evans et al., 1996). They can prevent the formation of free radical even sequestering metal ions by chelating the inorganic reaction catalyst (Leopoldini et al., 2011).

1.4.1. Classification of phenolic compounds

Polyphenols can be classified on the basis of different criteria. The most widely used is on the chemical structure. According to this consideration, polyphenols are divided in non-flavonoid phenols and flavonoid phenols. The non-flavonoid phenols include phenolic acids (benzoic acid and cinnamic acids) and stilbens. All the benzoic acids derive from *p*-hydroxybenzoic acid. Gallic, vanillic and syringic acid are examples of this kind of compounds. Chemically, cinnamic acid share the structure of the hydroxycinnamic acid. The most famous member of this class is caffeic acid. Stilbens are characterized by the presence of two benzene rings joined by an ethylene bridge, and multiple hydroxyl substitutes on the aromatic rings.

Flavonoids represent a large family of compounds which share the structure formed by a backbone of carbon atoms arranged into two benzene rings joined by a heterocycle. Quercetin is a well-known example of flavonoids.

1.4.1.1. Quercetin

Quercetin (3, 3', 4', 5, 7-pentahydroxyflavone) is a plant-derived flavonoid and it is widely distributed in fruits, vegetables, leaves and grains such as capers, green tea, apples, berries, celery, broccoli, and onions. Quercetin shows antioxidant, anti-inflammatory, anti-atherogenic and anti-carcinogenic activities. The U.S. Food and Drug Administration has not approved any health claims for this flavonoid. In comparison with other polyphenols, its purification process is easier, thus lead to a competitive market price. It has been estimated that the daily dietary intake of flavonoids is approximately 20 mg and quercetin is the major fraction of such intake (Figure 1.19).

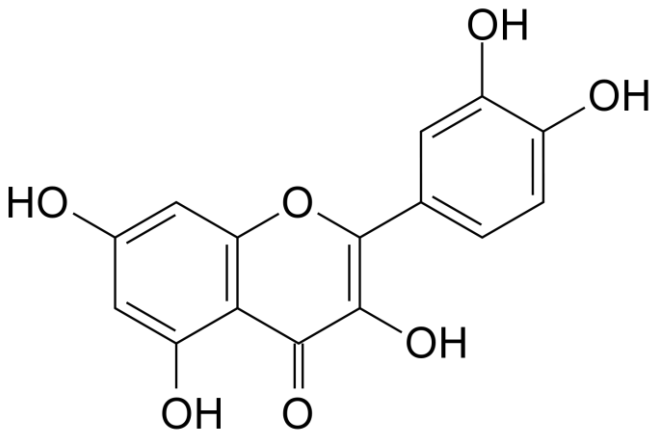

Figure 1.19: chemical structure of the flavonoid quercetin (adapted from McKay et al., 2015).

CHAPTER II

2. FUNCTIONALIZATION WITH BIOACTIVE COMPOUNDS OF BIODEGRADABLE ELECTROSPUN VASCULAR SCAFFOLDS

2.1.INTRODUCTION

In the Western World, atherosclerosis-related diseases, including coronary and peripheral arterial pathologies, are one of the most common cause of morbidity and mortality. In some cases, in order to restore the blood flow, preserving all the functions of the downstream tissue, is necessary to introduce an arterial bypass in the patient (Hu et al., 2012) or to replace a diseased blood vessel (Wippermann et al., 2009). If autologous veins or artery are not available for different reasons (previous harvest, anatomical defects and anomalies, disease progression, other vascular problems etc.), artificial vascular substitutes are required (Nerem & Seliktar, 2001). Current treatment strategies include the use of auto- or allografts or the use of stents which are not yet a definitive solution. The limited availability of suitable autogenous and allograft veins for complete coronary revascularization and the frequency of post-surgery occlusion of small-diameter synthetic prostheses has attracted several investigators to focus their attention on the fabrication of alternative biocompatible small caliber grafts. During the last decade, different type of vascular grafts have been used to bypass or replace stenosed vessels. Non-degradable synthetic grafts (e.g. poly (ethylene terephthalate) fibers, and expanded polytetrafluoroethylene) have been successfully implanted as vascular substitutes for aortic and iliac reconstruction (Konig et al., 2009). When they are used as analogues for small-caliber vessels (inner diameter < 6 mm), many drawbacks have been reported: increased frequency of infection, absence of endothelialization after the implantation, possible short-term thrombosis and myointimal hyperplasia, presence of dystrophicic calcification and aneurysm (Wilson et al., 1990), compliance mismatch between the native tissue and the artificial material, and the related inflammatory response to the foreign materials (Lee et al., 2012). Thus, there is a need for the development of scaffolds that can collectively overcome these above-mentioned drawbacks. Blends of biodegradable and biocompatible poly (ε-caprolactone) (PCL) and poly (glycerol sebacate) (PGS) are among the materials that have been successfully used in vascular tissue engineering. The composition is biodegradable and biocompatible

and offers mechanical properties comparable to the native vessel. In addition, it has been shown that PCL:PGS scaffolds support the growth of human umbilical vein endothelial cells (Sant et al., 2011) and human mesenchymal stem cells (Tong et al., 2011). Thus, this chemical composition is promising for small-caliber engineering vascular grafts. Until today, different approaches have been studied to fabricate high-performing small-caliber blood vessel grafts, including collagen porous materials (Shen et al., 2008), cell seeded or not biodegradable polymers through 3D printing, electrospinning, film casting, self-assembling methodologies, and decellularized matrices from animals (Teebken et al., 2000) and humans (Gui et al., 2009). In the last years, electrospinning has considered one of the most promising technique in the field of vascular tissue engineering since a microstructure very similar to extracellular matrix is formed during the whole process. During electrospinning the solvents evaporates quickly and a high electrical field charges the solidified polymers that are deposed onto a roto-translating collector.

Gelatin is a hydrophilic protein obtained by the partial hydrolysis of collagen. Collagen is the main constituent of bones, cartilages, skin, and , in general, of extracellular matrix in animals (Gomez-Guillen et al., 2011). In this work, it was used to make impermeable to water the polymeric scaffold.

Among antioxidants, there is a class of compounds, known as polyphenols, that show antinflammatory activity both *in vitro* and *in vivo*. Quercetin (3, 3', 4', 5, 7-pentahydroxyflavone) is one of the most prominent dietary antioxidant present in different kinds of fruit (apple, grapes, berries), vegetables (red onions, celery, broccoli, and beverages) (Kobuchi et al., 1999; Singh Baghel et al., 2012). It plays various beneficial health effect, not only acting as scavenger towards peroxynitrites and hydroxyl radicals (Boots et al., 2008), but even protecting against osteoporosis (Wattel et al., 2004), cancer (Ranelletti et al., 2000), cardiovascular diseases (Russo et al., 2012), and inflammation (Crespo et al., 2008). Despite the majority of tissue engineering research is focused on the finding of a perfect candidate scaffold mimicking biochemical, physiological, mechanical and architectural characteristics of the native tissues. However, polymeric scaffolds could provoke inflammation after the implantation of the material and in the worst cases its rejection. The counteracting of the implanted-related inflammation by functionalized biomaterials, represents today a new challenge. In fact, the post-surgical inflammation is able to affect negatively the cellular attachment and their growth on the bioprosthesis, inducing many damages to the microstructure of the biomaterials, compromising its physico-chemical and mechanical properties, leading, in the worst case, to the rejection of the graft.

The functionalization of polymeric scaffold with $CaCO_3$ nanoparticles aimed to create a good model of scaffold being able to attract cells during the release of the protein encapsulated in the nanoparticles themselves.

Finally, polymeric scaffolds were functionalized with rapeseed and salmon lecithin. Rapeseed lecithin is formed by esterified mono- and poly-unsaturated fatty acids (PUFA), like oleic, linoleic, and linolenic

acids while salmon lecithin is characterized by a high content of eicosapentaenoic and docosahexaenoic acids (Bouarab et al., 2014). These PUFAs act both directly (e.g. by replacing arachidonic acid as an eicosanoid substrate, inhibiting arachidonic acid metabolism, and inhibiting the production of inflammatory mediators) and indirectly (e.g. by altering the expression of inflammatory genes through effects on transcription factor activation) (Khalfoun et al., 1997; Calder, 2006).

2.2.MATERIALS AND METHODS

In this section, materials and methods used during the research activity concerning the fabrication of pure polymeric and functionalized vascular grafts are presented. In details, after a short section on chemicals, a part regarding the materials and the methods to fabricate and to functionalize with bioactive compounds the polymeric vascular scaffold is described.

2.2.1. Chemicals

Poly (ε-caprolactone) (PCL) (Mn = 80.000 g/mol), glycerol, sebacic acid, gelatin from bovine and porcine bones, quercetin, bovine serum albumin (BSA), tetrahydrofuran (THF), anhydrous chloroform, absolute ethanol, and Dulbecco's phosphate-buffered saline (DPBS, pH = 7.4) were purchased from Sigma-Aldrich (St. Louis, MO, USA).

Poly (glycerol sebacate) (PGS) was synthetized as described by Wang et al. (2002). Briefly, glycerol and sebacic acid were added in a 2:3 molar ratio and melted at 120°C under argon gas flow for 24 hours before the pressure was reduced below the atmospheric pressure over 5 hours. The reaction mixture was kept at 120°C and under vacuum for 48 hours after which it was obtained a highly viscous pre-polymer.

Molecular weight of PGS was determined using gel permeation chromatography (GPC, Agilent 1100 series, USA). PGS was dissolved in THF and 20 μL of the solution was injected to a column (Agilent PLgel 5 μm MIXED-D, 7.5 × 300 mm) at 25 °C and at flow rate of 1 mL/min.

Water used for the preparation of solutions and washing operations was purified by Milli-Q® system (Millipore, Molsheim, France).

2.2.2. Cell mediums and reagents

Two different types of cells were used for the experimentation, human endothelial cell line EA. hy 926 and human mesenchymal stem cells (hMSC). EA. hy 926 were cultivated in Dulbecco's Modified Eagle Medium (DMEM) high glucose with L-glutamine (Euroclone, Milan, Italy) with the addition of 10 % of fetal bovine serum (v/v) (Carlo Erba, Milan, Italy) and penicillin/streptomicin 1 % (v/v) (Ge Healthcare, Pasching, Austria). hMSC were collected from Wharton's jelly (WJ) from connective tissue of human umbilical cord. In this case, umbilical cords were used after mother information and agreement, applying the guidelines ratified by the University Hospital Center of Nancy (agreement TCG/11/R11). Cells were collected after enzymatic digestion of the WJ using a collagenase solution at 1 mg/mL (Sigma-Aldrich, France) during 18 hours at 37°C. hMSC were cultivated using DMEM (Gibco, France) after the addition of 10 % of fetal bovine serum (v/v), 2 mM of L-glutamine, 2.5 g/L of fungizone®, 100 IU/mL of penicillin and 100 μg/mL of streptomycin. Cells were collected and grown in an incubator at 37°C and 5 % CO_2 and culture medium was changed every 3 days of cultivation. Trypsin-EDTA was purchased from Carlo Erba (Milan, Italy), 3-(4, 5-dimethylthiazol-2-yl)-5-(3-carboxymethoxy-phenyl)-2-(4-sulfophenil)-2H-tetrazolium) (MTS) from Promega (Madison, WI, USA) and TNFα from Biovision Inc. (Milpitas, CA, USA).

2.2.3. Fabrication of vascular prostheses

2.2.3.1. Preparation of spinning solution

PCL (10, 15 and 20 %, w/v) and PGS solutions (20 %, w/v) were prepared dissolving the polymers in a mixture of chloroform:ethanol (9:1, v/v) under magnetic stirring (Heidolph Mr 2002, Kelheim, Germany) for at least 12 hours at room temperature (25 ± 1°C). Three different type of spinning solution were prepared during the research, pure polymeric solutions (PPS) consisting of PCL, PGS or a combination of them, polymeric solution with calcium carbonate nanoparticles ($CaCO_3$), polymeric solution with free quercetin (Q), and polymeric solution with rapeseed and salmon lecithin (RL an SL, respectively). In order to prepare PCL:PGS solutions at different volume ratios (0:1, 1:0, 1:1, 2:1, 3:1, respectively), the stock solutions at 20 % (w/v) were mixed for at least 2 hours at room temperature. In the case of quercetin-functionalized scaffold (QS), both the polymeric solutions were prepared using a constant percentage of polymers (20 %, w/v) in chloroform and an ethanolic solution of quercetin (5.5 mg/mL), instead of pure ethanol, with the same solvent ratio reported above (9:1, v/v). Even in this case, the two polymers solutions were mixed keeping always constant at 1:1 (v/v) the ratio between them and they were mixed at the same conditions

reported before in glass amber bottles under magnetic stirring for at least two hours before being electrospun. In order to obtain nanoparticles-functionalized scaffold (NS), the two polymer solutions (20 %, w/v each) were then combined only in a ratio 1:1 and it was added an equivalent of 0.1 % (w/v) of $CaCO_3$ nanoparticles and stirred again for 45 minutes. To fabricate rapeseed and salmon lecithin-functionalized scaffold (RLS and SLS, respectively), lecithins were weighted and the two polymers solutions (20 %, w/v each) were added to them in a ratio 1:1. Three different concentration for both the lecithins were studied (0.5, 1.0 and 5.0 mg/mL). RLS and SLS were characterized only in terms of morphology studies (SEM) and they were analysed using FTIR. This research is still ongoing as collaboration between University of Genova and University of Nancy.

2.2.3.2. Density and viscosity of the spinning solution

At first, to understand if the pure polymeric solutions were suitable for the electrospinning process, both their density and their viscosity were calculated.

Density of each pure polymeric solution was measured by weighing the same volume of each sample (5 mL) at room temperature. Each solution was placed in a 5-mL Pyrex single metric scale graduated cylinder, it was kept at 25°C for 15 min, and the mass of the sample (after taring the cylinder) was determined by a four-digit analytical balance (model AE240, Mettler-Toledo, Milan, Italy). Density was mathematically calculated by dividing mass of the sample by volume. The density results are the mean of at least four independent measurements.

The solution viscosity measurements were performed by using Cannon Fenske glass capillary kinematic viscometers (Fisher Scientific, Pittsburgh, PA, USA) at room temperature. Kinematic viscosity (ν) expressed in centistokes, was calculated measuring the flow time (t) and instrument constant (c) provided by the viscometer manufacturer, using the following equation:

$$v = ct \qquad \text{(Equation 2.1)}$$

Dynamic viscosity (μ_L), expressed in centipoise, was calculated from the kinematic viscosity (v) and the density of the solution (ρ) using the equation:

$$\mu_L = \rho v \qquad \text{(Equation 2.2)}$$

2.2.3.3. Fabrication of small diameter tubular scaffolds via electrospinning

The electrospinning apparatus (Spinbow, Bologna, Italy) used to fabricate small diameter tubular scaffolds consisted of a high voltage power supply (PCM series, Spellman, NY, USA) to negatively charge the polymeric solution, a grounded roto-translating aluminium cylindrical drum (2 or 5 mm outer diameter and 13 cm in length) to collect fibers, and a syringe pump (KDS-100, KD Scientific, Holliston, MA, USA) to control the feed flow rate. In the preliminary experiments, operative parameters of the electrospinning process were varied. In detail, voltage (from 14 to 20 kV), distance from needle to collector (from 15 to 18 cm), and flow rate (from 0.60 to 2.20 mL/h) were used. Among all these experiments, electrospun homogeneous grafts could be obtained only working with a flow rate between 1.10 and 2.20 mL/h and with the maximum distance (18 cm) between the needle and the collector. Low voltage, low distance, and low flow rate were not suitable for our electrospinning. At short distance of needle to collector and under a low voltage, the formation of beads and fibrous non-homogenous fragile constructs were noticed. High voltage of 20 kV resulted to instability of the jet and fusion of fibers. Rotation and translating speed were kept at minimum to minimize their effect on the graft microarchitecture. Once determined the optimal working conditions, 1.50 mL polymeric solutions were loaded into a 5 mL glass syringe (FORTUNA® OPTIMA®, Poulten & Graf GmbH, Wertheim, Germany) and extruded from a 16G flat needle tip at a vertically distance of 18 cm onto a cylindrical collector. The potential was set at 17 kV, the flow rate was 1.10 (working with 2 mm collector) or 2.20 mL/h (working with 5 mm collector) and, in any case, the rotation and the translation speed were 500 rpm and 600 mm/min, respectively. Fibers were collected at room temperature and in dark conditions. All electrospun constructs were then placed in a desiccator overnight to allow the completely evaporation of the solvents. In Table 2.1, 2.2, 2.3, and 2.4 are reported all the different conditions used during the synthesis of PPS, QS, NS, RLS, and SLS, respectively. The following figures are representative pictures of the final electrospun construct made of PCL:PGS (1:1, v/v) (Figure 2.1) and functionalized with Q (Figure 2.2), or with nanoparticles (Figure 2.3), or with RL (Figure 2.4).

Table 2.1: process parameters and operating conditions during electrospinning of PPS.

Process parameters	Operating conditions
needle diameter (G)	16
orientation of the needle	vertical
collector outer diameter (mm)	2
distance between needle and collector (cm)	18
rotational speed (rpm)	500
translation speed (mm/min)	600
right limit (mm)	115
left limit (mm)	15
flow rate (mL/h)	2.20
voltage (kV)	17.0
electrospun volume (mL)	1.50

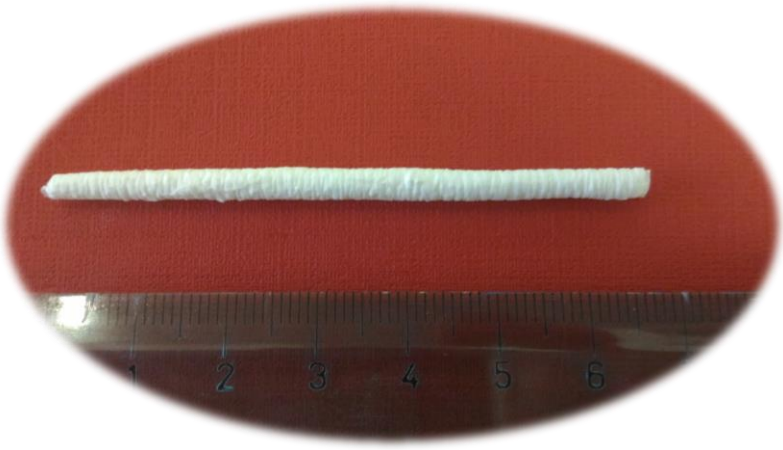

Figure 2.1: representative scaffold made of PCL:PGS (1:1).

Table 2.2: process parameters and operating conditions during electrospinning of QS.

Process parameters	Operating conditions
needle diameter (G)	16
orientation of the needle	vertical
collector outer diameter (mm)	5
distance between needle and collector (cm)	18
rotational speed (rpm)	500
translation speed (mm/min)	600
right limit (mm)	115
left limit (mm)	15
flow rate (mL/h)	1.10
voltage (kV)	17.0
electrospun volume (mL)	2.00

Figure 2.2: representative scaffold made of PCL:PGS (1:1) (left) and one functionalized with Q (right).

Table 2.3: process parameters and operating conditions during electrospinning of NS.

Process parameters	Operating conditions
needle diameter (G)	16
orientation of the needle	vertical
collector outer diameter (mm)	2
distance between needle and collector (cm)	18
rotational speed (rpm)	500
translation speed (mm/min)	600
right limit (mm)	115
left limit (mm)	15
flow rate (mL/h)	2.20
voltage (kV)	17
electrospun volume (mL)	1.50

Figure 2.3: representative scaffold made of PCL:PGS (1:1) and functionalized with $CaCO_3$ nanoparticles.

Table 2.4: process parameters and operating conditions during electrospinning of RLS and SLS.

Process parameters	Operating conditions
needle diameter (G)	16
orientation of the needle	vertical
collector outer diameter (mm)	5
distance between needle and collector (cm)	18
rotational speed (rpm)	500
translation speed (mm/min)	600
right limit (mm)	115
left limit (mm)	15
flow rate (mL/h)	1.10
voltage (kV)	17
electrospun volume (mL)	2.00

Figure 2.4: representative scaffold made of PCL:PGS (1:1) and functionalized with RL.

As reported in Table 2.1, 2.2, 2.3 and 2.4, needle diameter, orientation of the needle, distance between needle and collector, voltage, rotational and translation speed, right and left limit were kept constant for each type of samples. Adding free Q, RL, and SL to the polymeric solution, it was not possible to fabricate a homogeneous scaffold, applying the same operating conditions used for PPS and NS. Furthermore, two collectors with a different outer diameters were used during the research. A 2 mm collector was employed to have polymeric constructs to be potentially implanted in rats (*Rattus norvegicus*) and a 5 mm collector was utilized to have polymeric constructs to be potentially implanted in rabbit (*Oryctolagus cuniculus*).

Working with the thicker collector, it was necessary to halve the flow rate and to increase from 1.50 to 2.00 mL the electropsun volume in order to obtain comparable scaffolds.

2.2.3.4. Surface coating of the scaffolds with gelatin

With the aim of reducing the porosity and the excessive water permeability of PCL:PGS (1:1, v/v) scaffolds, a coating with gelatin of the external surface of the scaffolds was performed. To obtain surface coated scaffolds, they were completely immersed in a gelatin solution (67 mg/mL, w/v) and maintained under mechanical agitation (agitator model Kirk 510, Bicasa, Monza Brianza, Italy) for 1 hour at 37 ± 2°C at a constant rotational speed of 135 rpm (Figure 2.5). After that, gelatin-coated scaffolds were placed under an UV lamp for 1 hour to allow gelatin cross-linking on the surface (Pulieri et al., 2007). At the end of these total two hours, the gelatin-coated scaffolds were put again into a desiccator overnight. The coating with gelatin was performed for both PPS (1:1, v/v) and QS. Hereinafter, PCL:PGS (1:1, v/v) coated with gelatin will be called Gelatin Coated Scaffold (GCS) and QS coated with gelatin will be reported as Quercetin-functionalized and Gelatin Coated Scaffold (QGCS).

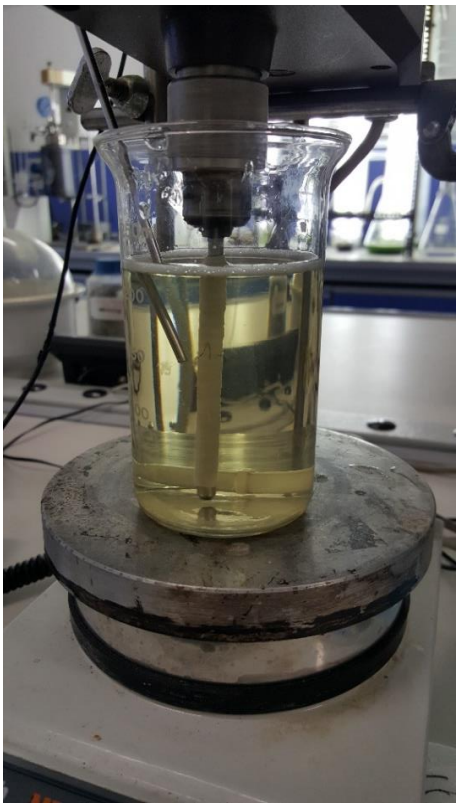

Figure 2.5: coating process with gelatin.

2.2.4. Characterization methods for the scaffolds

2.2.4.1. Scanning Electron Microscopy (SEM) analysis

Scaffold morphology was studied using LEO scanning electron microscope Model Stereoscan 440 for PPS, a SEM Hitachi 2500 (Tokyo, Japan) for NS and GCS, and the Quanta FEG 650 SEM (ThermoFisher Scientific, USA) for QS, QGCS, RLS and SLS. Fibers mean diameters were measured using image processing software (Image J, USA) in at least three different images. For each sample, the diameters of about 60 fibers were taken into account to have a meaningful statistical value.

2.2.4.2. Atomic Force Microscopy (AFM)

AFM images of PCL:PGS (1:1, v/v) and QS were recorded using a AFM (Bruker, Karlsruhe, Germany). Non conductive silicon nitride cantilevers of conical shape were purchased from Bruker (NPG-10 Bruker, Camarillo, USA).Experiments were performed at room temperature, using small pieces of each scaffold.

2.2.4.3. Fourier Transform Infrared spectroscopy (FTIR)

FTIR spectra for PPS (PCL:PGS, 1:1) QS, RLS and SLS were obtained using a Tensor 27 mid-FTIR spectrometer (Burker, Karlsruhe, Germany), equipped with a diamond ATR (attenuated total reflectance) module and a DTGS (deuterated triglycine sulfate) detector. Scanning rate was fixed to 10 kHz and 100 scans were performed for both reference (air) and samples between 400 and 4000 cm^{-1} at a resolution of 4 cm^{-1} at room temperature. At first, an initial reference spectrum was recorded. Next, a small piece of the different samples was directly put on the diamond crystal of the optical cell and a minimum of four independent analysis were done for each sample. All the data were treated using OPUS software (Bruker, Karlsruhe, Germany). Crude absorbance spectra were smoothened, centred and normalized using OPUS software.

2.2.4.4. Contact angle measurements of the scaffolds

The hydrophilicity of the PCL:PGS (1:1, v/v) and QS scaffolds was done by a goniometer (Digidrop, GBX instruments, France) equipped with three different syringes. They were used to drop 0.48 μL of three different liquids with different polarity (deionized water, glycerol and diiodomethane) on the flat surfaces of the different studied materials. The contact angle was measured by a video contact angle system.

2.2.4.5. Mercury porosimetry

Mercury porosimetry has been widely used to analyze the pore characteristics of various scaffold types (Loh & Choong, 2013; Skotak et al., 2011). Pore size distribution, bulk and apparent density, and porosity were measured using two porosimeter devices (Pascal 140 and 240, ThermoQuest, Rodano, Italy). A fragment of tubular scaffold (3 cm in length) was weighted and placed into the dilatometer, and the void space in the chamber was filled with mercury. Operative pressure range were 0.1–400 kPa and 0.1–200 MPa for Pascal 140 and 240, respectively. Test was performed in triplicate and all data were analyzed with the software SOL.I.D. (SOLver of Intrusion Data), Ver. 1.5.0. Mercury porosimetry was performed to understand the different behaviour in terms of water permeability of GCS in comparison to PCL:PGS, (1:1, v/v).

2.2.4.6. Water permeability test

It was evaluated the value of pressure that made permeable the studied scaffolds. For this test, scaffolds were cut in small pieces and cannulated by the connection of one end of the scaffold to a water reservoir after closing the other end by a flow valve (Figure 2.6). The pressure of the water was increased since it achieved diastolic and systolic values (80-120 mmHg in healthy conditions). Therefore, water passed through the scaffold and pressure was monitored during time since the graft started to be leaky. Once reached the pressure at which the water leakage occurred, the flux was maintained constant for one minute more and permeated water was collected in a beaker. After that, the volume of collected water was measured and permeability of the scaffold (τ) was calculated, as reported by Madhavan et al. (2013), using the following equation:

$$\tau = \frac{V}{A} \qquad \text{(Equation 2.3)}$$

where:

- τ is the permeability of the graft (mL/cm^2/min);
- V is the volume of the fluid passing through the graft (mL/min);

- A is the cross-sectional area of the aperture in the sample holder (cm^2).

Tests were performed with PPS (only with PCL:PGS, 1:1), GCS, and QGCS.

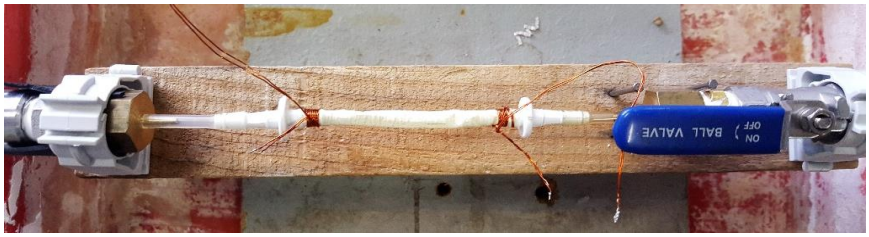

Figure 2.6: set-up of the equipment used during the water permeability test.

2.2.4.7. *In vitro* degradation and fluid up-take

An essential characteristic of biomaterials is their degradability during time. To test the mass loss in function of time, samples were first cut into small cylindrical pieces (5 x 2 mm^2), lyophilized (freeze-dryer Christ model Alpha1-2 LDplus, Osterode am Harz, Germany), and then incubated at 37°C after immersion in 1.5 mL of DPBS for a total period of 28 days or 8 weeks. At each time point (1, 7, 14, and 28 days for PPS, GCS and NS and 2, 3, 4, 5, 6, 7, 8 weeks for QS and QGCS) triplicate sample pieces were taken out, washed three times with deionized water, and lyophilized with the same freeze-dryer reported above for 24 hours after which they were reweighted. The percentage of degradation of each sample was calculated by dividing the mass loss by the initial dry mass.

To study the fluid-uptake, tubular scaffolds were cut as described above, weighted, and then immersed in DPBS. After 2, 4, 7, and 24 hours for PPS, GCS, and NS and after 2, 4, 8, and 24 hours for QS and QGCS, the excess DPBS on their surface was removed and the scaffolds were weighted again. The fluid uptake percentage was calculated by the following equation:

$$Fluid\ uptake\ (\%) = \frac{m_w - m_0}{m_0} \times 100 \qquad \text{(Equation 2.4)}$$

where m_0 and m_w are the mass of the sample before and after immersion, respectively.

Different samples (n = 3) of each scaffold type were tested.

2.2.4.8. Influence of gelatin coating on degradation rate

To understand if the coating with gelatin influenced, positively or negatively, the degradation rate of the PCL:PGS blends, degradation of coated scaffold (GCS) was study under a mathematical point of view, following these equations:

$m_{s(t)} = m_{s(f)} + m_{g(f)}$

$m_{g(f)} = m_{g(i)} - m_{g(r)}$ and substituting the term $m_{g(f)}$ in the equation

$m_{s(t)} = m_{s(f)} + \left(m_{g(i)} - m_{g(r)}\right)$

$m_{s(f)} = m_{s(t)} - \left(m_{g(i)} - m_{g(r)}\right)$ (Equation 2.5)

The mass loss percentage was calculated following this formula:

$Mass\ loss\ (\%) = \frac{m_{s(i)} - m_{s(f)}}{m_{s(i)}}$ (Equation 2.6)

where:

$m_{s(i)}$: mass of the scaffold before the coating process;

$m_{s(t)}$: total mass of the scaffold (mass of the polymer and of the gelatin);

$m_{s(f)}$: mass of the polymer after the degradation and release study;

$m_{g(f)}$: mass of the residual gelatin on the scaffold after degradation and release study;

$m_{g(i)}$: mass of the initial gelatin deposed on the scaffold;

$m_{g(r)}$: mass of the released gelatin during the study.

2.2.4.9. Gelatin release from GCS

In order to quantify the released gelatin from coated scaffolds during time, entire GCS were cut into small pieces and put into a 50 mL test tube with 5 mL of PBS. Then, they were incubated at 37 ± 2°C, in order to mimic the physiological conditions of human body, in the same incubator described before, used for degradation and fluid up-take assays. At regular intervals (after 1, 2, 3, 4, 8, 24, 48, and 72 h), 10 % of the solution was collected and it was replaced by the same volume of fresh PBS. After freeze drying of the samples, the bicinchoninic acid assay (BCA) (Euroclone, Milan, Italy) allowed to calculate the concentration of the released gelatin through UV-Visible spectroscopy at 562 nm.

The BCA assay is a convenient tool, as it permits to work with small volumes of sample: in fact, only 5 µL of the sample were mixed with 125 µL of the BCA reagent in an centrifuge tube and placed into the incubator at 37 ± 2°C for 30 minutes. After that, it was possible to record the absorbance values of the sample with a plate reader (Microplate Reader Tecan, Männendorf, Switzerland). The BCA reagent is

composed of 50 part of reagent A (bicinchoninic acid, sodium carbonate, sodium tartrate, and sodium bicarbonate in 0.1 M NaOH, pH 11.25) and 1 part of reagent B (4 % cupric sulfate).

The assay is based on a reaction of reduction in which Cu^{2+} becomes Cu^{+} in presence of proteins in an alkaline conditions. The Cu^{+} ions thus formed are detected by conversion into a violet-coloured substance by reaction with bicinchoninate. The absorbance at 562 nm of the Cu(I)-$(bicinchoninate)_2$ complex is directly proportional to protein concentration over a broad working range (20-2000 μg/mL). The absorbance of the samples was related to the concentration of the protein using an opportune calibration curve obtained with standard bovine serum albumin (Figure 2.7).

The relation between the absorbance of albumin at 562 nm and its concentration was given by the following linear equation (R^2= 0.9894) (Eq. 2.7):

$$Abs_{562} = 0.1887 \times C \qquad \text{(Equation 2.7)}$$

where:

- Abs_{562} is the absorbance of bovine serum albumin at 562 nm;
- C is bovine serum albumin concentration expressed in mg/mL.

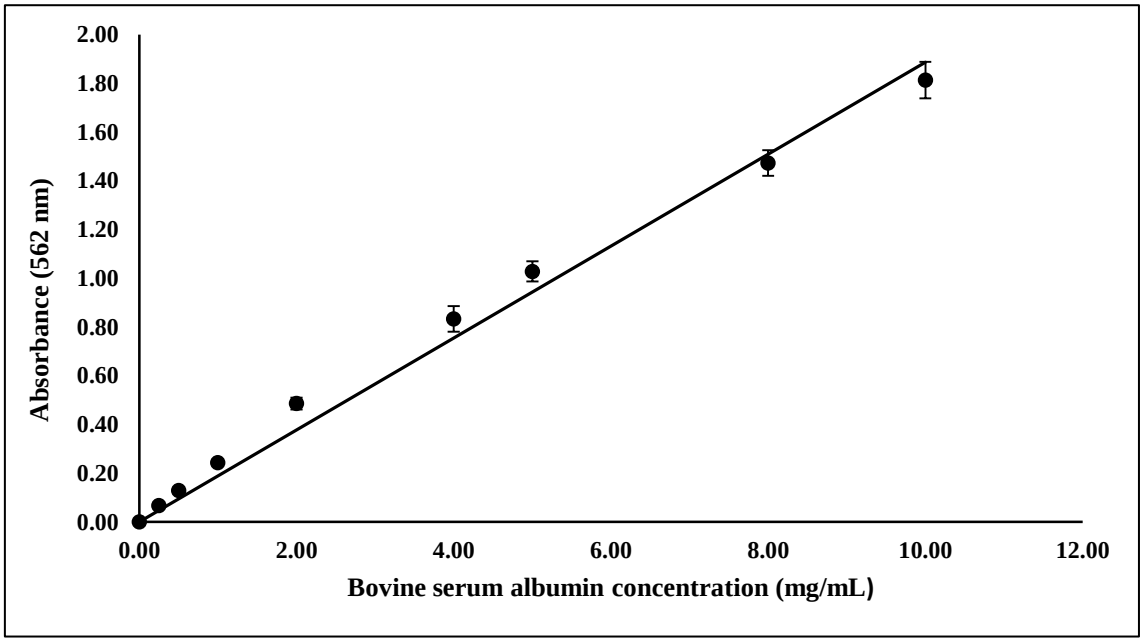

Figure 2.7: calibration curve for the quantification of gelatin released from GCS.

Results are presented in terms of percentage of the total amount of gelatin that originally covered the scaffold. The total amount of gelatin layer was evaluated by subtracting the mass of the scaffold after the gelatin coating process and the original mass. This procedure was repeated six times and the average value was taken into account for calculations.

2.2.4.10. Quercetin release from QS and QGCS

To evaluate the release of quercetin, QS and QGCS were cut in small pieces, immersed in 5 mL of PBS at pH = 7.4 and maintained at 37 ± 2°C in the same incubator described above. Daily, for 54 days, 10 % of the solution was collected and it was replaced by a same volume of fresh PBS. Samples were frozen at -20°C and before spectrophotometric analysis, they were lyophilized with the same freeze-dryer described above. Then, samples were resuspended in a solution of water:ethanol 50:50 (v/v) and they were analysed using a SPECTROStar Nano plate reader (BMG LABTECH, Ortenberg, Germany). At first, it was done a spectrum analysis (from 300 to 500 nm) of the collected samples to identify the absorbance with the highest absorption (Figure 2.8).

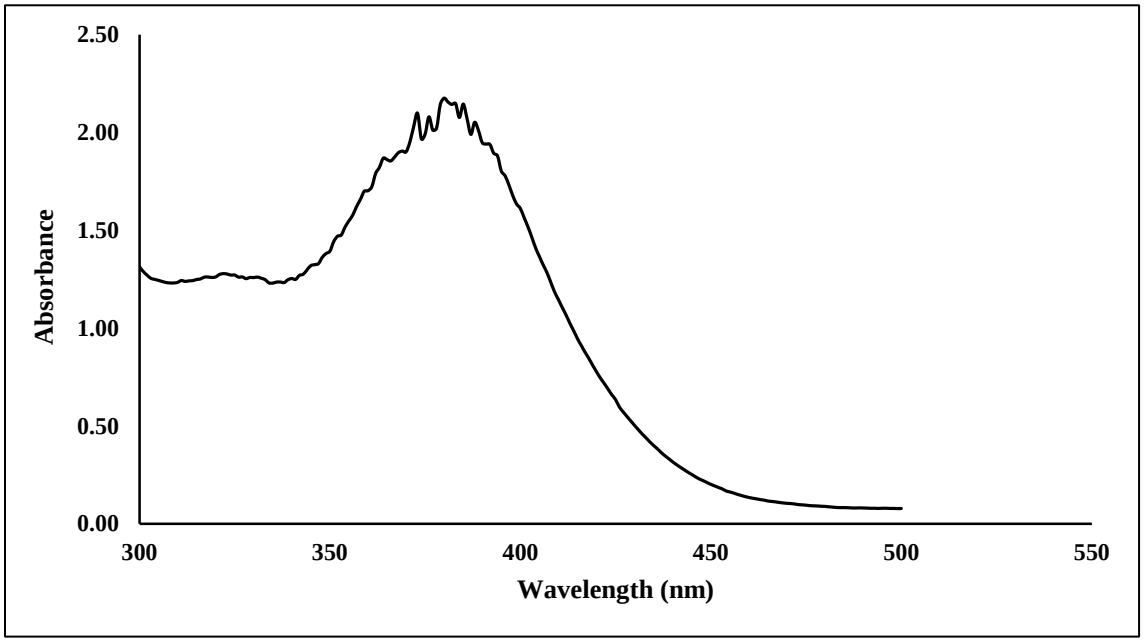

Figure 2.8: spectrum of quercetin in ethanol:PBS (50:50, v/v).

Once verified that the maximum peak of absorbance corresponded to 380 nm, a calibration curve was made with standard solutions of quercetin in a mixture of PBS:ethanol 50:50 (v/v) obtaining the following equation 2.8:

$Abs_{380} = 13.755 \times C$ ($R^2 = 0.9939$) (Equation. 2.8)

where:

• $Abs_{380}$is the absorbance of quercetin at 380 nm;

• C is quercetin concentration expressed in mg/mL.

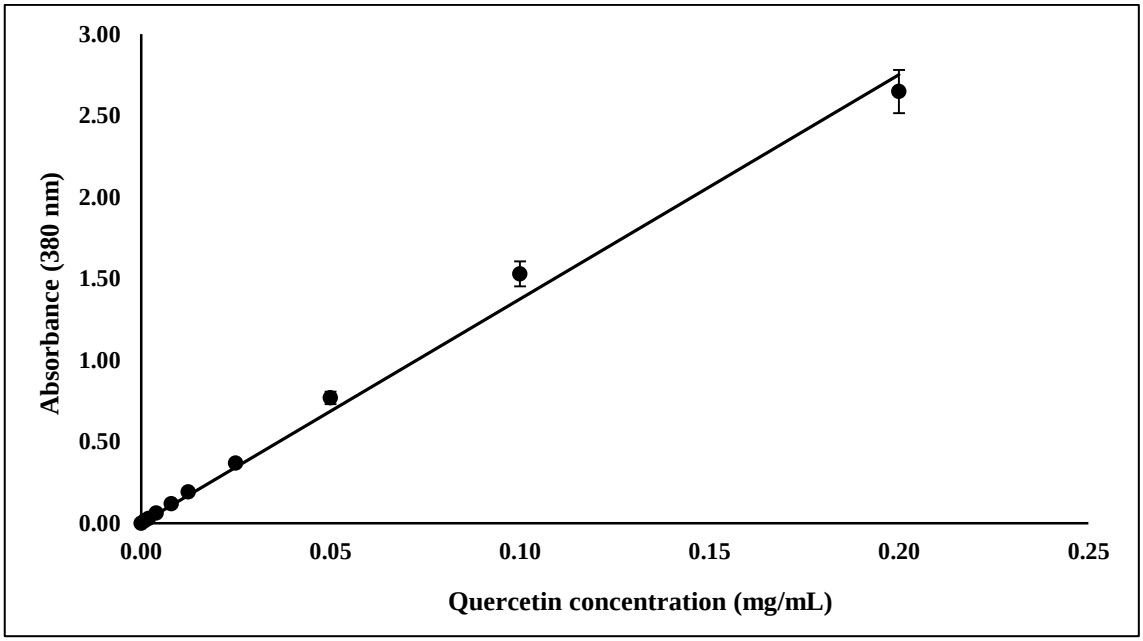

Figure 2.9: calibration curve for the quantification of quercetin.

The total amount of quercetin in electrospun scaffold was evaluated through solid/liquid extraction (SLE) using ethanol as unique solvent. Briefly, an entire scaffold was cut into small pieces and it was put in 2 mL of absolute ethanol and agitated under magnetic stirring for 2 days at room temperature. This extraction was made in triplicate. After this procedure, 150 μL of the extracting solvent was collected, its absorbance analysed at 380 nm and quercetin concentration calculated using an opportune calibration curve (Figure 2.9).

Results are presented in terms of percentage of the total amount of quercetin that originally was present in the scaffold.

2.2.4.11. BSA release from NS

For BSA release analysis, scaffold were cut, weighted, immersed in 5 mL of PBS and mildly shaken at 220 rpm in the same incubator previously reported at 37°C. At each measurement time-point (1, 2, 3, 4, 8 h and from day 1 to 28), an aliquot of 0.5 mL was removed and replaced with an equal volume of the same buffer. The protein concentration was determined by UV-visible spectrophotomer (BioPhotometer Eppendorf, Hamburg, Germany) at 562 nm through the bicinchoninic acid (BCA) assay. The relation between the absorbance of albumin at 562 nm and its concentration was given by the following linear equation (R^2= 0.9957) (Equation 2.9):

$$Abs_{562} = 0.5859 \times C + 0.0348 \quad \text{(Equation 2.9)}$$

where:

• $Abs_{562}$is the absorbance of bovine serum albumin at 562 nm;

• $C$is bovine serum albumin concentration expressed in mg/mL.

This equation describes the curve reported in Figure 2.10.

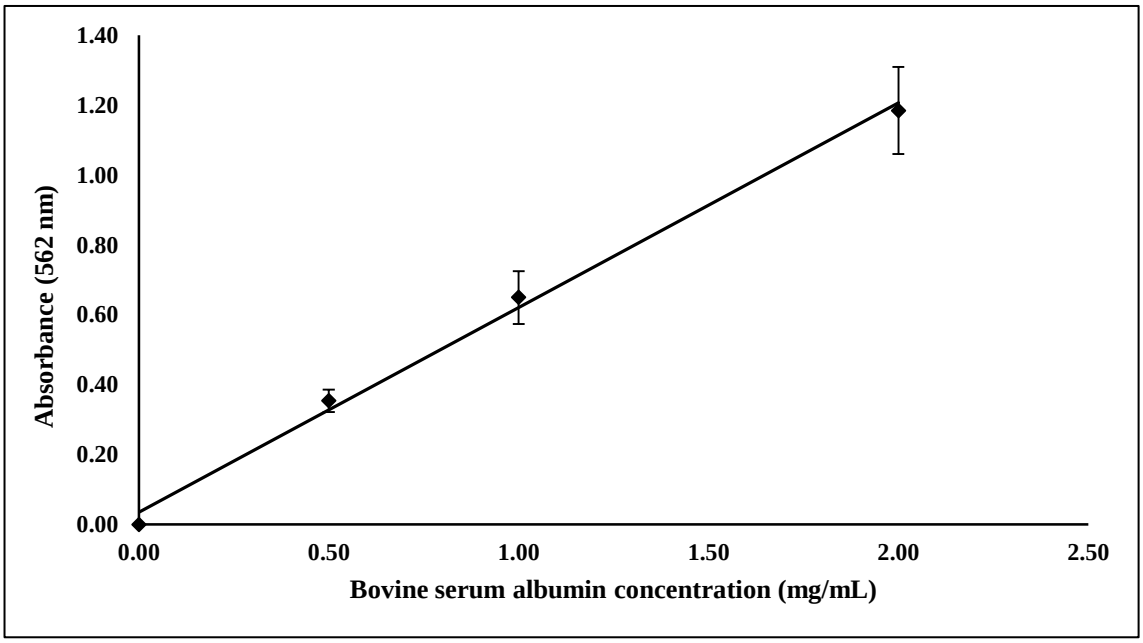

Figure 2.10: calibration curve for the quantification of BSA released from NS.

All the measures were done in triplicate.

2.2.4.12. Mechanical characterization and suture retention strength

Mechanical loading tests were performed on the electrospun grafts in the axial direction using uniaxial Z0.5 test machine (Zwick Roell, Ulm, Germany). Each tubular scaffold was cut to obtain rectangular specimen (n = 3, length = 30 mm, width = 2 mm) with the short edge of each sample originally oriented circumferentially on the original tube. The thickness of each sample was measured using a digital caliper (Series 209, Mitutoyo, USA). Every segment was clamped at its cut ends and the crosshead speed was set at 20 mm/min with a preload of 0.1 N. Young's modulus was calculated taking into account stress and strain values between 0.5-2 % of strain (about 25 data points) through a MATLAB algorithm. For each type of scaffold, the measurements were done at least four times. In the case of GCS and QGCS, mechanical tests were performed using both dry and wet samples, after their immersion in a solution of NaCl (0.9 %,

w/v) for 5 minutes. Mechanical loading tests were also performed on QS after one month of degradation in PBS, in order to analyse their behaviour even during degradation. Suture retention test was performed in accordance to American National Standard Institute/Association for the Advancement of Medical Instruments (ANSI/AAMI). The samples were prepared as described above and a single loop of 5-0 Vascufil™ suture (Covidien™) was created at approximately 2 mm from one free end. The suture loop and the opposite end of the graft were secured to the grips of the same tensile machine described above. In this case, to pull the suture, an extension rate of 1 mm/s was used and suture retention strength was taken as the maximum force recorded. The preload was set at 0.05 N.

2.2.4.13. Cytotoxicity evaluation using endothelial cells

Recent studies, in line with this, reported that electrospun PCL:PGS constructs promote cell adhesion and proliferation compared to PCL scaffolds (Sant et al., 2011), because of their enhanced hydrophilicity in comparison to hydrophobic PCL. Two different test were performed in order to assess the biocompatibility of PPS. One was done seeding endothelial cells directly on the surface of PPS, after having cut them to have a suitable dimension for a 96-well plate with an autopsy punch. The second was done using Trans-well system but only in the case of PCL:PGS (1:1, v/v) scaffolds. Scaffolds were sterilized under UV light for 1 h, and washed with 1 % penicillin–streptomycin. To study the potential cytotoxicity of grafts and by-products generated during their degradation rather than studying the interaction between cells and grafts, scaffolds were placed in the Transwell-clear multiwell inserts (Corning Costar Corporation, MA, USA) without any direct contact with endothelial cells. The graft was introduced in the cell culture system for 24 h after cell seeding to do not interfere with a proper cell attachment. The adopted protocol is described in different publications (Burdick et al., 2002; Trudel & Massia, 2002; Wang et al., 2013). Before interactions with the scaffold, the human vascular endothelial cell line EA. hy 926 was plated at a seeding density of 2 x 10^5/well in a 24-well plate in complete medium. Cell viability was evaluated using the colorimetric CellTiter96® AQ_{ueous} One Solution Cell Proliferation Assay (Promega, WI, USA) according to the manufacturer's instructions. Briefly, at any time point (1, 2, 3, and 7 days), 20 % 3-(4, 5-dimethylthiazol-2-yl)-5-(3-carboxymethoxyphenyl)-2-(4-sulfophenil)-2H-tetrazolium) reagent was added directly to the culture wells, and tetrazolium was bioreduced by cells into a colored formazan product soluble in the culture medium. Thereafter, aliquots were transferred into a 96-well plate and the quantity of formazan was measured by a spectrophotometric plate reader (Microplate Reader Tecan, Männendorf, Swiss) at 492 nm. The first protocol was adopted for all PPS scaffolds, QS, GCQS, RLS, and SLS while the use of the Trans-well system was adopted in the case of PCL:PGS (1:1, v/v) GCS, and NS.

2.2.4.14. Hemocompatibility

Hemocompatibility is a fundamental factor to determine the application of implantable biomaterials, especially vascular prosthesis. For hemocompatibility tests, blood was collected from healthy volunteers by venipuncture into ethylenediaminetetraacetic acid (EDTA) anticoagulant vacutainer tubes. For hemolysis test, each scaffold was cut (50 mm^2 in area) and rinsed three times with distilled water. Then hemolysis test was performed by placing the scaffold in a solution of 0.9 % NaCl or deionized water. Then, 0.1 mL of human fresh blood was added to the solution. After 30 min, erythrocytes membranes were broken and hemoglobin was released in the solution. At the end of the incubation time (30 min), the supernatants of all the samples were collected and transferred into cuvettes to measure their absorbance at 540 nm, which is the wavelength were there is a maximum of absorbance in haemoglobin spectrum. Hemoglobin was chosen since it is one of the most abundant proteins expressed by erythrocytes. Similarly, 0.1 mL of fresh blood was added to 5 mL of distilled water and 0.9 % NaCl using, respectively, as positive and negative controls. Positive and negative controls are necessary to exclude erythrocyte disruption not directly caused by the samples. At the end of the incubation, all the samples were centrifuged at 3.000 rpm for 5 min. The supernatants were carefully collected and transferred into cuvettes to determine the absorbance at 540 nm (spectrophometer Lambda 25, PerkinElmer, Milan Italy). The hemolysis percentage (HR) was calculated by the following equation:

$$HR\ (\%) = \frac{A_s - A_n}{A_p - A_n} \times 100 \qquad \text{(Equation 2.10)}$$

where A_s, A_p, and A_n are the absorbance values of haemoglobin in the sample, in the positive and negative controls, respectively.

The anticoagulant properties of electrospun scaffold were registered by the kinetic clotting time method (Imai & Nose, 1972). The coagulation is an extremely complicated process where different cells and molecules play a fundamental role. After a detailed research in the literature, free hemoglobin appeared as one of the most common parameters analyzed to study the anticoagulant properties of materials (Meng et al., 2010; Zhang et al., 2013; Elahi et al., 2014; Shen et al., 2015). A total of 64 μL of EDTA blood was dropped on the inner surface of the samples (32 mm^2), followed by the addition of 16 μL of $CaCl_2$ (0.2 mol/L) solution, and mixed uniformly. After predetermined intervals of time (5, 30, and 60 min), the specimens were put into 16 mL of distilled water and incubated at 37°C for 5 min. The concentration of the free hemoglobin in water was measured by monitoring the absorbance at 540 nm using the same spectrophotometer described above. Glass was used as reference thrombogenic material (Motlagh et al., 2006). All the hemocompatibility analysis were performed using as reference poly (ethylene terephthalate) and expanded poly (tetrafluoroethylene).

2.2.4.15. *In vivo* suturability test

All animal treatments were approved by the S.S.D. Animal Facility, IRCCS AOU San Martino - IST. Wistar rats (Charles River Laboratories International Inc., MA, USA) were anesthetized feeding isoflurane with a starting flow of 3-4 mL/h. Then the flow was kept constant at 1.5 mL/h with addition of O_2 at 30 mL/min during the surgical procedure. Under general anesthesia and after subrenal aortic clamping, aorta was resected and the vascular graft was implanted. Electrospun PCL:PGS (1:1, v/v) blend coated with gelatin (GCS) graft of 3 cm in length was sutured to the aorta in an end-to-side fashion using monofilament 10-0 Vascufil™ sutures (Covidien™). The implantation of GCS was done in two animals. This test has to be considered a preliminary test and it was only done to assess the practical suturability of the electropsun vascular prosthesis with native vessels.

2.2.4.16. Anti-inflammatory activity of QS

PCL:PGS (1:1, v/v) constructs (control) and GCQ scaffolds were cut in cylindrical pieces (0.5 cm in diameter × 0.5 cm in length) and they were sterilized using a solution of penicillin/streptomycin (1 %) for at least three hours, in order to avoid possible contamination once in contact with human cells. 5×10^4 EA hy 926 were seeded in each well using Transwell-clear multiwell (Corning Costar Corporation, MA, USA). The material was put into each insert and as a result there was no a direct contact between the cells and the scaffold. After 24 hours, the medium was replaced with serum free medium and cells were treated with TNF-α (1 ng/ml, Biovision). After 24 hours, the conditioned media (CM) were collected and centrifuged to remove cellular debris and stored at -20°C before analysis. Matrix Metalloprotease 9 (MMP-9) expression was observed using optical densitometry of gelatinolytic bands (gel analysis system, GeneGenius, Syngene, Cambridge, UK). The same quantity of proteins, estimated by BCA assay, from CM were loaded on SDS-acrylamide gel cast with 0.28 % (w/v) gelatin (type A), rinsed two times in 2.5 % Triton-X-100 for 30 minutes. After that, the samples were incubated for 18 hours in 40 mM Tris–HCl, 0.2 M NaCl, 10 mM $CaCl_2$ at 37°C for 18 hours and then stained with 0.2% Coomassie blue and destained in ethanol:water:acetic acid (50:40:10, v/v).

2.2.4.17. Statistical analysis

All the experiments were performed at least in triplicate and the results were expressed as mean values and standard deviations. The analysis of variance (ANOVA) and the Tukey's post hoc test were used to

highlight statistically significant differences among the different studied samples. Multiple comparison of the mean values was performed by the least significant difference test at $p < 0.05$. For data analysis, the Statistica v 8.0 software (StatSoft, Tulsa, OK, USA) was used.

2.3.RESULTS AND DISCUSSION

In this section of the thesis, tables and figures concerning all the data obtained investigating electrospun vascular scaffolds are presented and critically discussed. In the order, the attention will be focused on Pure Polymeric Scaffolds (PPS), Gelatin-Coated polymeric Scaffolds (GCS), Quercetin-functionalized polymeric Scaffolds (QS), Quercetin-functionalized and Gelatin-Coated polymeric Scaffolds (QGCS), Nanoparticles-functionalized polymeric Scaffolds (NS), and Rapeseed and Salmon Lecithin-functionalized polymeric Scaffolds (RLS and SLS, respectively). In every section regarding GCS, QS, QGCS, NS, RLS, and SLS, the PPS made of poly (ε-caprolactone) and poly (glycerol sebacate) (PCL:PGS, 1:1) has to be considered as the control. In fact, it was fabricated using the same polymeric mixture of the others scaffolds but without the bioactive compounds present in the functionalized counterpart.

2.3.1. Pure polymeric scaffolds (PPS)

2.3.1.1. Density and viscosity of the spinning solutions

In general, the concentration of the polymers in the spinning solution plays a pivotal role at first on the electrospinning process and after on the physicochemical and biomechanical properties of electrospun products. The synthetized PGS resulted to have a molecular weight of 2673 Da with a polydispersity index (PDI) equal to 1.98. The effects on the properties of the grafts due to PCL concentration as well as those due to the addition of PGS to the spinning solution, were studied. During the preliminary tests, three different concentrations of PGS (10, 15, and 20 %, w/v) were taken into account (data not showed). However, because of their low viscosity, it was not possible to fabricate scaffold with a well-defined architecture working with PGS alone at 10 and 15 % (w/v) via electrospinning. As a result, concentration of PGS was limited to 20 % (w/v) to facilitate the electrospinning process itself. The properties of the different spinning solutions, such as density and viscosity, were measured and they are reported in Table 2.5. The density of the different polymeric solutions resulted to be in the range from 1.25 ± 0.09 to 1.38 ± 0.6 g/mL. An increase in PCL concentration did not significantly influence the density of the solutions ($p < 0.05$). A glass capillary kinematic viscometers was used to measure the viscosity of solutions. As expected, the viscosity of the PCL solution significantly increased ($p < 0.05$) by increasing the concentration of the polymer from 10 to 20 %. The addition of PGS (20 %, w/v) to the PCL solution resulted to a reduction in the viscosity of solution from 4.54 ± 0.02 to 1.10 ± 0.13 Pa·s for PCL:PGS (1:1, v/v) and

2.45 ± 0.12 for PCL:PGS (3:1, v/v). PGS solution is known to have a low viscosity, thus, the mixture of PCL and PGS solutions showed a lower viscosity in comparison to those made of PCL alone. Even the viscosity of solutions plays an important role during the electrospinning process and it influences the generated construct. Low-viscosity solutions cannot generate fibrous structures, while too viscous solutions require a higher voltage to form fibrous scaffold (Tamayol et al., 2013).

Table 2.5: viscosity and density values of PCL and PCL:PGS blend solutions with different concentrations and ratios between the two polymers.

Sample	Density (g/mL)	Viscosity (Pa·s)
PCL (10 %)	1.30 ± 0.13^{a}	0.32 ± 0.02^{b}
PCL (15 %)	1.32 ± 0.04^{a}	1.69 ± 0.02^{a}
PCL (20 %)	1.35 ± 0.09^{a}	4.54 ± 0.02^{e}
PCL:PGS (1:1)	1.25 ± 0.02^{a}	1.10 ± 0.13^{c}
PCL:PGS (2:1)	1.32 ± 0.09^{a}	1.47 ± 0.03^{a}
PCL:PGS (3:1)	1.38 ± 0.06^{a}	2.45 ± 0.12^{d}

Results are mean of three measurements ± SD. Different letters do refer to statistically significant differences among results for each column ($p < 0.05$), ANOVA with Tukey's multiple comparison test.

2.3.1.2. Scanning Electron Microscopy (SEM) analysis of PPS

Representative SEM images of internal (Figure 2.11, top) and external (Figure 2.11, bottom) surfaces of electrospun scaffolds, made of PCL 20 % and PCL:PGS (1:1, v/v) showed randomly oriented bead free fibers. The fabricated scaffolds were porous with uniform morphology. In the inner surfaces of scaffolds (Figure 2.11 A and 2.11 C), some fiber fusion was observed. It could be caused by the presence of mineral oil used for covering the drum collector to allow an easy extrusion of the scaffold at the end of the electrospinning process. Fiber diameters are reported in Table 2.6 for internal and external surfaces of the scaffolds. The microfibers had diameters between 3.94 ± 1.39 and 5.57 ± 1.55 μm. These results demonstrated that the average of fiber diameter was not statistically different ($p < 0.05$) for internal and external surfaces of the studied polymers. However, the scaffold containing PGS resulted to have fibers with greater diameter when compared to only PCL fibers. The same trend was also noticed by Sant et al. (2011). They found that at the same electrospinning condition, an increase in PGS content in the PCL:PGS blend resulted to increase fiber diameter. As described by Ghasemi-Mobarakeh et al., (2008), thickness of

electrospun nanofibers influences cell proliferation by providing better substrate with more dimensional stability. The microfiber scaffolds can be potentially advantageous with respect to the nanofibers scaffolds by their larger pores between the fibers which can facilitate cellular infiltration and/or nutrient diffusion during cell culturing (Pham et al., 2006; Balguid et al., 2009). It is chosen to present only PCL 20 % and only PCL:PGS (1:1, v/v) because of they represented the scaffold with the highest amount of PCL and PGS, respectively.

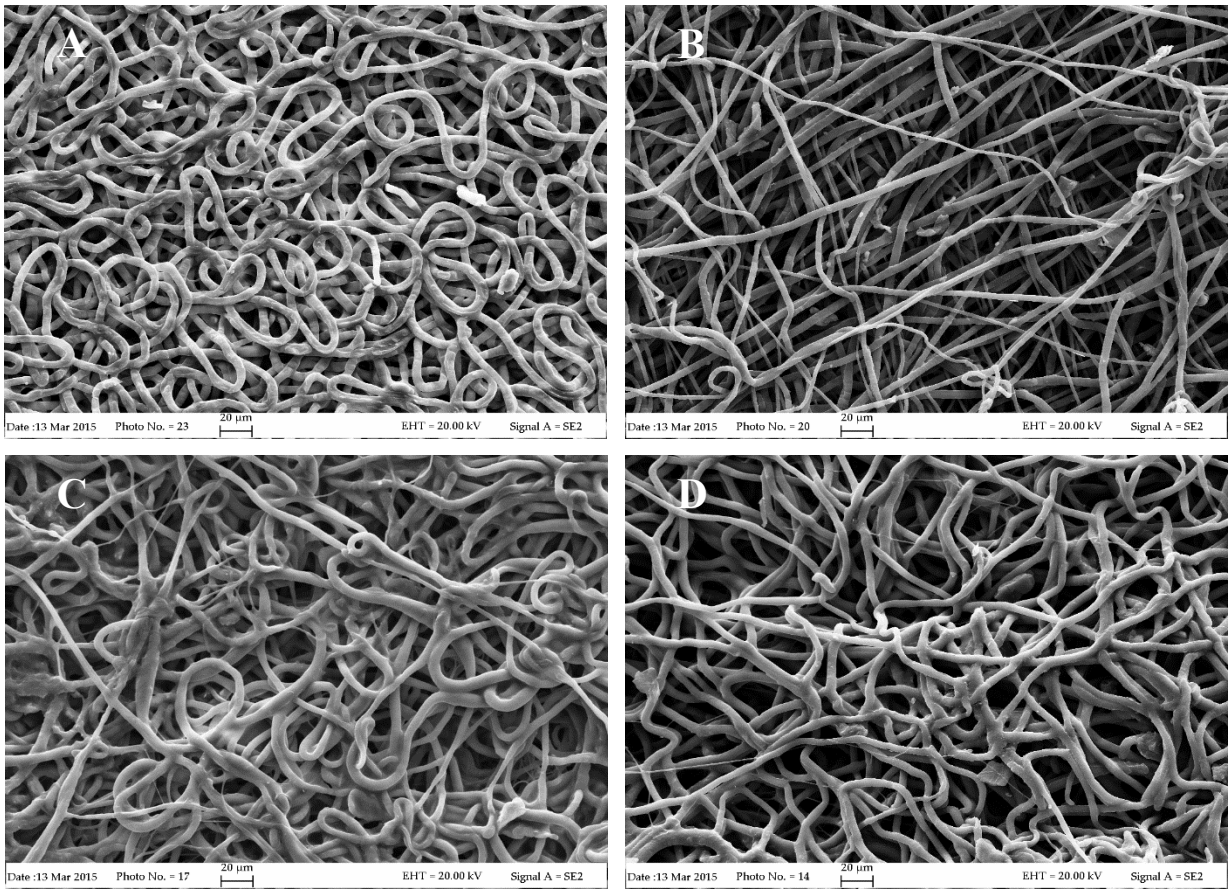

Figure 2.11: representative SEM micrographs of (A) internal and (B) external surfaces of electrospun scaffolds made of PCL 20 % and of (C) internal and (D) external surfaces of electrospun scaffolds made of PCL:PGS (1:1, v/v).

Table 2.6: fiber diameter for internal and external surfaces of PCL 20 % and PCL:PGS (1:1).

Sample	Internal diameter (µm)	External diameter (µm)
PCL (20 %)	3.94 ± 1.40^{a}	$4.80 \pm 0.80^{a,c}$
PCL:PGS (1:1)	$5.11 \pm 1.11^{b,c}$	5.57 ± 1.55^{b}

Results are mean of at least one hundred measurements ± SD. Different letters do refer to statistically significant differences among results for each column ($p < 0.05$), ANOVA with Tukey's multiple comparison test.

2.3.1.3. Contact angle measurements

Contact angle measurements were carried out to study the wettability of PCL:PGS (1:1, v/v) scaffold. Once a solvent drop was put on the scaffold, it was completely unstable and adsorbed in few seconds, with all the solvents employed during the analysis. Since the instability of the drop on the surface of the material, it was not possible to measure the contact angle. These observations demonstrated that the PCL:PGS (1:1, v/v) scaffold was hydrophilic. However, the high porosity of PCL:PGS (1:1, v/v) played an important role allowing the drop of the solvent to disappear among the numerous pores. This observation was in completely accordance with the work published by Sant et al. (2011).

2.3.1.4. Thickness and porosity of PPS

The thickness of scaffolds is a fundamental parameter to take under consideration before the implant of the prostheses. The thickness of electrospun scaffolds were measured using a digital caliper and resulted to be from 0.32 to 0.73 mm (Table 2.7). The increase in PCL in the solution resulted to increase the thickness of scaffold ($p < 0.05$). The sample containing PCL:PGS (1:1, v/v) resulted to have an intermediate thickness (0.46 ± 0.11 mm), thus providing a good substrate for cell proliferation. The porosity of scaffolds in tissue engineering plays a crucial factor affecting biocompatibility properties of the samples. Data reported in Table 2.7 show that the porosity of samples ranged from 68.19 ± 0.02 % for PCL:PGS (1:1, v/v) to 78.97 ± 2.96 % (PCL 15 %). These values are in agreement with the values reported in the literature for PCL electrospun sheets (Wang et al., 2009; Liu et al., 2012; Salehi et al., 2014). Pertinent literature suggests that a porosity range from 60 to 90 % can facilitate cell spreading, penetration, and proliferation.

Table 2.7: thickness and porosity of PCL and PCL:PGS blend scaffolds.

Sample	Thickness (mm)	Porosity (%)
PCL (10 %)	0.32 ± 0.11^{c}	$71.90 \pm 5.29^{a,b}$
PCL (15 %)	0.49 ± 0.16^{a}	78.97 ± 2.96^{b}
PCL (20 %)	0.68 ± 0.09^{b}	$76.26 \pm 0.77^{a,b}$
PCL:PGS (1:1)	0.46 ± 0.11^{a}	68.19 ± 0.02^{a}
PCL:PGS (2:1)	0.51 ± 0.12^{a}	$73.96 \pm 0.01^{a,b}$
PCL:PGS (3:1)	0.73 ± 0.12^{b}	$73.10 \pm 0.90^{a,b}$

Results are mean of three measurements ± SD. Different letters do refer to statistically significant differences among results for each column ($p < 0.05$), ANOVA with Tukey's multiple comparison test.

2.3.1.5. Water permeability

Showing highly porosity and highly hydrophilic properties, all the scaffold made of PGS were leaky even applying low pressure of water. This test confirmed that their porosity and their wettability were too much high to be employ like vascular graft. Working with these samples, it was not possible to calculate the permeability of the grafts.

2.3.1.6. *In vitro* degradation and fluid uptake of PPS

The biomaterial degradation is a key factor which can influence cell adhesion, proliferation, and the neoforming tissue architecture, reorganization, and integration. Degradability of biomaterials is a possible drawback in tissue engineering. It is associated to the polymer creep and weakening and should be kept in consideration. When a scaffold is used as prosthesis, slow degradation and integrity of the sample enable host body to gradually replace the implanted scaffold with native tissue over an extended period of time (Salehi et al., 2014). As can be seen from Figure 2.12 (A), weight loss was more evident in the samples of PCL:PGS blends during 28 days of incubation when compared to the only PCL samples. A notable weight loss (approximately 11 %) was noticed after the first day of soaking for PCL:PGS samples, whereas PCL samples were resulted to be more stable and very slowly degradable after the same soaking period. The addition of relatively hydrophilic PGS into the blends enhanced the water adsorption and thus faster

biodegradation. The maximum degradation was observed for the sample composed of PCL:PGS (1:1, v/v) which resulted to lost 20 % of the initial weight after 28 days of soaking. This behaviour was in agreement with those reported by other research groups working with PGS (Sant et al., 2011; Salehi et al., 2014). Kharaziha et al. (2013) explained that the degradation of PGS scaffolds at 37°C in DPBS was caused by the decomposition of ester bonds into its sebacic and glycerol monomers. In one of their experiments, Sant et al. (2011) showed only a 6 % mass loss of PCL scaffolds under accelerated degradation conditions (0.1 mM NaOH solution, at 37°C) in 7 days, compared with a 16 % of mass loss for the PCL:PGS (1:2, v/v) electrospun scaffolds. Salehi et al. (2014) attributed the fast degradation of the PCL:PGS scaffolds (15 %) after 24 h of incubation at 37°C in DPBS to the hydrolytic mechanism of materials which involves surface and bulk degradation.

The fluid uptake of biomaterials is an important factor that can influence cellular adhesion, proliferation, and growth and consequently affects their specific applications in the biological and biomedical field. The water uptake of electrospun scaffolds was assessed. The samples were kept at physiological conditions (37°C and DPBS) and water uptake was calculated after 2, 4, 7, and 24 hours. As can be seen from the Figure 2.12 B, for all samples, the percentage of fluid uptake resulted to be almost constant after 2 h of soaking up to 24 h. After 24 h of soaking, the maximum percentage of uptake was noticed for PCL 20 % (296 %) and the lowest value was observed for PCL:PGS (1:1, v/v) (166 %). PCL is known to be a hydrophobic polymer and it was expected that the addition of hydrophilic PGS could increase the water uptake of sample; however, the microstructure is another factor affecting the water uptake property of the electrospun samples. In this regard, the lowest fluid uptake of PCL:PGS samples with respect to PCL scaffolds could be attributed to their lower porosity already described in Section 2.3.1.4.

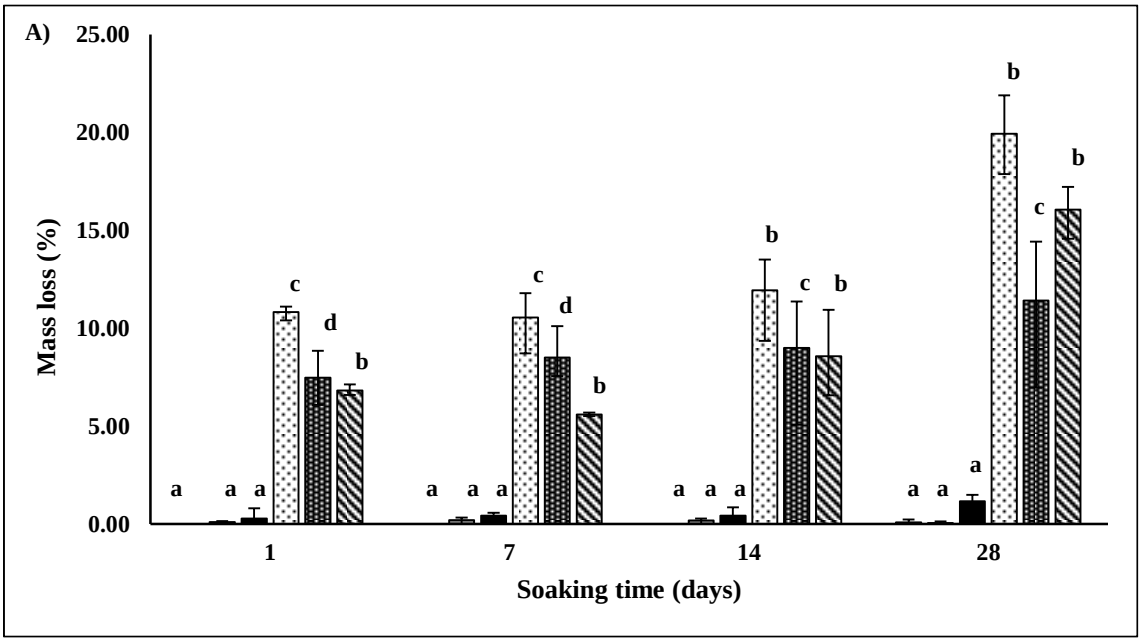

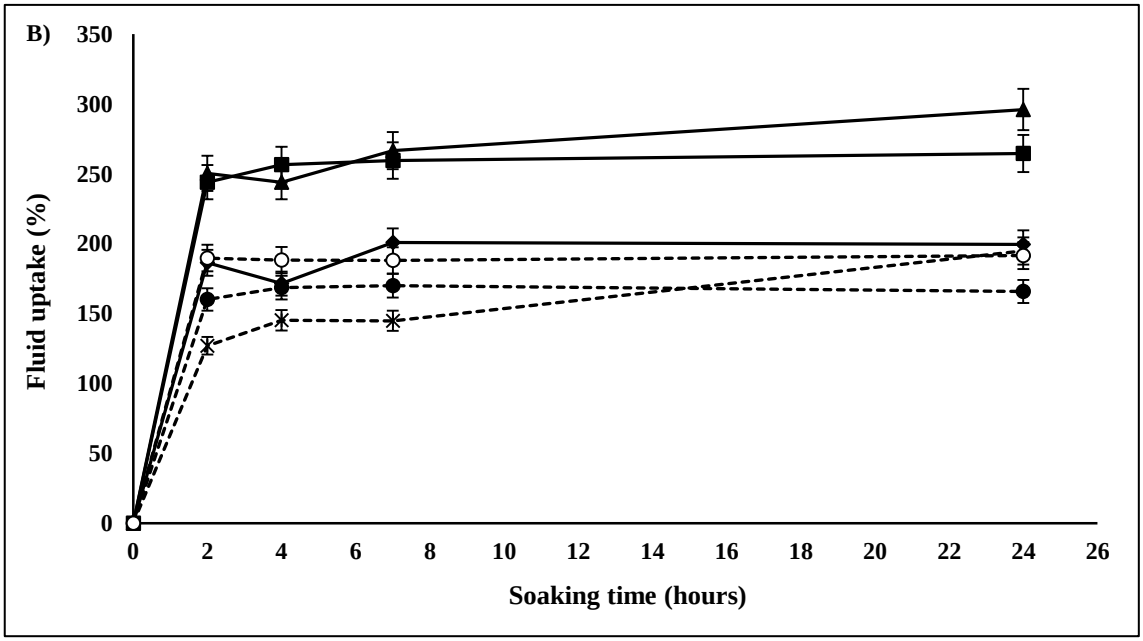

Figure 2.12: (A) mass loss and (B) fluid uptake of electrospun scaffolds with different percentage of PCL and different blend ratio of PCL:PGS. Mass loss: □ PCL (10 %), ▩ PCL (15 %), ■ PCL (20 %), ⊡ PCL:PGS (1:1), ▩ PCL:PGS (2:1), ▨ PCL:PGS (3:1). Fluid uptake: PCL (▬): ♦ PCL (10 %), ■ PCL (15 %), ▲ PCL (20 %), PCL:PGS (▬ ▬): ● PCL:PGS (1:1), * PCL:PGS (2:1); ○ PCL:PGS (3:1).

Results are mean of three measurements ± SD. Different letters do refer to statistically significant differences among results for each day ($p < 0.05$), ANOVA with Tukey's multiple comparison test.

2.3.1.7. Mechanical characterization of PPS

In vascular surgery, prostheses are tightly fixed by pins, are treated with medical glue and sutured and, once implanted, they are physiologically subject to a relative constant high pressure. Hence, it is necessary to fabricate mechanically stable bioprostheses to avoid their rupture during surgery and for all the post-surgery period. To do that, mechanical properties of the electrospun scaffolds were studied in terms of Young's modulus, tensile strength, and elongation.

Tensile strength of PCL samples increased with the percentage of PCL in the pre-polymer dispersion from 1.16 to 2.37 MPascal (Table 2.8). The corresponding increase in elongation at rupture, that for the PCL 20 %, displayed a value about seven times higher than PCL (10 %), was strictly linked with a growth of the specimen plasticity and can be explained with a change in the internal microstructure of the polymer as well as of the scaffold. Young's modulus instead seemed to reach a maximum value in the PCL (15 %) with a minimum for PCL (10 %). This trend, that surprisingly was opposite to the change of the specimen porosity (maximum in PCL 15 %) (Table 2.8) might be due to a more interconnected network of the

randomly polymer wires produced during the electrospinning, as a consequence of different values of the pre-polymer viscosity. A progressive increase in Young's modulus with the amount of PGS dispersed, from 4.25 to 7.61 MPascal, and consequently a reduction of elongation at rupture, from 453 % to 218 %, can be observed (Table 2.8). This increase in scaffolds' rigidity toward values of Young's modulus about three times higher than the one of native human artery might be considered inopportune. However, this fact is make up for an ultimate tensile strength and an elongation at rupture elevated in comparison with the human vascular tissue and therefore with higher values of their toughness. Among all samples, PCL (10 %) resulted to have Young's modulus (2.48 ± 0.19 MPascal) and tensile strength (1.16 ± 0.24 MPascal) comparable with native human artery (2.58 ± 0.34 and 1.13 ± 0.06 MPascal, respectively). However, elongation at rupture was higher when compared to native human artery. As reported by Sant et al. (2011), photocured acrylated PGS films have shown elastic modulus from 0.15 to 30 MPa with ultimate elongation up to 200 %. In other works, thermally cured PGS films resulted to have ultimate tensile strength less than 1 MPa and ultimate elongation about 200–400 % (Wang et al., 2002). The fabricated PCL:PGS (1:1, v/v) scaffolds in this study resulted to have similar elasticity but higher ultimate strength without any thermal or photo-crosslinking process. Biomimetic Young's modulus, suture retention, and tensile strength combined with high elongation at rupture make the fabricated PCL:PGS (1:1, v/v) graft promising for engineering human arteries.

The anastomotic strength is one of the physical factors concerning the conventional grafts. A method to assess this property is the measurement of suture retention strength, a parameter depending on the wire diameter, on the needle size, and on the thickness of tissue (Mine et al., 2010). In this work, for each specific type of PPS, the retention strength is to be evaluated, independently from the thickness of scaffold. For this reason, the force was normalized, by dividing the thickness of sample by the value obtained from the test, performed according the protocol ANSI/AAMI. The normalized values of suture retention strength (Table 2.8) displayed a maximum for the PCL (15 %) but with a high standard deviation. Also for the copolymer PCL:PGS, the specific strength, ranging between 5.98 and 3.84 N/mm, is comparable with the one obtained in the case of natural artery (4.09 N/mm). The value abnormally low in PCL (10 %) can be due to the excessive thinness of the sample and to its different microstructures.

Table 2.8: mechanical properties of PCL and PCL:PGS blend scaffold.

Sample	Young's modulus (MPa)	Tensile strength (MPa)	Elongation (%)	Normalized suture retention (grams-force/mm)
PCL (10 %)	2.48 ± 0.19^{b}	1.16 ± 0.24^{a}	84.16 ± 7.95^{b}	0.42 ± 0.18^{a}
PCL (15 %)	4.25 ± 0.22^{a}	1.84 ± 0.75^{a}	282.76 ± 127.72^{a}	6.80 ± 4.17^{a}
PCL (20 %)	$3.87 \pm 0.36^{a,c}$	$2.37 \pm 0.60^{a,b}$	643.30 ± 30.68^{d}	5.75 ± 2.31^{a}
PCL:PGS (3:1)	4.25 ± 0.21^{a}	1.78 ± 0.31^{a}	453.11 ± 19.38^{c}	4.94 ± 1.20^{a}
PCL:PGS (2:1)	5.39 ± 0.84^{d}	$1.89 \pm 0.45^{a,b}$	242.83 ± 39.38^{a}	5.98 ± 2.45^{a}
PCL:PGS (1:1)	7.61 ± 0.92^{e}	3.14 ± 1.47^{b}	218.48 ± 27.72^{a}	3.84 ± 2.72^{a}
Native human artery	$2.58 \pm 0.34^{b,c}$	1.13 ± 0.06^{a}	46.54 ± 11.32^{b}	4.09 ± 2.12^{a}

Results are mean of three measurements ± SD. Different letters do refer to statistically significant differences among results for each column ($p < 0.05$), ANOVA with Tukey's multiple comparison test.

2.3.1.8. Biocompatibility of PPS

To demonstrate the absence of cytotoxicity effects on human endothelial cells EA. hy 926, they were put in contact for 24, 72, and 96 hours with PPS. Cell proliferation in presence of the scaffold was evaluated trough the MTS assay. Working with pure PCL, it was noticeable that the proliferation during the first 24 hours was higher in comparison with those scaffold containing both PCL and PGS. Among PCL:PGS scaffolds, by increasing the amount of PCL in the scaffold, there was an increase in cellular growth after 24 hours, in a ratio dependent manner. After 72 and 96 hours of contact with PCL scaffold (15 and 20 %), endothelial cells significantly reduced their metabolic activity (Figure 2.13 A). This cellular behaviour found an explanation in the fact that PCL is a hydrophobic material and probably it made difficult the diffusion of nutrients and metabolites between the attached cells and the medium. On the contrary, the presence of the hydrophilic PGS allow cells to grow even after 3 and 4 days after their seeding. These data are completely consistent with those presented by Sant et al. (2013). To confirm once more the biocompatibility of PGS in the scaffold, the electropsun grafts with the highest percentage of PGS (PCL:PGS, 1:1) were tested alone using the same cells reported above but performing the experiments with a Trans-well system over a longer period (7 days) (Figure 2.13 B). In fact, recent studies have reported that electrospun PCL:PGS constructs promote cell adhesion and proliferation compared to PCL scaffolds (Sant et al., 2011), because of their enhanced hydrophilicity in comparison to hydrophobic PCL. For this reason, biological test with only PCL:PGS scaffolds was decided to perform. The viability of EA. hy 926 on days

1, 2, 3, and 7 is shown in Figure 2.13 (B). Cell proliferation, evaluated through the mitochondrial metabolic activity, indicated that cells grown in the presence of electrospun scaffolds with no significant differences when compared with cells grown on a tissue culture plate as a negative control. The increasing absorbance values during the culture period demonstrated that proliferation can occur in the presence of the studied scaffolds without any cytotoxic event. The results suggest that PCL:PGS (1:1, v/v) blends can promote cell growth and thus may be used for bioengineering vascular prosthesis.

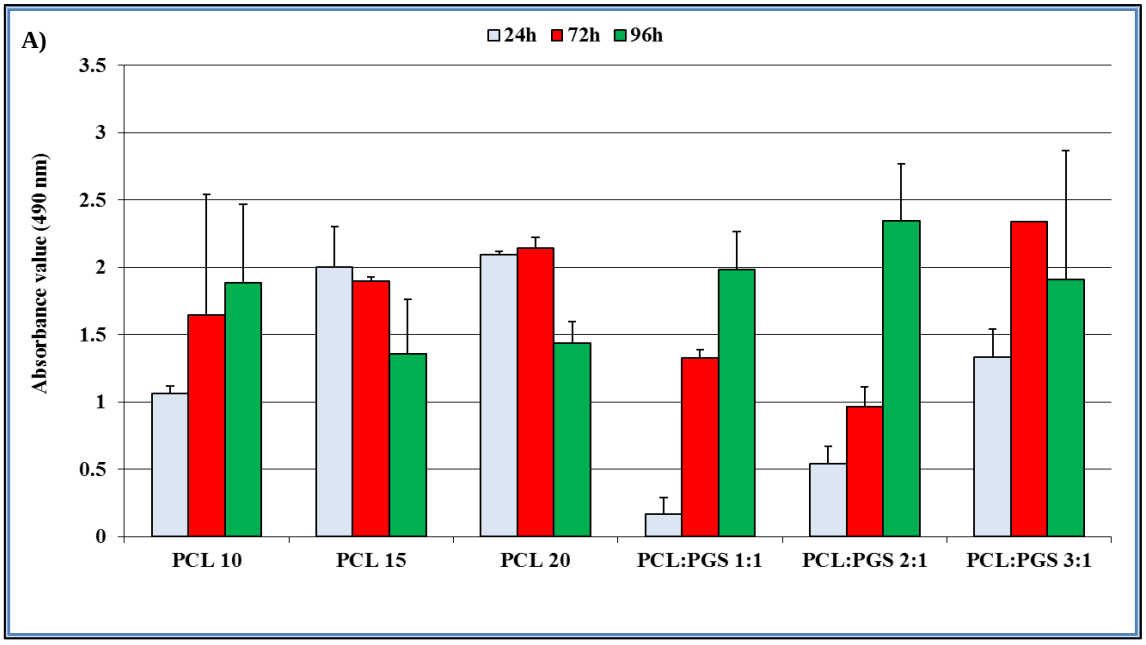

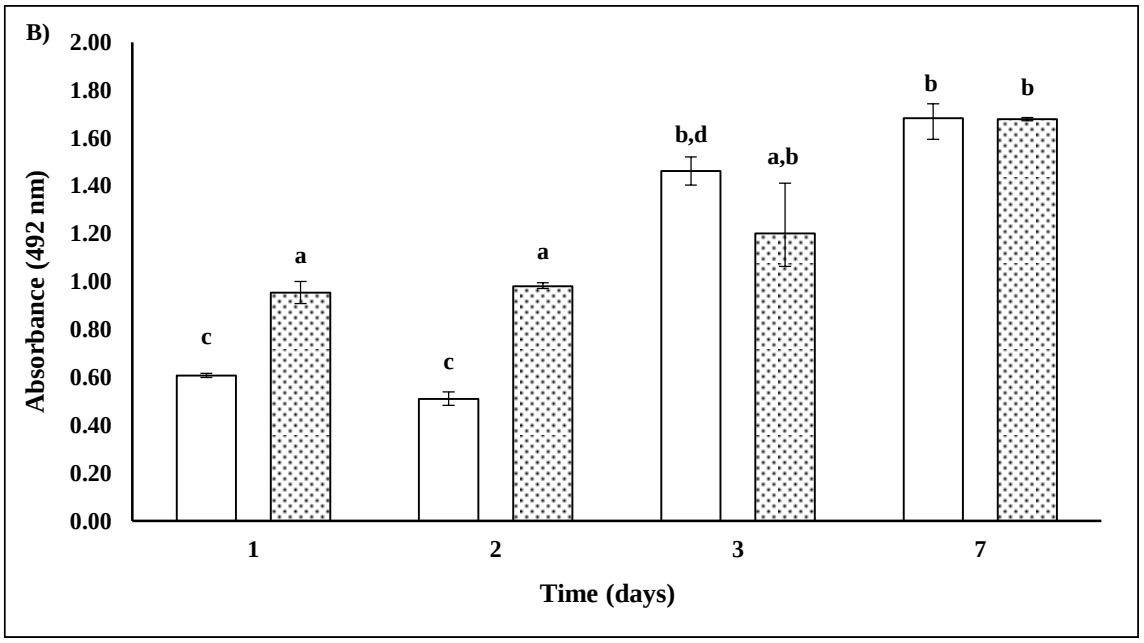

Figure 2.13: cell viability of all the electrospun (A) PPS and (B) PCL:PGS (1:1) scaffold by MTS assay.

☐ control, ⚄ PCL:PGS (1:1).

Results are mean of three measurements ± SD. Different letters do refer to statistically significant differences among results ($p < 0.05$), ANOVA with Tukey's multiple comparison test.

2.3.1.9. Hemocompatibility of PPS

When blood contacts solid material surface, many physiological reactions such as thrombus formation and red blood cells disruption can occur. Therefore, hemocompatibility represents one of the most important parameters to take into account working with vascular prostheses (Elahi et al., 2014). In this work, the hemocompatibility of electrospun scaffolds was evaluated by hemolysis and kinetic clotting time method. The blood clotting behavior in the presence of scaffolds is shown in Figure 2.14 (A). The aim of *in vitro* dynamic clotting time test is to measure the clotting time influenced by the presence of materials. The absorbance of free hemoglobin in the solution varies with time; the higher the absorbance, the better the antithrombotic properties. Figure 2.14 A shows that blood incubated with PCL and PCL:PGS blends had a significantly higher absorbance than glass almost at each fixed time point. Glass ws used as a reference thrombogenic material (Motlagh et al., 2006). PCL:PGS (1:1, v/v) samples showed the best anticoagulant properties with an absorbance of 0.533 after 30 minutes. Furthermore, it may be seen that, after 5 minutes, scaffolds made only by PCL are less efficient in comparison to those made by PCL and PGS together.

Hemolysis percentage is a parameter to express quantitatively the breakage of erythrocytes after the contact with materials. Figure 2.14 (B) shows that with the increasing PCL content in PCL:PGS blend, the hemolysis percentage decreased, probably because the surface roughness depends on the presence of PGS. Nevertheless, the data suggest that PCL at different percentages and PCL:PGS blend scaffold were highly

compatible with human blood. In fact, for each kind of sample, the hemolysis percentage resulted < 5, with no significant differences between them.

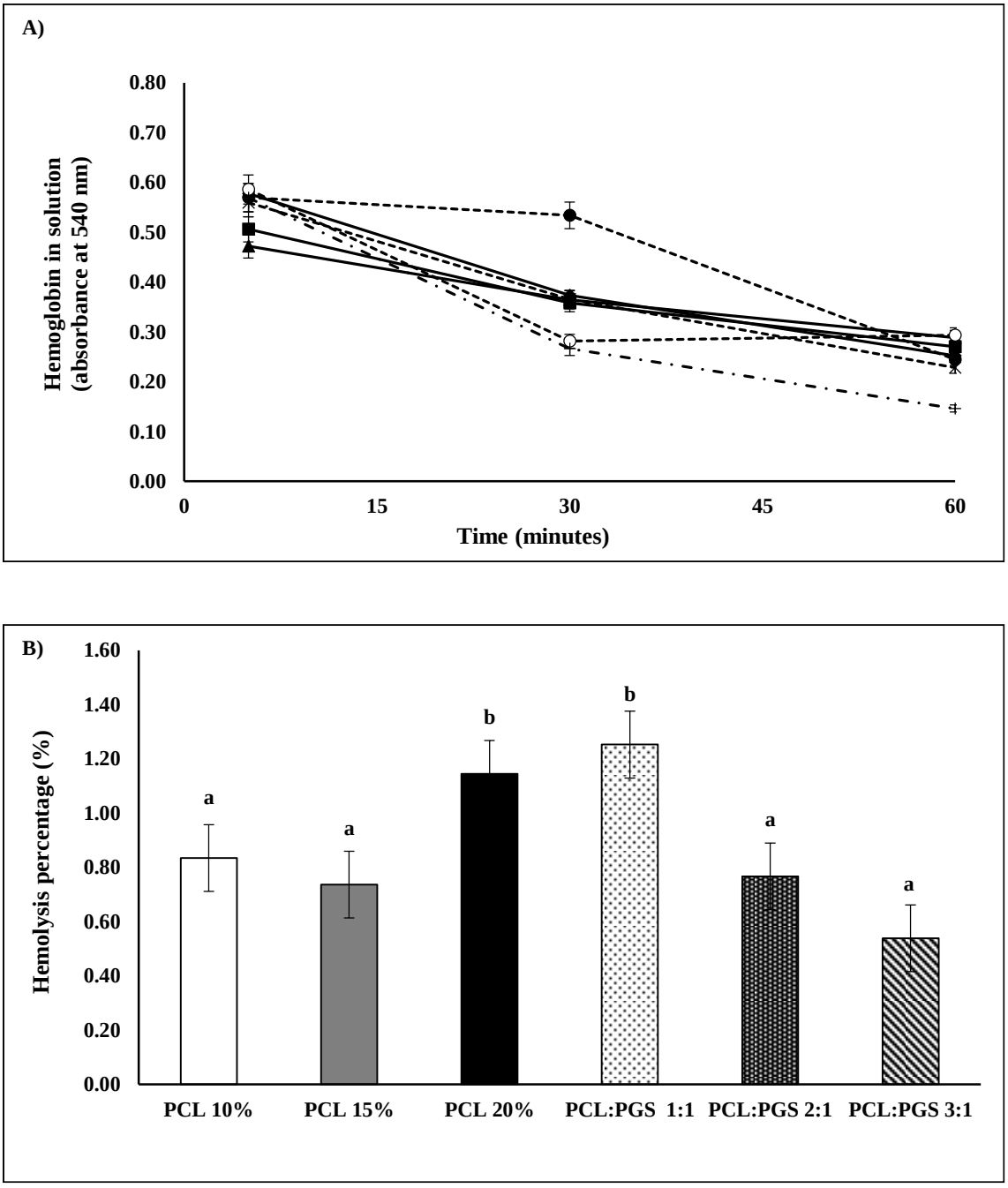

Figure 2.14: hemocompatibility of electrospun scaffolds with different percentage of PCL and different blend ratio of PCL:PGS. (A) Kinetics of clotting time and (B) hemolysis percentage. Clotting time: PCL (▬): ♦ PCL (10 %), ■ PCL (15 %), ▲ PCL (20 %), PCL:PGS (▬ ▬): ● PCL:PGS (1:1), * PCL:PGS (2:1); ○ PCL:PGS (3:1), (▬ ▪) + glass.

Results are mean of three measurements ± SD. Different letters do refer to statistically significant differences among results ($p < 0.05$), ANOVA with Tukey's multiple comparison test.

2.3.1.10. Conclusion

In this study regarding PPS, electrospun small-diameter (2 mm) tubular grafts were successfully fabricated as a suitable replacement for small diameter vessels. Degradable and porous grafts generated from 20 % (w/v) of PCL and PGS solution, mixed together in the ratio 1:1(v/v), offered good biomimetic mechanical properties and comparable suture retention with the native human artery. Fabricated tubular scaffolds of PCL:PGS 1:1 (v/v) were nontoxic to human vascular endothelial cell line EA. hy 926 and they showed good anticoagulation property with a low hemolysis percentage. Taking together all these data, we were able to select among all PCL and PGS-based material, PCL:PGS (1:1, v/v) as a good candidate for vascular tissue engineering. For this reason, only PCL:PGS (1:1) blend was functionalized with bioactive compounds.

This work was partially published as: "Tailored electropsun small diameter graft for vascular prosthesis", International Journal of Polymeric Biomaterials 66, (2017) 635-643, by **Ferrari P.F.**, Aliakbarian B., Lagazzo A., Tamayol A., Palombo D., Perego P.", partially presented as "Effect of electrospinning parameters on mechanical properties of engineered small diameter vascular grafts" at the 64th international Congress of the European Society of Cardiovascular and Endovascular Surgery (ESCVS) 2015, Istanbul, Turkey, by Aliakbarian B., **Ferrari P.F.**, Perego P., Palombo D, and published in The Journal of Cardiovascular Surgery, abstract book, Vol. 56 – Suppl. 1 to n° 2, 94.

2.3.2. Gelatin coated polymeric scaffold (GCS)

The vessel prosthesis show often a suitable porosity to allow the metabolic exchanges of the cells during the building of the regenerated tissue. However, after the implantation of porous prosthesis, these pores commonly could generate high blood loss. As a result, it is mandatory to seal the pores with a biocompatible and adsorbable filling agent (Fleckenstein & Werner, 1988). In this thesis, in order to reduce the porosity, the water permeability, and to increase the biocompatibility, PCL:PGS (1:1, v/v) scaffolds were coated with gelatin. We chose gelatin as coating agent because of its extremely well-known physicochemical properties, its commercial availability at low cost, its high biocompatibility and its low antigenicity (Zhang et al., 2005; Pulieri et al., 2007).

2.3.2.1. Scanning Electron Microscopy (SEM) analysis of GCS

In PCL:PGS (1:1, v/v) and GCS scaffolds, fibers appeared randomly distributed and they were bead-free (Figure 2.15). The presence of gelatin (Figure 2.15, A and B) did not affect the structure of the electrospun scaffolds in comparison with uncoated PCL:PGS (1:1, v/v) (Figure 2.15, C and D). Both the inner and the outer surfaces of GCS exhibited microfibers, without any differences between GCS and control. The coating with gelatin did not interfere with the diameter of fibers ($p < 0.05$) (Table 2.9).

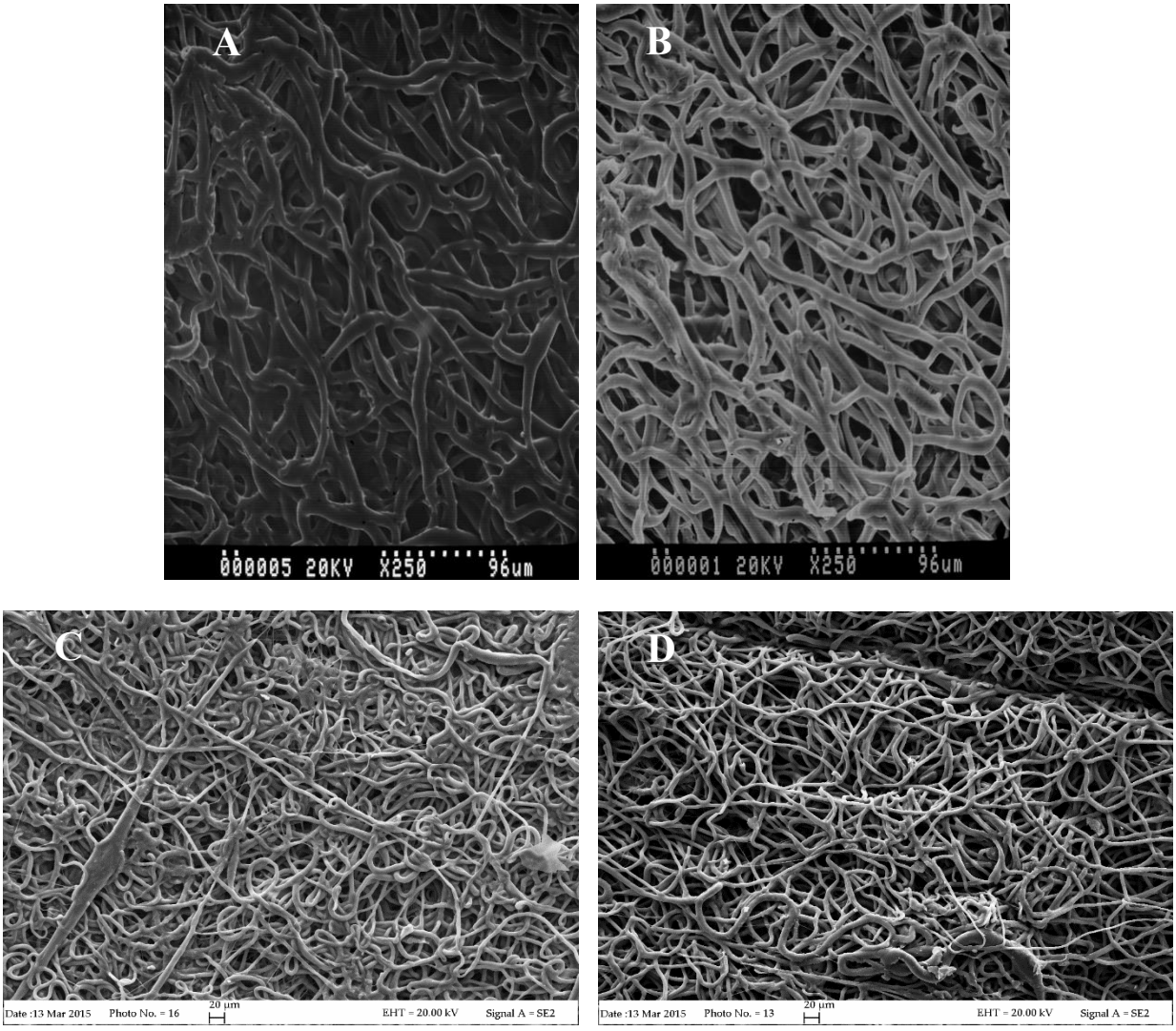

Figure 2.15: representative SEM micrographs of gelatin coated (A) internal and (B) external scaffold surfaces and of (C) internal and (D) external surfaces of PCL:PGS (1:1) without coating.

Table 2.9: fiber diameters of GCS and PCL:PGS (1:1).

Sample	Fiber diameter (µm)
GCS	5.50 ± 1.34[a]
PCL:PGS (1:1)	5.29 ± 1.31[a]

Results are mean of at least one hundred measurements ± SD. Different letters do refer to statistically significant differences among results ($p < 0.05$), ANOVA with Tukey's multiple comparison test.

2.3.2.2. Thickness and porosity of GCS

The thickness of GCS and PCL:PGS (1:1, v/v) was measured and resulted to be 0.46 ± 0.11 and 0.43 ± 0.11 mm, respectively (Table 2.10). Data suggested that surface modification did not increase scaffold thickness and therefore the gelatin layer can be considered at a sub-millimeter level. In general, porosity of biomaterials plays a pivotal role due to its influence to favour cellular colonization and growth on the prosthesis. Porosity is defined as the measure of the open pore volume, known as the void fraction (Lawrence & Madihally, 2008). In the case of GCS, porosity was significantly lower (43.49 ± 10.85 %) in respect of PCL:PGS (1:1, v/v) (68.19 ± 0.02 %) (Table 2.10). This fact can be attributed to the formation of a uniform layer during gelatin coating that is able to occlude the pores of the scaffolds.

Table 2.10: thickness and porosity of GCS and PCL:PGS (1:1).

Sample	Thickness (mm)	Porosity (%)
GCS	0.43 ± 0.11^{a}	43.49 ± 10.85^{b}
PCL:PGS (1:1)	0.46 ± 0.11^{a}	68.19 ± 0.02^{a}

Results are mean of three measurements ± SD. Different letters do refer to statistically significant differences among results for each column ($p < 0.05$), ANOVA with Tukey's multiple comparison test.

2.3.2.3. Water permeability of GCS

Water permeability was greatly decreased by gelatin surface modification. In fact, in the case of PCL:PGS (1:1, v/v), first water drops were already registered at 0.2 atm, while working with GCS there was not water leakage until 0.7 atm was reached.

2.3.2.4. *In vitro* degradation, fluid uptake and release of gelatin from GCS

Degradation rate of biomaterials is a key factor that has to be considered once studying tissue architecture reorganization and integration. In fact, during a fast degradation, scaffolds do not represent a good substrate for cell attachment and growth while, during a slow degradation, biomaterials go under a process of calcification and hardening, losing their mechanical properties. As can be seen from Figure 2.16 (A), mass loss was more evident with GCS. In fact, during the first period of degradation, also gelatin is released from the scaffolds, lowering their weights. Mass loss, in this case, is the sum of two different processes,

degradation of the polymers and release of gelatin. However, the degradation profile was very similar between GCS and the PCL:PGS (1:1, v/v).

In addition, it was studied if the degradation of the polymeric scaffold was accelerated in presence of gelatin or not using equation 2.5, presented in Section 2.2.4.8. In particular, we focused our attention only on the 24 hours of releasing of gelatin and degradation of the polymers. Our aim was to understand if the releasing of gelatin had an effect on the degradation rate of the polymeric scaffolds. To do that, we performed releasing and degradation experiments starting from the same samples. After 24 hours, it was noticed that the degradation rate of the coated polymer was remarkably higher in the case of GCS (Table 2.11). Probably, the release of gelatin, that was physically deposed onto the surface of the scaffold, caused an instability of the polymers with a subsequent co-release of the components of the scaffold.

Figure 2.16 (B) shows the fluid uptake profile of the studied materials during 24 hours. The presence of gelatin induced an increase of fluid uptake during the first hours. GCS presented a peak of fluid uptake after 2 hours (248 %) and after 24 hours this parameter decreased (144 %) as a consequence of a concomitant gelatin release. As shown in Figure 2.17, the majority of gelatin (58.96 %) was released within the 8 hours and the total amount of released gelatin was 70.64 % after 72 hours. In conclusion, the release of gelatin from the scaffolds is responsible of the different behaviour between GCS and PCL:PGS (1:1, v/v) in degradation rate and fluid uptake profiles.

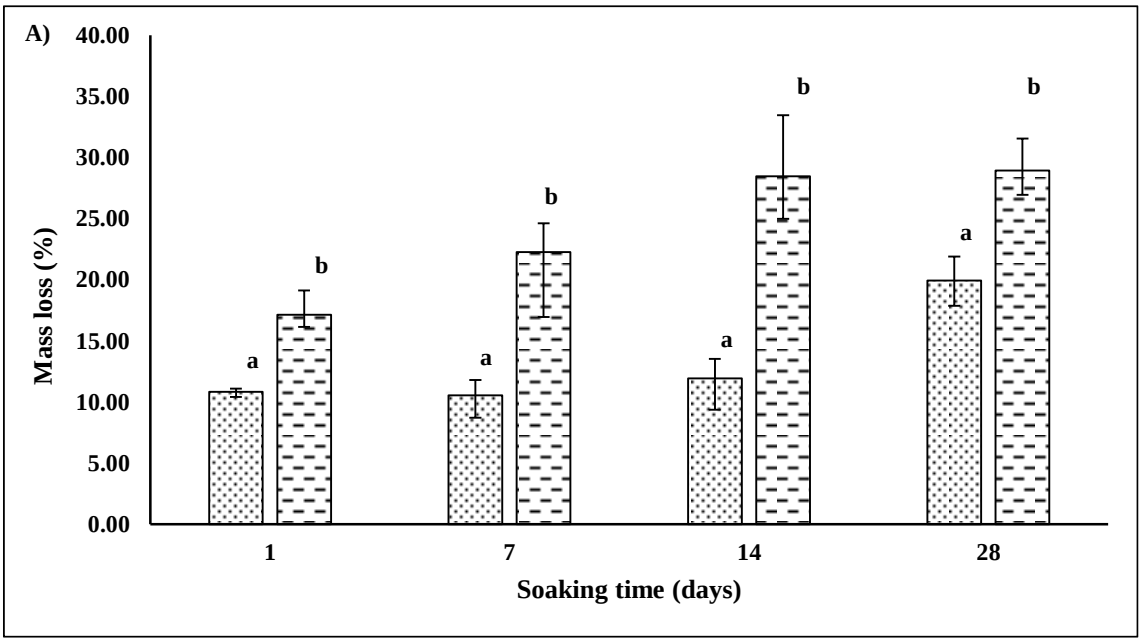

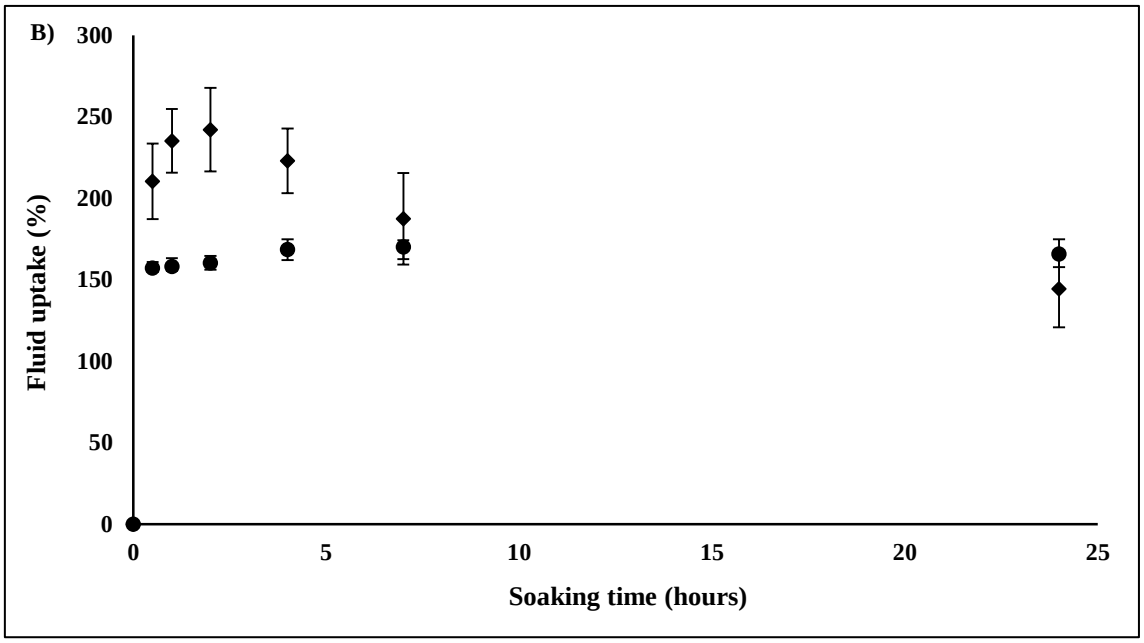

Figure 2.16: (A) mass loss (B) and fluid uptake of PCL:PGS (1:1) and GCS. Mass loss: ⚄ PCL:PGS (1:1). ⚀ GCS. Fluid uptake: (♦) GCS, (●) PCL:PGS (1:1).

Results are mean of three measurements ± SD. Different letters do refer to statistically significant differences among results for each day ($p < 0.05$), ANOVA with Tukey's multiple comparison test.

Table 2.11: degradation of the polymer in presence of gelatin or not after 24 hours.

Sample	Degradation (%)
GCS	26.13 ± 4.12^{a}
PCL:PGS (1:1)	10.82 ± 0.37^{b}

Results are mean of three measurements ± SD. Different letters do refer to statistically significant differences among results ($p < 0.05$), ANOVA with Tukey's multiple comparison test.

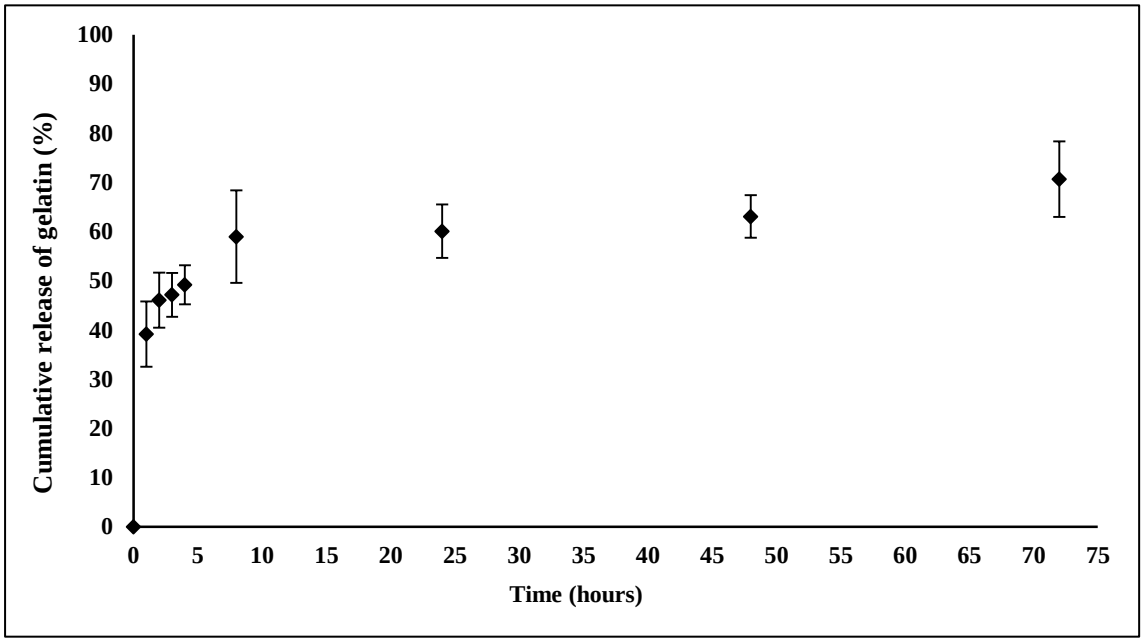

Figure 2.17: cumulative release of gelatin from GCS.

2.3.2.5. Mechanical properties of GCS

With the aim of comparing mechanical properties between PCL:PGS (1:1, v/v) and GCS, Young's modulus, tensile strength and elongation were calculated (Table 2.12). Dry GCS showed a very different behaviour under a mechanical point of view in comparison with all the other samples. Considering Young's modulus, statistically significant differences ($p < 0.05$) were reported only in the case of dry GCS that presented a modulus approximately nine times higher in respect with PCL:PGS (1:1, v/v). In complete accordance with Meng et al., (2010), the presence of gelatin decreased the mechanical properties of PCL:PGS (1:1,v/v) scaffold. This hardening property was overcome by immersing GCS in a NaCl solution (0.9 %, w/v) for 5 minutes. After that, surprisingly, all the tested samples showed a comparable tensile strength without any relevant differences ($p < 0.05$). The hardening of the polymeric samples caused by the surface modification with gelatin was responsible of low values in elongation. Following vascular surgery procedures, even in this case, GCS and PCL:PGS (1:1) scaffolds were immersed in a NaCl solution (0.9 %) and their mechanical responses were investigated. Wet samples were considered nearer than dry samples to the final application of the prostheses, and therefore, taken together, all these data suggested that the coating of PCL:PGS scaffolds with gelatin did not modify the mechanical properties of control (uncoated samples).

Table 2.12: mechanical properties of GCS and PCL:PGS (1:1).

Sample	Young's modulus (MPa)	Tensile strength (MPa)	Elongation (%)
GCS (dry)	62.02 ± 8.81^{b}	4.00 ± 1.21^{a}	12.79 ± 4.44^{b}
PCL: PGS (1:1) (dry)	6.21 ± 2.13^{a}	2.33 ± 0.75^{a}	482.34 ± 193.44^{a}
GCS (wet)	8.63 ± 2.02^{a}	3.27 ± 1.44^{a}	327.56 ± 74.36^{a}
PCL:PGS (1:1) (wet)	8.05 ± 0.86^{a}	2.89 ± 0.81^{a}	516.66 ± 63.13^{a}

Results are mean of three measurements ± SD. Different letters do refer to statistically significant differences among results for each column ($p < 0.05$), ANOVA with Tukey's multiple comparison test.

2.3.2.6. Biocompatibility of GCS

Different studies have suggested that gelatin is able to enhance biocompatibility of biomaterials promoting cell adhesion and proliferation (Ghasemi-Mobarakeh et al., 2008). In our case, only the external surface of the scaffold was coated with gelatin with the aim of reducing water permeability. In order to study whether our scaffolds were responsible to release toxic molecules, they were put in Transwell-clear multiwell inserts and the EA. hy 926 cell viability after 1, 2, 3 and 7 days was monitored through MTS assay. The results, expressed as percentage values with respect to the control, are shown in Figure 2.18. After 1 and 2 days, a significant increase in cell viability was noticed. No statistically significant differences ($p < 0.05$) were observed between the cells grown on a tissue culture plate as control and the cells grown in presence of GCS and PCL:PGS (1:1) after one week.

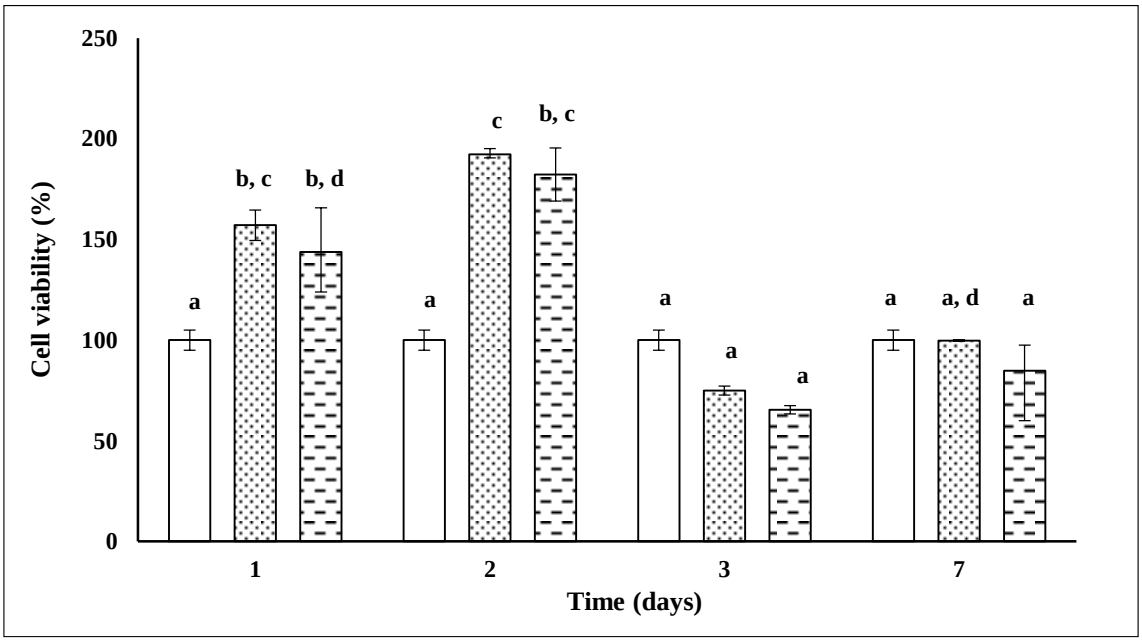

Figure 2.18: cell viability of PCL:PGS (1:1) and GCS by MTS assay. ☐ control, ⚄ PCL:PGS (1:1), and ⚄ GCS.

Results are mean of three measurements ± SD. Different letters do refer to statistically significant differences among results ($p < 0.05$), ANOVA with Tukey's multiple comparison test.

2.3.2.7. Hemocompatibility of GCS

Hemocompatibility of electrospun scaffolds was evaluated registering the absence of material-derived erythrocytes disruption. Figure 2.19 shows that working with GCS it was dramatically diminished the hemolysis percentage, probably because of the gelatin coating, reducing the porosity of the scaffolds, caused a decrease of the roughness of PCL:PGS scaffolds. Considering that, for both GCS and PCL:PGS (1:1, v/v) this parameter was always < 5 % and we can conclude that they were highly hemocompatible (Sternberg et al; 2015). Studying hemolysis, the biodegradable electrospun scaffolds were compared to the current commercial prostheses, poly (ethylene terephthalate) and expanded poly (tetrafluoroethylene).

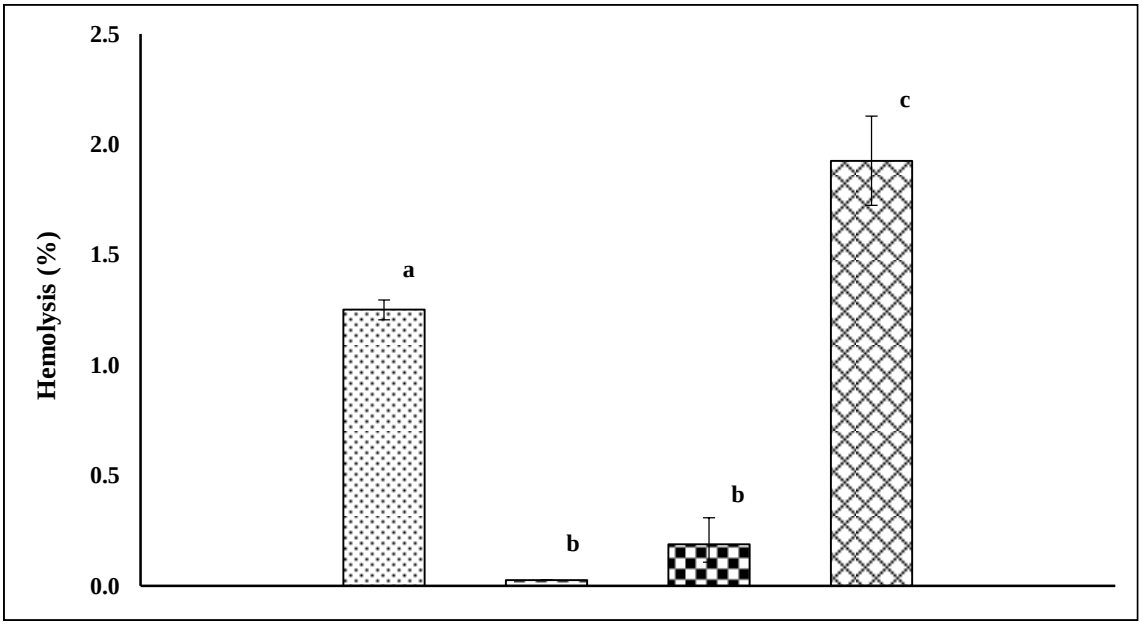

Figure 2.19: hemolysis of PCL:PGS (1:1), GCS, poly (ethylene terephthalate) and expanded poly (tetrafluoroethylene). ⚄ PCL:PGS (1:1), ⚄ GCS, ⚄ poly (ethylene terephthalate), and ⚄ expanded poly (tetrafluoroethylene).

Results are mean of three measurements ± SD. Different letters do refer to statistically significant differences among results ($p < 0.05$), ANOVA with Tukey's multiple comparison test.

2.3.2.8. *In vivo* suturability test with GCS

Once evaluated the impermeability of GCS through the water permeability test, a feasibility study to confirm the in vivo suturability of the scaffolds was assessed. GCS (2 mm in diameter) were implanted in two White Star rats with the aim of replacing the native aorta (Figure 2.20). Baseline structural integrity and host responses were evaluated. No evidence of trans-graft leakage of blood was demonstrated when the GCS were implanted in rats. No bleeding occurred throughout the entire duration of the surgery.

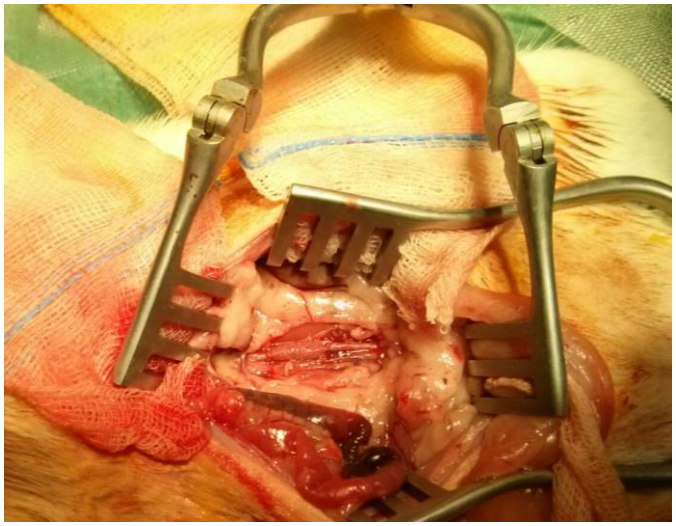

Figure 2.20: implantation of GCS in White Star rat.

2.3.2.9. Conclusions

During this research, small diameter tubular grafts as vascular prostheses by electrospinning were fabricated. Fibrous, degradable, porous, bio- and hemocompatible scaffolds of PCL:PGS (1:1, v/v) showed good mechanical properties. Oppositely, these scaffolds exhibited an excessive water permeability even at low pressure. In order to overcome this drawback, scaffolds were coated with gelatin. The coating made of gelatin influenced the degradation rate of the studied polymers, but it didn't alter their fluid uptake properties. Furthermore, the surface modification with gelatin did not alter thickness, fiber diameters, mechanical properties, when they were wet, biocompatibility, and hemocompatibility of PCL:PGS scaffolds. The coating with gelatin was responsible of the water impermeability of the scaffolds Taking together all these data, GCS could be used to be surgically implanted in animal model as arterial graft.

This work was partially published as: "Small diameter vascular grafts coated with gelatin". Chemical Engineering Transactions 57, 2017 by **Ferrari P.F.**, Aliakbarian B., Palombo D., Perego P., partially presented as: "Functionalizing small diameter vascular grafts with gelatin" at the 65th international Congress of the European Society of Cardiovascular and Endovascular Surgery (ESCVS) 2016, Belgrade, Serbia, by Aliakbarian B., **Ferrari P.F.**, Perego P., Palombo D, and published in The Journal of Cardiovascular Surgery, abstract book, Vol. 57 – Suppl. 2 to n° 2, 73.

2.3.3. Quercetin-fuctionalized scaffolds (QS) and Quercetin-functionalized and gelatin coated scaffolds (QGCS)

Herein the effect of incorporating free quercetin on the properties of the scaffolds is investigated. Quercetin (Q) is a naturally occurring polyphenolic flavonol present in several food and beverages (e.g. onions, broccoli, apples, tea, and red wine). It shows different beneficial activity on the body, being an antioxidant and a free-radical scavenger (Harborne & Baxter, 1999; Gomathi, et al., 2003). It protects against cardiovascular pathologies (Tribolo et al., 2008), inflammation (Boots et al., 2008), and tumorigenesis (Murakami et al., 2008). After implantation, scaffolds could induce immunological reactions in response to injury due to the presence of a foreign material in the body, leading to acute inflammation (Lee et al., 2012). In this part of the research, PCL:PGS (1:1, v/v) scaffolds were functionalized with quercetin to evaluate its effects on inflammatory response. On the basis of the previous study concerning gelatin coating, even in this case, after functionalization with quercetin, scaffolds were coated with gelatin.

2.3.3.1. Scanning Electron Microscopy (SEM) analysis of QS and QGCS

In tissue engineering it is necessary characterized the scaffold matrix in terms of the microscale thickness of the single fibers. When a biomaterial is made only by of a bed of fibers, the fiber stickness is done from the diameter of an individual fiber (Lawrence & Madihally, 2008). As a result of this, representative SEM images of internal and external scaffold surface of QS, QGCS, and PCL:PGS (1:1, v/v) were collected (Figure 2.21). These images were useful for evaluating the microarchitecture of the functionalized scaffold. The presence of free quercetin in the spinning solution did not interfere with the fiber formation process during electrospinning. Morphologically, scaffolds consisted of fibers with a random orientation and disposure. In any case, fibers, both for the internal and the external surface, can be considered as microfibers. Their diameter ranged is for each kind of graft around 5 μm (Table 2.13). Typical microstructure of PCL:PGS (1:1, v/v) functionalized with quercetin matched well with the morphological properties for pure PCL:PGS (1:1, v/v), described in Section 2.3.1.2. The presence of few fused fibers in the internal surface of the scaffold (QS and PCL:PGS (1:1)) was a consequence of using mineral oil on the aluminium collector with the aim of easily extruding the construct after the electrospinning process. As a result, there was no significant differences ($p < 0.05$) between QS and PCL:PGS (1:1, v/v), both for the internal and external surface. Similarly, the gelatin coating step did not alter the fiber diameter. Considering QGCS, fibers appeared sticky for the presence of the gelatin and more undefined in comparison with QS and PCL:PGS (1:1, v/v).

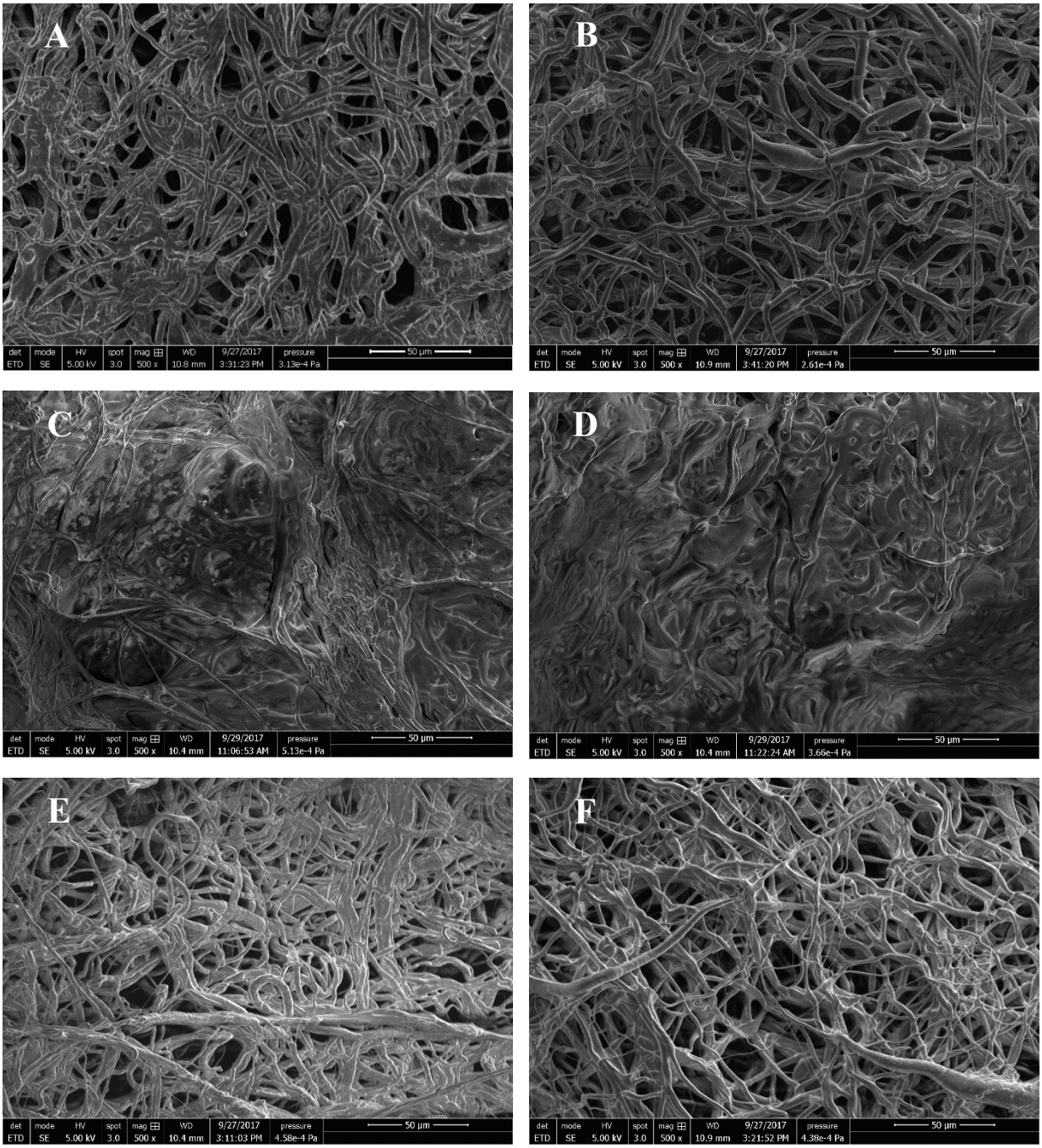

Figure 2.21: representative SEM micrographs of (A) internal and (B) external surfaces of QS, of (C) internal and (D) external surfaces of QGCS, and of (E) internal and (F) external surfaces of PCL:PGS (1:1).

Table 2.13: fiber diameter of QS, QGCS, and PCL:PGS (1:1).

Sample	Diameter (µm)
QS	4.12 ± 1.06[a]
QGCS	3.96 ± 0.47[a]
PCL:PGS (1:1)	4.01 ± 0.92[a]

Results are mean of at least one hundred measurements ± SD. Different letters do refer to statistically significant differences among results ($p < 0.05$), ANOVA with Tukey's multiple comparison test.

2.3.3.2. Atomic Force Microscopy (AFM) analysis of QS

SEM analysis represents a good technique to characterize the microstructure of fibers but it is not useful to evaluate the roughness of the scaffold surface (Kim et al., 2009). Therefore, to further characterize the scaffold surfaces, AFM analysis were carried out using QS and PCL:PGS (1:1, v/v) as control. The structures of the electrospun fibers was imaged, mapping variations in surface properties. Adhesive interactions are shown as darker regions whereas repulsive interactions are shown as brighter regions in the collected images. Figure 2.22 shows representative images of the surfaces of scaffolds obtained by AFM.

A

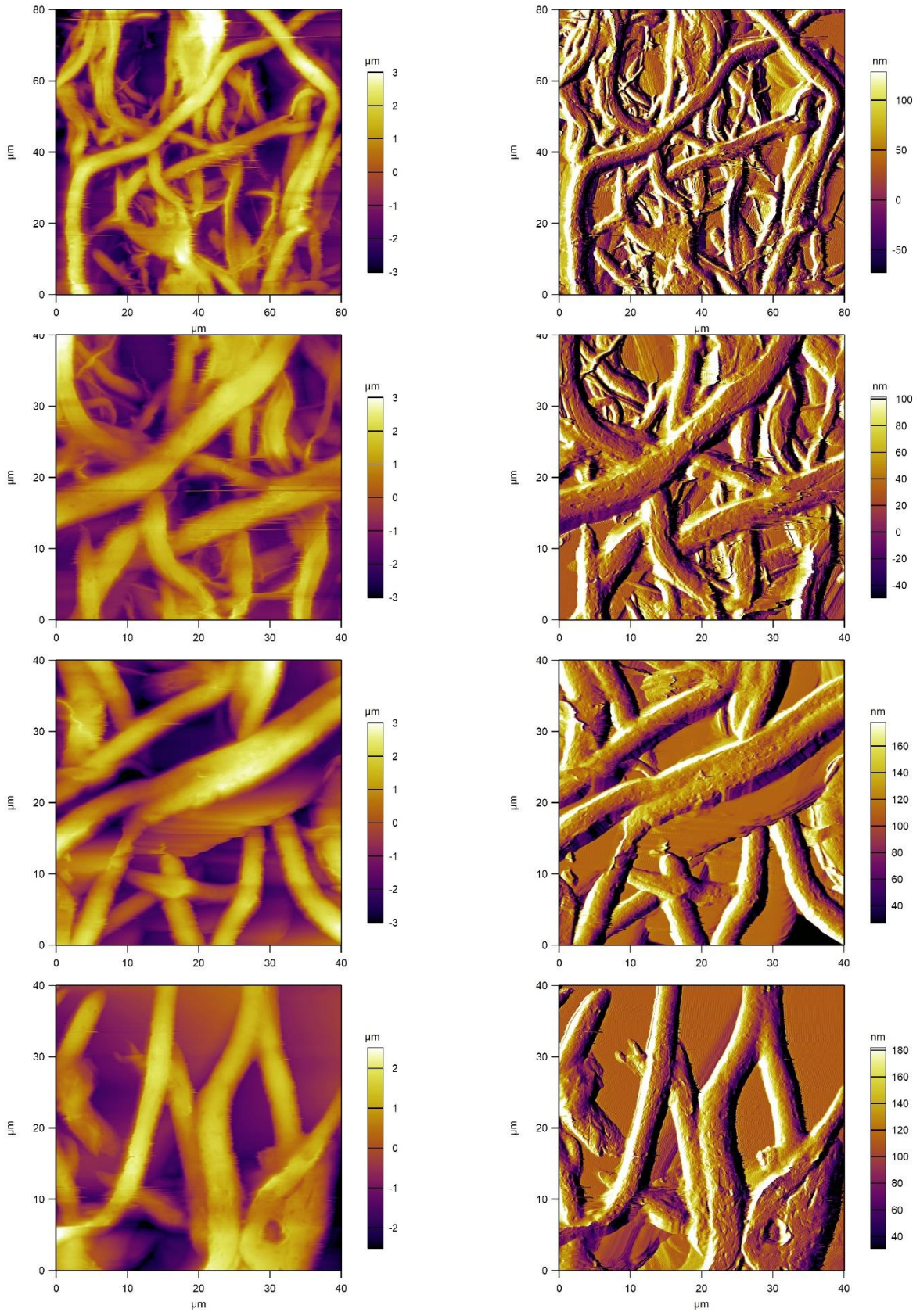

B

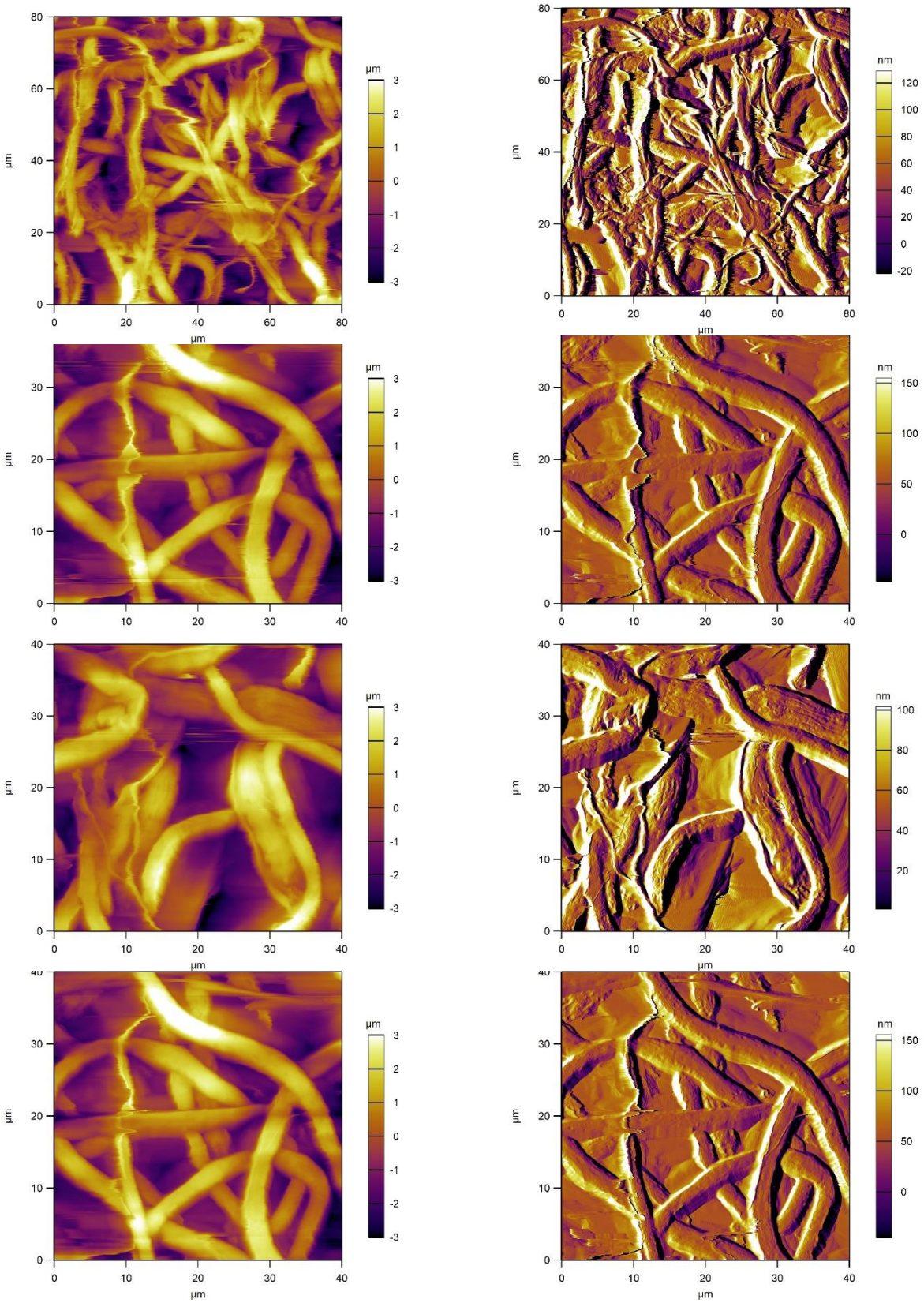

Figure 2.22: AFM height (left) and deflection (right) images of (A) QS and (B) PCL:PGS (1:1) external surfaces.

A

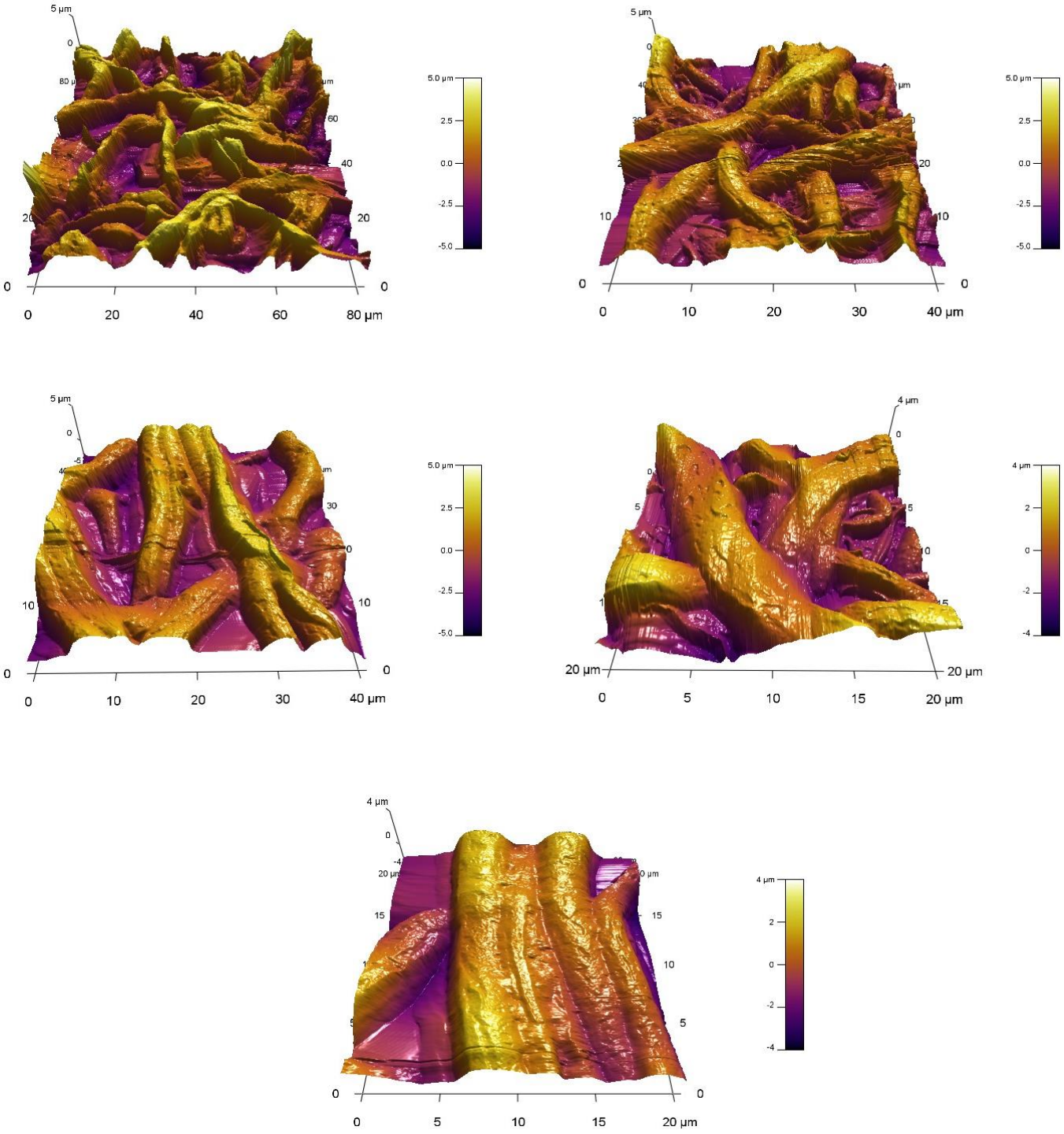
5 µm
0
80 µm
60
40
20
0
0 20 40 60 80 µm
5.0 µm
2.5
0.0
-2.5
-5.0
5 µm
0
40 µm
30
20
10
0
0 10 20 30 40 µm
5.0 µm
2.5
0.0
-2.5
-5.0
5 µm
0
40 µm
30
10
0
0 10 20 30 40 µm
5.0 µm
2.5
0.0
-2.5
-5.0
4 µm
0
20 µm
15
10
5
0
0 5 10 15 20 µm
4 µm
2
0
-2
-4
4 µm
0
20 µm
15
10
5
0
0 5 10 15 20 µm
4 µm
2
0
-2
-4

B

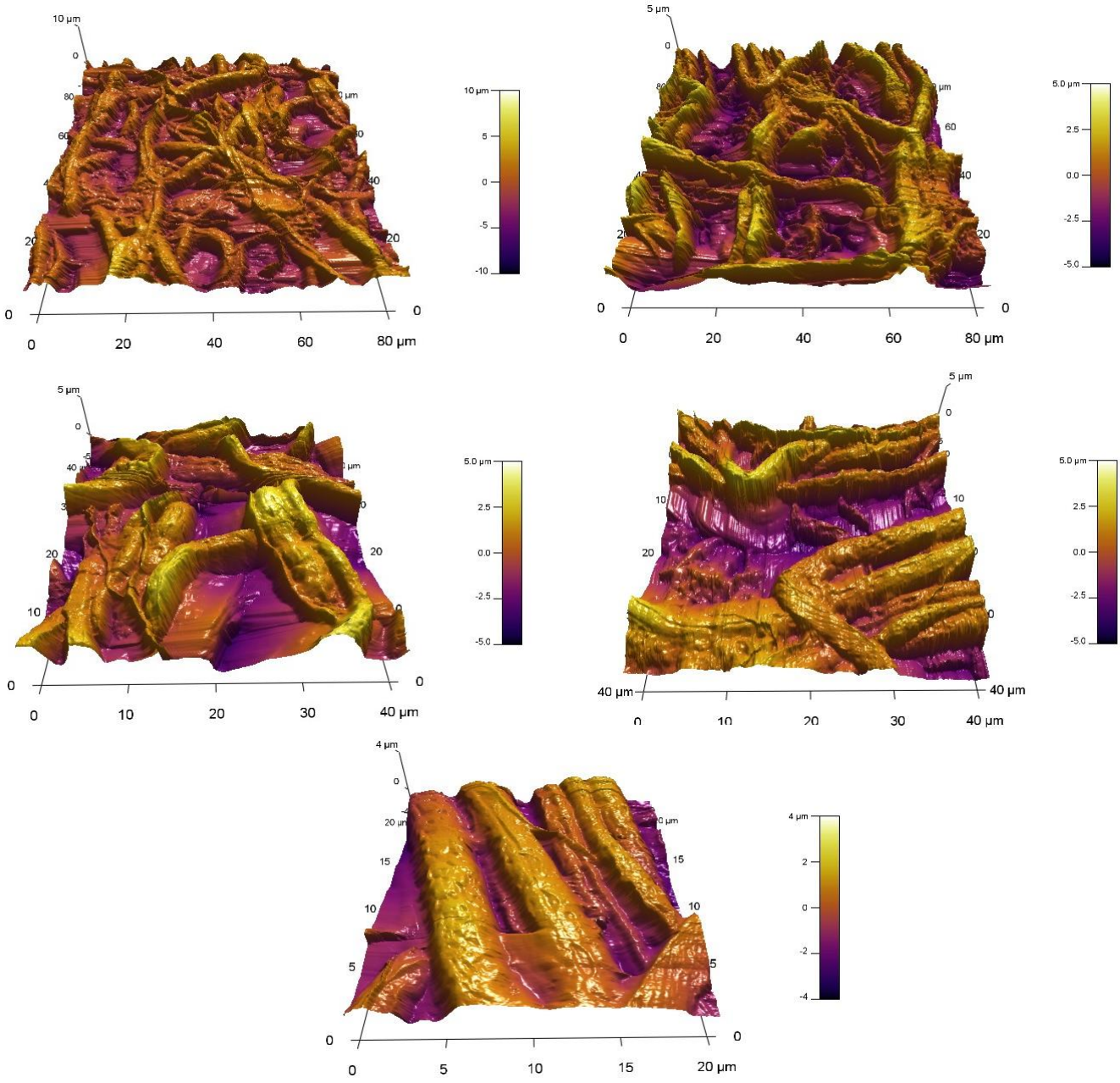

Figure 2.23: AFM 3D images of (A) QS and (B) PCL:PGS (1:1). Figures on the left and on the right are from a different area,

AFM studies confirmed the micrometric dimension of fibers forming both PCL:PGS (1:1, v/v) and QS. Fibers resulted to be randomly distributed and bead-free. The AFM 3D images (Figure 2.23) demonstrates that fibers have cylindrical-like geometries. Furthermore, AFM studies validated the presence of many pores among the fibers of the electrospun scaffolds. In general, the presence of quercetin did not make changes to the properties of the PCL:PGS (1:1, v/v) scaffolds.

2.3.3.3. FTIR spectroscopy of QS

Figure 2.24 shows FTIR spectra in the wavenumber ranging from 4000 to 400 cm^{-1} for QS and PCL:PGS (1:1, v/v). FTIR spectroscopy was used to study possible changes in polymeric materials during the fabrication process due to the addition of free quercetin. In the PCL:PGS (1:1, v/v) spectrum, it was possible to notice some aspects that derive from the two component alone, PCL and PGS. One of this was the presence of esters peaks related to PCL at 1724 and 1170 cm^{-1}. Regarding PGS, there were different stretch vibration peaks for the alkyl group ($-CH_2$) at 2929, 2851, and 1384 cm^{-1}. An intense signal was present at both 1734 and 1165 cm^{-1}; it has to be attributed to a carboxyl groups (C-O and C=O). In PCL:PGS (1:1, v/v) samples the most important change, in comparison with the two pure polymers, is between 3300 and 2500 cm^{-1}. These new shoulders were strictly related to the PGS, indicating an increase in hydroxyl group in the blend sample. FTIR spectra of pure PCL and PGS were not reported but they could be easily find on FTIR data bank. In the QS, the low concentration of quercetin and the most intense bands related to the two polymers prevented the detection of the free quercetin characteristics bands. FTIR spectra of QS and PCL:PGS (1:1, v/v) did not show any differences in their absorbance pattern. As a result, it was possible to notice that the chemical composition of the scaffold was not compromised adding free quercetin during the fabrication process.

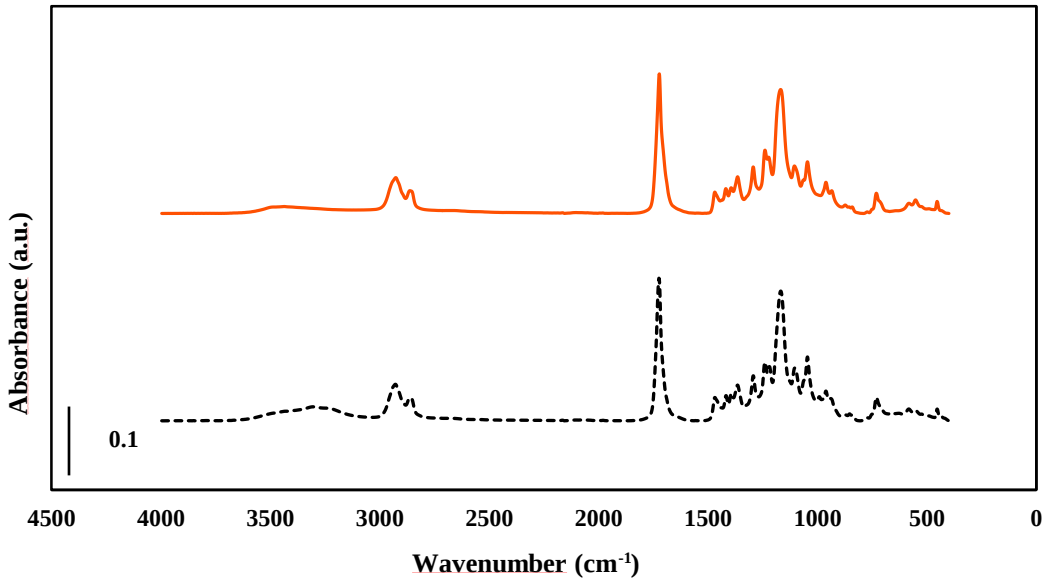

Figure 2.24: FTIR spectra of QS (▬) and PCL:PGS (1:1) (▬ ▬).

2.3.3.4. *In vitro* degradation and fluid uptake of QS and QGCS

In general, biomaterial degradation plays a pivotal role in the formation of the new tissue since it can influence positively or negatively cell adhesion and proliferation. Biodegradability could be considered a possible disadvantage in tissue engineering, especially when it is associated with polymer creep and weakening during time. As shown in Figure 2.25, degradation tests were performed until 8 weeks. The mass loss percentage in the case of PCL:PGS (1:1, v/v) after 4 weeks was about 20 %, according to data observed by other authors (Salehi et al., 2014). Comparing these data with those collected working with QS, it was noticeable that the addition of quercetin in the scaffold did not interfere with the degradation kinetic. In fact, QS and PCL:PGS (1:1, v/v) showed the same degradation trend over 8 weeks. A complete different behaviour was remarkable for QGCS. After 4 weeks, its mass loss reached about 45 %, a higher value in comparison with both QS and PCL:PGS (1:1, v/v). This rapid kinetic of degradation was just a superimposed effect due to the presence of gelatin as coating agent. Samples lost more mass since they were releasing gelatin. Probably, the polymer that formed QGCS showed a degradation kinetic similar to the other samples but it was not possible to take into account the mass loss directly related to the gelatin release because of the co-release of quercetin from the same scaffold.

Fluid uptake of biomaterials is an important factor that affects their specific applications for biological and biomedical applications. In particular, working with scaffolds for vascular tissue engineering, the swelling of the material due to the adsorption of liquids should be considered when a surgical implant is planned. The diameter of the bioprosthesis should not change after fluid uptake to have a correct anastomosis between the vessel and the graft. The samples were immersed in PBS and kept at 37°C for a period of 24 hours (Figure 2.25). After 4 hours of immersion, fluid uptake percentage reached a steady-state for all the analyzed samples. In details, it was 111.26 ± 9.18, 101.31 ± 7.85, and 112.19 ± 3.32 for QS, QGCS, and PCL:PGS (1:1, v/v), respectively. Interestingly, QGCS samples exihibited a more sustained fluid up-take in comparison with QS and PCL:PGS (1:1, v/v), in the first hours, with a peak after 2 hours of soaking time. This was due to the presence of gelatin that, being hydrophilic, could capture at first more water than the polymer itself. However, after this initial phase, the fluid uptake percentage decreased, reaching lower values. The mass loss that was registered during the fluid uptake experiments was attributable to a contemporary release of gelatin from the scaffold during time. In fact, as preously reported (Section 2.3.2.4), gelatin had a significant release during the first hours of immersion in PBS.

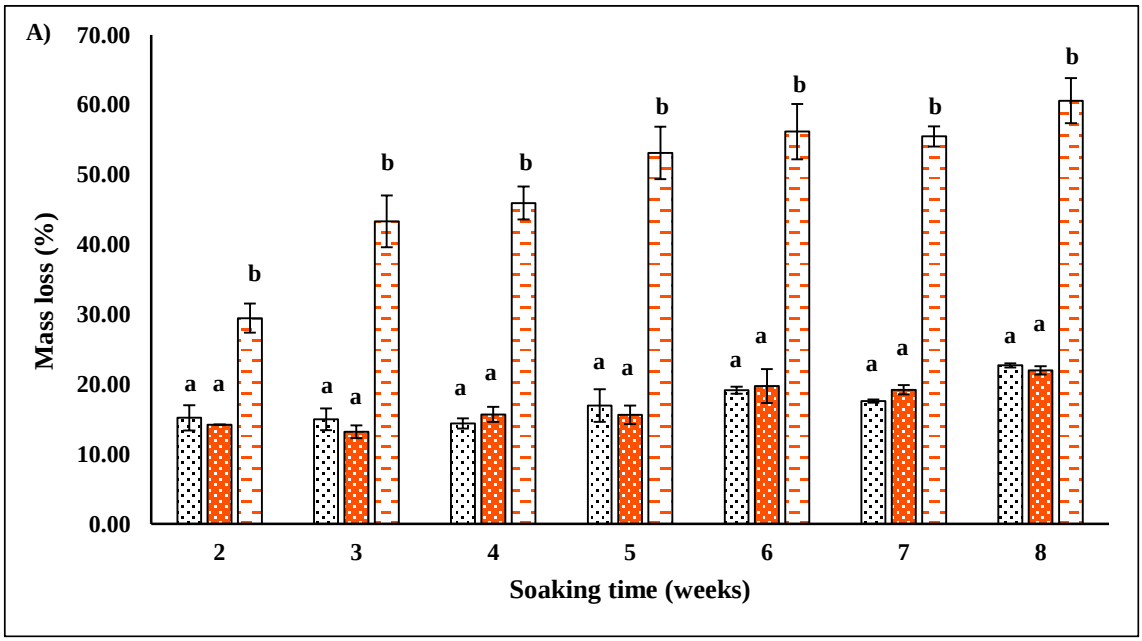

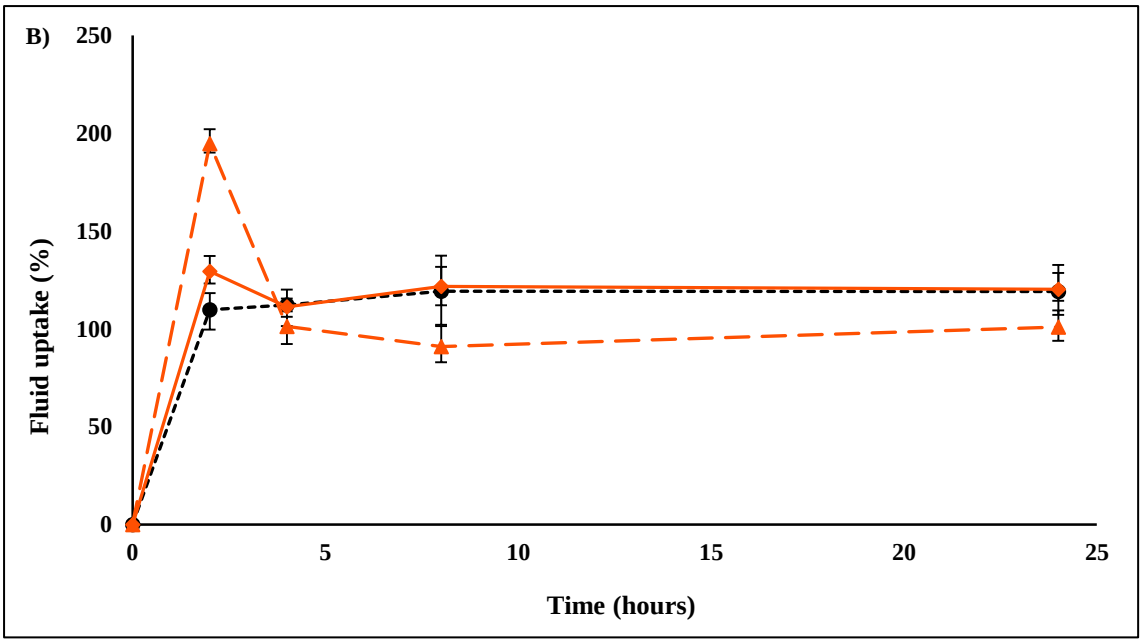

Figure 2.25: (A) mass loss (B) and fluid uptake of PCL:PGS (1:1), QS, and QGCS. Mass loss: ⬚ PCL:PGS (1:1), ⬚ QS, ⬚ QGCS. Fluid uptake: PCL:PGS (1:1) ● (▬ ▬), QS ♦ (▬▬), QGCS ▲ (▬ ▬).

Results are mean of three measurements ± SD. Different letters do refer to statistically significant differences among results for each day ($p < 0.05$), ANOVA with Tukey's multiple comparison test.

2.3.3.5. Quercetin release from QS and QGCS

Figure 2.26 refers to the release of quercetin in PBS at 37°C for a period of 54 days. As regards to QS, the amount of released quercetin during the first 10 days was very low. Then, the release accelerated reaching

1 % of the total quercetin in the electrospun scaffold after 19 days and a final value of 2.14 % (0.59 ± 0.13 mg) at the end of the experiment. This pretty poor release of quercetin was probably related to the low solubility of this compound in aqueous solutions. Comparing the results obtained working with QGCS, it was found that the two curves showed the same release trend, meaning that the coating with gelatin did not interfere with the release kinetic. However, QGCS displayed a higher release of quercetin, taking into account the same intervals, in comparison with QS: after 19 days and at 54 days the amount of released quercetin was 2.79 and 4.51 % (1.19 ± 0.06 mg), respectively. Probably, there was more than only one explanation to this trend. First, when gelatin left the scaffold, it induced a co-release of superficial quercetin. Second, the presence of a coating with gelatin preserved quercetin from oxidation and this is reflected in an enhanced detection of quercetin using spectrophotometry. In fact, in this second case, the percentage of the released quercetin could be the same but working with QS a part of released Q was oxidized. During the spectrophotometric analysis, in fact, only the active quercetin and not the oxidized form, is detected. This interesting aspect will need a more detailed studies to prove which is the correct hypothesis. Q was chosen as anti-inflammatory molecule with whom functionalize PCL:PGS (1:1, v/v) scaffold, after a detailed research in literature. As reported by Kobuchi et al. (1999), it shows an anti-inflammatory effect after 24 hours at a concentration of 1 μM. This concentration is always overcome by the released quercetin from the scaffolds in (QS and QGCS). Regarding these data, these samples were considered promising for the subsequent experiments with human endothelial cells.

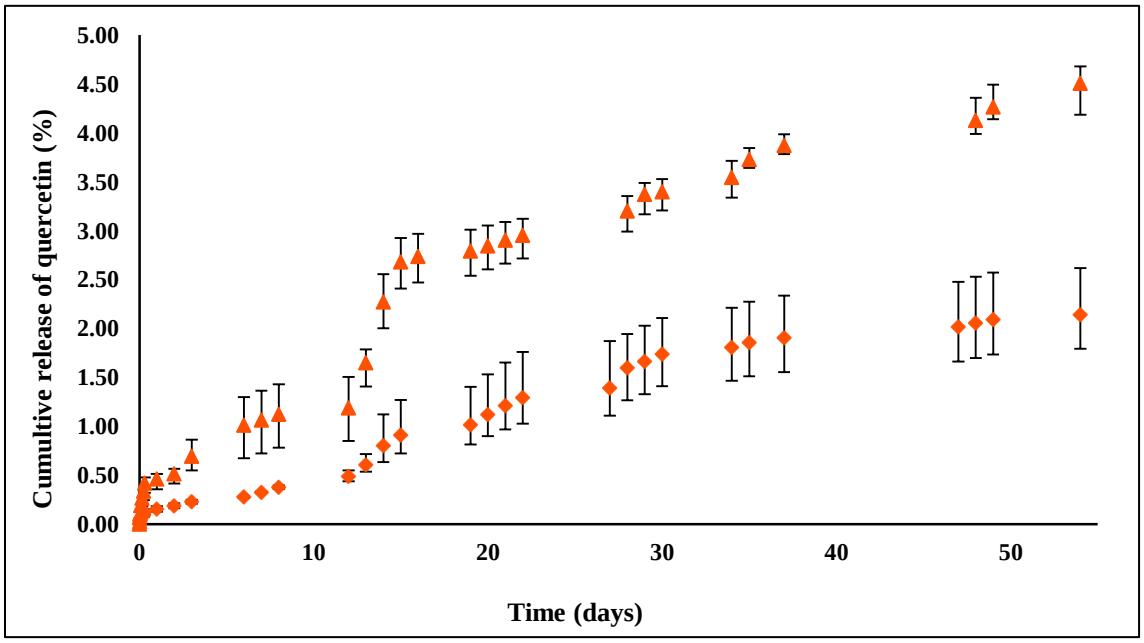

Figure 2.26: cumulative release of quercetin from QS ♦ (—) and QGCS ▲ (- - -).

2.3.3.6. Water permeability of QS and QGCS

The presence of gelatin coating allowed us to perform the water permeability test. This coating was responsible of a less water permeability in comparison with PCL:PGS (1:1, v/v). QGCS showed a 0 % water permeability at a pressure of 0.2 bar (correpsonding to 150 mmHg), a value closer to the systolic blood pressure in a healthy person (120 mmHg). The first water drops appeared on the surface of QGCS when the applied pressure was 0.3 bar (225 mmHg). The permeability of the graft was 0.34 mL/cm^2/min, a value extremely low in comparison with those reported in literature (e.g. Madhavan et al., 2013). Under a microscopic point of view, the capability of coated samples to be impermeable at water at 0.2 bar could be found an explanation in their 3D microstrucutre. As previously reported (Section 2.3.2.2), the porosity of GCS was lower (43.49 ± 10.85 %) in respect with PCL:PGS (1:1, v/v) (68.19 ± 0.02 %). This property justified the decrease of water permeability, working with GCS and QGCS. The water permeability test confirmed that gelatin was a cheap and necessary coating agent for PCL:PGS (1:1, v/v) scaffold. Data are summerized in Table 2.14.

Table 2.14: water permeability of QS, QGCS, and PCL:PGS (1:1) at 0.2 bar.

Sample	Pressure (bar)	Water permeability (%)
QS	0.2	100
QGCS	0.2	0
PCL:PGS (1:1)	0.2	100

2.3.3.7. Mechanical characterization of QS and QGCS

In order to compare the mechanical properties of QS and QGCS with those of PCL:PGS (1:1, v/v), we focused our attention on Young's modulus, tensile strength and elongation percentage of the scaffold (Table 2.15). QS and PCL:PGS (1:1, v/v) showed a comparable Young's modulus, tensile strength and elongation percentage. The addition of quercetin to the polymer did not change its mechanical properties. Conversely, QGCS exhibited, under a mechanical point of view, a different behaviour in comparison with QS and PCL:PGS (1:1): the Young's modulus and the tensile strength were higher while the elongation percentage was lower. Figure 2.27 (A) shows representative stress-strain curves of dry PCL:PGS (1:1, v/v), QS, and QGCS. In general, QGCS samples presented a more brittle and harder behaviour, possessing a Young's modulus from 12 to 20 times bigger and a lower elongation percentage (from 5 to 10 times lower). This

hardening properties, due to the presence of a layer of gelatin on the surface of the scaffold, was overcome by immersing QGCS in a NaCl solution (0.9 %, w/v) for at least 5 minutes, following a common vascular surgery procedure before implanting grafts. Surprisingly, the wet state restored the ductile properties of QGCS in terms of Young's modulus and tensile strength, deleting the hardening behaviour of dry gelatin. Figure 2.27 (B) reported the stress-strain curve for wet GCQS. The condition of rehydration facilitated the sliding of polymer chains under mechanical deformation (Kharaziha et al., 2013). Samples in wet condition were considered to correspond better than samples in dry condition to the final application of the vascular prostheses, and therefore, all these data suggested that the coating with gelatin did not modify the mechanical properties of the scaffold when they were wet. There were no differences among dry and wet samples made of PCL:PGS (1:1, v/v) and QS (data not shown).

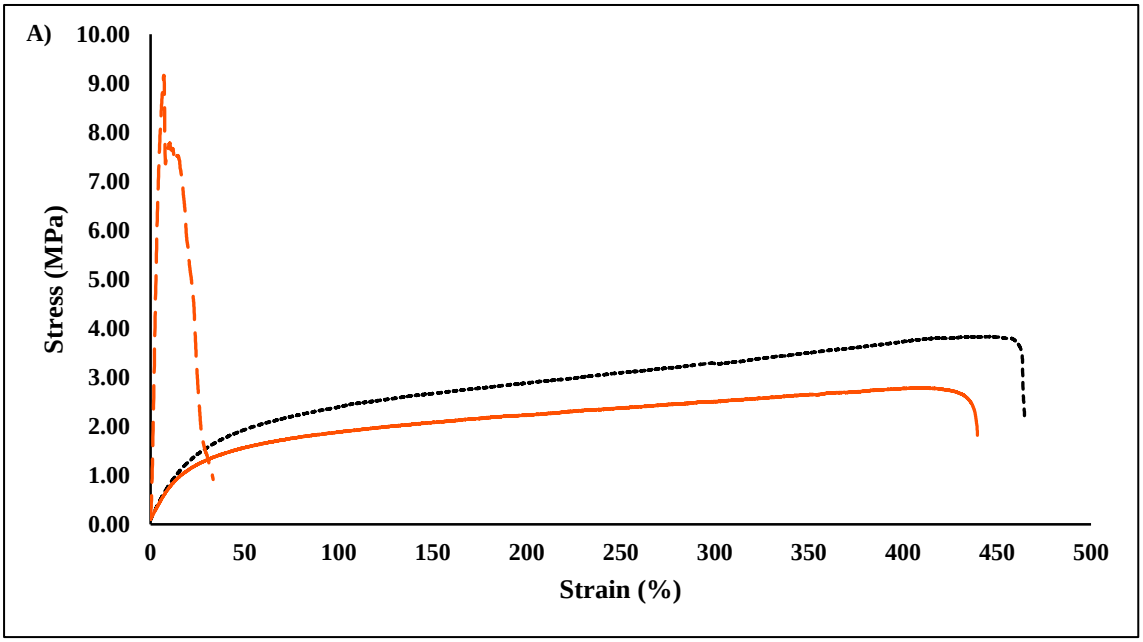

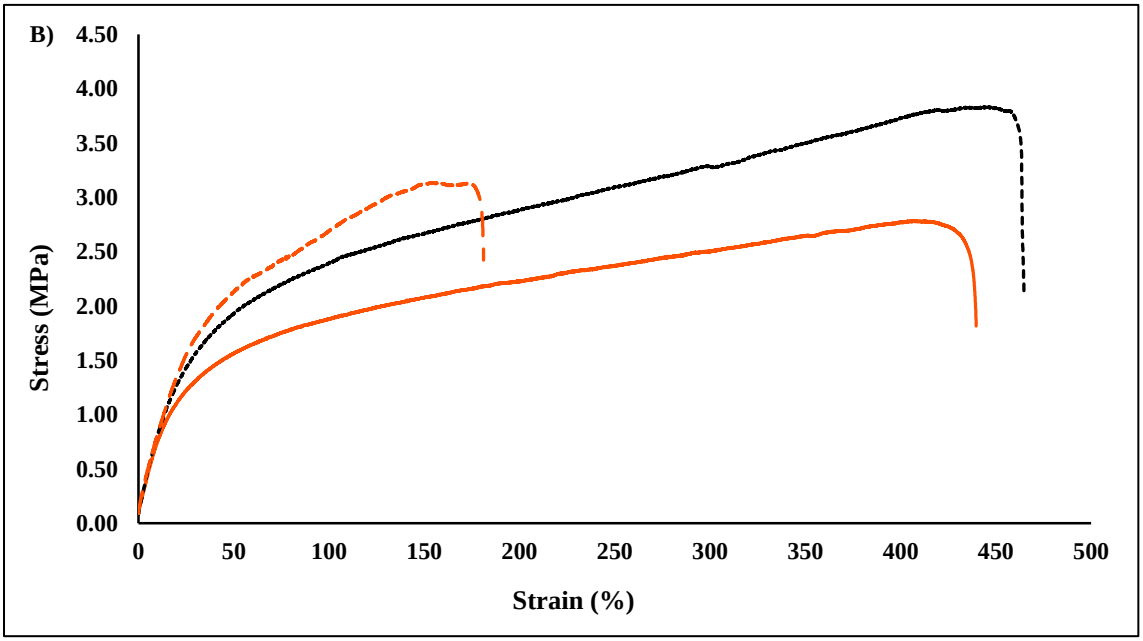

Figure 2.27: representative stress-strain curves for (A) dry samples of PCL:PGS (1:1), dry samples of QS, and dry samples of QGCS and (B) dry samples of PCL:PGS (1:1), dry samples of QS, and wet samples of QGCS. PCL:PGS (1:1) (▬ ▬), QS (▬▬) and QGCS (▬ ▬).

Table 2.15: mechanical properties of QS, QGCS, and PCL:PGS (1:1).

Sample	Young's modulus (MPa)	Tensile strength (MPa)	Elongation (%)
QS_{dry}	6.65 ± 2.34^{a}	2.68 ± 0.62^{a}	450.94 ± 86.19^{a}
$QGCS_{dry}$	221.09 ± 5.61^{b}	7.26 ± 0.97^{c}	32.45 ± 7.60^{c}
$QGCS_{wet}$	9.82 ± 2.09^{a}	$3.25 \pm 0.16^{a,b}$	199.56 ± 28.98^{b}
PCL:PGS $(1:1)_{dry}$	7.92 ± 0.25^{a}	4.57 ± 0.56^{b}	505.76 ± 35.12^{a}

Results are mean of three measurements ± SD. Different letters do refer to statistically significant differences among results for each column ($p < 0.05$), ANOVA with Tukey's multiple comparison test.

Furthermore, it was investigated the mechanical properties of QS after one month of degradation (Figure 2.28). The process of degradation of the polymers did not interfere with the mechanical behaviour but the breaking point in the degraded samples was lower. Probably, this fact was due to fibers weakening during degradation time.

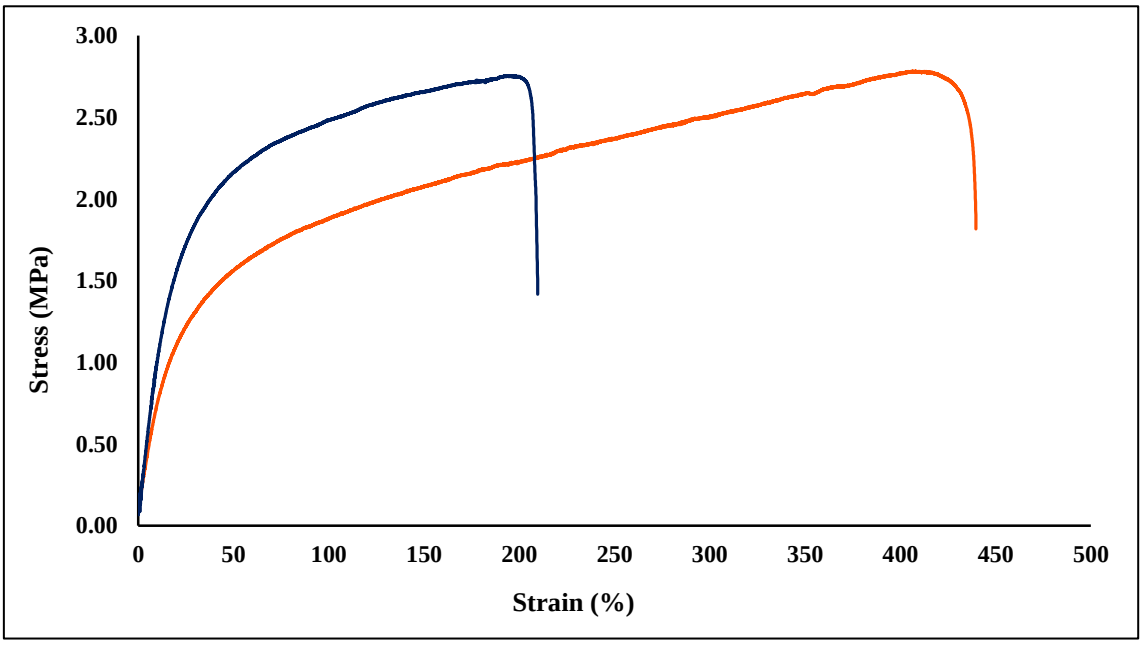

Figure 2.28: representative stress-strain curves for native QS (—) and after one month (—) of soaking in PBS.

2.3.3.8. Biocompatibility of QS and QGCS

Biocompatibility of QS and QGCS were assessed using both human endothelial and mesenchymal stem cells. Before testing the cell cytotoxicity of QS and QGCS, the cell viability in presence of free quercetin solubilized in ethanol was assessed. The cellular growth was monitored even in presence of ethanol alone, using the same volume of solvent that was necessary to prepare the solution with the different concentrations of quercetin. These preliminary experiments were performed to be sure that an eventual cytotoxicity was exclusively due to the tested quercetin and not due to the ethanol. Figure 2.29 shows the curve of human endothelial growth over a period of 8 days in presence of different concentrations of quercetin. Treating the cells with 5 and 10 μM of quercetin, there was no cell cytotoxicity. At the highest concentration of quercetin (50 μM), endothelial cells showed the same growth rate in comparison with the control and the lowest concentration of the drug but they stopped to grow, reaching a plateau phase after 6 days of culture. The presence of ethanol interfered with the cellular growth only in the presence of the huge amount of the solvent, not in the other cases. Thus, the partial cytotoxicity highlighted working with the highest concentration of quercetin (50 μM), probably, was due to an excessive amount of ethanol instead of the presence of the quercetin itself.

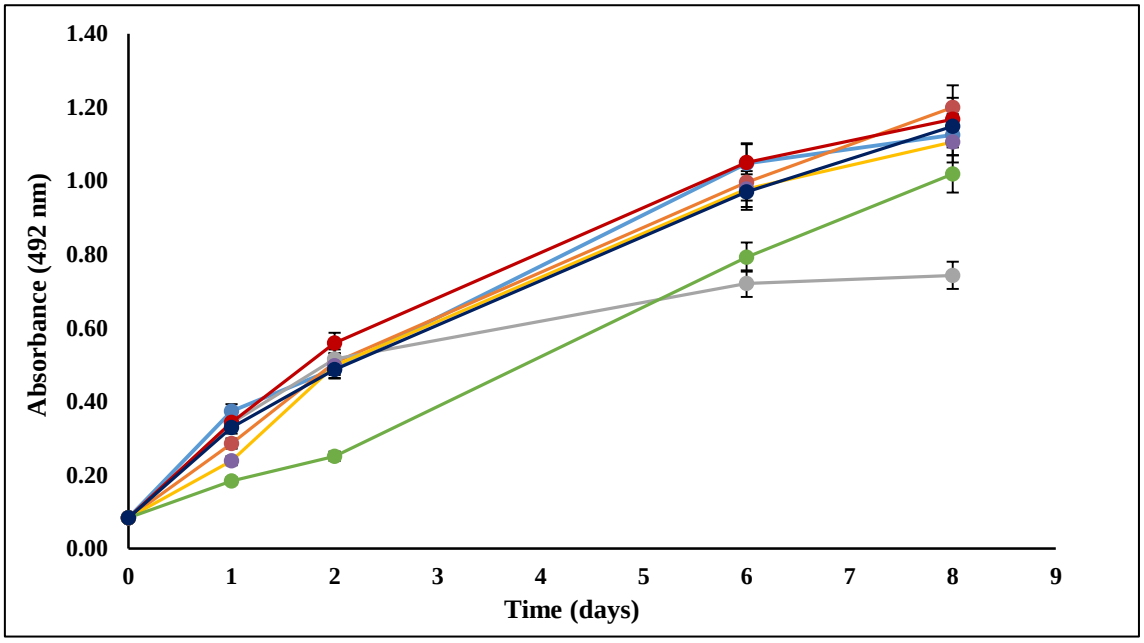

Figure 2.29: Cell viability quantified by MTS assay. Cells were treated with: 5 μM Q (—), 10 μM Q (—), 50 μM Q (—), the volume of ethanol present in 5 μM Q (—), the volume of ethanol present in 10 μM Q (—), the volume of ethanol present in 50 μM Q (—), and no treatment (—).

The second step was represented by putting in contact endothelial cells and hMSC with QS and QGCS to prove their non-toxicity. As reported in Figure 2.30, the presence of the biomaterials in the cellular medium

didn't interfere with cellular proliferation after 1 and after 4 days, working with endothelial cells. The same trend was found working with hMSC. Taking into account the previous studies regarding the quercetin release from QS and QGCS, these data confirmed that the released amount was no cytotoxic both for endothelial and hMSC cells.

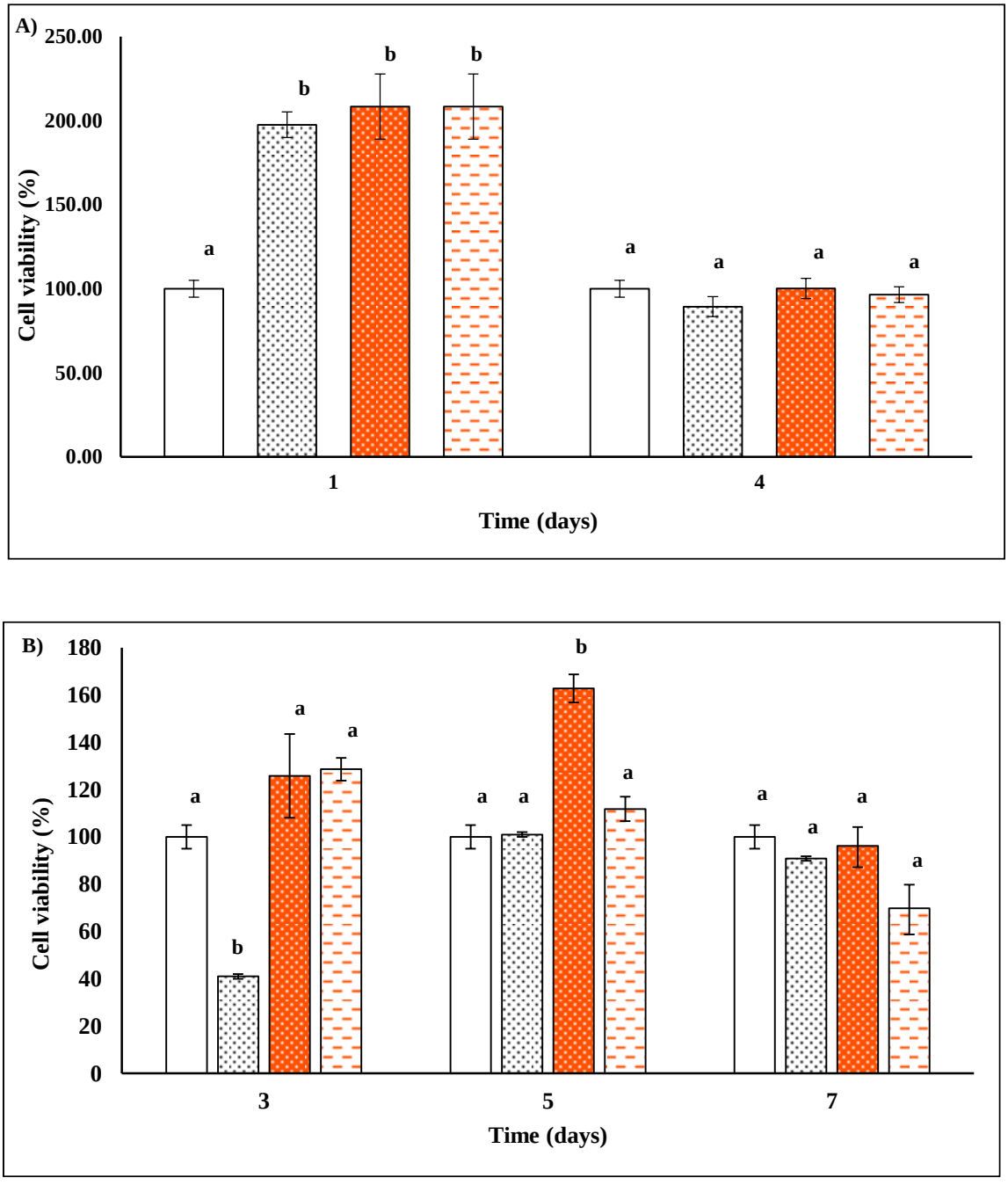

Figure 2.30: cell viability of PCL:PGS (1:1), QS, and QGCS on (A) endothelial cells and on (B) hMSC. ☐ control, ⁙ PCL:PGS (1:1), ■ QS, and ▭ QGCS.

Results are mean of three measurements ± SD. Different letters do refer to statistically significant differences among results ($p < 0.05$), ANOVA with Tukey's multiple comparison test.

2.3.3.9. *In vitro* anti-inflammatory activity of QS

The anti-inflammatory activity of QS was verified studying the relative expression of one of the most significant inflammatory marker expressed by endothelial cells. Matrix Metallo-Protenaise 9 (MMP-9), also known as gelatinase B, is one member of the zinc-metalloproteinases family and it is involved in the degradation of the extracellular matrix. In particular, one of its substrates is represented by gelatin. This is the reason why, during the research activity, described in this thesis, it was decided to evaluate its expression. In fact, MMP-9 could have a crucial role in degrading the coating made of gelatin of QGCS after the implantation. Endothelial cells where treated with Tumor Necrosis Factor α (TNF-α) to reproduce *in vitro* the inflammatory response that occurs after the implantation of the graft. TNF-α is a cell signalling protein involved in the inflammation process. It is able to induce the expression of many mediators of inflammation, including MMP-9. The level of MMP-9 activity was detected by zimography in the conditionated media of TNF-α-stimulated endothelial cells put in contact with PCL:PGS (1:1, v/v) and QS. The presence of TNF-α induced a clear expression of MMP-9 in endothelial cells as shown in Figure 2.31.

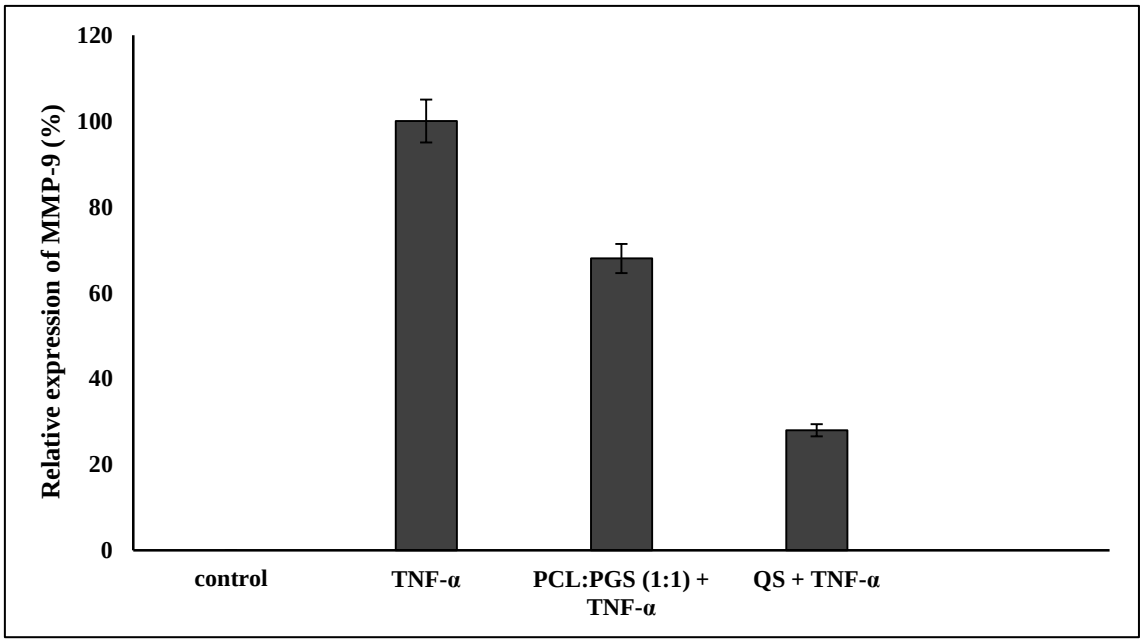

Figure 2.31: relative expression of MMP-9. Data are normalized on the expression obtained with the treatment with TNF-α. Results are mean of three measurements ± SD.

Among all the reported data there are statistically significant differences ($p < 0.05$).

The presence of the PCL:PGS (1:1, v/v) is slightly able alone to down-modulate the expression of MMP-9 ($p < 0.05$). When cells were treated with TNF-α and put in contact with QS, a higher down-modulation of MMP-9 was obtained. The released quercetin from the scaffold was able to decrease the expression of MMP-9 induced by TNF-α. This data are in completely agreement with those reported by Chakraborty et al. (2012), Scoditti et al. (2012), Pan et al. (2015) who demonstrated that one of the cellular response induced by the treatment with quercetin of different kind of cells was the decrease of the expression of MMP-9.

2.3.3.10. Conclusions

This part of the research was addressed to obtain functionalized scaffold incorporating a well-known antioxidant, quercetin. The presence of quercetin did not modify the physicochemical properties of the pure PCL:PGS (1:1, v/v) scaffold and in order to obtain an usable scaffold, it was coated with gelatin. The presence of gelatin ameliorated the release of quercetin during time. The presence of both quercetin and gelatin did not remarkably changes the physicochemical, mechanical, and biological properties of the scaffold. In addition, QS was able to reduce the expression of one of the most important inflammatory markers, MMP-9. For all these reasons, QGCS could be regarded as a promising substitute in vascular tissue engineering.

This work will be partially published as: "Fabrication and functionalization with quercetin of biodegradable vascular prostheses through electrospinning" by **Ferrari P.F.**, Aliakbarian B., Garibaldi S., Arab-Tehrany E., Kahn C., Palombo D., Perego P. 2017 (submitted), partially presented as: "Engineered small diameter vascular grafts with anti-inflammatory properties" at the 66th international Congress of the European Society of Cardiovascular and Endovascular Surgery (ESCVS) 2017, Thessaloniki, Greece, by Aliakbarian B., **Ferrari P.F.**, Palombo D., Perego P., and published in The Journal of Cardiovascular Surgery, abstract book, Vol. 58 – Suppl. 2 to n° 3, 14.

2.3.4. Nanoparticles-functionalized Scaffolds (NS)

The $CaCO_3$ particles used to functionalize the scaffolds described in this section were prepared as described in the Section 3.2.3 using a concentration of PAANa of 1900 μg/mL. They were directly added to the spinning solution before the electrospinning process at the concentration of 0.10 % (w/v).

2.3.4.1. Scanning Electron Microscopy (SEM) analysis of NS

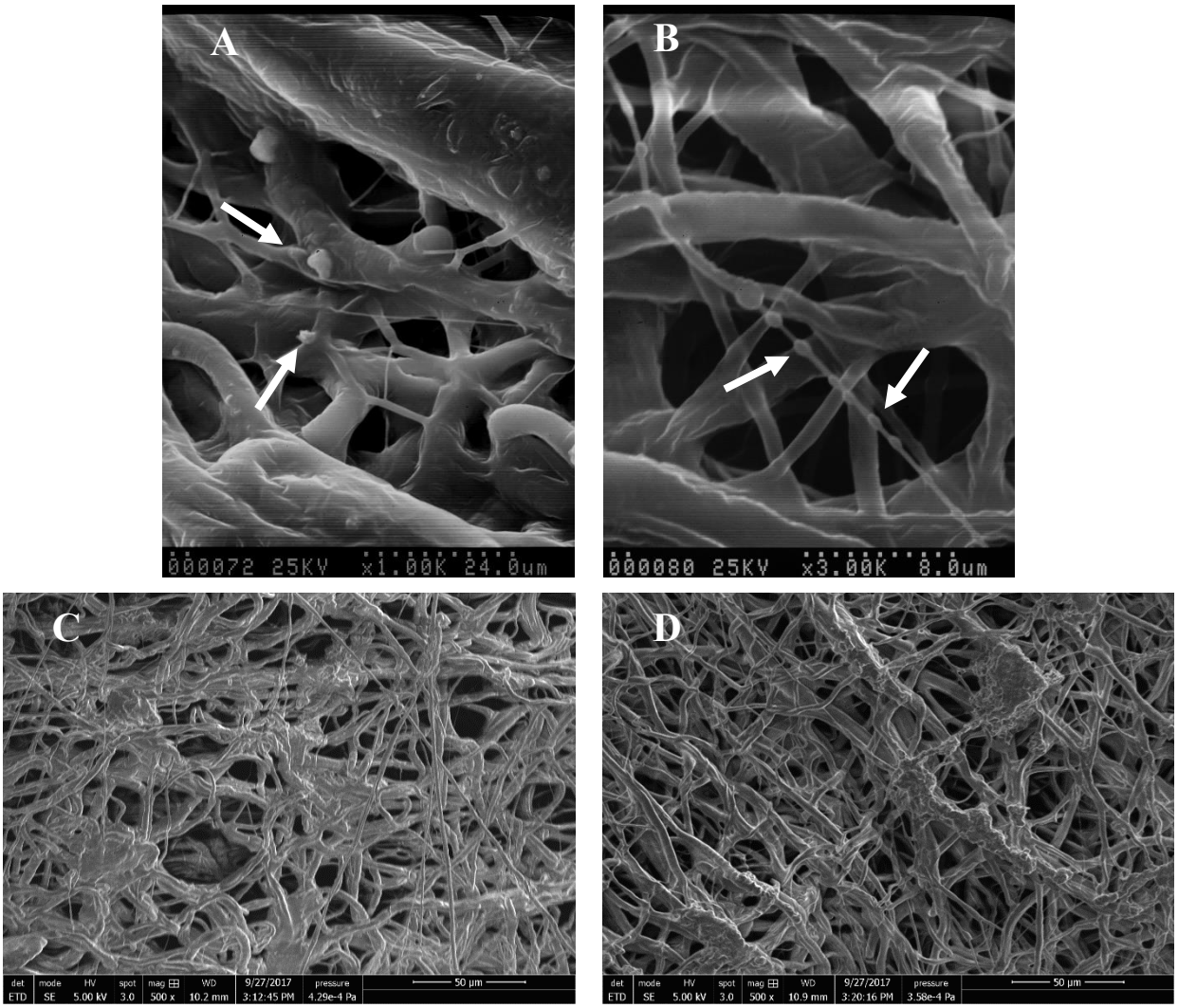

Figure 2.32: representative SEM micrographs of (A) internal and (B) external surfaces of NS and of (C) internal and (D) external surfaces of PCL:PGS (1:1) (images at different magnification).

In Figure 2.32 representative SEM images of internal and external scaffold surface for NS and PCL:PGS (1:1, v/v) are presented. These images were used to confirm the presence of $CaCO_3$ particles in the microarchitecture of the functionalized scaffold. Even in this case, scaffolds presented a random orientation of microfibers. It was noticed a significant difference ($p < 0.05$) in the diameter distribution of the fibers. NS showed fibers that were half of those possessed by PCL:PGS (1:1, v/v). Probably, during the electrospinning process, the presence of nanoparticles served as guide for the formation of the fibers that resulted to be smaller in comparison with the control (Table 2.16). In both the internal and the external surface of NS is possible to put in evidence the presence of the nanoparticles among the electrospun fibers.

Table 2.16: fiber diameter of NS and PCL:PGS (1:1).

Sample	Internal diameter (μm)	External diameter (μm)
NS	2.46±1.75[b]	2.41±1.04[b]
PCL:PGS (1:1)	5.11±1.11[a]	5.57±1.55[a]

Results are mean of at least one hundred measurements ± SD. Different letters do refer to statistically significant differences among results for each column ($p < 0.05$), ANOVA with Tukey's multiple comparison test.

2.3.4.2. Thickness and porosity of NS

Table 2.17 reports the thickness and the porosity of NS and PCL:PGS (1:1, v/v), respectively. No changes were observed measuring the thickness between these two kinds of samples. With respect to porosity, a very subtle difference between the NS and the control was highlighted.

Table 2.17: thickness and porosity of NS and PCL:PGS (1:1).

Sample	Thickness (mm)	Porosity (%)
NS	0.51 ±0.14[a]	71.39±0.16[b]
PCL:PGS (1:1)	0.46 ± 0.11[a]	68.19 ± 0.02[a]

Results are mean of three measurements ± SD. Different letters do refer to statistically significant differences among results for each column ($p < 0.05$), ANOVA with Tukey's multiple comparison test.

2.3.4.3. *In vitro* degradation and fluid uptake of NS

The mass loss and the fluid uptake of NS was compared with PCL:PGS (1:1, v/v) as a function of time in Figure 2.33 (A and B), respectively. A remarkable mass loss after the first day was noticed, both for PCL:PGS (1:1, v/v) and NS. In NS, the presence of nanoparticles provoked a higher specific surface area between the polymeric matrix and nanoparticles themselves. Therefore, a more conspicuous degradation during time were expected. At first, mass loss was more evident in the case of NS (13.03 ± 1.07 %) in comparison with PCL:PGS (1:1, v/v) (10.82 ± 0.37 %). In the two subsequent measurements (after 7 and 14 days), the degradation remained more marked for NS with respect to the control. In the last measurement (after 28 days) the mass loss of NS seemed to be stabilized while there was an increase in the mass loss percentage of the control.

The fluid uptake of PCL:PGS (1:1, v/v) samples resulted to be almost constant just after 2 hours. NS, after 4 hours of incubation absorbed 23 % more water than the control; after 24 hours of soaking time NS absorbed 50 % more water in comparison with the control. Taking into account all these experimental results, it could be speculated that a higher rate of degradation and fluid uptake for NS were due to different reasons. First, the degree of crystallinity of the polymeric blend in NS was reduced by the presence of the $CaCO_3$ nanoparticles. This fact could led to an acceleration in the biodegradation rate of NS due to a possible mobility of the backbone chains and the amorphous region of the polymeric matrix (Lee et al., 2005). Another factor influencing the degradation of NS was its higher porosity. As reported by Cui et al., (2006), the porous structure of electrospun fibers results in a faster matrix breakdown. The higher porosity of NS could be one of the reasons for its faster degradation during the initial phase of the experiments. In fact, the difference between the breaking speed of a chemical bond of polymeric materials and the distribution of water into the polymer matrix is directly linked with the degradation mechanism of biodegradable polymers. The last factor influencing the degradation rate and the fluid upatke could be the difference in the fibers diameter. The thickness of the fiber is related to their stability in aqueous solutions, thickener are the fibers, more unstable they are.

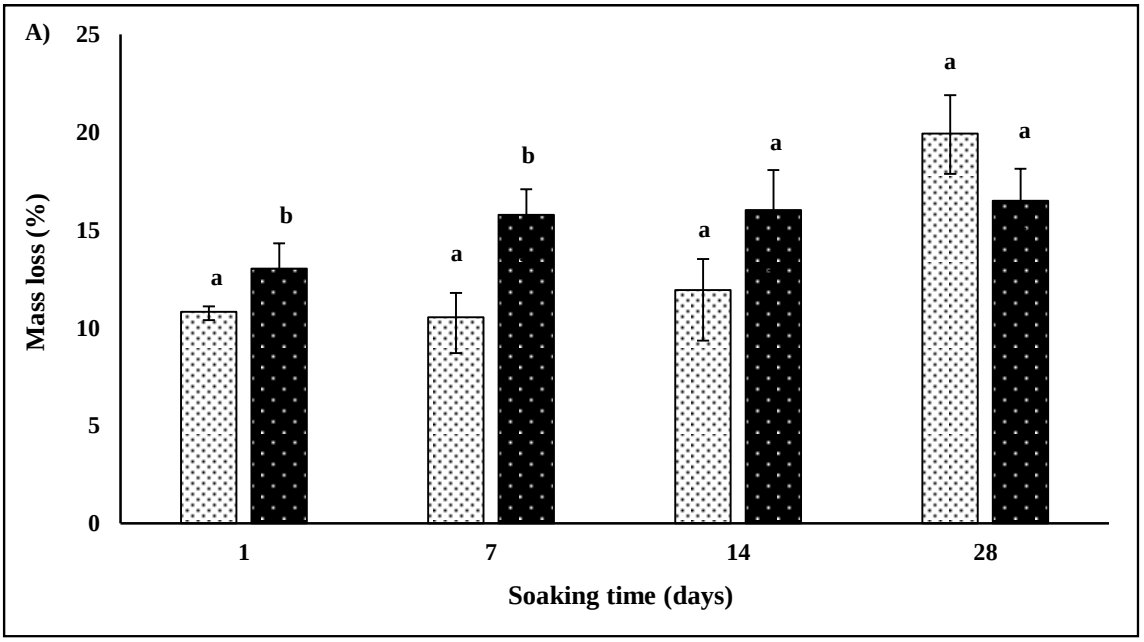

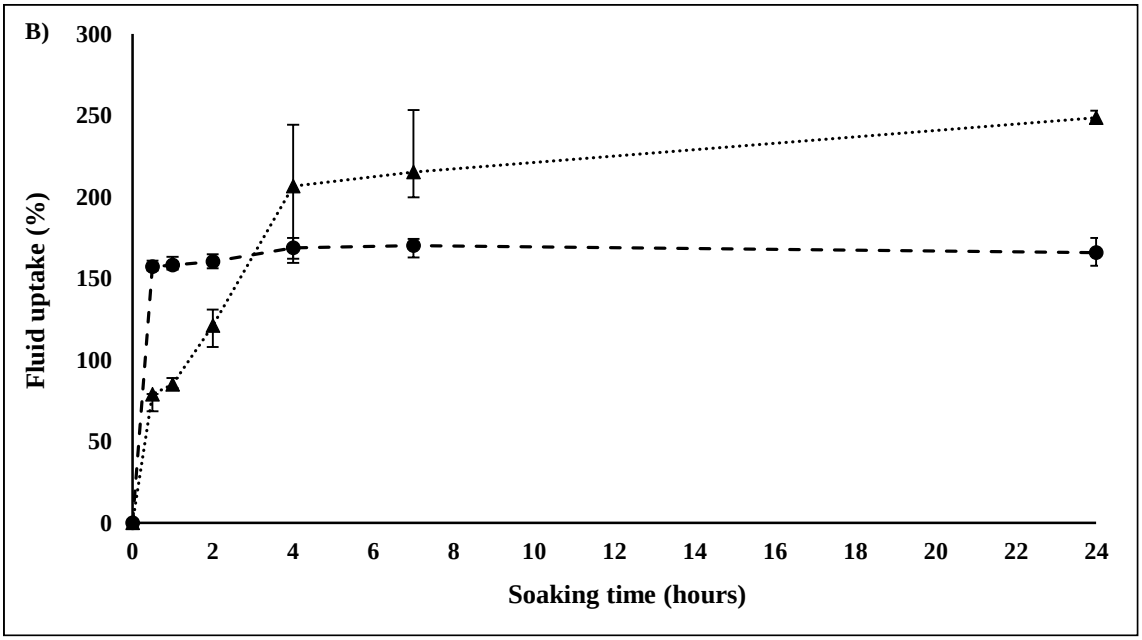

Figure 2.33: (A) mass loss and (B) fluid uptake of PCL:PGS (1:1) and NS. Mass loss: ⚃ PCL:PGS (1:1) and ■ NS. Fluid uptake: PCL:PGS (1:1) ● (▬ ▬), NS ▲ (▪ ▪ ▪ ▪).

Results are mean of three measurements ± SD. Different letters do refer to statistically significant differences among results for each day ($p < 0.05$), ANOVA with Tukey's multiple comparison test.

2.3.4.4. Release of BSA from the scaffold

In Figure 2.34 the profile of the cumulative amount of released BSA from the scaffold over a period of 21 days is reported. The initial inner structure and the dispersion of the nanoparticles within the fibers of the scaffold has to be considered as a critical factor governing the release kinetic of the entrapped drug. In the initial phase, a pronounced burst release was observed. Later the release of BSA became gradual. Reporting a linear release of the protein, it has to be considered that the molecules at first dispersed throughout the polymeric matrix. Then, the presence of an extremely porous matrix allowed the diffusion of the drug out of the scaffold making it possible a constant release of the protein from the inner part. During the entire studied interval, the 86 % of the total encapsulated protein was released. Considering that the aim of this part of the research was to fabricate a general model of scaffold releasing chemoattractant agents, growing factor or differentiation molecules, this could be considered a promising result. In fact, for example, cells need continuously the molecular stimulation to keep their phenotype and to proliferate on the surface of the scaffold.

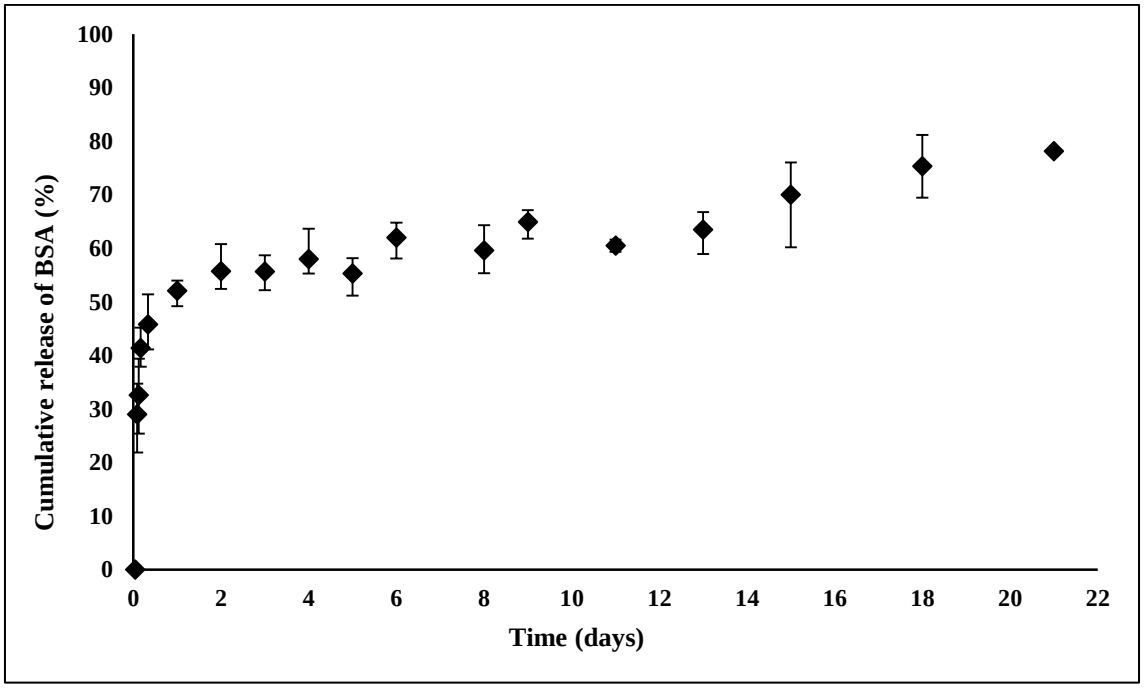

Figure 2.34: cumulative release of BSA from NS.

2.3.4.5. Mechanical characterization of NS

Mechanical integrity is a fundamental property requiring of biomaterials. A well-built scaffold is not only be able of promoting cell attachment and proliferation, supporting cellular growth, but it is also able of maintaining its mechanical stability for all the surgical period required to repair the injured tissue. Table 2.18 shows Young's modulus, tensile strength and elongation for both PCL:PGS (1:1, v/v) and NS. As shown in Figure 2.35, PCL:PGS (1:1, v/v) and NS initially presented a linear stress increase. All the scaffold were largely stretched with increasing strain and the stress drop was seen with visible scaffold breakage. Clearly, all the value for the NS were significantly higher ($p < 0.05$). The incorporation of $CaCO_3$ nanoparticles within the fibrous scaffold was responsible of the observed improving in the tensile strength, Young's moduls, and elongation when it was compared with the control.

Table 2.18: Young's modulus, tensile strength, and elongation percentage of NS and PCL:PGS (1:1).

Sample	Young's modulus (MPa)	Tensile strength (MPa)	Elongation (%)
NS	4.91 ± 1.37^{b}	2.01 ± 0.26^{a}	576.99 ± 132.5^{b}
PCL: PGS (1:1)	7.61 ± 0.92^{a}	3.14 ± 1.47^{a}	218.48 ± 27.72^{a}

Results are mean of three measurements ± SD. Different letters do refer to statistically significant differences among results for each column ($p < 0.05$), ANOVA with Tukey's multiple comparison test.

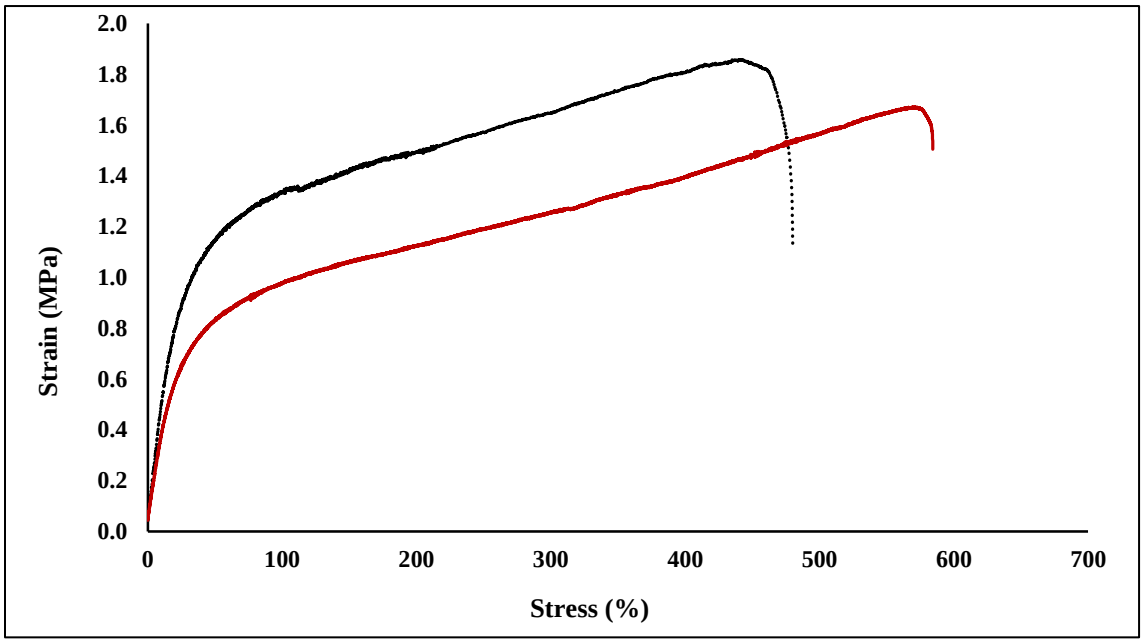

Figure 2.35: representative stress-strain curves for PCL:PGS (1:1) (▬ ▬) and NS (▬▬).

2.3.4.6. Biocompatibility of NS

Biocompatibility is a fundamental precondition of any material that is meant to be implanted in an organism. These materials indeed should be highly tolerable by cells that will be in contact with them. For this reason, it was decided to test the cellular viability of our scaffolds on a human endothelial cell line. To perform this analysis, cell viability was evaluated through the mitochondrial metabolic activity. Three different conditions were compared: control cells (cells without any kind of biomaterials), cells in contact with PCL:PGS (1:1, v/v) and cells in contact with NS. The results are reported in Figure 2.36. No significant differences were found comparing the growth of the cell in presence of the electrospun scaffolds and the control. The increasing values of absorbance during the entire period of cell culturing demonstrated that proliferation occurred in presence of both scaffolds without any cytotoxic event.

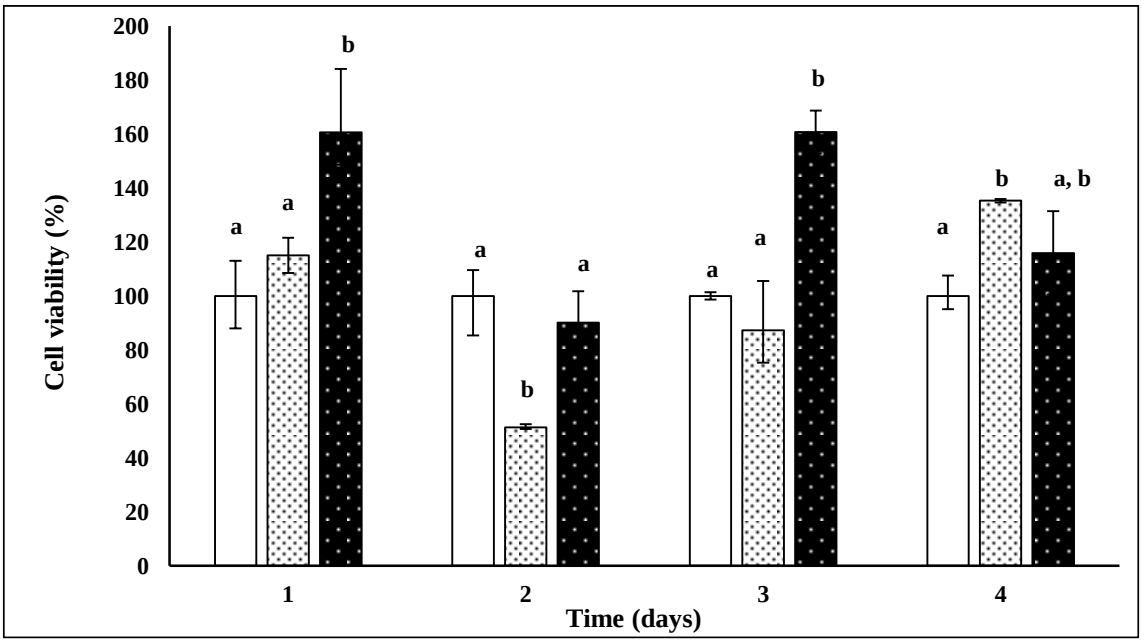

Figure 2.36: cell viability of PCL:PGS (1:1) and NS. ☐ control, ⁙ PCL:PGS (1:1), and ■ NS.

Results are mean of three measurements ± SD. Different letters do refer to statistically significant differences among results ($p < 0.05$), ANOVA with Tukey's multiple comparison test.

2.3.4.7. Hemocompatibility of NS

In this part of the research, the hemocompatibility was evaluated focusing the attention on the blood clotting time and hemolysis. The scope of the *in vitro* clotting time test is to measure the influence of the material on the clotting time. The absorbance of hemoglobin in the solution varied during time, and the higher is the absorbance, better are the anti-thrombotic properties of the scaffold. As indicated in Figure 2.37, after 5 minute PCL:PGS (1:1, v/v) and poly (ethylene terephthalate), with an absorbance equal to 0.533 and 0.575, respectively, howed an absorbance value similar to the glass coverslip, used as a reference thrombogenic material, while the other tested material showed lower values. NS, after 30 minutes, present a lower value of absorbance in comparison with the PCL:PGS (1:1, v/v) and poly (ethylene terephthalate). This value was still comparable to that of expanded poly (tetrafluoroethylene). The last point of the kinetic indicated that all the tested materials, after 60 minutes, had higher absorbance with respect to the glass, indicating a lower thrombogenic activity. PCL:PGS (1:1, v/v), after 5 and after 30 minute of incubation with blood, showed the best anticoagulant properties. Poly (ethylene terephthalate) and expanded poly (tetrafluoroethylene) were chosen as reference materials because nowadays they are currently used in vascular surgery. Hemolysis percentage is a parameter that expresses quantitatively the breakage of red cells after the contac with a material. Materials are classified by the percentage of induced hemolysis as: hemolytic if the this parameter is over 5 %, slightly hemolytic if this value is between 2 and 5 %, and not-hemolytic if this

parameter is low than 2 % (Sterner et al., 2015). Figure 2.37 (B) shows the hemolysis percentage of PCL:PGS (1:1, v/v), NS, poly (ethylene terephthalate) and expanded poly (tetrafluoroethylene). Analysis of the obtained data highlighted that the presence of the nanoparticles in the scaffold significantly reduced the number of disrupted red cells, both with respect to PCL:PGS (1:1, v/v) and expanded poly (tetrafluoroethylene). There was no statistically differences between the percentage of hemolysis in the case of NS and poly (ethylene terephthalate). All these data suggested that both electrospun scaffolds, PCL:PGS (1:1, v/v) and NS were highly compatible with human blood.

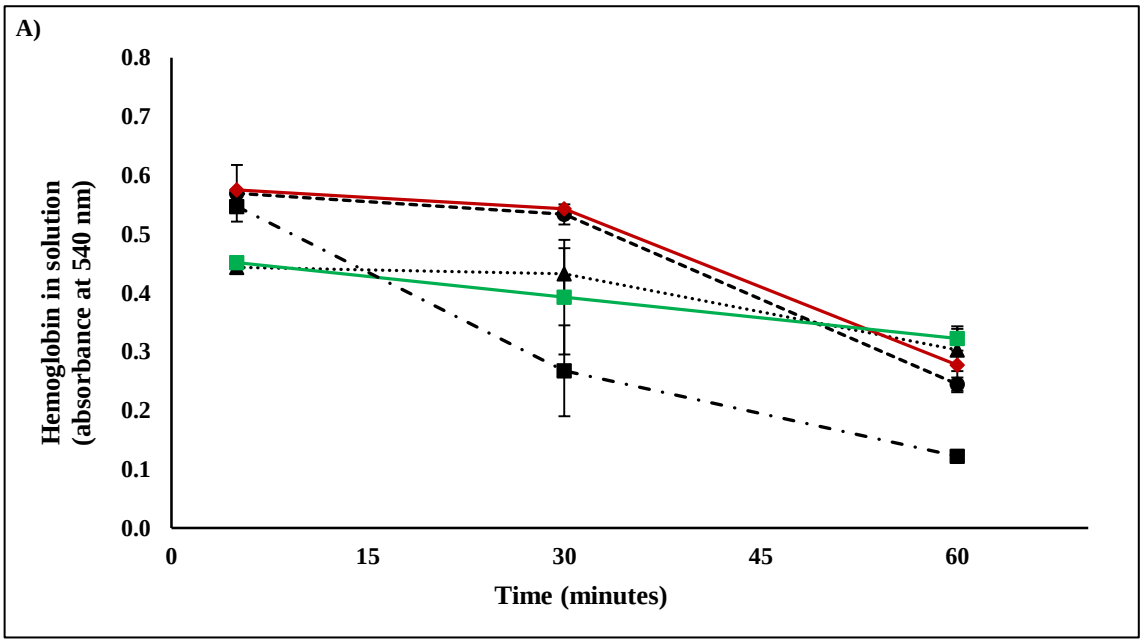

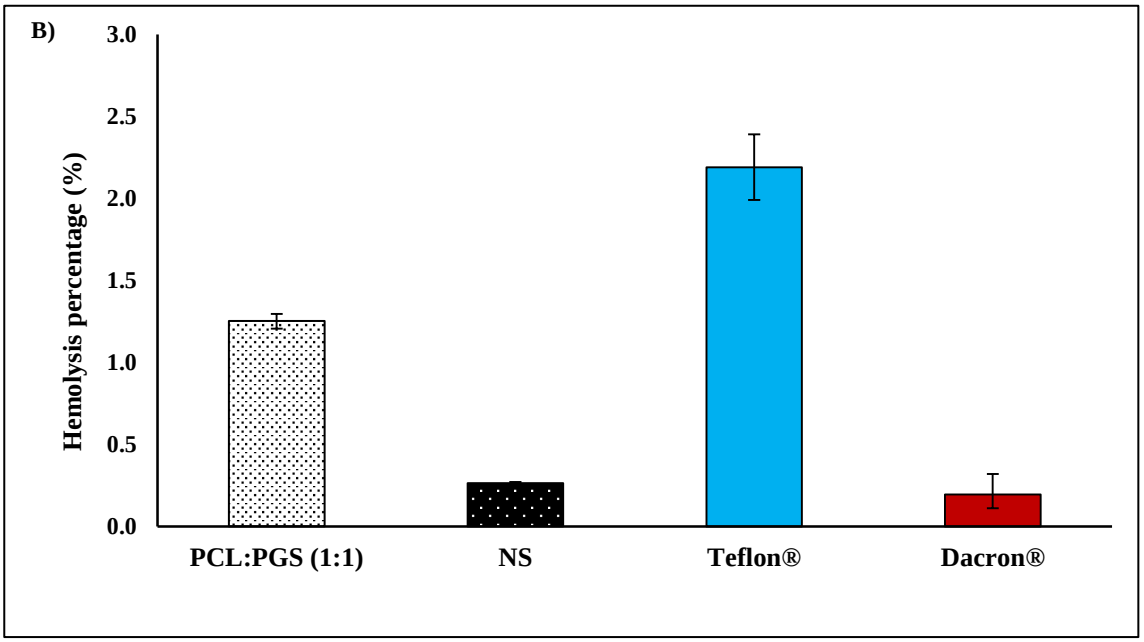

Figure 2.37: hemocompatibility of PCL:PGS (1:1) and NS. (A) Kinetics of clotting time and (B) hemolysis percentage. Clotting time: PCL:PGS (1:1) ● (▬ ▬), NS ▲ (▪ ▪ ▪ ▪), poly (ethylene terephthalate) ♦ (▬▬), expanded poly (tetrafluoroethylene) ■ (▬▬), and glass + (▬ ▪). Result are mean of three measurements ± SD.

2.3.4.8. Conclusions

The scope of this part of the research was to functionalize PCL:PGS (1:1. v/v) with calcium carbonate ($CaCO_3$) nanoparticles encapsulating bovine serum albumin (BSA). Nowadays tissue engineering is promoting the concept of "active" scaffold. Historically, scaffolds were born to replace temporarily a damaged organ until its new development. These scaffolds are generally considered as "passive" scaffold since they offer only the 3D structure to host the cells that are the responsible of the rebuilding of a new working organ. Today, next to this concept of "scaffold as a framework for cells", scaffolds play a fundamental role in each step of the replacement of the damaged organ. It has to counteract the post-implantation inflammatory response, to recruit the correct cell population from the blood releasing chemoattractants, to induce differentiation or trans- differentiation of the attached cells. For all these reasons, this part of the research was dedicated to create a model of scaffold incorporating nanoparticles loaded with a model protein, BSA. In the future, for example, BSA could be replaced with growing factors and chemoattractant agents.

This work was partially presented as: "Functionalization of PCL:PGS electrospun scaffold with protein loaded nanoparticles" at Summer school on Biomaterials and Regenerative Medicine, Riva del Garda, Italy, 2016 by **Ferrari P.F.**, Aliakbarian B., Pastorino L., Palombo D., Perego P. and it will be partially presented

as. “Biodegradable small diameter vascular prostheses functionalized with protein-loaded nanoparticles” at the 67th international Congress of the European Society of Cardiovascular and Endovascular Surgery (ESCVS) 2018, Strasbourg, France, by **Ferrari P.F.**, Aliakbarian B., Palombo D., Perego P.

2.3.5. Lecithin-functionalized polymeric scaffolds (RLS and SLS)

In the last part regarding the functionalization of PCL:PGS (1:1, v/v) scaffold, rapeseed and salmon lecithin were added to the spinning solution at different concentration (0.5, 1.0, and 5.0 mg/mL). Lecithin is a naturally occurring mixture of the diglycerides of stearic, palmitic, and oleic acid, linked to the choline ester of phosphoric acid. Because of its chemical composition, it shows amphiphilic properties. It is commonly found in different tissues of living plants and animals (Wenninger et al., 2000). This kind of functionalization was done in order to have on the scaffolds a surface mimicking the endothelial and the erythrocyte membranes (Zhang et al., 2012). Furthermore, the presence of lecithin in scaffolds serve as building block of cellular plasmatic membranes (Wang et al., 2008). This part of the research was designed in collaboration with Professor Elmira Arab-Tehrany during the last period of the Ph.D., at University of Nancy. For this reason a lot of experiments are still ongoing. RLS and SLS were morphologically characterized using SEM, their chemical structure was studied using FTIR analysis and biocompatibility studies were performed.

2.3.5.1. Scanning Electron Microscopy (SEM) analysis of RLS and SLS

The morphology of electrospun fibers is strictly dependent on different processing parameters such as (1) viscosity of polymer solution that depends on the concentration of the polymers and on the temperature of the process, (2) working voltage, (3) flow rate of the spinning solution, (4) distance between needle tip and the rotating collector, and (5) inner diameter of the needle (Fujihara et al., 2005). As a consequence of this consideration and in order to obtain the same morphology of the scaffolds previously studied, all the parameters of the electrospinning process for both RLS and SLS were kept constant, as reported in Section 2.2.3.3. For all the studied concentration of rapeseed lecithin, fibers appeared randomly distributed, as it was shown in the case of PCL:PGS (1:1, v/v) without the occurrence of bead defects (Figure 2.38 and Figure 2.39). There were no significant differences between the fiber diameters for all the tested concentration of lecithin (Table 2.19). No differences were noticed between RLS, SLS and PCL:PGS (1:1, v/v) in terms of morphology as well as there were no differences among RLS and SLS despite of their

different origin (plant or animal). In general, the presence of both rapeseed and salmon lecithin did not interfere with the microarchitecture of the electropsun scaffold.

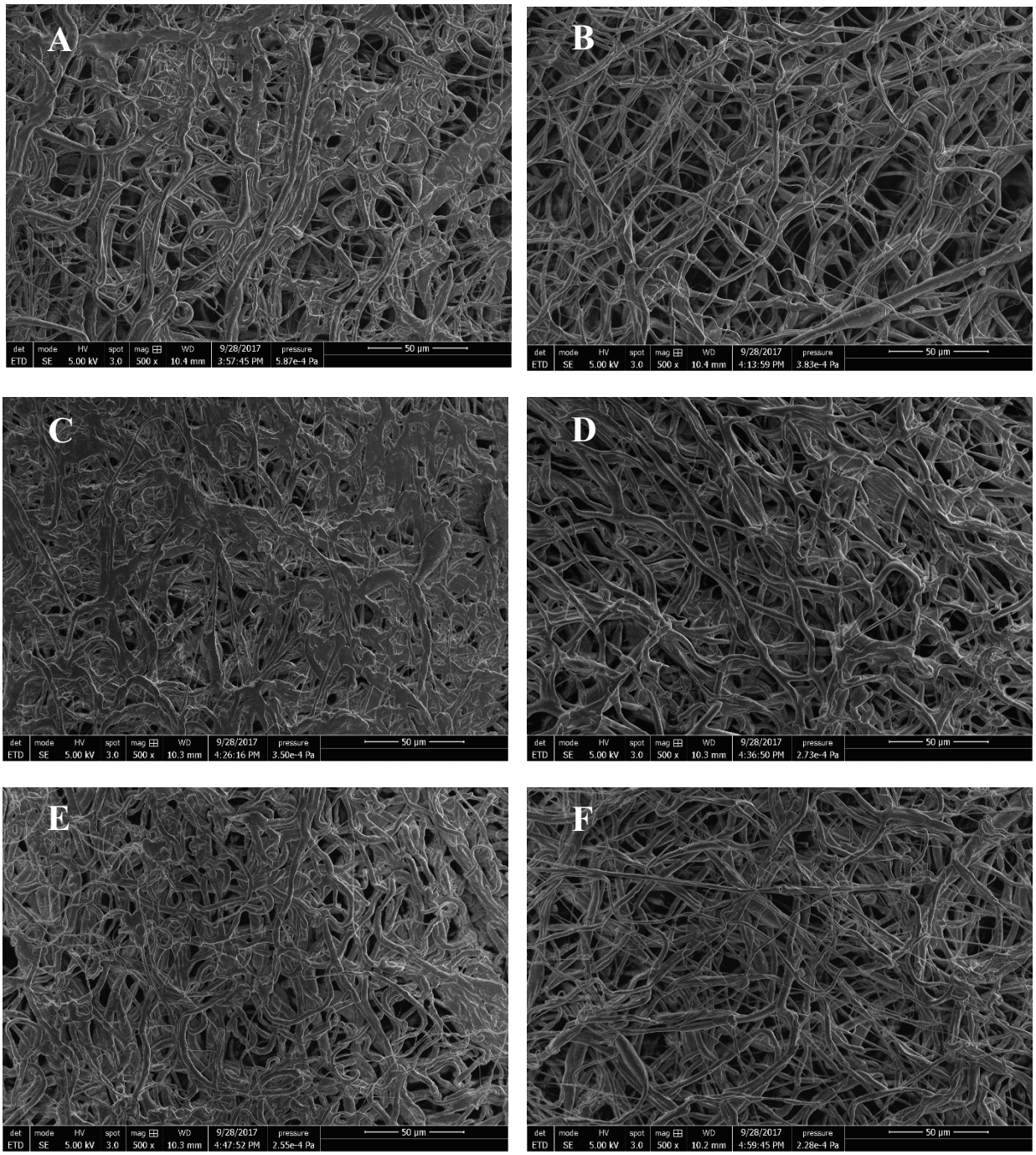

Figure 2.38: representative SEM micrographs of internal (left) and external (right) surface of RLS made with (A and B) 0.5, (C and D) 1.0, and (E and F) 5.0 mg/mL of rapeseed lecithin.

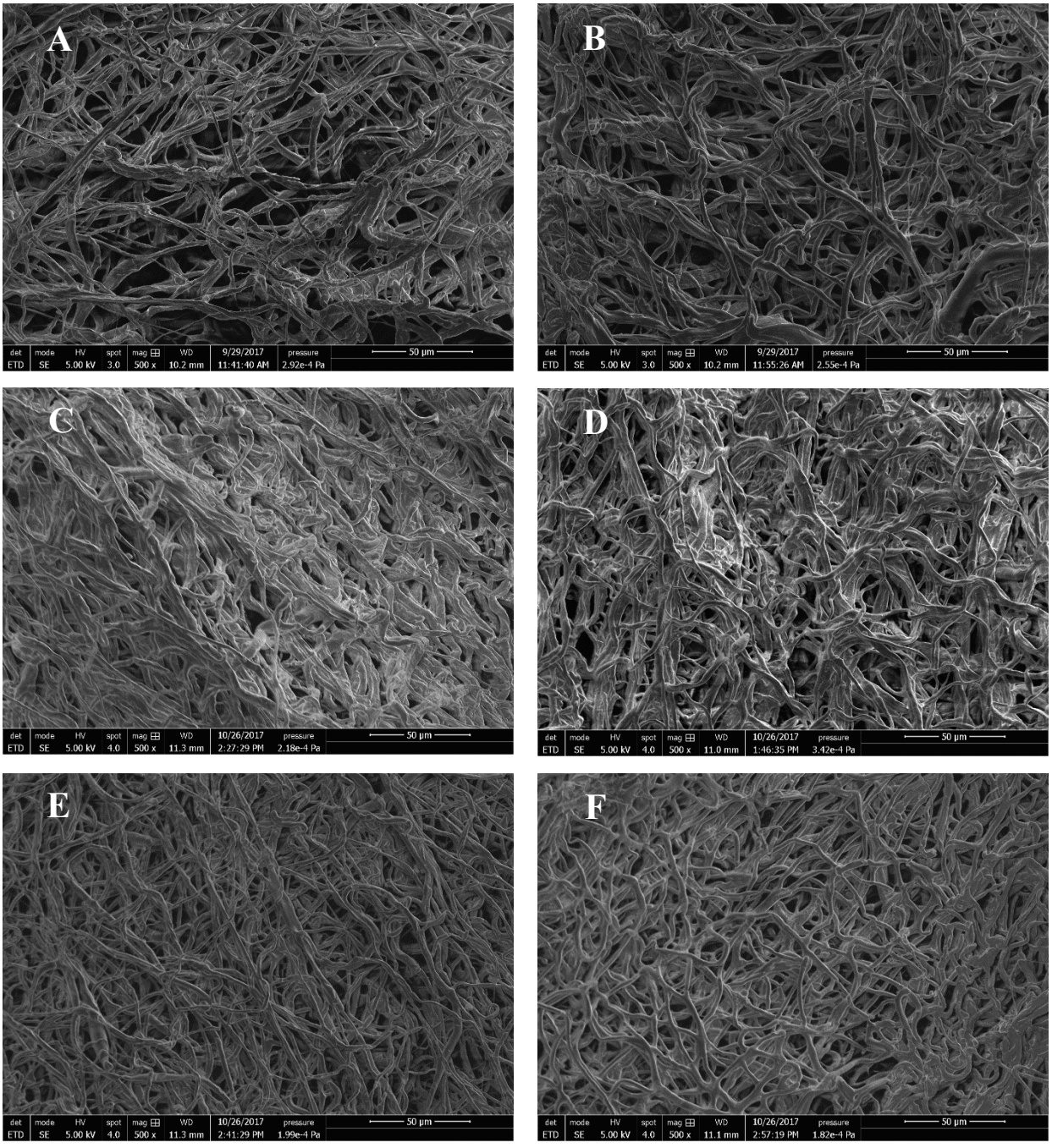

Figure 2.39: representative SEM micrographs of internal (left) and external (right) surface of SLS made with (A and B) 0.5, (C and D) 1.0, and (E and F) 5.0 mg/mL of salmon lecithin.

Table 2.19: fiber diameter of RLS and SLS.

Sample	Diameter (µm)
RLS (0.5 mg/mL)	3.45 ± 0.97^{b}
RLS (1.0 mg/mL)	3.51 ± 0.90^{b}
RLS (5.0 mg/mL)	3.55 ± 0.84^{b}
SLS (0.5 mg/mL)	3.53 ± 0.73^{b}
SLS (1.0 mg/mL)	3.57 ± 1.03^{b}
SLS (5.0 mg/mL)	3.35 ± 0.88^{b}
PCL:PGS (1:1)	4.01 ± 0.92^{a}

Results are mean of three measurements ± SD. Different letters do refer to statistically significant differences among results for each column ($p < 0.05$), ANOVA with Tukey's multiple comparison test.

2.3.5.2. FTIR spectroscopy of RLS and SLS

Figure 2.40 shows FTIR spectra in the wavenumber ranging from 4000 to 400 cm^{-1} for RLS (Figure 2.40 A), SLS (Figure 2.40 B), and PCL:PGS (1:1, v/v). FTIR data were collected to evaluate potential changes in polymeric materials due to the addition of free rapeseed and salmon lecithin, respectively. For all the samples, the low concentration of lecithin and the most intense bands related to the two polymers (PCL and PGS) prevented the detection of the characteristic bands of the components of lecithin. FTIR spectra of RLS, SLS, and PCL:PGS (1:1, v/v) did not show any difference in their absorbance pattern. As a result, it was possible to notice that the chemical composition of the scaffold was not compromised adding free rapeseed or salmon lecithin during the fabrication process of the scaffolds.

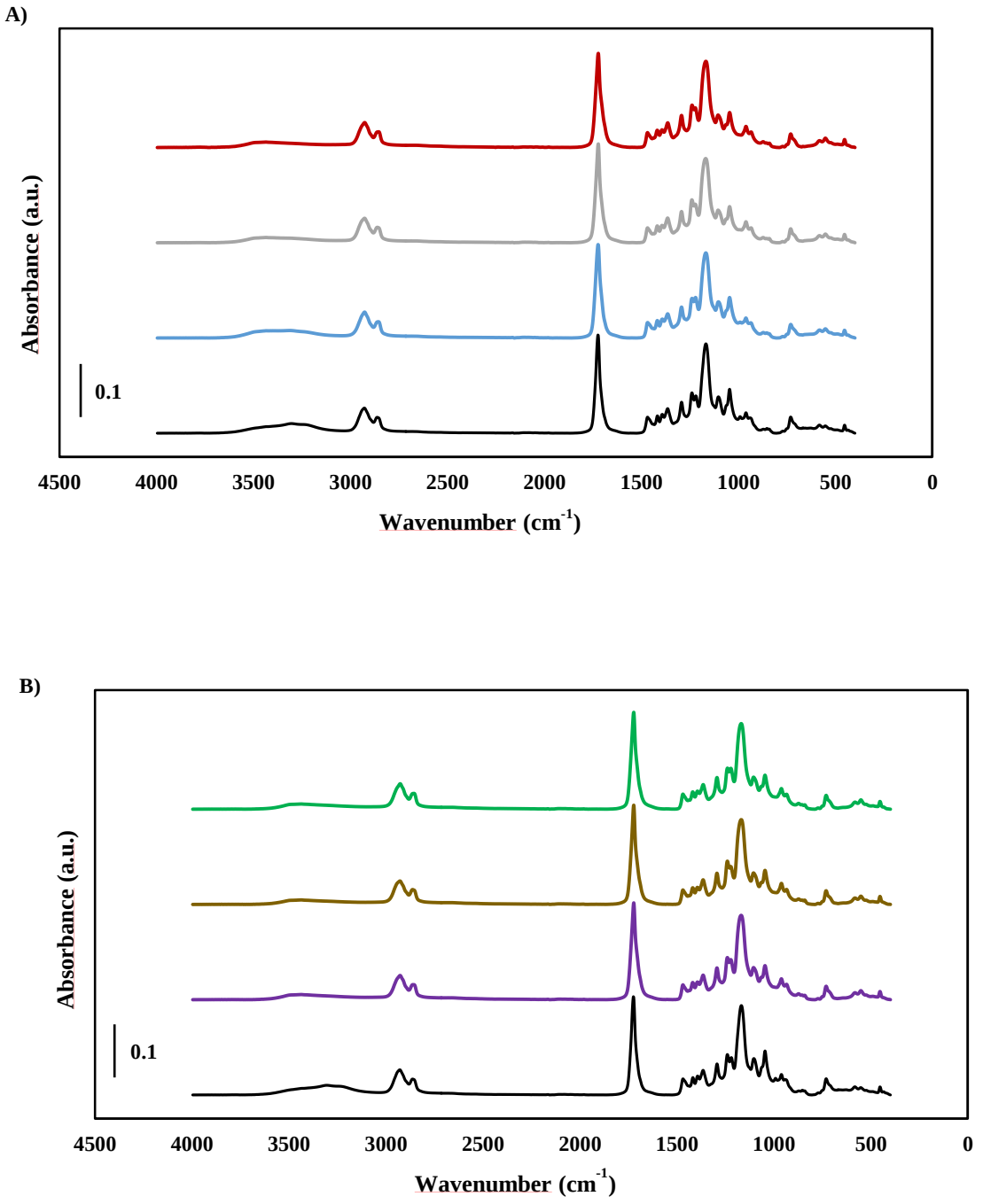

Figure 2.40: FTIR spectra of (A) PCL:PGS (1:1) (▬) and of RLS with: 0.5 (▬), 1.0 (▬), and 5.0 mg/mL (▬) of rapeseed lecithin; (B) FTIR spectra of PCL:PGS (1:1) (▬) and of SLS with: 0.5 (▬), 1.0 (▬), and 5.0 mg/mL (▬) of salmon lecithin.

2.3.5.3. Biocompatibility of RLS and SLS

Figure 2.41 (A and B) refers to the biocompatibility data obtained working with scaffolds functionalized with RL or SL. These preliminary data suggest that there was not difference between the scaffolds functionalized with RL and SL in terms of biocompatibility, but their biocompatibility was different from that presented by the control. In fact, for both the materials, cell viability was comparable to the control only after 5 days of incubation. After 3 days, the cell viability was lower than that of the cells seeded without the scaffold. In the majority of cases, a decrease in cell viability is common working with scaffold in the first hours. It depends on the surface of the material and on the number of cells that are able to attach to them. Only the attached cells will survive and proliferate in the days after. The same trend was observed after 7 days. In general, these data have to be confirmed performing other test with cells such ad lactate dehydrogenase assay (LDH) and DNA quantification.

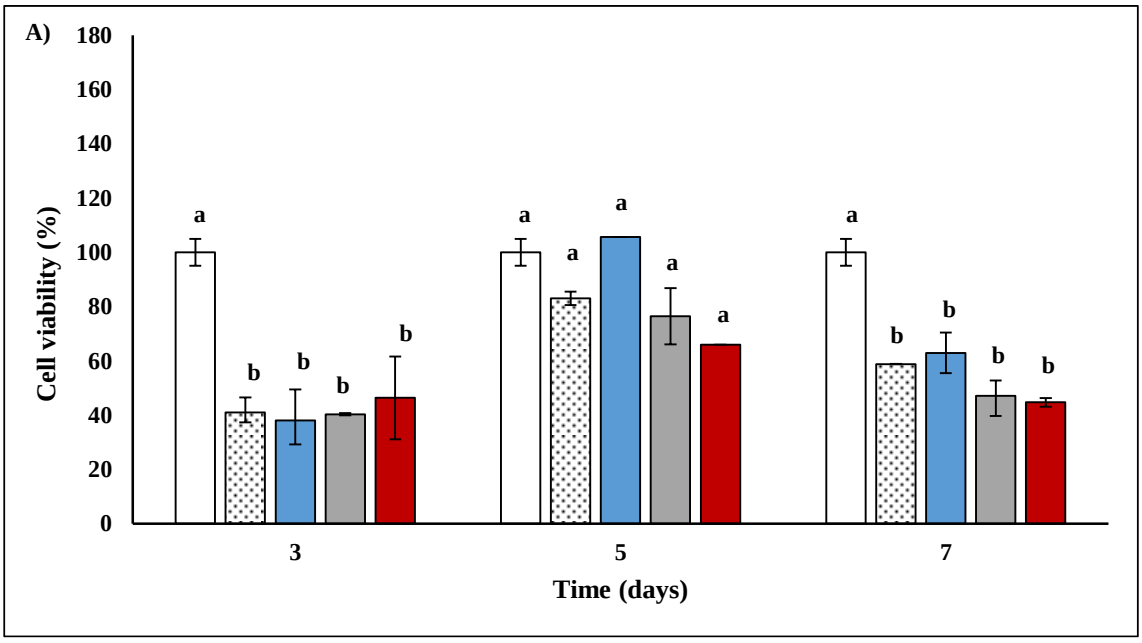

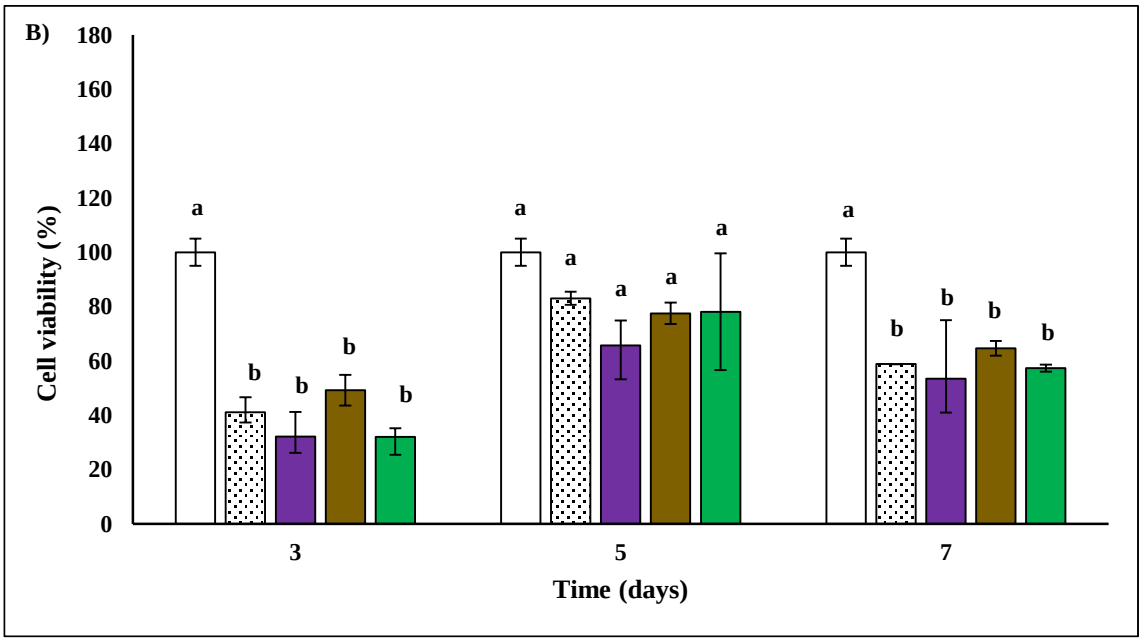

Figure 2.41: cell viability of (A) RLS and (B) SLS at different concentration of lecithin. RLS: ☐ control, ⊡ PCL:PGS (1:1), ■ 0.5, ■ 1.0, and ■ 5.0 mg/mL. SLS: ☐ control, ⊡ PCL:PGS (1:1), ■ 0.5, ■ 1.0, and ■ 5.0 mg/mL.

Results are mean of three measurements ± SD. Different letters do refer to statistically significant differences among results ($p < 0.05$), ANOVA with Tukey's multiple comparison test.

2.3.5.4. Conclusions

The functionalization of PCL:PGS (1:1) scaffolds with rapeseed and salmon lecithin was done in collaboration with University of Nancy and this research activity is still ongoing. Morphological analysis of fibers demonstrated that the presence of rapeseed or salmon lecithin at different concentration did not tamper the microstructure of the electropsun scaffolds. FTIR analysis showed that the fuctionalization with rapeseed and salmon lecithin did not create strong chemical interaction of lecithin with the two polymers used to prepare the scaffolds. Finally, as a result of the first set of experiments, it seemed that hMSC did not appreciate the presence of lecithin in the biomaterial, presenting a reduced cell viability in comparison with the control after 3 and 7 days of contact with the scaffolds.

CHAPTER III

3. DEVELOPMENT OF NANODELIVERY SYSTEMS: CALCIUM CARBONATE NANOPARTICLES

3.1. INTRODUCTION

Over the last years, several systems to nano-encapsulate bioactive molecules, such as polymeric particles (Soppimath et al., 2001; (Mora-Huertas et al., 2010), nanoliposomes (Mozafari et al., 2008) , nanoemulsion (Lovelyn & Attama, 2011), and mineralized nanoparticles (Boyjoo et al., 2014), have been proposed in the literature. Among them, calcium carbonate-based nanoparticles are considered a good tool for drug delivery nanosystems because of their cost-effectiveness (He et al., 2008), good biocompatibility (Kurapati & Raichur, 2013), the possibility to modulate the particle size acting on the chemical composition (Lauth et al., 2014), and the capability to load a wide range of molecules (Wang et al., 2010). One of the most common approaches to confine biological compounds in calcium carbonate ($CaCO_3$) particles is complex coacervation. In general, coacervation is defined as liquid/liquid phase separation of colloids into a two-phase system. Simple coacervation consists of a partial desolvation of biomolecules (Nicolas et al., 2013) while complex coacervation presumes that at least one component is a charged colloid (e.g. poly (acrylic) acid), PAANa, that interacts with oppositely charged ions (e.g. Ca^{2+}) (Kaempfe et al., 2013). Nowadays, another goal of innovative drug therapy protocols is to control the release of drugs at the therapeutically optimal dose regimen directly into the tissue/organ where they are needed. For this purpose, $CaCO_3$ nanoparticles have been considered a good template for the electrostatic self-assembling layer-by-layer (LbL) technique. This method exploits the alternate deposition of positively charged (e.g. chitosan, poly-L-arginine) and negatively charged polymers (e.g. dextran sulphate, poly-γ-glutammate) in order to fabricate nanostructured films enveloping nanoparticles (Ariga et al., 2011). Concerning the drug delivery systems, the LbL-based particles confine active agents increasing both their stability and that of the nanoparticles on which they are deposited and inducing a more sustained release of the encapsulated drugs (Johnston et al., 2006). Additionally, the LbL technique introduces the possibility to immobilize guidance molecules, such as receptors and antibodies, at the outer surface of the shell architecture. In immunotherapy, antibodies are able to recognize and to drive drug-loaded nanoparticles to the

pathological site. In fact, they are an important class of targeting molecules, as they exhibit high specificity and selectivity for cellular antigens. The presence of targeting molecules on polyelectrolyte layers can be achieved both by noncovalent and covalent attachment to the surface. Working with charged polymers makes it possible to functionalize the particles with antibodies operating with electrostatic interactions (Kamphuis et al., 2010). Thus, multilayered immune-nanoparticles are perfect candidates for the construction of site-selective drug delivery/release systems. Although cancer therapy is the main target of drug delivery carriers, recently they have been evaluated for the treatment of different degenerative diseases, such as cardiovascular diseases. In fact, from a pharmacological point of view, this nano-sized system gets into the hematic flow and it is guided by the antibodies to the pathological site, such as an atherosclerotic plaque.

3.2.MATERIALS AND METHODS

In this section, materials and methods used during the research activity concerning the encapsulation of bioactive compounds (proteins and polyphenols) in calcium carbonate ($CaCO_3$) nanoparticles are presented. In details, after a short section on chemicals, the materials and the methods used to synthetize and to characterize this nanosystem are reported.

3.2.1. Chemicals

Poly (acrylic acid) sodium salt (PAANa, Mw = 8000 g/mol, 45 % in water), poly-L-arginine hydrochloride (Mw = 15000-70000 g/mol), chitosan (medium Mw), dextran sulfate sodium salt (average Mw = 9000-20000 g/mol), bovine serum albumin (BSA), standard polyphenols (tyrosol, caffeic, vanillic and *p*-coumaric acid), calcium chloride ($CaCl_2$, purity = 97 %), sodium carbonate (Na_2CO_3, purity ≥ 99.5 %), sodium chloride (NaCl), ethylenediaminetetraacetic acid (EDTA), Folin-Ciocalteu reagent, absolute ethanol, methanol, acetic acid, and Dulbecco's phosphate-buffered saline (DPBS, pH = 7.4) were purchased from Sigma-Aldrich (St. Louis, MO, USA).

Water used for the preparation of solutions and washing operations was purified by Milli-Q® system (Millipore, Molsheim, France).

3.2.2. Cell mediums and reagents

Human endothelial cell line EA. hy 926 were used for the experimentation. They were cultivated in Dulbecco's Modified Eagle Medium (DMEM) high glucose with L-glutamine (Euroclone, Milan, Italy) with the addition of 10 % of fetal bovine serum (v/v) (Carlo Erba, Milan, Italy) and penicillin/streptomicin 1 % (v/v) (Ge Healthcare, Pasching, Austria). Cells were collected and grown in an incubator at 37°C and 5 % CO_2 and culture medium was changed every 3 days of cultivation. Trypsin-EDTA was purchased from Carlo Erba (Milan, Italy), 3-(4, 5-dimethylthiazol-2-yl)-5-(3-carboxymethoxy-phenyl)-2-(4-sulfophenil)-2H-tetrazolium) (MTS) from Promega (Madison, WI, USA) and TNFα from Biovision Inc. (Milpitas, CA, USA) and Instant ELISA immunoassay for the detection of IL-6 from Bender MedSystems (Vienna, Austria).

ENCAPSULATION OF BOVINE SERUM ALBUMIN IN CALCIUM CARBONATE PARTICLES

3.2.3. Synthesis of calcium carbonate nanoparticles incorporating bovine serum albumin

Calcium carbonate ($CaCO_3$) nanoparticles were synthesized via a combination of complex coacervation and mineralization method, as described by Lauth et al., (2014). Briefly, 4 mL of PAANa aqueous solution with two different final concentrations (700 and 1900 mg/mL) were each mixed with an equal volume of 24 mmol/L of $CaCl_2$ solution and maintained under agitation at 900 rpm for 1 min using a magnetic stirrer (Falc Instruments, Treviglio, Italy). After the complexation time between Ca^{2+} ions and PAANa, 4 mL of a 12 mmol/L Na_2CO_3 solution was added with 4 mL of the previous one. Na_2CO_3 was added to the mix in order to stabilize the droplets by forming fully mineralized $CaCO_3$ nanoparticles. The samples were then centrifuged at 16 500 × g for 5 min (centrifuge Hettich Rotina 35 R, Tuttlingen, Germany). The obtained nanoparticles were then washed three times with water with the aim of removing the uncapsulated BSA and the excess of PAANa and freeze dried (freeze dryer Christ Alpha 1–2 LD_{plus}, Osterode am Harz, Germany) for 24 hours. The lyophilized nanoparticles were stored at room temperature until analyses were performed. To prepare protein-loaded nanoparticles, BSA, at a final concentration of 550 mg/mL, was directly dispersed in the aqueous solution prior to the addition of PAANa and $CaCl_2$. These nanoparticles were used even to functionalize the scaffold (nanoparticles-functionalized polymeric scaffold, NS), Section 2.3.4.

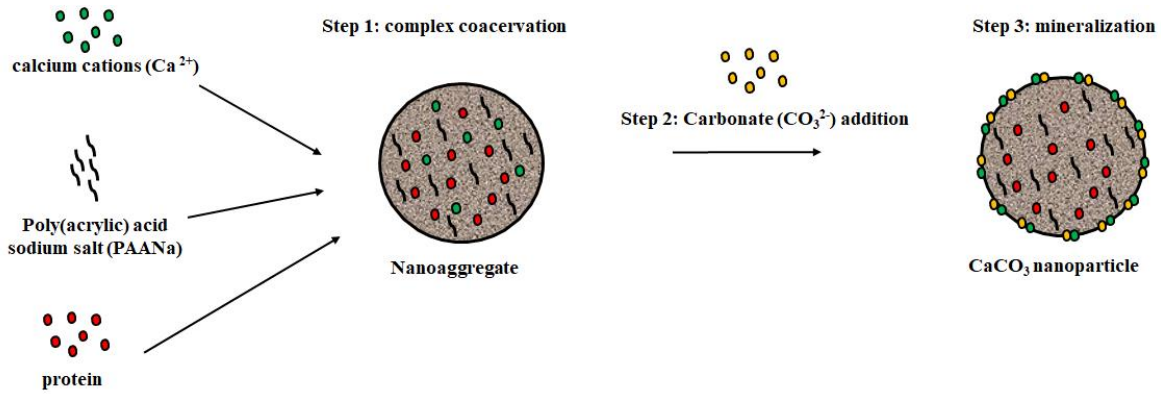

Figure 3.1: schematic representation of $CaCO_3$ nanoparticles synthesis.

3.2.4. Scanning Electron Microscopy (SEM) analysis

To obtain a morphological analysis of the particles, the samples were prepared by putting a small drop onto a glass slide at room temperature for 12 hours allowing the complete evaporation of the water. These glass slides were then metallized with gold by using a Polaron SEM coating system and $CaCO_3$ particle morphology was observed with a scanning electron microscope (SEM Hitachi 2500, Tokyo, Japan). Particle diameters were measured on SEM images using GNU Image Manipulation Program (GIMP) v. 2.8 software in at least three images of each sample. In order to obtain a meaningful statistical value for every image, at least 20 particle diameters were taken into account.

3.2.5. Transmission Electron Microscopy (TEM) analysis

TEM was used to investigate the nanostructure of $CaCO_3$ particles with a negative staining method. Samples were diluted 10-fold with ultrapure water in order to decrease the concentration of the particles. An equal volume of ammonium molybdate solution (2 %, w/v) and of the samples were put together for 3 minutes at room temperature. Then, this solution was dropped on a Formvar-carbon coated copper grid (8200 mesh, 3 mm diameter HF 36) for 5 minutes. Filters papers was used to drawn off the excess of liquid. The grid was dried at room temperature and micrographs were collected using a Philips CM Transimission Electrone Microscope operating at 200 kV (Colas et al., 2007).

3.2.6. Entrapment efficiency of bovine serum albumin in $CaCO_3$ nanoparticles

The amount of BSA entrapped in the $CaCO_3$ nanoparticles was evaluated separating unentrapped BSA from nanoparticles by centrifuging them at 16 060 × g for 5 minutes for three times. All the supernatants were collected and the concentration of BSA was determined through spectrophotometric analysis using BCA assay. When the sample were too diluted, it was necessary to freeze dried them to concentrate the protein before registering absorbance. At the end of the three centrifugation, the pellet was treated with EDTA that induced a total breakage of the $CaCO_3$ nanoparticles. As a consequence of that, it was possible to detect with BCA assay the concentration of encapsulated BSA.

BSA entrapment and loading efficiency were calculated as reported by Papadimitriou & Bikiaris (2009)

$$\text{BSA entrapment efficiency (\%)} = \frac{(weight\ of\ BSA\ in\ nanoparticles)}{(weight\ of\ BSA\ fed\ initially)} \times 100 \qquad \text{(Equation 3.1)}$$

$$\text{BSA loading (\%)} = \frac{weight\ of\ BSA\ in\ nanoparticles}{weight\ of\ nanoparticles} \times 100 \qquad \text{(Equation 3.2)}$$

3.2.7. Synthesis of multilayered $CaCO_3$ nanoparticles, immobilization and detection of anti-rabbit IgG

In order to obtain ultrathin films covering $CaCO_3$ nanoparticles the Layer-by-Layer (LbL) electrostatic self-assembly technique was adopted, as reported by Paini et al., (2015 A) in which the LbL assembly of chitosan/dextran was confirmed by Quartz Crystal Microbalance with dissipation monitoring (QCM-D) analysis (see Section 3.3.14). 20 mg of nanoparticles was dispersed in 1 mL of each polyelectrolyte solution (0.5 mg/mL in pure acidified water at pH = 5) and shaken for 15 minutes on a laboratory shaker (Falc Instruments, Treviglio, Italy). The shell assembly started with the deposition of positively charged chitosan. Then the samples were centrifuged at 16060 × g for 5 minutes (centrifuge Heraeus Instruments, Osterode am Harz, Germany) and the supernatant was separated from the precipitated nanoparticles. The particles were washed centrifuging them three times in acidified water at the same conditions reported above. This procedure was repeated until the multilayered structure was completed. The obtained multilayered nanoparticles were then rinsed by pure water. In the second part of the research chitosan was replaced by poly-L-arginine. This second polycation was chosen for its better solubility in NaCl 0.15 M (0.5 mg/mL), avoiding to use acetic acid and continuous stirring overnight necessary in the case of chitosan. The entire shell architecture was (poly-L-arginine/dextran)$_2$/poly-L-arginine.

At the end of the multilayers deposition procedure, 1.95 mg of horseradish peroxidase-linked anti-rabbit IgG (HRP-linked IgG) (Cell Signaling Technology, Danvers, MA, USA) was added to the $CaCO_3$ nanoparticles, shaken for 1 h at room temperature, centrifuged as described earlier, and washed four times (Habibi et al., 2011). The resulting shell architecture was (chitosan/dextran)$_2$/chitosan/anti-IgG. After that, 5 mL of nanoparticles with immobilized antibody was spotted onto a nitrocellulose membrane (Ge Healthcare, Piscataway, NJ, USA). On the same membrane an equal volume of multilayered nanoparticles without antibody immobilization was spotted as negative control. The samples were dried for few minutes at room temperature, washed with approximately 20 mL of phosphate-buffered saline (PBS) and visualized by ECL chemiluminescence assay (Merck Millipore, Darmstadt, Germany) using a UVItec system (Cambridge, UK).

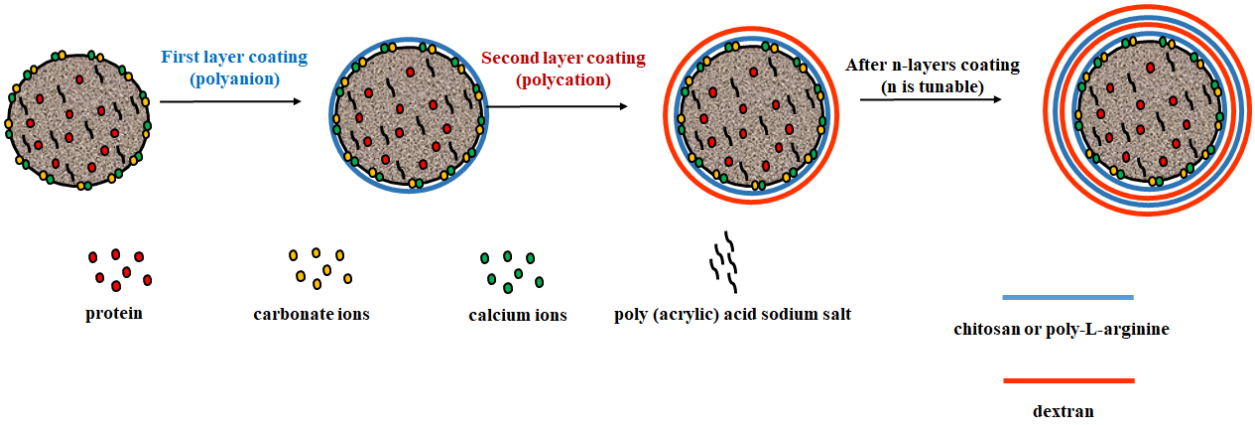

Figure 3.2: schematic representation of LbL deposition on $CaCO_3$ nanoparticles.

3.2.8. BSA release from nanoparticles

To investigate the release behaviour of BSA, 20 mg of both multilayered and non-multilayered $CaCO_3$ nanoparticles were resuspended in 550 mL of PBS at pH = 7.4 and maintained at 37 °C (incubator Heraeus, Hanau, Germany) until 72 hours were reached. At different time-points (2, 3, 4, 8, 24, 48, and 72 h), the samples were centrifuged with the same centrifuge described earlier and 350 mL of the supernatant was collected and replaced with an equal amount of fresh PBS. Released BSA was quantified by the bicinchoninic acid assay (Novagen, EMD Chemicals Inc., CA, USA) at 562 nm using a Biophotometer (Eppendorf, Hamburg, Germany).

3.2.9. Mathematical models for BSA release from particles

In order to evaluate if the release of BSA from multilayered and non-multilayered nanoparticles showed a different kinetic, different mathematical models were applied to the experimental data:

1) first order model: when the release of the drug from the particles follows a first order kinetic, it can be expressed by the equation:

$$\frac{dC_A V}{dt} = kA\,(C_{Ae} - C_A) \qquad \text{(Equation 3.3)}$$

where C_{Ae} is the concentration at $t \to \infty$ and C_A is the concentration at time t.

Considering that: $a = \frac{A}{V}$, where A is the surface of solid/liquid interface and V is the volume of the medium used during the release studies, the equation will be:

$$\frac{dC_A}{dt} = k \cdot a\,(C_{Ae} - C_A)$$

$$\frac{dC_A}{(C_{Ae} - C_A)} = k \cdot a\,dt$$

$$\frac{-d\,(C_{Ae} - C_A)}{(C_{Ae} - C_A)} = k \cdot a\,dt$$

that has to be integrated considering the initial conditions:

$t = 0$, $C_A = 0$, $C_{Ae} - C_A = C_{Ae}$

$$-\int_{C_{Ae}}^{C_{Ae}-C_A} \frac{d\,(C_{Ae} - C_A)}{(C_{Ae} - C_A)} = \int_0^t k \cdot a\,dt$$

$$-\ln\left(\frac{C_{Ae} - C_A}{C_{Ae}}\right) = k \cdot a \cdot t$$

$$\frac{C_{Ae} - C_A}{C_{Ae}} = \exp(-k \cdot a \cdot t)$$

$$1 - \frac{C_A}{C_{Ae}} = \exp(-k \cdot a \cdot t)$$

$$\frac{C_A}{C_{Ae}} = (1 - \exp(-k \cdot a \cdot t))$$

$$C_A = C_{Ae}(1 - \exp(-k \cdot a \cdot t)) \qquad \text{(Equation 3.4)}$$

As reported by (Dash et al., 2010), this model can be used to describe the water-soluble drug release in porous matrices.

2) second order model:

$$\frac{dC_A}{dt} = k_{II}\,(C_{Ae} - C_A)^2$$

$$\frac{dC_A}{dt} = k_{II}\,(C_{Ae} - C_A)^2$$

$$\frac{dC_A}{(C_{Ae} - C_A)^2} = k_{II}\, dt$$

$$\frac{-d(C_{Ae} - C_A)}{(C_{Ae} - C_A)^2} = k_{II}\, dt$$

$$\int_{C_{Ae}}^{C_{Ae}-C_A} -(C_{Ae} - C_A)^{-2}\, d\,(C_{Ae} - C_A) = \int_0^t k_{II}\, dt$$

$$\left[\frac{1}{(C_{Ae} - C_{A)}} - \frac{1}{C_{Ae}}\right] = k_{II}\, t$$

$$\frac{C_{Ae}}{{C_{Ae}}^2 - C_{Ae}C_A} = k_{II} \cdot t \qquad \text{(Equation 3.5)}$$

3) Power law: a very simple, but comprehensive, semi-empirical equation to describe drug release from particles is the so-called power law:

$$\frac{M_t}{M_\infty} = kt^n \qquad \text{(Equation 3.6)}$$

where M_t and M_∞ are the absolute cumulative amount of released drug at time t and at infinite time, respectively, k is a constant that takes into account structural and geometric properties of the studied system, and n is a model parameter, indicative of the mechanism of drug release (Siepmann and Peppas, 2001).

3.2.10. *In vitro* cytotoxicity assay

To assess the maximum non-cytotoxic concentrations of multilayered and non-multilayered nanoparticles, the MTS assay (CellTiter 96® AQ_{ueous} One Solution Cell Proliferation Assay, Promega, USA) was performe (Biradar et al., 2011). Briefly, human endothelial EA. hy 926 cells were seeded into a flat-bottom 96 well-plate with a density of 6×10^3 cells/well with complete medium and incubated at 37 °C with 5 % CO_2. Nanoparticles were sterilized by exposing them to UV light for few hours. After 24 hours of cell incubation, multilayered and non-multilayered nanoparticles were added to the medium at different concentrations (40, 80, 160, and 320 μg/mL). After appropriate time intervals (1, 2, 3, and 7 days), 20 mL of 3-(4,5-

dimethylthiazol-2-yl)-5-(3-carboxymethoxyphenyl)-2-(4-sulphophenyl)-2H-tetrazolium (MTS) was added directly to the culture wells and it was bioreduced by cells into formazan. After 1 hour of incubation, the amount of formazan was measured at 492 nm by a plate reader (Microplate Reader Tecan, Männedorf, Switzerland). All experiments were assessed in triplicate and results are expressed as a percentage of the control (100 %).

3.2.11. Cell treatment, zimography for MMP-9 and ELISA for IL-6

To demonstrate the absence of an inflammatory response due to the treatment with multilayered nanoparticles two inflammation-related markers were taken into consideration. One of them was Matrix MetalloProteinase 9 (MMP-9) and interleukin 6 (IL-6). EA. hy 926 endothelial cells (80 % confluence) were set in serum-free medium, pre-treated or not with multilayered nanoparticles at different concentrations (20, 40, 80, 160 μg/mL) for 1 hour and incubated. The cells considered as positive control were treated only with TNF-α (100 ng/mL) and the cells considered as negative control were not-treated. After 24 hours, conditionated media were collected, centrifuged at 13000 rpm for 5 minutes to remove cells and cellular debris and immediately frozen. To detect MMP-9, an equivalent protein amount (estimated by BCA method) from conditionated media were loaded on SDS-acrylamide gel cast with 0.28 % (w/v) gelatine (type A), run at 6/8°C in an ice bath, rinsed twice for 30 minutes in 2.5 % Triton-X-100, incubated for 12 hours at 37°C in 40 mM Tris-HCl, 0.2 M NaCl, 10 mM $CaCl_2$, stained with 0.2 % Coomassie blue in 50 % methanol, 10 % acetic acid and destained in methanol:acetic acid. MMP-9 expression was evaluated by optical densitometry of gelatinolytic bands. IL-6 levels in the conditionated media were measured using an ELISA immunoassay kit according to the manufacturer's instructions (Bender MedSystems, Vienna, Austria).

3.2.12. Hemocompatibility of $CaCO_3$ nanoparticles

The majority of protocols in the targeted therapy involves a direct contact between the vectors and the blood cells. An ideal drug delivery system has to be safe, not inducing the disruption of red cells and the activation of the immune system. For this reason, it is essential to study the hemocompatibility of drug incorporating vectors. In this research hemocompatibility of $CaCO_3$ nanoparticles was studied in terms of hemolysis and blood coagulation. To verify if multilayered nanoparticles were able to induce a damage in the erythrocytes membranes, the whole blood collected from a healthy volunteer by venipuncture was transferred into ethylenediaminetetraacetic acid (EDTA) anticoagulant vacutainer tubes and immediately used for the analysis. The first step consisted in centrifuging 1.0 mL of whole blood at 200 × *g* for 5 minutes, with the aim of separating red blood cells from the serum. Then, erythrocytes were washed three times with NaCl

0.9 % and diluted ten times. Freeze dried nanoparticles were resuspended in an isotonic solution obtaining different concentrations (20, 40, 80,160 μg/mL). One part of the diluted solution was mixed to four parts of the nanoparticles and they were incubated for 2 hours at 37°C. After that, samples were centrifuged and the supernatant was read at 540 nm with the same plate reader described above. To perform the coagulation assay, freeze dried nanoparticles were suspended in PBS at the different concentration mentioned above. One part of the nanoparticles suspension was mixed with ten parts of blood and they were incubated for 1 hour. After the incubation time, they were centrifuged at 2500 × *g* for 10 minutes to induce the sedimentation of blood cells. 100 μL of the supernatant (plasma) was transferred in a water bath at 37°C and the same volume of $CaCl_2$ (0.025 M) was added. Starting from this moment, the coagulation time was registered for each sample.

3.2.13. Confocal microscopy analysis

To study if the endothelial cells were able to internalize the multilayered nanoparticles, confocal microscopy analysis were performed. Briefly, EA. hy 926 were seeded onto glass microscopy slides and after 24 hours nanoparticles were added to the cell culture. After 18 hours of incubation, the cells were washed three times with PBS, fixed with paraformaldehyde (3 % in PBS) for 10 minutes, and washed twice in PBS. To prevent the autofluorescent signal from paraformaldehyde, the slides were treated with NH_4Cl (30 mM) for 10 minutes and then fetal bovine serum (10 % in PBS) to saturate all the aspecific sites. After that, cells were mounted with Mowiol medium on coverslips, and imaged using an Axiovert 200 m SP LSM 500 META confocal laser-scanning microscope (Zeiss, Jena, Germany).

ENCAPSULATION OF ANTIOXIDANTS IN CALCIUM CARBONATE PARTICLES

This part of the research was partially done in collaboration with Doctor Marco Paini during his Ph.D.

3.2.14. Preparation and engineering of calcium carbonate particles by Layer-by-Layer self-assembling technique and release of polyphenols

Calcium carbonate particles were prepared by mixing together calcium chloride ($CaCl_2$) and sodium carbonate (Na_2CO_3). The chemical reaction was the following:

$$CaCl_2 + Na_2CO_3 \rightarrow CaCO_3 + 2NaCl$$

10^8 $CaCO_3$ particles were coated using dextran and chitosan as layers. For each layer, particles were put in contact with the polysaccharide under continuous agitation for 20 minutes. After the deposition of the first layer, the suspension was centrifuged at 800 × g for 5 minutes to separate the excess of polysaccharide. The particles were then washed three times with Milli-Q water. The final shell architecture was $(chitosan/dextran)_4$ or $(chitosan/dextran)_8$. Then the core of the nanoparticles was dissolved using an EDTA solution at a concentration of 0.5 M at pH 7 followed by three washing steps in pure water. As a standard phenolic compounds, a mixture of tyrosol, caffeic, vanillic and *p*-coumaric acid was used. To prepare the loading solution, 2.5 mg were weighted per mL of pure water and of solutions with ethanol:water at different ratios (80:20, 65:35 and 50:50, v/v). Folin-Ciocalteu assay was performed to determine the concentration of these antioxidant in the loading solutions and it was expressed as mg of caffeic acid equivalent (CAE) per mL. Particles with four bilayers were incubated with 35 mL of the loading solution for 24 hours with continuous stirring at 300 rpm in dark conditions. Then, particles were centrifuged (800 × g for 5), and the supernatant was collected and used to calculate the encapsulation efficiency according to the following equation:

$$Entrapment\ efficency\ (\%) = \frac{TPC - C_{sup}}{TPC} \times 100 \qquad \text{(Equation 3.7)}$$

where TPC is total phenolic concentration of the initial solution

C_{sup} is the phenolic concentration after the loading step, both evaluated using Folin-Ciocalteu assay. Briefly, 0.5 mL of Folin-Ciocalteu reagent and 1.0 mL of Na_2CO_3 saturated solution were added to 4.8 mL of deionized water and 0.2 mL of diluted sample. The final volume was adjusted with deionized water and samples were incubated for 60 minutes in dark conditions. Then the absorbances of the samples were read using a UV-Vis spectrophotometer (Lambda 25, Perkin Elmer, Wellesley, USA) at 725 nm. A calibration curve using methanolic solutions of caffeic acid (10-1000 μg/mL) were performed and it is reported in the Figure 3.3.

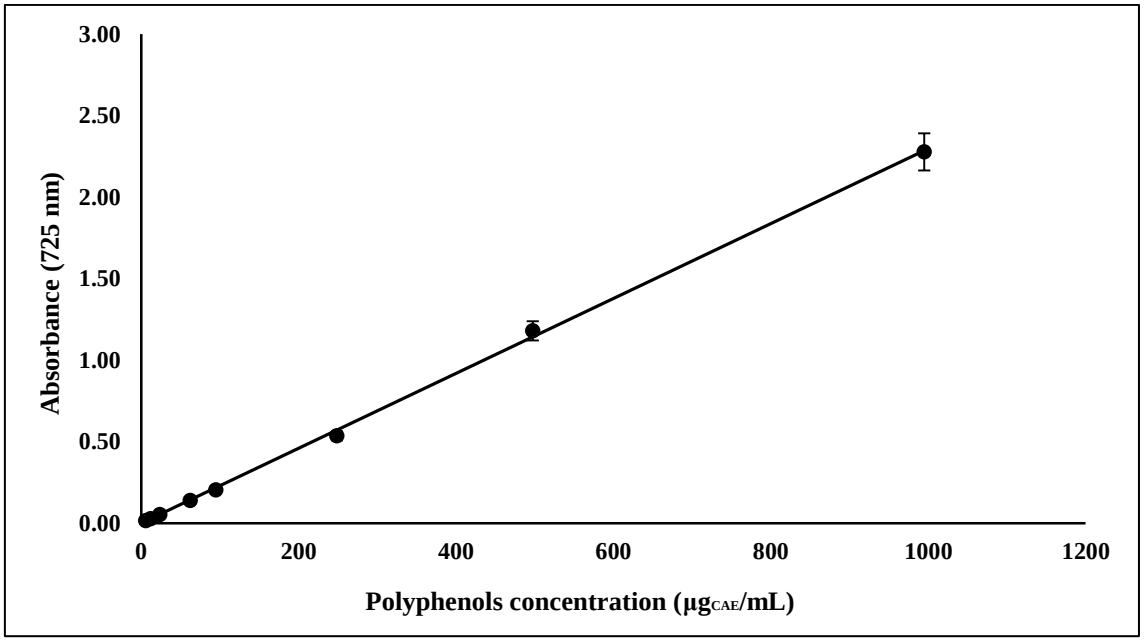

Figure 3.3: calibration curve for the quantification of total polyphenol concentration.

$Abs_{725} = 0.0023 \times TP$ (R^2= 0.993) (Equation 3.8)

where TP is total polyphenol yield expressed as milligrams of CAE.

With the aim of characterizing particles for pharmaceutical purposes, the release of encapsulated polyphenols was monitored during 240 minutes in total. Briefly, loaded particles were centrifuged at 2500 rpm for 5 minutes and then resuspended in acidified deionized water. At 0, 15, 30, 45, 60, 120, 180, and 240 minutes, 20 % of the solution was collected and it was analysed by Folin-Ciocalteu assay with the aim of quantifying the total phenolic compounds released. The concentration of polyphenols was calculated through spectrophotometric analysis and it was expressed as mg_{CAE} per mL of acidified water.

After loading of polyphenols, SEM images, using a Zeiss Supra microscope, were collected.

3.2.15. Quartz crystals microbalance (QCM) with dissipation monitoring

QCM-Z500 (KSV Instruments, Helsinki, Finland) with dissipation monitoring was used to study the build-up of chitosan/dextran multilayers. This technique is widely described in literature (Kannisto et al., 2011) and is usefull to evaluate simultaneously the normalized resonant frequency (Δf) and energy dissipation shifts (ΔD). The quartz crystal with gold plateled polished electrodes is exited at its fundamental frequency (5 MHz) and at the 3rd, 5th, 7th, 9th and 11th overtones (12, 25, 35, 45 and 55 MHz). When a mass is deposited onto the surface of the crystal, there is a decrease of the oscillation frequency. If the deposited mass is

rigidly attached to the crystal, the decrease of the frequency is proportional to the mass and can be calculated using the Sauerbrey's equation (Sauerbrey, 1959) (Equation 3.9)

$$\Delta f = -\frac{2f_0^2}{A\sqrt{\rho_q \mu_q}}\,\Delta m \qquad \text{(Equation 3.9)}$$

in which Δf is the frequency change (Hz), f_0 is the frequency of resonance, A is the crystal area, ρ_q and μ_q represent density and shear modulus of quartz, respectively, and Δm is the mass change. Working with viscoelastic materials, the deposited mass introduces a dissipative energy damping. The QCM-D response of a viscoelastic material can be modeled using a Voigt-based model (Voinova et al., 1998) and the thickness of added layers can be calculated. Before the experiments, the quartz crystal was washed with H_2SO_4 at 150 °C for 20 minutes followed by washing in pure water. A liquid chamber with a volume of 2.0 mL was used during the experiments. Chitosan and dextran solutions were alternatively introduced into the chamber and left in contact with the quartz crystal. Unabsorbed polysaccharides were washed with pure water. Data analysis was done using the QCM Impedance Analysis software (KSV Instruments, version 3.11).

3.2.16. Statistical analysis

All the experiments were performed at least in triplicate and the results were expressed as mean values and standard deviations. The influence of multilayered and non-multilayered $CaCO_3$ nanoparticle concentration on endothelial cells growth was assessed by the analysis of variance (ANOVA) and the Tukey's post hoc test. Multiple comparison of the mean values was performed by the least significant difference test at $p < 0.05$. For data analysis, the Statistica v 8.0 software (StatSoft, Tulsa, OK, USA) was used.

3.3.RESULTS AND DISCUSSION

3.3.1. Influence of PAANa concentration on $CaCO_3$ particle size

Drug carrier morphology is an important factor for the interaction of the nanoparticles with the target cells and therefore this aspect was investigated through SEM and TEM images analysis (Figure 3.4, 3.5, and 3.6). With the aim of investigating the influence of PAANa concentration on the size of the native (without protein) and BSA-loaded $CaCO_3$ nanoparticles, two different concentrations of the polymer (700 and 1900 mg/mL) were studied. It was revealed that synthesized nanoparticles showed a homogeneous spherical geometry using PAANa at both concentrations. In the case of native particles, the final size was highly dependent on the PAANa concentration. Indeed, those obtained with a PAANa concentration of 700 mg/mL (Figure 3.4 A) were evidently larger (diameter of 802.93 ± 103.01 nm) than those produced with a concentration of 1900 mg/mL (diameter of 212.17 ± 60.56 nm) (Figure 3.4 B). In complete accordance with results reported by Lauth et al., (2014), an increase in the polymer concentration caused a reduction in the size of the resulting particles. The electrostatic interaction between carboxylic groups of PAANa and calcium cations in aqueous solution leads to the self-assembly of small complexes, known as complex coacervate droplets, that sequester from the aqueous polymer solution. The coacervate droplets are transformed into stable particle through the addition of carbonate ions in the solution. The size of native coacervates is strictly influenced by the polymer concentration. A higher concentration of PAANa causes an increase in the number of nucleation sites and inhibits the particle growth with a reduction of particle size. In fact, the electrostatic stabilization of coacervate droplets due to high net charge on the droplets surface makes them less prone to aggregation and growth keeping their nanosize (Lauth et al., 2014). BSA-loaded nanoparticles were prepared with a final concentration of the protein equal to 550 mg/mL. The encapsulation of bovine serum albumin (BSA) did not significantly ($p < 0.05$) affect the circular shape at both concentrations of PAANa. In particular, the BSA-loaded particles made with 700 mg/mL (Figure 3.4 C) and 1900 mg/mL of PAANa (Figure 3.4 D) showed the same trend reported for native nanoparticles. An increase in the polymer concentration caused a decrease in the particle diameter. Furthermore, BSA-loaded nanoparticles were smaller for the two studied polymer concentrations, 283.98 ± 78.65 and 151.90 ± 31.66 nm for PAANa at 700 and 1900 mg/mL, respectively. Table 3.1 summarizes average diameters of native and BSA-loaded particles calculated by GNU Image Manipulation Program (GIMP).

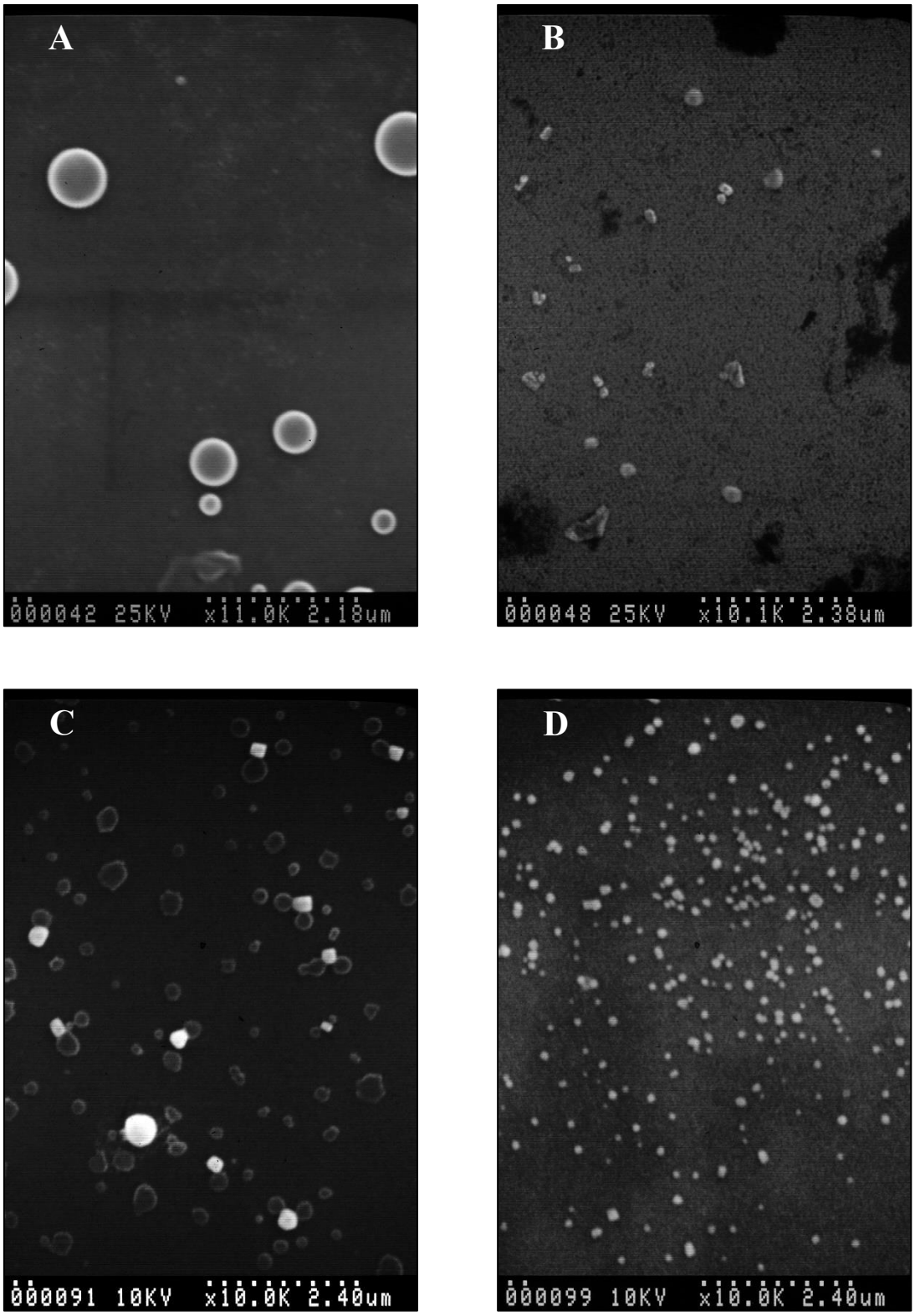

Figure 3.4: representative SEM images of the nanoparticles obtained with different concentrations of PAANa: (A) native nanoparticles with 700 mg/mL, (B) native nanoparticles with 1900 mg/mL, (C) BSA-loaded nanoparticles with 700 mg/mL, and (D) BSA-loaded nanoparticles with 1900 mg/mL.

Table 3.1: average diameters of native and BSA-loaded nanoparticles obtained with 700 and 1900 μg/mL of PAANa.

Sample	Native nanoparticles diameter (nm)	BSA-loaded nanoparticles diameter (nm)
PAANa (700 μg/mL)	802.93 ± 103.01[a]	212.17 ± 60.56[c]
PAANa (1900 μg/mL)	283.98 ± 78.65[b]	151.90 ± 31.66[d]

Results are mean of three measurements ± SD. Different letters do refer to statistically significant differences among results for each column ($p < 0.05$), ANOVA with Tukey's multiple comparison test.

In the case of multilayered nanoparticles, the mean diameter resulted to be higher. This fact was probably due to the presence of chitosan. In fact, it was a sticky polysaccharides and induce the fusion between single nanoparticles (Figure 3.5 B).

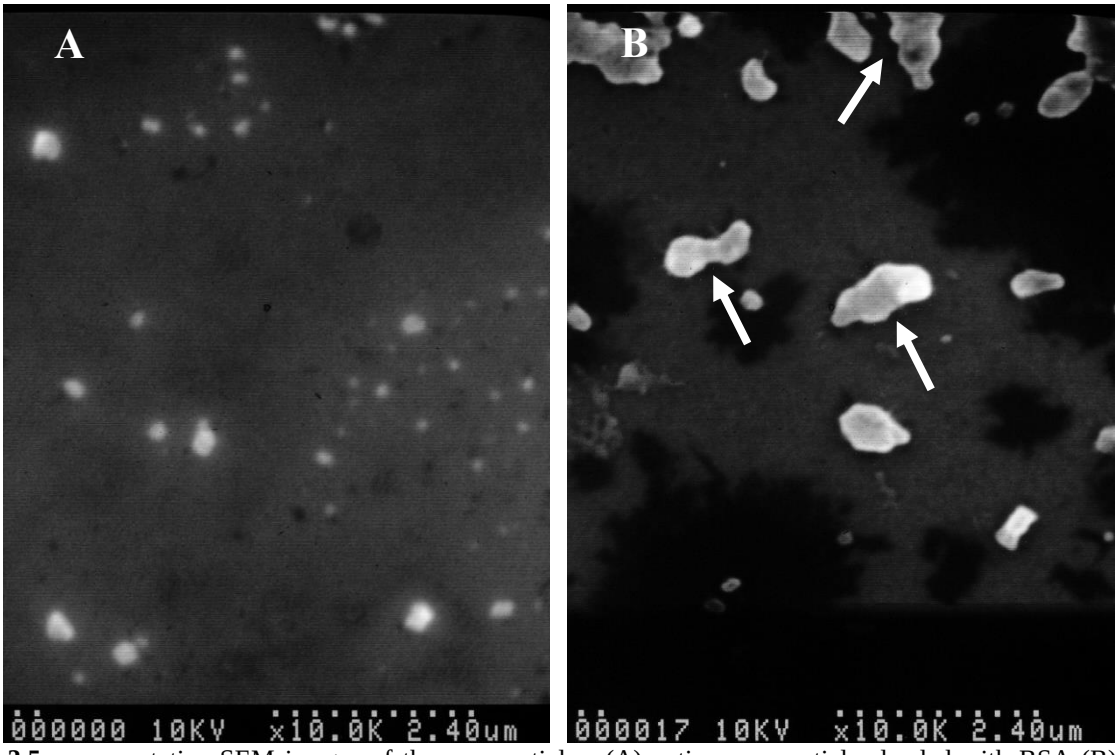

Figure 3.5: representative SEM images of the nanoparticles: (A) native nanoparticles loaded with BSA (B) mutilayered nanoparticles with shell architecture (chitosan/ dextran)$_2$/chitosan. White arrows indicate the fusion between the nanoparticles.

Table 3.2: average diameters of native and nanoparticles with layers of chitosan/dextran.

Samples	Mean diameter (nm)
BSA-loaded nanoparticles (native)	151.90 ± 31.66^a
Immuno-nanoparticles with chitosan/dextran	317.63 ± 50.94^b

Results are mean of three measurements ± SD. Different letters do refer to statistically significant differences among results ($p < 0.05$), ANOVA with Tukey's multiple comparison test.

3.3.2. TEM observations of $CaCO_3$ nanoparticles with layers of chitosan/dextran

The TEM images (Figure 3.6) confirmed that both native nanoparticles (Figures 3.6 A and B) and BSA-loaded nanoparticles (Figures 3.6 C and D) had a well-defined circular shape. Furthermore, it was confirmated the mean dimeter of the studied nanosystem. Both SEM and TEM images showed the low polydispersity of the samples.

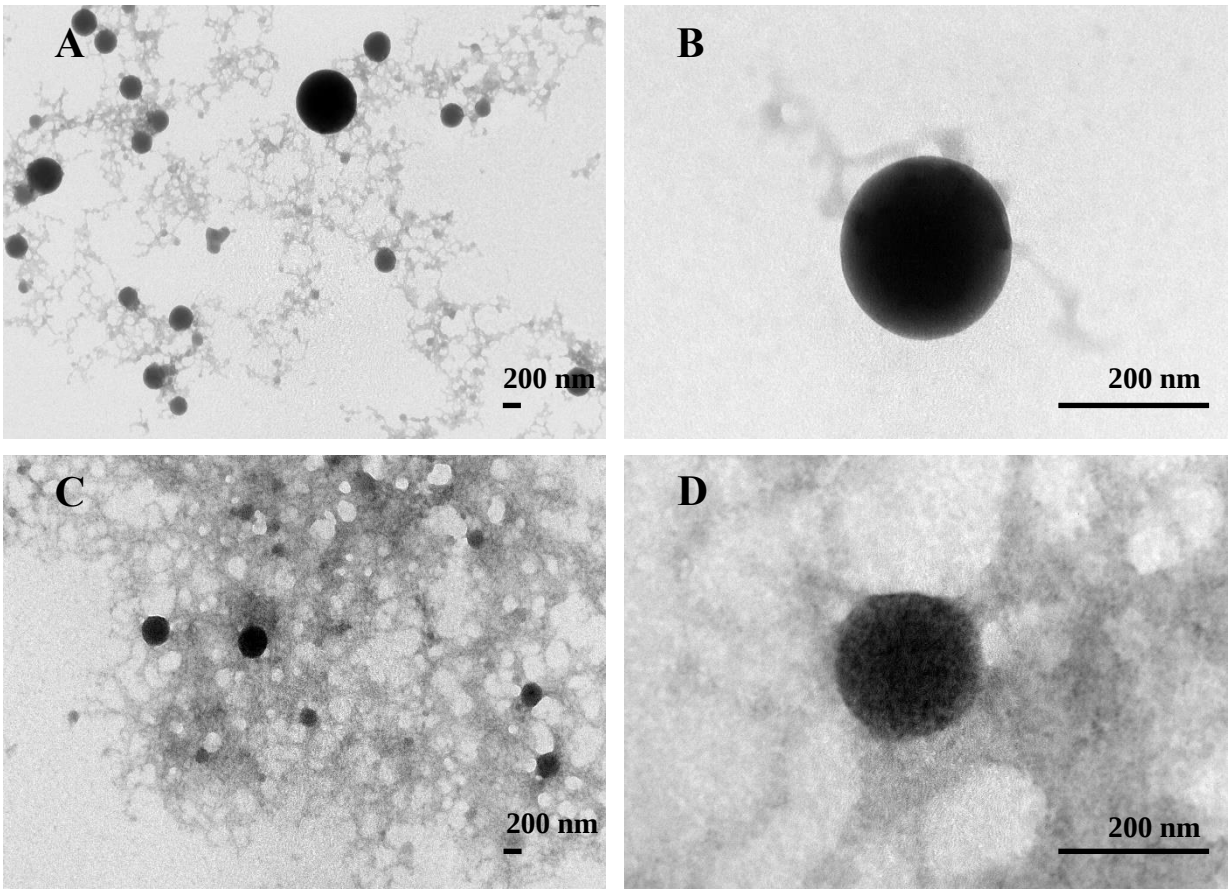

Figure 3.6: representative TEM images of (A and B) native nanoparticles and of (C and D) BSA-loaded nanoparticles obtained with different magnification.

3.3.3. BSA entrapment efficiency and BSA loading

The entrapment efficiency and loading of a protein into a nanosized system are two important parameters to consider when working in the field of drug delivery. To evaluate the amount of BSA encapsulated into $CaCO_3$ nanoparticles, BSA entrapment efficiency and loading were calculated. In accordance with Lauth et al., (2014) a low entrapment efficiency of BSA (9.61 ± 0.75 %) was probably due to the electrostatic repulsion between PAANa and BSA, since both of them are negatively charged at the neutral pH used during the synthesis process. For all the experiments, 2.24 mg of BSA were encapsulated per 20 mg of $CaCO_3$ nanoparticles, resulting in a BSA loading of 11.20 ± 0.87 %.

3.3.4. Detection of chemiluminescent signal from anti-rabbit IgG attached to the particles

Chemiluminescence is the light produced by a chemical reaction. The enzyme horseradish peroxidase (HRP) catalyzes luminol oxidation by hydrogen peroxide and produces a high and durable chemiluminescence (Díaz et al., 1998) Driving molecules, such as antibodies, are an essential component of targeted therapy, since they are able to address the functionalized particles exactly where the bioactive compounds should be released. In our work, we attached HRP linked IgG at the outer layer of the capsules. Figure 3.7 shows the presence or absence of a chemiluminescent signal after the spotting of the particles onto a nitrocellulose membrane. The chemiluminescent signal was noticed only for nanoparticles functionalized with HRP-linked IgG (Figure 3.7 a). Indeed, the clear signal confirmed the immobilization of antibodies on the surface of the particles. No signal was detected in the case of nanoparticles where no antibodies were added during the sample preparation (Figure 3.7 b). This sample has to be considered as a good control of the experiment.

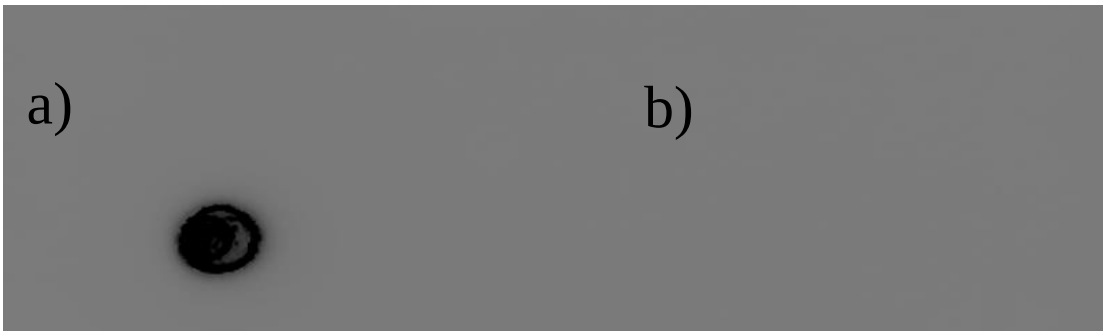

Figure 3.7: chemiluminescent signal from (a) nanoparticles functionalized with HRP-linked IgG and (b) nanoparticles without HRP-linked IgG (control).

3.3.5. Release profile of BSA from particles

Close to the pathological tissue/organ, two different types of therapeutic agents release in the disease site have been described: instant release (burst release) and slow release over a protracted period (sustained release). The former is needed when the capsules are addressed to intracellular uptake (e.g. gene transfection and inhibition of intracellular pathways), whereas the latter is preferred when they should remain extracellular and/or should have constant levels of drug release during time. A sustained release can be achieved by slow diffusion of the molecules through an intact capsule wall, by gradual release of therapeutic molecules through a slowly degrading capsule wall, or through covered nanoparticles with polymeric films (Park et al., 2005; Wood et al., 2005). The cumulative amount of BSA released from multilayered and non-multilayered nanoparticles over a time span of 72 hours is shown in Figure 3.8. Non-multilayered nanoparticles exhibited a faster release compared to the multilayered ones. Indeed, with non-multilayered particles 99.33 ± 4.97 % of the total protein (2241.06 ± 175.86 mg) was released in 2 hours and it remained stable until 72 hours, showing a burst release. It could be assumed that, in this case, BSA is encapsulated close to the surface of the particles and this fact avoids a full dissociation of the carrier. Burst release of the protein could be expected working with inorganic porous carriers such as $CaCO_3$. In the case of multilayered constructs, the cumulative curve was considerably slower and at the end of the experiment the BSA released was 77.34 ± 1.21 % of the entire encapsulated protein (20.17 ± 0.90 mg). The more sustained protein release profile over time from LbL-based nanoparticles could be explained by the fact that the presence of different thin films delayed BSA release. In conclusion, the existence of different layers of chitosan/dextran was essential to avoid BSA burst release.

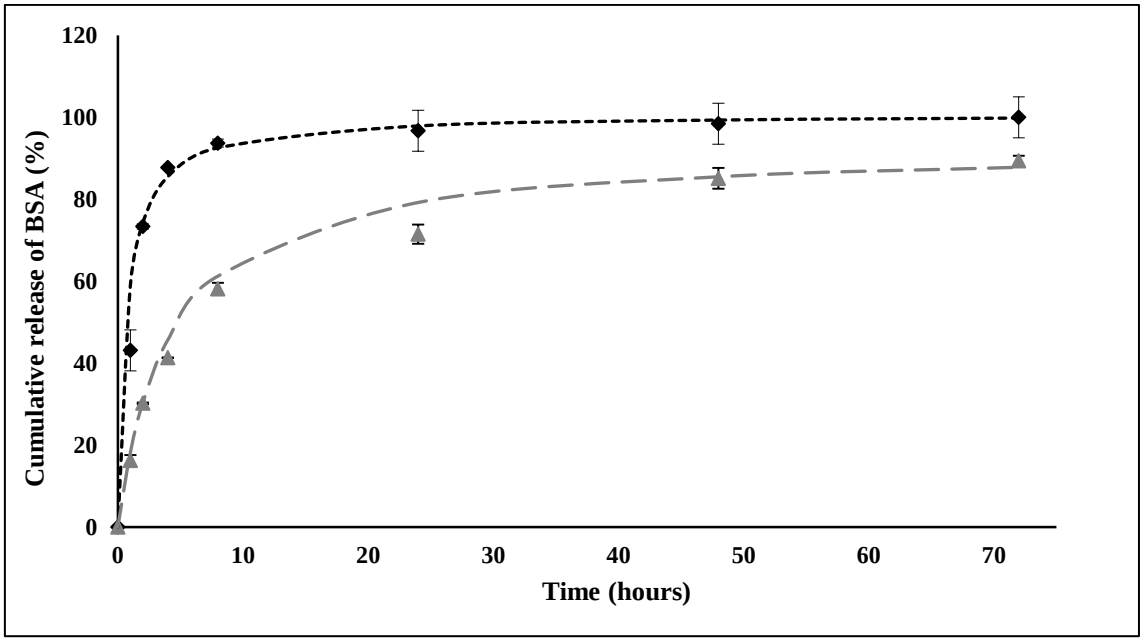

Figure 3.8: release profile of BSA from non-multilayered (♦) and multilayered (▲) nanoparticles. Dashed lines refer to second order model applied to experimental data. (▬ ▬) non-multilayered nanoparticles, (▬ ▬) multilayered nanoparticles.

Table 3.3: kinetic parameters of first, second order, and power law model for BSA release from native and multilayered nanoparticles. k_I refers to first order model, k_{II} to the second order model, and k to power law.

Model	Sample	Model parameters	R^2
First order model	native particles	k_I = 0.3957	0.8508
	multilayered particles	k_I = 0.1176	0.9551
Second order model	native particles	$k_{II} = 3.92 \times 10^{-5}$	0.9998
	multilayered particles	$k_{II} = 1.65 \times 10^{-4}$	0.9941
Power law model	native particles	k = 26796 n = 0.072	0.7883
	multilayered particles	k = 419 n = 0.310	0.9593

Different mathematical models, as described in Section 3.2.9, were applied to experimental data to confirm a different behavior in delivery BSA comparing native and multilayered nanoparticles. Among the studied models, the best fitting was described applying the second order model. It presented a R^2 equal to 0.9941 and 0.9998 for multilayered and native particles, respectively (Table 3.3). Indeed, its k values, ($\boldsymbol{k_{II}}$), highlighted that there was a different trend in releasing BSA. The $\boldsymbol{k_{II}}$ value calculated for the native particles showed a more accelerated release of the drug in comparison with the multilayered counterpart. Experimentally, it was obtained a burst release working with native nanoparticles and a more sustained release working with multilayered particles. In particular, the presence of an architecture of (chitosan/ dextran)$_2$/chitosan delayed significantly the release of the encapsulated protein from the multilayered nanoparticles. Figure 3.8 shows the experimental data and the second order models fitting. The different behavior in releasing BSA from the two nanosystems was found even applying a first order model. Power law model has to be considered the worst applied mathematical model due to its R^2 values.

3.3.6. Cell toxicity using $CaCO_3$ nanoparticles with layers of chitosan/dextran

A possible cytotoxicity of multilayered and non-multilayered $CaCO_3$ nanoparticles was evaluated under *in vitro* conditions, taking into account the effect of nanoparticles on the proliferation of EA. hy926 endothelial cells, through the MTS assay. Untreated cells, as well as cells treated with different concentrations of $CaCO_3$ nanoparticles (40, 80, 160, and 320 μg/mL) for 1, 2, 3 and 7 days, were subjected to the MTS assay for cell viability determination. Figure 4 shows the results obtained, expressed as a percentage value with respect to the control. No statistically significant differences ($p < 0.05$) were noticed between the control and the cells incubated with 40, 80, and 160 μg/mL of non-multilayered nanoparticles. It was possible to highlight that the higher concentration (320 μg/mL) induced a partial cytotoxicity already after 2 days of incubation and cell viability remained constant until 7 days (Figure 3.9 A). Consequently, these results indicated that the maximum non-cytotoxic concentration of non-multilayered nanoparticles amounted to 160 μg/mL. Taking into account data from multilayered nanoparticle experiments, we found that no relevant differences ($p < 0.05$) with the lower concentrations (40 and 80 μg/mL) with respect to the control were noticed. Even in the case of cells treated with multilayered nanoparticles, there was a decrease of cell viability after 2 days, after which it remained stable until the end of the experiment. Furthermore, considering cells treated with the higher concentrations (320 μg/mL), it was noticed that cell viability started to reduce, as in the case of treatment with 160 μg/mL, after 2 days of incubation and drastically decreased in a time-dependent manner (Figure 3.9 B). This cell toxicity can be understood referring to external factor, such as the higher molecular weight of multilayered capsules in comparison to the non-multilayered ones. As a consequence, sedimentation of capsules on the bottom of Petri dishes during cell

culture could determine a competition for space between cells and nanoparticles. This factor could be the one responsible for nanoparticle toxicity, as reported in previous studies (An et al., 2009; Habibi et al., 2011; Liu et al., 2005).

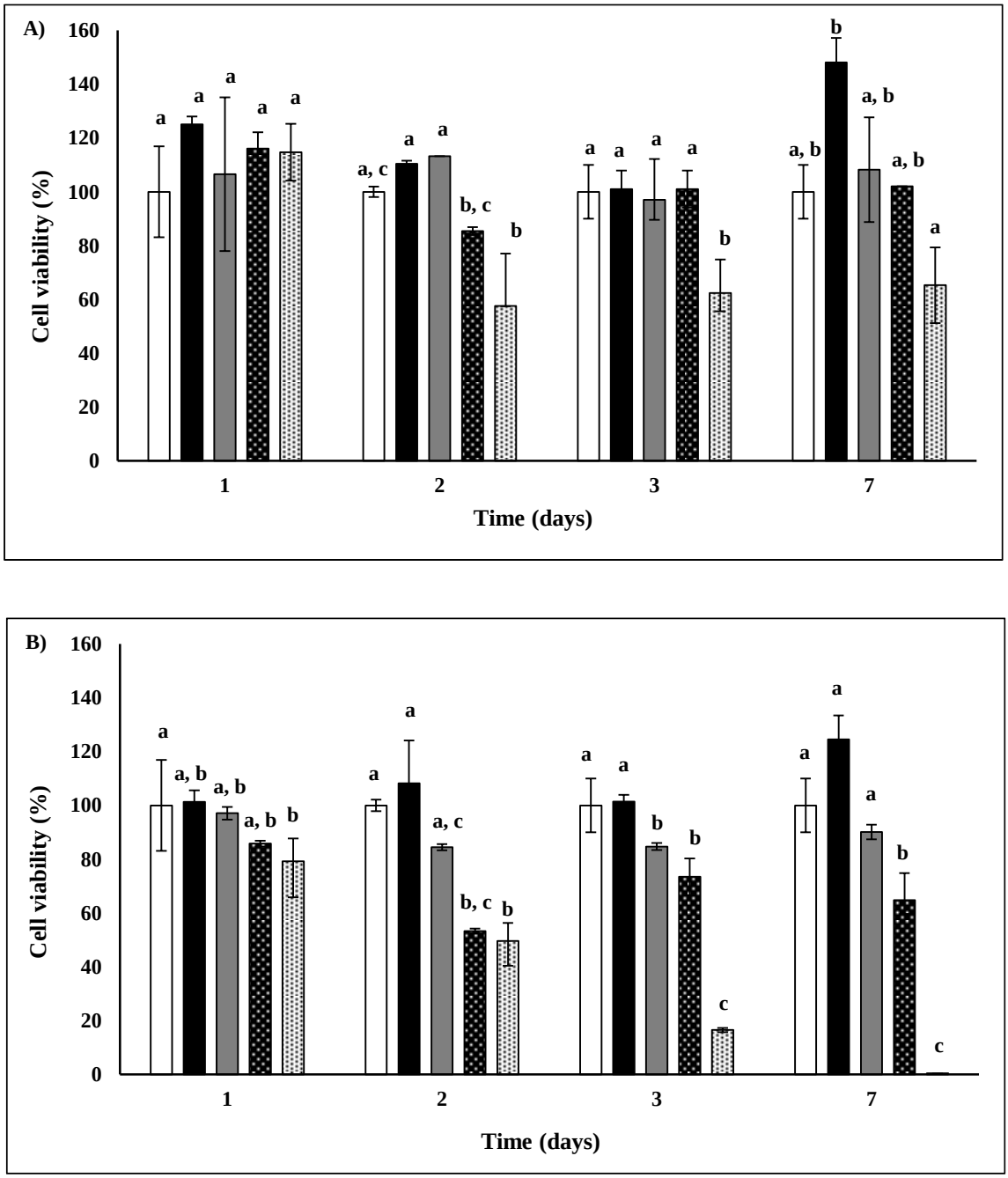

Figure 3.9: cell viability of $CaCO_3$ (A) non-multilayered and (B) multilayered with chitosan/dextran nanoparticles by MTS assay. ☐ control, ■ 40 μg/mL, ■ 80 μg/mL, ■ 160 μg/mL, ▨ 320 μg/mL.

Results are mean of three measurements ± SD. Different letters do refer to statistically significant differences among results ($p < 0.05$), ANOVA with Tukey's multiple comparison tes).

3.3.7. SEM analysis of $CaCO_3$ nanoparticles with layers of poly-L-arginine/dextran

SEM images revealed the presence of fully mineralized $CaCO_3$ nanoparticles with a well-defined round shape. No differences were observed comparing immuno-nanoparticles and native nanoparticles. The presence of multi-layers did not interfere with the entire 3D structure of the nanoparticles. Table shows the mean diameter of native nanoparticles, particles with a shell architecture (chitosan/ dextran)$_2$/chitosan, and particles with a shell architecture (poly-L-arginine/ dextran)$_2$/poly-L-arginine.

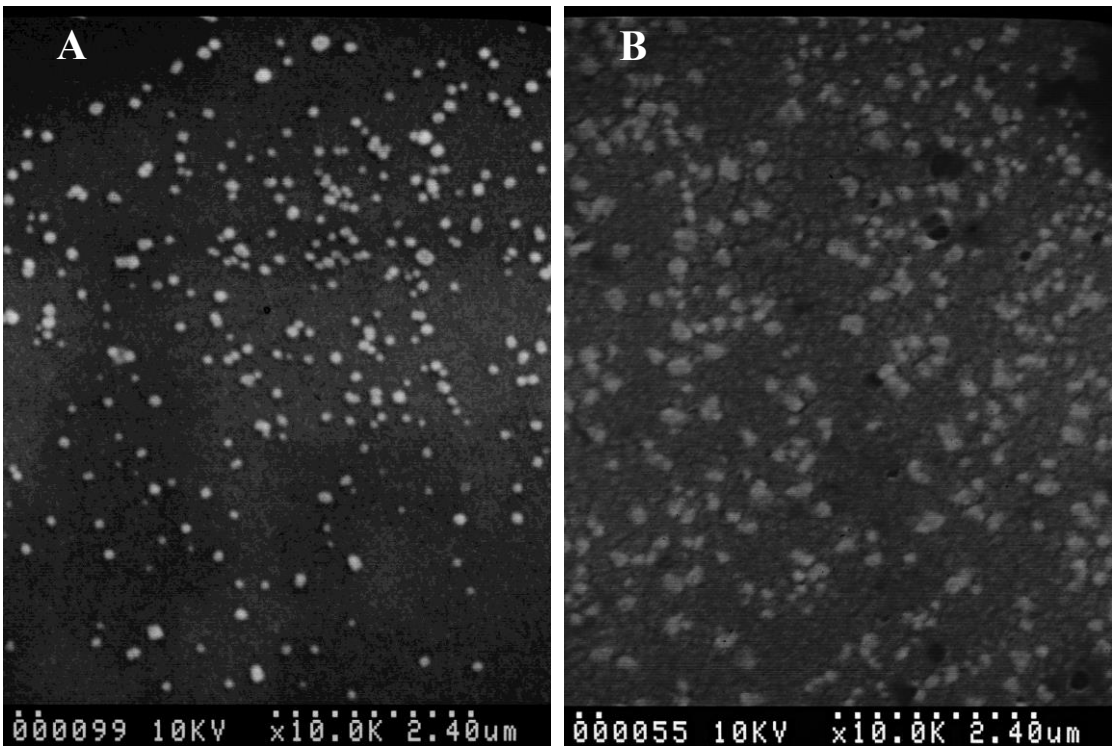

Figure 3.10: representative SEM micrographs of the nanoparticles: (A) native nanoparticles, (B) nanoparticles with shell architecture (poly-L-arginine /dextran)$_2$/ poly-L-arginine.

Table 3.4: average diameters of native and nanoparticles with layers of poly-L-arginine/dextran.

Samples	Mean diameter (nm)
BSA-loaded nanoparticles (native)	151.90 ± 31.66[a]
Immuno-nanoparticles with poly-L-arginine/dextran	194.24 ± 41.99[a]

Results are mean of three measurements ± SD. Different letters do refer to statistically significant differences among results ($p < 0.05$), ANOVA with Tukey's multiple comparison test.

3.3.8. Cell viability using $CaCO_3$ nanoparticles with layers of poly-L-arginine/dextran

One of the most important parameter to take into account when working with biomaterials and nanomaterials is to demonstrate if they are biocompatible when are in contact with the targeted cells. In this case, endothelial cells will be addressed by nanoparticles (Ferrari et al., 2017). As a consequence, the biocompatibility was assessed until three days and for any time no differences were noticed between the control (cells without nanoparticles) and the four different concentration tested (Figure 3.11).

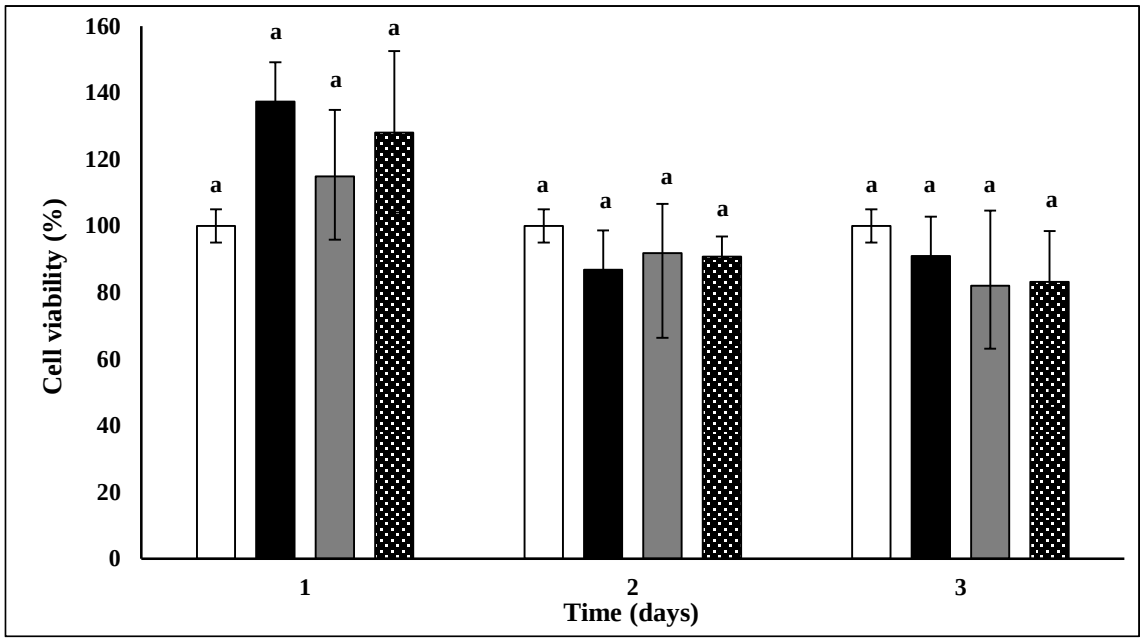

Figure 3.11: cell viability of $CaCO_3$ nanoparticles with layers of poly-L-arginine/dextran by MTS assay. ☐ control, ■ 40 μg/mL, ▒ 80 μg/mL, ▩ 160 μg/mL.

Results are mean of three measurements ± SD. Different letters do refer to statistically significant differences among results ($p < 0.05$), ANOVA with Tukey's multiple comparison test.

3.3.9. Expression of MMP-9 and IL-6 after nanoparticles treatment

Exogenous materials could be provoke a possible inflammation response when injected in the body. To verify if synthetized $CaCO_3$ nanoparticles could be able to induce an inflammatory response, MMP-9 and IL-6 expression was evaluated after 24 hours of incubation with endothelial cells. Figure 3.12 shows an

induction of MMP-9 by TNF α and no expression was registered treating cells with different nanoparticles concentration (20, 40, 80 and 160 μg/mL). No differences regarding MMP-2 expression were noticed.

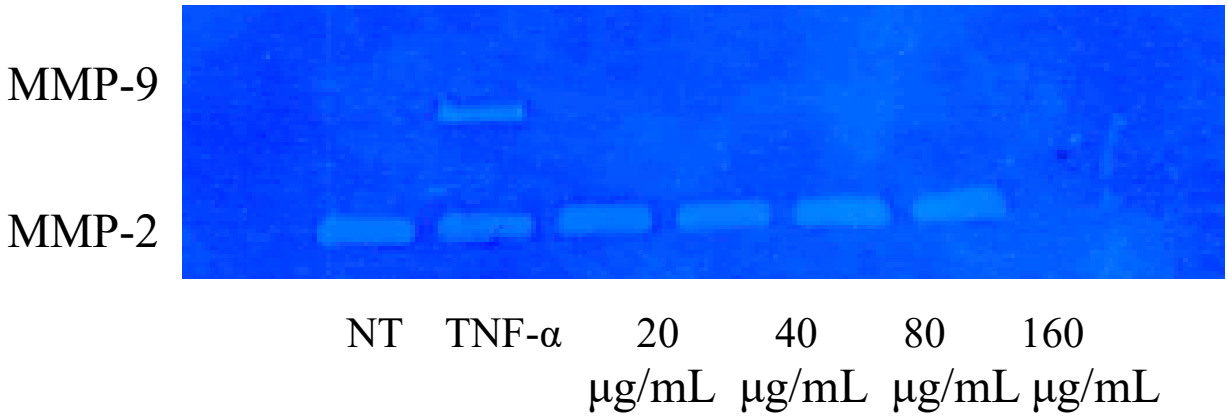

Figure 3.12: gel zymography of MMP-2 and MMP-9 of endothelial cells treated with different concentrations of immunonanoparticles (20, 40, 80 and 160 μg/mL). NT: not-treated; TNF-α: treated with tumor necrosis factor-α.

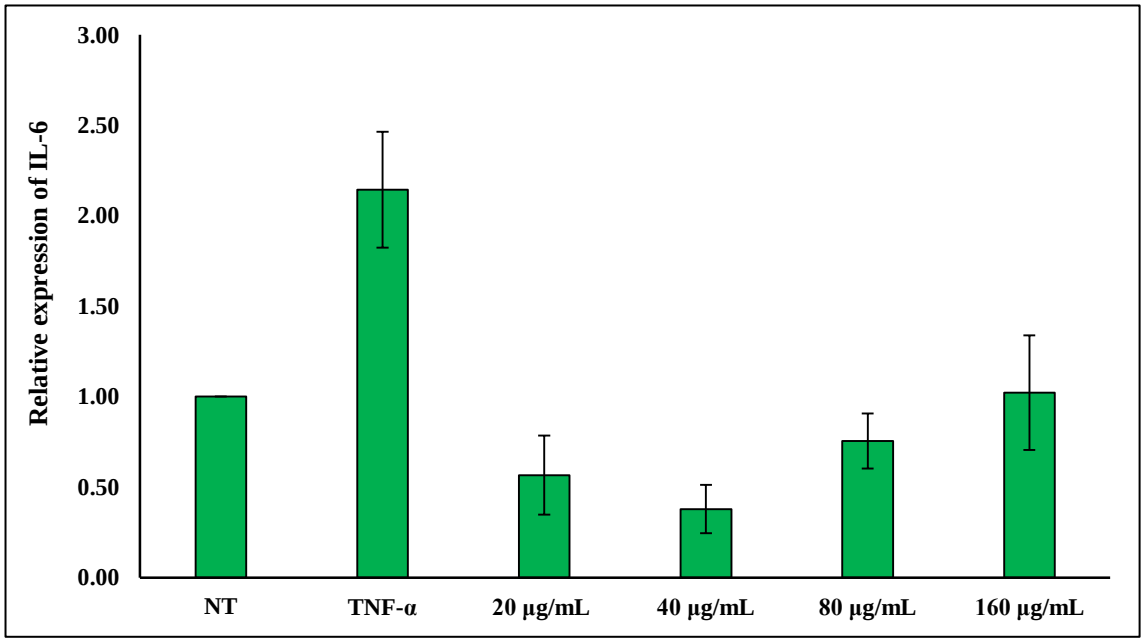

Figure 3.13: relative expression of IL-6 in endothelial cells treated with different concentrations of immunonanoparticles (20, 40, 80 and 160 μg/mL). NT: not-treated; TNF-α: treated with tumor necrosis factor-α. Results are mean of three measurements ± SD.

During inflammation different mediators are released by cells to induce recruitment of leukocytes from blood, their rolling and, finally, their diapedesis in the inflamed tissue. Interleukins are a very large group of molecules involved in the immune system and in the inflammation response. Among them, interleukin 6 (IL-6) is one of the molecule responsible in inducing the expression of acute phase proteins (Gabay, 2006). TNF-α, acting as a pro-inflammatory cytokine, causes a high expression of IL-6 in endothelial cells. The treatment of these cells with the multilayered nanoparticles di not provoke the expression of IL-6 in the culture. In any case, even testing the highest concentration of particles (160 μg/mL), there was not a higher expression of IL-6 in comparison with the control (NT) (Figure 3.13).

3.3.10. Hemocompatibility of nanoparticles

Being an injectable product, a possible hemolysis of the nanoparticles should be considered as an essential factor to validate them biologically. When blood contacts solid material surface, such as inorganic nanocarriers, many physiological reactions such as thrombus formation and red blood cells disruption, can happen. Therefore, hemocompatibility represents one of the most influent parameters to take into consideration working with drug delivery systems (Mayer et al., 2009; Thasneem et al., 2011; Bender et al., 2012; Angelova &Yordanov, 2017). In this work, the hemocompatibility of electrospun $CaCO_3$ nanoparticles was evaluated by hemolysis. In general, materials are classified in non highly hemocompatible (< 5 % hemolysis), hemocompatible (within 10 % hemolysis) and non-hemocompatible (> 20 % hemolysis) (Pal & Pal, 2006). For all the tested concentrations, a hemolysis < 1 was reported (Figure 3.14). The maximum value was reached treating blood with 80 μg/mL but no dose-dependent behaviour was reported.

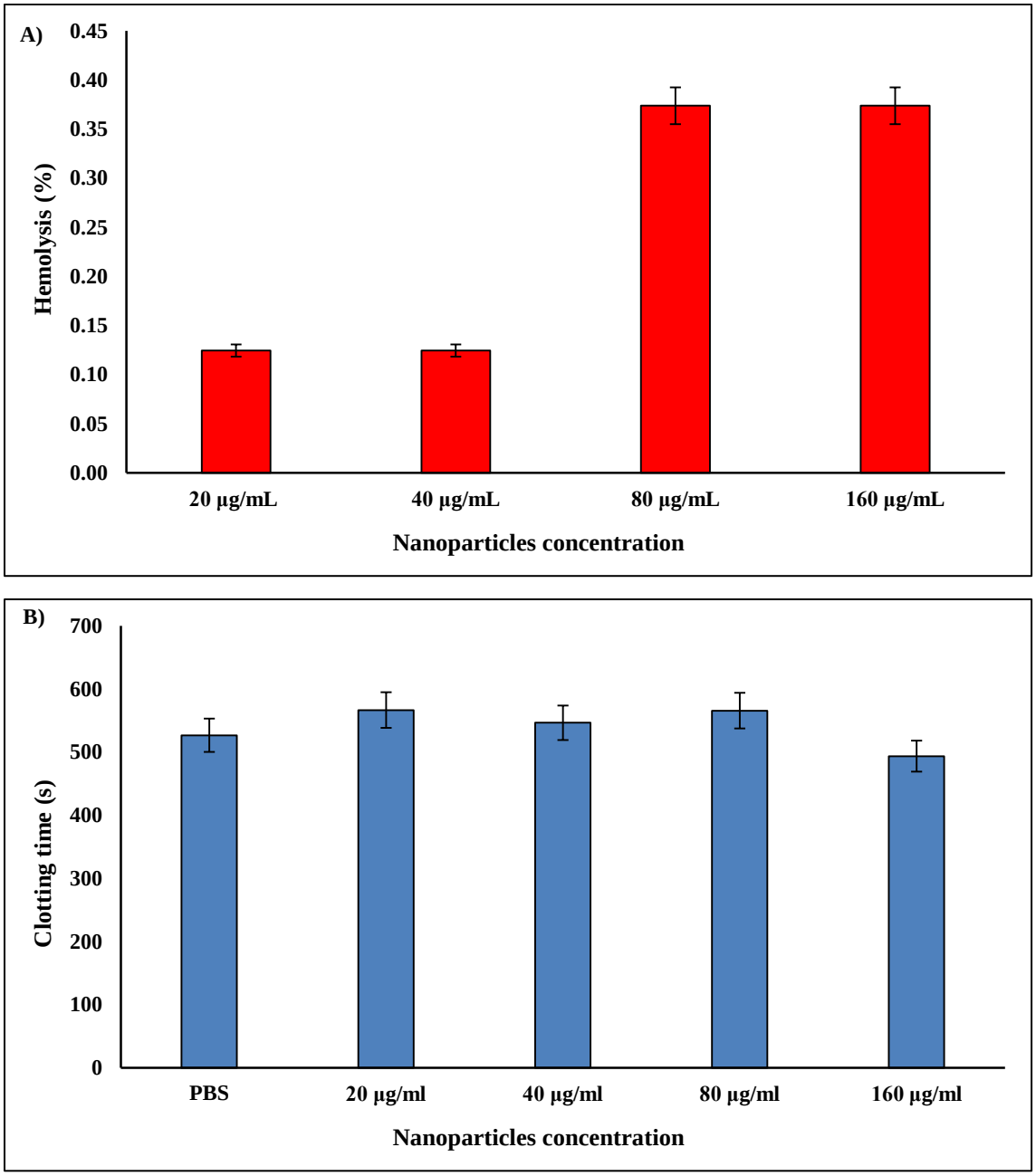

Figure 3.14: (A) hemolysis percentage and (B) clotting time of fresh blood after incubation with different concentration of nanoparticles. Results are mean of three measurements ± SD. PBS: phosphate-buffered saline.

3.3.11. Confocal microscopy analysis

To qualitatively evaluate the up-take of the nanoparticles by endothelial cells, fluorescence microscopy analysis were performed. The fluorescence images of endothelial cells after culture in the media containing

the $CaCO_3$ nanoparticles modified with an IgG linked to a fluorophore are shown in Figure 3.15. Confocal microscopy of the cells exposed to the multilayered nanoparticles demonstrated their presence in the cytoplasm of the cells. The capability of endothelial cells to internalize $CaCO_3$ multilayered nanoparticles, could be useful in drug delivery protocol. In particular, it represents an advantage when the drug encapsulated is represented by a molecule acting on an intracellular molecule. In this case the potential inhibitor of a cytosolic or nuclear molecule could be protect into the nanoparticles before be internalized from the cells. Once into the cell, it could play its therapeutic role. In Figure 3.15, are reported confocal microscopy images before and after washing. The washing step was necessary to remove the particles that were non-specifically in contact with the endothelial cells.

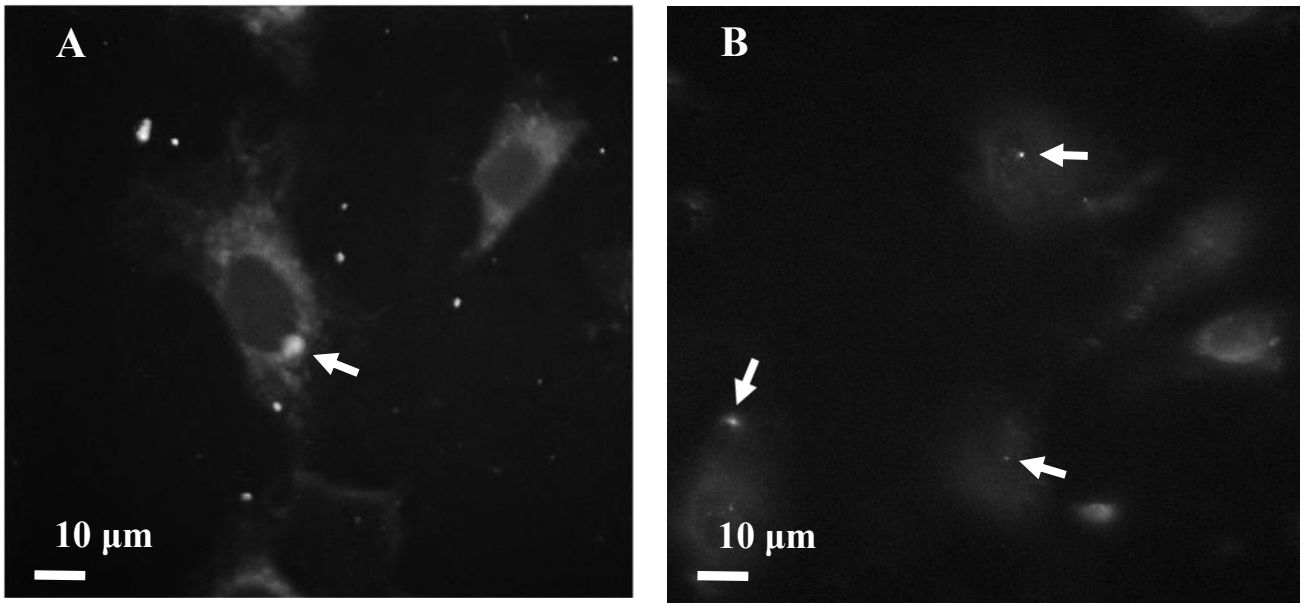

Figure 3.15: fluorescence photographs of phagocytized $CaCO_3$ nanoparticles (A) before and (B) after washing. White arrows indicate phagocytized nanoparticles.

3.3.12. Conclusions

The aim of this part of the work was to define a simple protocol for the synthesis of a delivery nanosystem loaded with BSA, as a model protein to be employed directly where the an ideal therapeutic proteins is needed. In this study, $CaCO_3$ protein-loaded nanoparticles were synthesized via combination of complex coacervation and mineralization. The synthesis process started with the complexation between Ca^{2+} ions, PAANa, and BSA within coacervates droplets, whose size can be tuned by the polymer concentration. In particular, we found that the higher the PAANa concentration, the smaller the diameter of the obtained nanoparticles, allowing us to fabricate particles of 151.9 nm in diameter with 1900 mg/mL of PAANa.

$CaCO_3$ particles proved to be a good template for LbL electrostatic self-assembling technique and multilayered nanoparticles with shell architecture (chitosan/ dextran)$_2$/chitosan were fabricated. BSA release from multilayered and non-multilayered nanoparticles was studied. For the former we described a typical burst release behavior while for the latter we noticed a sustained release during time. The biocompatibility data suggest that non-multilayered particles were well tolerated in comparison to the multilayered ones. In more details, the maximum concentration of non-multilayered nanoparticles that could be employed is twice the concentration of multilayered particles. Based on these results, we can conclude that the present work can be considered a very simple, cost effective, and easy scale up method to synthesize and to functionalize $CaCO_3$ nanoparticles with natural polymeric multilayers and antibodies. In order to increase the biocompatibility of multilayered nanoparticles and with the aim of preventing the fusion phenomenon between nanoparticles, chitosan was replaced with poly-L-arginine. The fully mineralized $CaCO_3$ nanoparticles, even in this case, exhibited spherical morphology and were successfully loaded with BSA. Antibodies were successfully immobilized on the surface of multi-layered nanoparticles These nanocarriers resulted to be biocompatible and hemocompatible at all the tested concentrations (20, 40, 80 and 160 μg/mL). No inflammatory response, in terms of MMP-9 and IL-6 was noticed.

This work was partially published as: "Engineered $CaCO_3$ nanoparticles with targeting activity: a simple approach for a vascular intended drug delivery system". The Canadian Journal of Chemical Engineering 95: 1683-1689, 2017 by **Ferrari P.F.**, Aliakbarian B., Zattera E., Pastorino L., Palombo D., Perego P., partially presented as: "Engineered $CaCO_3$ nanoparticles with targeting activity" at Convegno GRICU 2016, Anacapri, Italy by **Ferrari P.F.**, Aliakbarian B., Zattera E., Pastorino L., Palombo D., Perego P., and partially presented as: "An innovative drug delivery system for atherosclerosis" at the 66th international Congress of the European Society of Cardiovascular and Endovascular Surgery (ESCVS) 2017, Thessaloniki, Greece, by **Ferrari P.F.,** Aliakbarian B., Palombo D., Perego P. It has been awarded the "Young Vascular Award Session" as best oral presentation.

ENCAPSULATION OF POLYPHENOLS IN $CaCO_3$ PARTICLES

This work was the main topic of the Ph.D. thesis of Doctor Marco Paini and it was done in collaboration with him.

Following the same protocol reported for $CaCO_3$ nanoparticles encapsulating albumin, particles with chitosan/dextran layers were synthetized with the aim of entrapping polyphenols. In details, nanostructured capsules were loaded with a mixture of tyrosol, caffeic, vanillic and *p*-coumaric acid. To optimize the loading of these four compounds different ethanol:water ratios for the loading solution were studied. $(dextran/chitosan)_4$ particles were loaded with different loading solutions in which were dissolved the four polyphenols above mentioned, increasing the ethanolic fraction. In fact, it is well known that the solubility of the majority of polyphenols is higher in ethanol in respect with water. (Paini et al., 2016). The total polyphenol concentration of the different loading solution was calculate as reported in Section 3.2.14 and the quantity of the polyphenols entrapped into the particles was evaluated after 120 minutes of incubation.

Table 3.5: total polyphenol concentrations (TPCs, expressed as mg_{CAE}/mL) and amount of polyphenols (in mg_{CAE}) released from nanocapsules (11.3 µL) prepared in solutions with different ethanol:water ratio after 120 min of incubation in water**.**

Ethanol:water ratio (v/v)	**TPC (mg_{CAE}/mL)**	**Polyphenols released (mg_{CAE})**
0:100	5.2 ± 0.9 [a]	8.2 ± 0.1 [a]
20:80	6.6 ± 0.2 [a,b]	8.6 ± 0.1 [b]
35:65	7.9 ± 0.5 [b]	11.5 ± 0.7 [b]
50:50	10.4 ± 0.2 [c]	7.8 ± 1.4 [c]

Results are mean of three measurements ± SD. Different letters do refer to statistically significant differences among results for each column ($p < 0.05$), ANOVA with Tukey's multiple comparison test.

As it is shown in Table 3.5, a complete dissolution of the polyphenols mixture was obtain working with ethanol:water (50:50, v/v) with 10.4 ± 0.2 mg_{CAE}/mL (approximately equal to initial theoretical TPC). It was noticed that an increase in the solubility of polyphenols induced a larger amount of loaded compounds in the particles. A further increase higher than 50 % of ethanol resulted in a decrease in the quantity of released polyphenols. Probably, the presence of a high volume of ethanol induced the formation of large

defect in the shell of the particles. The ethanol:water (35:65, v/v) was selected for all the subsequent analysis because of it maximized the solubility of polyphenols without affecting the structural stability of the particles. Figure 3.16 shows a representative image of one polyphenol particles with shell architecture $(dextran/chitosan)_4$.

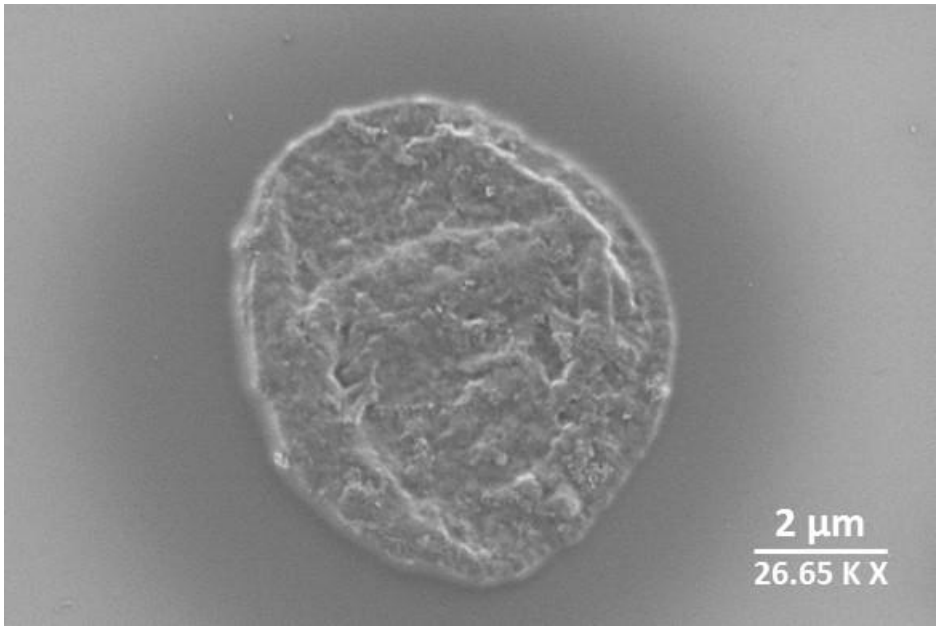

Figure 3.16: representative SEM micrographs of a $(dextran/chitosan)_4$ particle loaded with a polyphenolic solution made of ethanol:water (35:65, v/v).

3.3.13. Entrapment efficiency

The encapsulation efficiency of the nanoparticles loaded in pure water or in ethanol:water (35:65, v/v) was calculated referring to the equation 3.7. In the case of incubation with polyphenols in water, entrapment efficiency was 29.6 ± 2.0 %, whereas in the case of incubation with polyphenols in ethanol:water (35:65. v/v), it increased significantly ($p < 0.05$) to 42.0 ± 0.6 %. This augmented entrapment efficiency could be explained considering the higher solubility of polyphenols in ethanol and the stability of the polysaccharide shell working at this percentage of ethanol.

3.3.14. Release of polyphenols from $CaCO_3$ particles

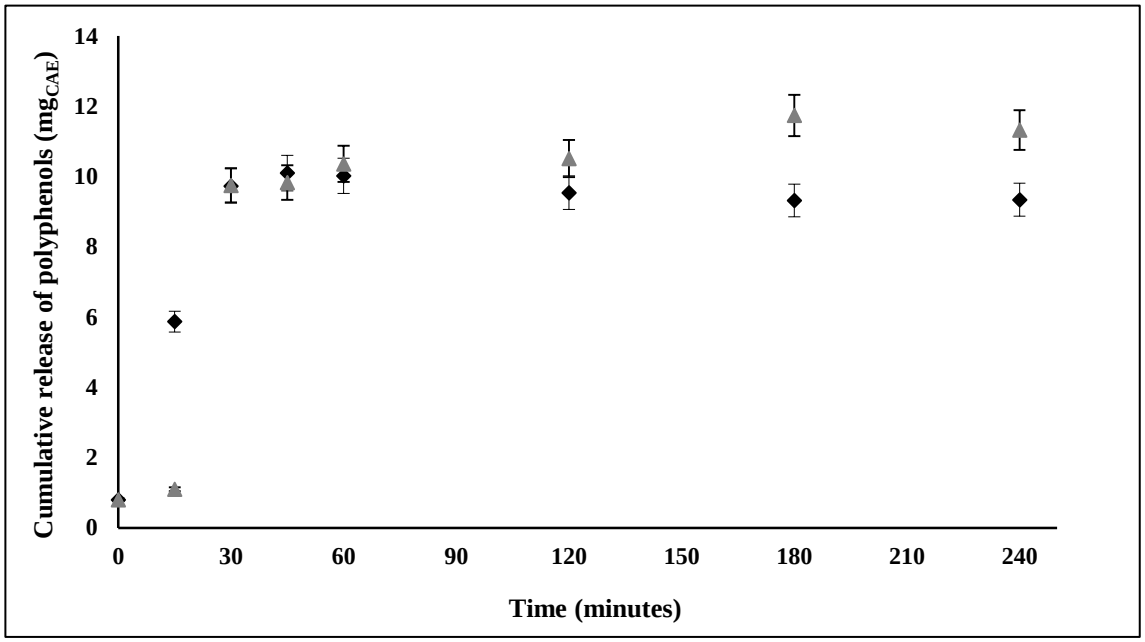

Figure 3.17: release profile of polyphenols from $CaCO_3$ particles prepared with ethanol:water (35:65) (♦) and water (▲) loading solution.

Figure 3.17 shows the release of polyphenols from $CaCO_3$ particles prepared using two different loading solutions, water and ethanol: water (35:65, v/v). Initially, at t_0 the release of polyphenols was not zero. Probably, it was due to the presence of polyphenols on the surface of the particles. After 15 minutes, the release was more evident in the case of polyphenols loaded with ethanol:water (35:65, v/v) in comparison with particles prepared in water. This behavior is to address to a higher solubility of polyphenols in ethanol instead of in water. The synthesis of $CaCO_3$ particles starting from a loading solution of ethanol:water (35:65, v/v), in fact, ensured a better dissolution of polyphenols in the mixture.

3.3.15. Quartz crystal microbalance with dissipation monitoring

The alternated deposition of chitosan and dextran layers was studied using QCM-D. The constitution of (chitosan/dextran)$_4$ is reported in Figure 3.18.

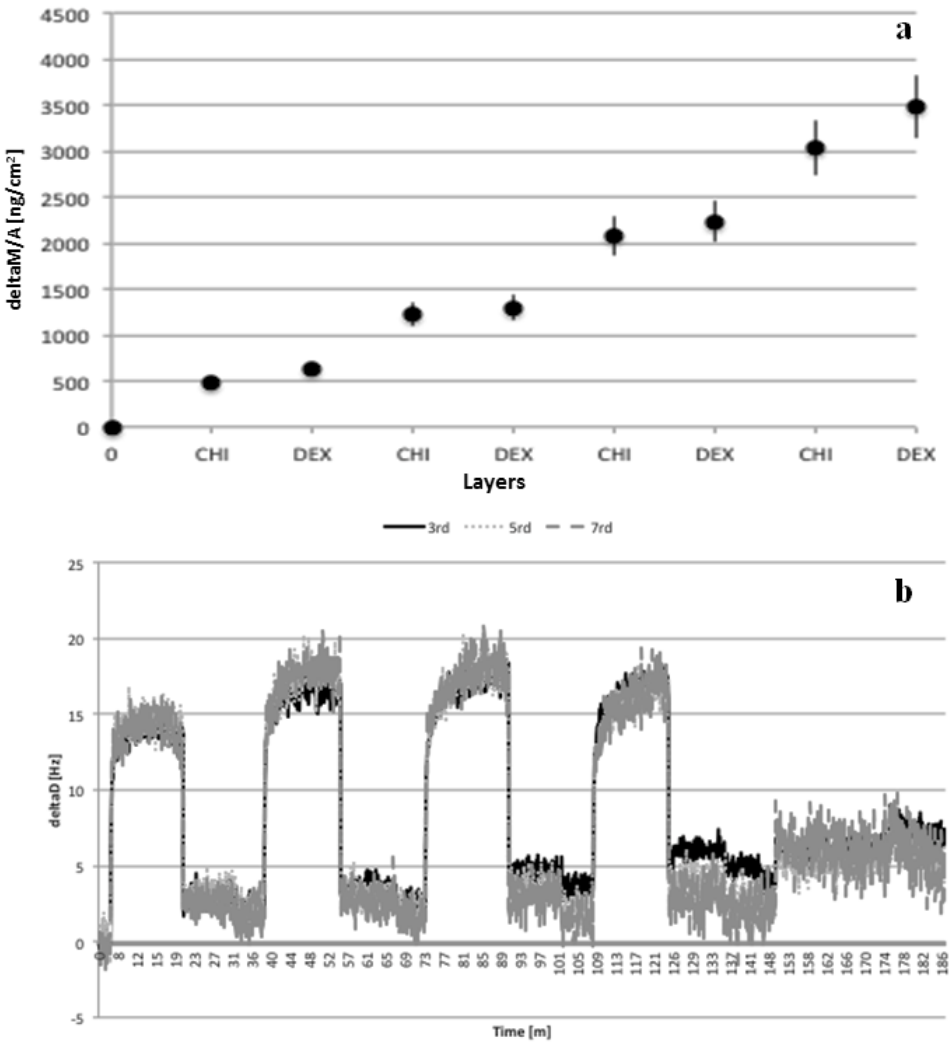

Figure 3.18: (a) plot of surface coverage as a function of layers during the alternated adsorption of chitosan and dextran; (b) dissipation changes measured by QCM-D during the build-up of a $(chitosan/dextran)_4$ multilayer. The data for the 3rd, 5th and 7th overtones are presented.

An increase in surface coverage (Figure 3.18 a) with each adsorption step indicated that a mass of the polysaccharide is deposed. ΔD was almost constant and it showed the strong interaction among the different layers. The harmonics of chitosan were well separated, while in the case of dextran they were superimpose. This behavior showed that chitosan had more viscoelastic properties than dextran. It was possible to calculate approximately the thickness of chitosan/dextran bilayer and it was 9 nm.

3.3.16. Conclusions

Nanostructured particles were successfully synthetized using $CaCO_3$ as template. The self-assembly Layer-by-Layer technique, using chitosan and dextran sulfate as polycation and polyanion, respectively allow us to obtain nanostructured particles. These particles were loaded with four different polyphenols with a good entrapment efficiency. QCM-D was carried out to characterize step-by-step the deposition of the polymers onto the surface of the particles. Considering all these data together, the polysaccharides capsules could be used to entrap a mixture of low water-soluble molecules, like polyphenols, in order to have an innovative drug delivery system.

CHAPTER IV

4. DEVELOPMENT OF NANODELIVERY SYSTEMS: RAPESEED LECITHIN NANOLIPOSOMES

4.1. INTRODUCTION

Bioactive compounds, like proteins and polyphenols, show a high susceptibility to environmental conditions (e.g. temperature, light, oxidation etc.). To protect these molecules to such adverse conditions and to increase, at the same time, their bioavailability, different encapsulation techniques are described in literature. Nowadays the most widespread encapsulation techniques are those addressed to liposome synthesis. Liposomes are self-organizing colloidal particles made of one or more lipid bilayer membranes that are able to entrap molecules in a confined core (Paini et al., 2015 B). The presence of amphiphilic membranes makes it possible to encapsulate both hydrophilic and hydrophobic compounds inside liposomes. One of the well-known group of molecules involved in the synthesis of liposome membranes is lecithin. It is extracted and purified from various natural sources, both from animal and vegetal kingdom. As reported by Arab Tehrany et al. (2012), lecithin from rapeseed is extremely rich in polyunsaturated fatty acids (PUFAs) which are considered as essential for healthy (Coonrod et al., 2008). This is the reason why lecithin was selected as source of phospholipids. Lecithin is able to self-organize in liposomes when it is sonicated in aqueous solutions. Liposomes are used as an excellent tool for increasing the bioavailability of extremely sensitive molecules, like proteins (Chang & Yeh, 2012) and of molecules poorly soluble in water (Kadri et al., 2016), as quercetin. Different techniques were described over the last years to synthetize small unilamellar vesicles: supercritical reverse phase evaporation (Otake et al., 2006), solvent injection (Schubert & Müller-Goymann, 2003), detergent dialysis (Alpes et al., 1986), sonication (Kisel et al., 2001), French press (Barenholzt et al., 1979), homogenization and membrane extrusion (Pupo et al., 2005). Among these, due to its cost-effectiveness, high reproducibility, possibility to be scaled up and its easy to handle properties, sonication is one of the most prevalent technique for liposome synthesis. In this part of the thesis, data about encapsulation of bovine serum albumin (BSA) and quercetin (Q) in liposomes through sonication are presented

4.2.MATERIALS AND METHODS

This section describes the materials and methods used to synthetize and to characterize the rapeseed lecithin nanoliposomes loaded with a model protein, bovine serum albumin (BSA), and a model antioxidant, quercetin (Q). This part of the research was done in collaboration with Professor Elmira Arab-Tehrany during the research period at University of Nancy, France. For this reason, a lot of experiments are still ongoing.

4.2.1. Chemicals

Q, BSA, absolute ethanol, methanol, formic acid (HPLC grade), and phosphate-buffered saline (PBS, pH = 7.4) were purchased from Sigma-Aldrich (St. Louis, MO, USA). Lecithin was extracted from rapeseed as described by Linder et al. (2002). Water used for the preparation of solutions and washing operations was purified by ELGA system (High Wycombe, UK).

4.2.2. Cell mediums and reagents

Two different types of cells were used for the experimentation, human mesenchymal stem cells (hMSC), and human fibroblast. hMSC were collected from Wharton's jelly (WJ) from connective tissue of human umbilical cord. In this case, umbilical cords were used after mother information and agreement, applying the guidelines ratified by the University Hospital Center of Nancy (agreement TCG/11/R11). Cells were collected after enzymatic digestion of the WJ using a collagenase solution at 1 mg/mL (Sigma-Aldrich, France) during 18 hours at 37°C. hMSC and human fibroblast were cultivated using DMEM (Gibco, France) after the addition of 10 % (v/v) of fetal bovine serum, 2 mM of L-glutamine, 2.5 g/L of fungizone®, 100 IU/mL of penicillin and 100 µg/mL of streptomycin. Cells were collected and grown in an incubator at 37°C and 5 % CO_2 and culture medium was changed every 3 days of cultivation.

4.2.3. Synthesis of BSA-loaded liposomes

At first, 50 mL of ultrapure water with two different concentrations of BSA, 0.5 and 2.0 mg/mL were prepared. 49 mL of this solution were added to 1.0 g of rapeseed lecithin in order to obtain a solution of 1

% (w/v). The suspension was mixed for at least 5 hours under magnetic stirring (600 rpm) in a nitrogen atmosphere and in dark conditions. Then, the mixture was subjected to sonication (Sonicator Vibra cell 75115, 500 watt, Bioblock Scientific Co.) at room temperature (25 ± 2°C) at 40 kHz for 8 minutes (1 s on and 1 s off) to obtain a homogeneous solution. BSA-loaded nanoliposomes were stored at 4°C in the dark before the analysis.

4.2.4. Measurement of liposome size, ζ-potential, and electrophoretic mobility

The size distribution, the zeta potential, and the electrophoretic mobility of the liposome suspensions were measured by dynamic light scattering (DLS), using a Malvern Zetasizer Nano ZS (Malvern Instrument Ltd., UK). The apparatus consisted of a 4 mW He/Ne laser emitting at 633 nm, a measurement cell, a photomultiplier and a correlator. In order to prevent false results due to multiple light scattering in the small interparticle space between liposomes, dilution was necessary (Sood et al., 2014). As a result of that, before each analysis, samples were diluted in ultrapure water (1:400) and samples were put in a standard capillary electrophoresis cell. Size, zeta-potential, and electrophoretic mobility measurements were carried out at 25°C with a fixed scattering angle of 173°, refractive index equal to 1.471 and absorbance equal to 0.01.

4.2.5. Entrapment efficiency of BSA in liposomes

To calculate the amount of BSA encapsulated in the nanoliposomes, an aliquot of the suspension was centrifuged at 10.000 rpm for 15 minutes at 4°C with an ultracentrifuge (Ultracentrifuge WX Ultra 80, Thermo Fisher Scientific, Waltham, MA, USA). Then, the supernatant was separated from the nanoliposomes and the concentration of untrapped BSA was measured through BCA assay, as reported previously. The entrapment efficiency was calculated as described in the case of $CaCO_3$ nanoparticles (Section 3.2.6).

4.2.6. Synthesis of quercetin-loaded liposomes

At first, 10 mL of a methanolic solution of quercetin (1.0 mg/mL) was added to 1.0 g of rapeseed lecithin in a completely dried round bottomed flasks. After rotary evaporation of methanol, the obtained thin homogeneous lipid film on the wall of the round bottomed flasks was hydrated with 49 mL of ultrapure water to obtain a solution of 1 % (w/v). The suspension was before mixed and later sonicated, as described before for BSA-loaded nanoliposomes.

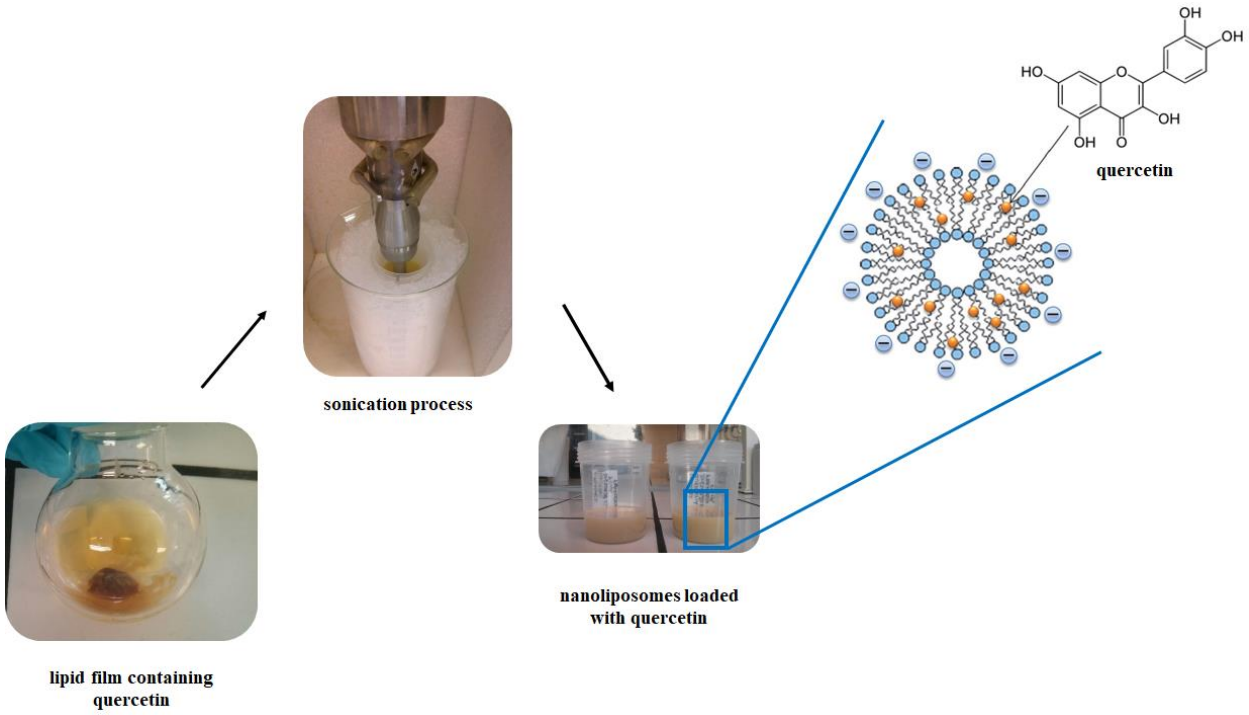

Figure 4.1: schematic representation of the synthesis of quercetin-loaded nanoliposomes.

4.2.7. Nanoparticle tracking analysis

Suspension made of liposomes were analysed by a NanoSight LM 10 instrument (NanoSight, Salisbury, UK). The instrument was equipped with a monochromatic laser beam at 405 nm and a sCMOS camera. Before the analysis, samples were diluted (1:4000) and for each sample, three videos of 60 s in duration were taken with a number of frames between 1516 and 1939, at 22°C. The liposomes movements were analysed by NTA software (version 2.1, Nanosight). The NTA software identified at first the particles and then track each particle on a frame-by-frame basis and its Brownian movement is tracked and measured from frame to frame. The two dimensional Stokes-Einstein equation is used by the software to calculate particle size, taking into account the speed of the particles themselves. NTA is able to analyze particles with a mean diameter between 10 and 2000 nm. NTA post-acquisition settings were optimized and kept constant among samples and each video was then analysed to give the mean vesicle size together with an estimation of the concentration .

4.2.8. Stability of quercetin-loaded liposomes

The quercetin-loaded and control (empty) nanoliposomes were stored in drying rooms at 4, 20, and 37°C for 2 months. Mean particle size, polydispersity index (PDI) and zeta-potential of all formulations were examined with DLS after 2, 5, 7, 14, 28 and 60 days.

4.2.9. Entrapment efficiency of quercetin in liposomes

The amount of quercetin encapsulated in the nanoliposomes was determined by centrifuging the suspension at 10.000 rpm for 15 minutes at 4°C with the same ultracentrifuge described above. After centrifugation, the supernatant was collected and freeze dried. The freeze-dried supernatant was resuspended in pure methanol. The concentration of quercetin was determined by a reversed-phase HPLC system (Shimadzu, Kyoto, Japan) equipped with a quaternary pump (LC-20AD), an auto-injector (SIL-10AD), an UV-Vis photodiode array detector, an Alltima^{TM} C18 column (5μm, 150 × 2.1 mm) (GRACE, Deerfield, IL, USA) at 30°C and data were analyzed with Labsolution data software. Samples were analyzed using ultrapure water:formic acid (99.5:0.5, v/v) as mobile phase A and acetonitrile:formic acid (99.9:0.1, v/v) as mobile phase B. Solvent gradient changed during the analysis according to the following conditions: from 10 to 80 % B in 20 minutes, from 80 to 100 % B in 10 seconds, isocratic at 100 % B for 4.50 minutes, from 100 to 10 % B in 10 seconds and isocratic at 10 % B for 6.50 minutes. A flow rate of 0.2 mL/min, an injection volume of sample of 10 μL and a detection from 190 to 800 nm was used.

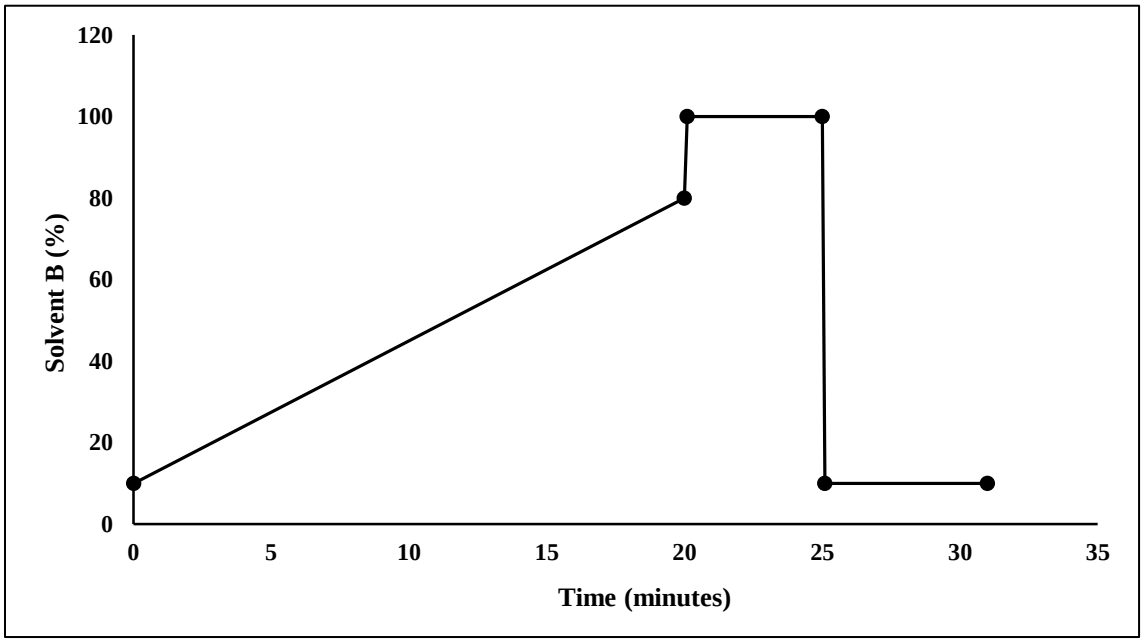

Figure 4.2: gradient for solvent B (0.1 % of formic acid in acetonitrile) during HPLC-DAD analysis of quercetin.

The concentration of quercetin was calculated by integration of peaks at 380 nm after approximatively 14.60 minutes (retention time) and using the calibration curve reported below:

$$Area = 16.51 \times 10^7 \times C \qquad (R^2 = 0.997) \qquad \text{(Equation 4.1)}$$

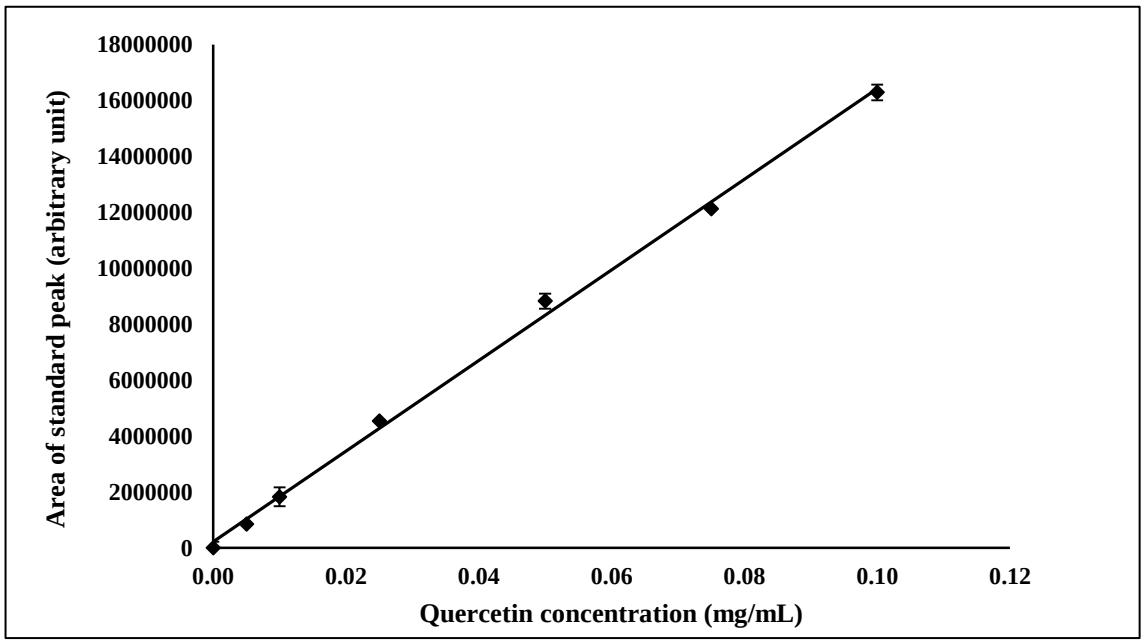

Figure 4.3: calibration curve for the quantification of quercetin by HPLC.

The entrapment efficiency was calculated by the equation:

$$Entrapment\ efficiency\ (\%) = \frac{initial\ drug - free\ drug}{initial\ drug} \times 100 \qquad \text{(Equation 4.2)}$$

4.2.10. Release of quercetin from nanoliposomes

To study the release of quercetin from nanoliposomes two different protocols were perfromed. The first step of both of them consisted of centrifuging the nanoliposome suspension three times at 1200 × g for 10 minutes (centrifuge Sorvall ST 8R, Thermo Fisher Scientific, Waltham, MA, USA) to remove the excess of insoluble quercetin, and after with the same ultracentrifuge and under the same conditions reported above. After that, the pellet (nanoliposomes) was resuspended in PBS and divided in 1.5 mL different aliquots. For the first protocol, at each time point (60 minutes, 1, 2, 7 and 14 days) the solution containing nanoliposomes was centrifuged at 10.000 rpm × 15 minutes at 4°C to separate the released quercetin from

the nanocarriers. 1.0 mL of the supernatant was collected, replaced with fresh PBS and freeze dried. Then, the freeze dried samples were resuspended in 150 µL of ethanol:water (50:50, v/v). The second protocol was applied considering that the solubility of quercetin in aqueous solution is low. As a result, it is released in forms of crystals and at pre-determinated intervals (the same reported for the first protocol) the samples were centrifuged at 3000 rpm for 10 minutes (Aditya et al., 2012). During the centrifugation, the released crystals of quercetin precipitated as a pellet which was redissolved in 150 µL of ethanol:water (50:50, v/v). To determine the concentrations of the released quercetin, the absorbance of all the samples was read at 352 nm, using a plate reader (Multiskan^{TM} GO Microplate Spectrophotometer, Thermo Scientific, Finland) taking into account the calibration curve reported below:

$Abs_{352} = 13.063 \times C$ ($R^2 = 0.9999$) (Equation 4.3)

where:

• Abs_{352} is the absorbance of quercetin at 352 nm;

• C is quercetin concentration expressed in mg/mL.

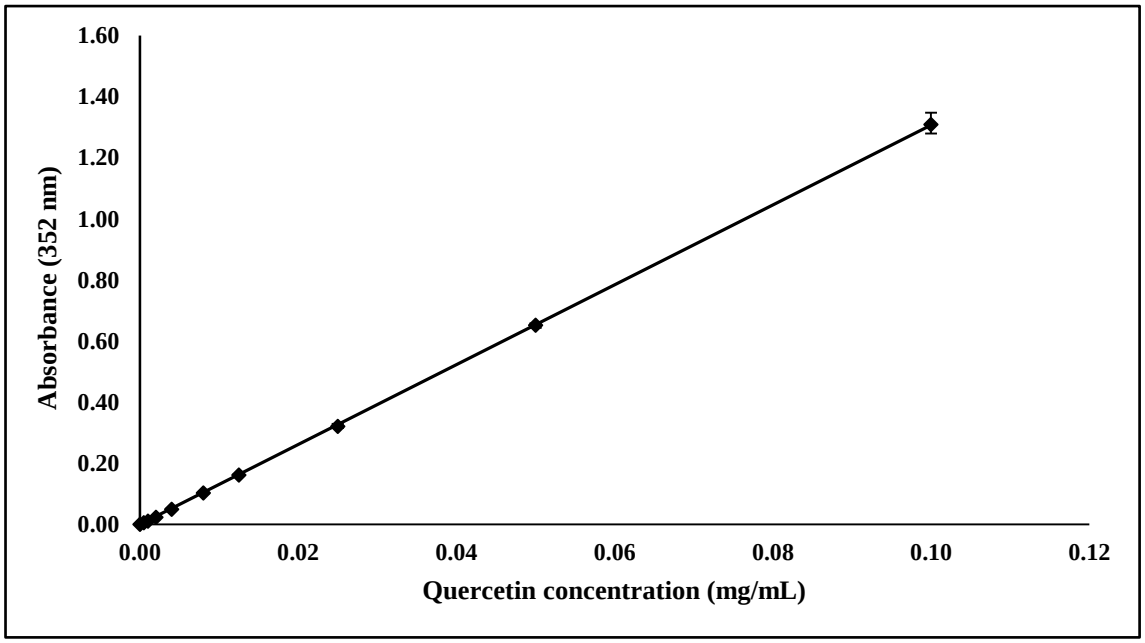

Figure 4.4: calibration curve for the quantification of quercetin by spectrophotometric analysis.

The release of quercetin was studied at three different temperature (4, 20, and 37°C), keeping the samples in dark conditions.

4.2.11. Rheological characterization of nanoliposome suspensions

Rheological studies of water-based solution containing nanoliposomes were performed using a Kinexus Pro rheometer (Malvern Instruments, Orsay, France). During all the rheological experiments, the system was covered with a hood to minimize water evaporation and to keep constant the temperature (25°C). Shear viscosimetry and oscillatory rheometry were studied. Steady-shear viscosity and shear stress measurements were determined using a cone-and-plate geometry (50 mm, 1°). For the steady-shear viscosity measurement, the shear rate was increased from 10^{-3} to 10^{3} s^{-1}. To determine the mechanical properties of the liposome dispersion, an amplitude sweep was first performed at a frequency of 1 Hz by changing the shear strain from 0.1 to 1000 % in order to determine the linear viscoelastic region. Based on this test, a value of strain within the linear region was then used in the subsequent frequency sweep analysis with the change of frequency between 0.01 and 10 Hz at 10 % of shear strain.

4.2.12. *In vitro* cytotoxicity assay

The adopted protocol to assess the biocompatibility of nanoliposomes was similar to that reported in section for $CaCO_3$ nanoparticles. Briefly, hMSC and fibroblasts were seeded into a flat-bottom 96 well-plate with a density of 5×10^3 cells/cm^2 with complete medium and incubated at 37 °C with 5 % CO_2. Nanoliposome dispersions (empty and quercetin-loaded) were sterilized by filtering them with 0.22 μm filters. After 24 hours of cell incubation, nanoliposome solutions were added to the medium at different concentrations (6.87-13.8 μg/mL and 0.33-0.67 mg/mL). In addition, free quercetin in ethanol at different concentrations (1, 10, 25 and 50 μM) and the same volume of ethanol used to dilute it were tested. After appropriate time intervals (1, 3, and 7 days), MTS assay was done. All experiments were assessed in triplicate and results are expressed as a percentage of the control (100 %).

4.2.13. Statistical analysis

All the experiments were performed at least in triplicate and the results were expressed as mean values and standard deviations. Multiple comparison of the mean values was performed by the least significant difference test at $p < 0.05$. For data analysis, the Statistica 8.0 software (StatSoft, Tulsa, OK, USA) was used.

4.3.RESULTS AND DISCUSSION

ENCAPSULATION OF BSA IN NANOLIPOSOMES

4.3.1. Measurement of size, ζ-potential and electrophoretic mobility of BSA-loaded nanoliposomes

The nanoliposome size was registered immediately after their synthesis. The BSA-loaded nanoliposomes were found to be smaller than the unloaded particles ($p < 0.05$). In fact, the mean size of control (empty) liposomes was 149.87 ± 1.19 nm, while after encapsulation of BSA, it decreased to 143.13 ± 2.08 and 138.18 ± 1.44 nm, working with 0.5 and 2.0 mg/mL of BSA, respectively (Table 4.1). This slightly decrease in size could be explained taking into account that there were no interaction between BSA (hydrophilic) and lipids, resulting in a well-defined separation between the core and the membranes of the liposomes. As a consequence, BSA remained in the core of the formed liposomes without affecting their mean size. The same trend was found working with $CaCO_3$ nanoparticles and BSA (Section 3.3.1). Liposome charge is an important factor that participates to liposome stability and entrapment efficiency (Maherani et al., 2012). The mixture of lipids employed for the synthesis of liposomes were negatively charged and this charge was maintained even after the sonication process. The presence of BSA, at the two studied concentrations, did not affect the ζ-potential and the electrophoretic mobility of the BSA-loaded liposomes, as shown in Table 4.1.

Table 4.1: mean particle size, polydispersity index, zeta potential and electrophoretic mobility of empty and BSA-loaded nanoliposomes.

Sample	Particle size (nm)	Polydispersity index	Zeta potential (mV)	Electrophoretic mobility (μmcm/Vs)
Empty liposome	149.87 ± 1.19[a]	0.27 ± 0.02	-41.13 ± 1.49[a]	-3.23 ± 0.12[a]
BSA-loaded liposome (0.5 mg/mL)	143.13 ± 2.08[b]	0.27 ± 0.02	-41.85 ± 0.71[a]	-3.28 ± 0.06[a]
BSA-loaded liposome (2.0 mg/mL)	138.18 ± 1.44[c]	0.26 ± 0.01	-40.33 ± 0.62[a]	-3.20 ± 0.05[a]

Results are mean of three measurements ± SD. Different letters do refer to statistically significant differences among results for each column ($p < 0.05$), ANOVA with Tukey's multiple comparison test.

4.3.2. Entrapment efficiency

The optimal encapsulation efficiency was reached when the lower amount of BSA was used. Working with the higher BSA concentration induced a decrease in the entrapment efficiency ($p < 0.05$) (Table 4.2). Probably, this fact was due to a difference in osmotic pressure between the internal and the external aqueous phase. The difference in osmotic pressure increased by increasing BSA loading, leading to a breakage of the lipophilic droplets. As a result, an exchange between the internal and the external aqueous phase occurred with a consequent loss of BSA (Lamprecht et al., 2000). These data are completely in agreement with a previous research published by Colletier et al. (2002).

Table 4.2: entrapment efficiency of BSA-loaded nanoliposomes.

Sample	Entrapment efficiency (%)
BSA-loaded liposomes (0.5 mg/mL)	47.31 ± 2.37^{a}
BSA-loaded liposomes (2.0 mg/mL)	37.27 ± 4.91^{b}

Results are mean of three measurements ± SD. Different letters do refer to statistically significant differences among results ($p < 0.05$), ANOVA with Tukey's multiple comparison test.

This part of the work about encapsulation of a model protein (BSA) in nanoliposomes is still ongoig. It will be studied the morphology (TEM analysis), the stability of liposomes at different temperatures over a period of 60 days, the kinetic of BSA release from the particles, the biocompatibility, and the possibility to attach covalently different antibodies on their surface to create a liposomal-based drug delivery system. However, it was decided to show these preliminary results to compare them with those obtained working with $CaCO_3$ nanoparticles loaded with the same protein.

4.3.3. Measurement of liposome size, ζ-potential and electrophoretic mobility of quercetin-loaded nanoliposomes

Working with liposomes, mean size, size distribution, ζ-potential and electrophoretic mobility are important physicochemical parameters that could be modulated acting on fatty acid composition, lipid classes, surface-active properties of lecithins as well as on the synthesis parameters (e.g. during sonication and homogenization) (Benedet et al., 2007; Arab Tehrany et al., 2012; Hasan et al., 2016). The range of these physicochemical parameters has to be fixed depending on the final application that the nanosystem will

possess (Calvagno et al., 2007). For example, in food industry it is preferable to have microsized vesicles instead of the nanosized ones. On the contrary, in the pharmaceutical and medical sectors it is more desirable the opposite condition to allow, for example, a better interaction between cells and nanoparticles. Mean size, size distribution, ζ-potential and electrophoretic mobility of liposomes (both empy and loaded with quercetin) were measured immediately after the sonication process using DLS and they are shown in Table 4.3.

Table 4.3: mean particle size, polydispersity index, zeta potential and electrophoretic mobility of empty and quercetin-loaded nanoliposomes.

Sample	Particle size (nm)	Polydispersity index	Zeta potential (mV)	Electrophoretic mobility (µmcm/Vs)
Empty liposome	185.82 ± 20.99[a]	0.31 ± 0.05	-44.58 ± 2.58[a]	-3.49 ± 0.20[a]
Quercetin-loaded liposome	204.04 ± 13.79[b]	0.32 ± 0.03	-46.09 ± 2.47[b]	-3.61 ± 0.19[b]

Results are mean of three measurements ± SD. Different letters do refer to statistically significant differences among results for each column ($p < 0.05$), ANOVA with Tukey's multiple comparison test.

The mean size of empty liposomes was 185.82 ± 20.99 nm, whereas after encapsulation of quercetin, it increased to 204.04 ± 13.79 nm (Table 4.3). This increase could be explained taking into account the interactions between lipids and quercetin. Hydrophobic interactions between lipid tails and quercetin may take place, allowing quercetin to come up to the bilayer. Since it has a planar configuration, quercetin showed a very high affinity for liposomes and it could easily intercalate into the well-organized structures of membrane phospholipids (Van Dijk et al., 2000). As a result, quercetin induced an enlargement of the phospholipid shell.

In addition to the liposomal size, DLS is also able to measure the polydispersity index. This parameter is a dimensionless number of the breadth of the distribution of particle size (Zweers et al., 2003). As reported in Table 4.3, the PDIs were between 0.31 and 0.32. This fact indicated that liposome size was well-controlled with a narrow dispersity.

To better understand the electrical surface charge of the liposome, which is a fundamental property that affects liposome behaviour, ζ-potential measurements were performed. The values of the ζ-potential give an idea of the stability of colloidal systems: to have a more stable colloidal dispersion, it is required the repulsion between particles and high potential values. In fact, if all particles in the suspension present a same large charge (positive or negative), they repulse each other and there will be no aggregation of the particles in the suspension (Mady et al., 2009). The negatively electrophoretic mobility of both empty and quercetin-loaded liposomes is the result of the anionic fraction of phospholipids present in rapeseed lecithin

(Chansiri et al., 1999). In Table 4.3, it can be seen that there were only slight statistical differences ($p < 0.05$) between the samples in terms of ζ-potential and electrophoretic mobility. All the presented results concerning mean size, size distribution, ζ-potential and electrophoretic mobility are consistent with ones reported by other authors working with rapeseed lecithin (Arab Tehrany et al., 2012; Hasan et al., 2014; Paini et al., 2015).

4.3.4. Nanoparticle tracking analysis

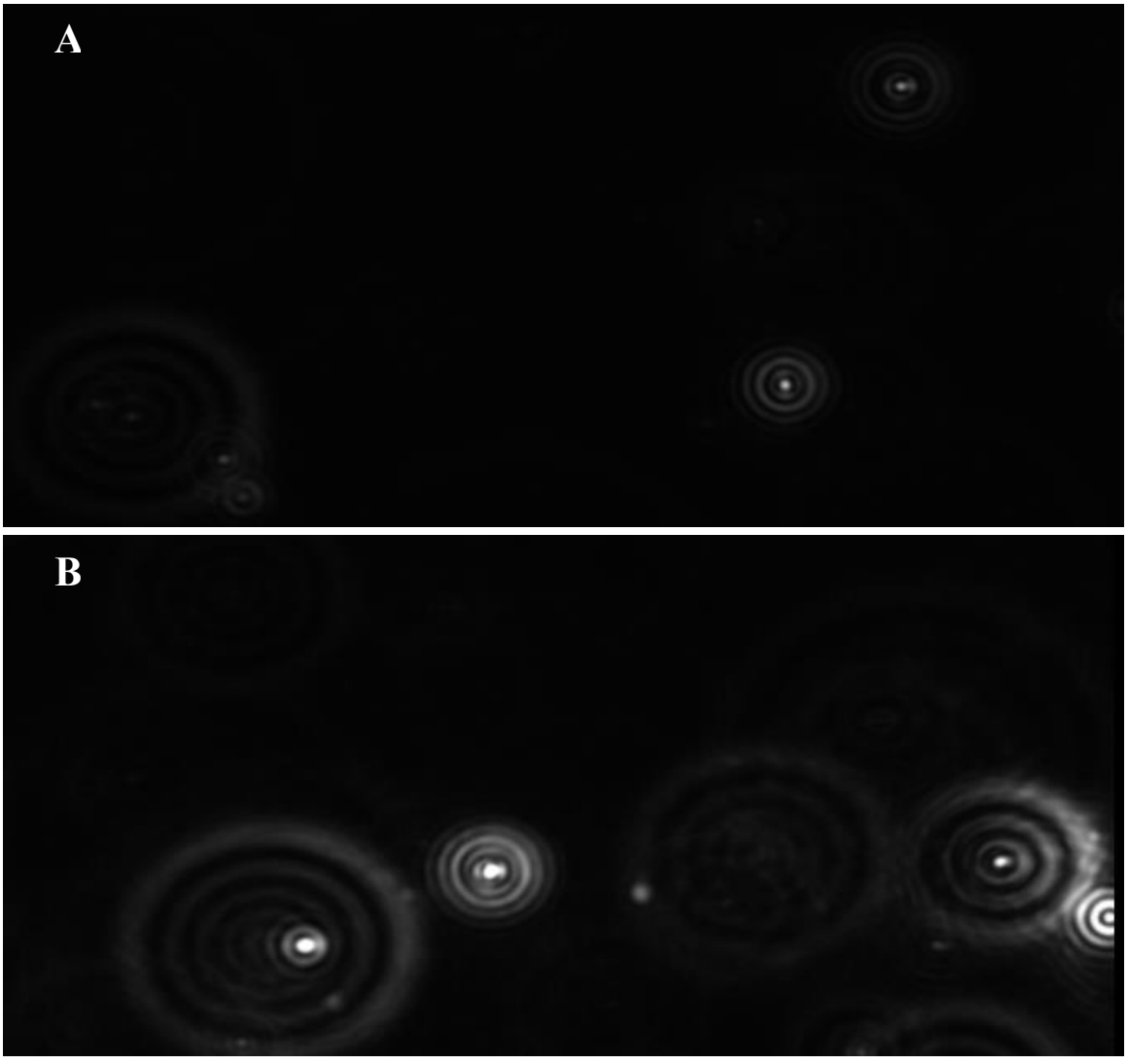

Figure 4.5: video frame for (A) empty and (B) quercetin-loaded nanoliposomes obtained with nanoparticles tracking analysis.

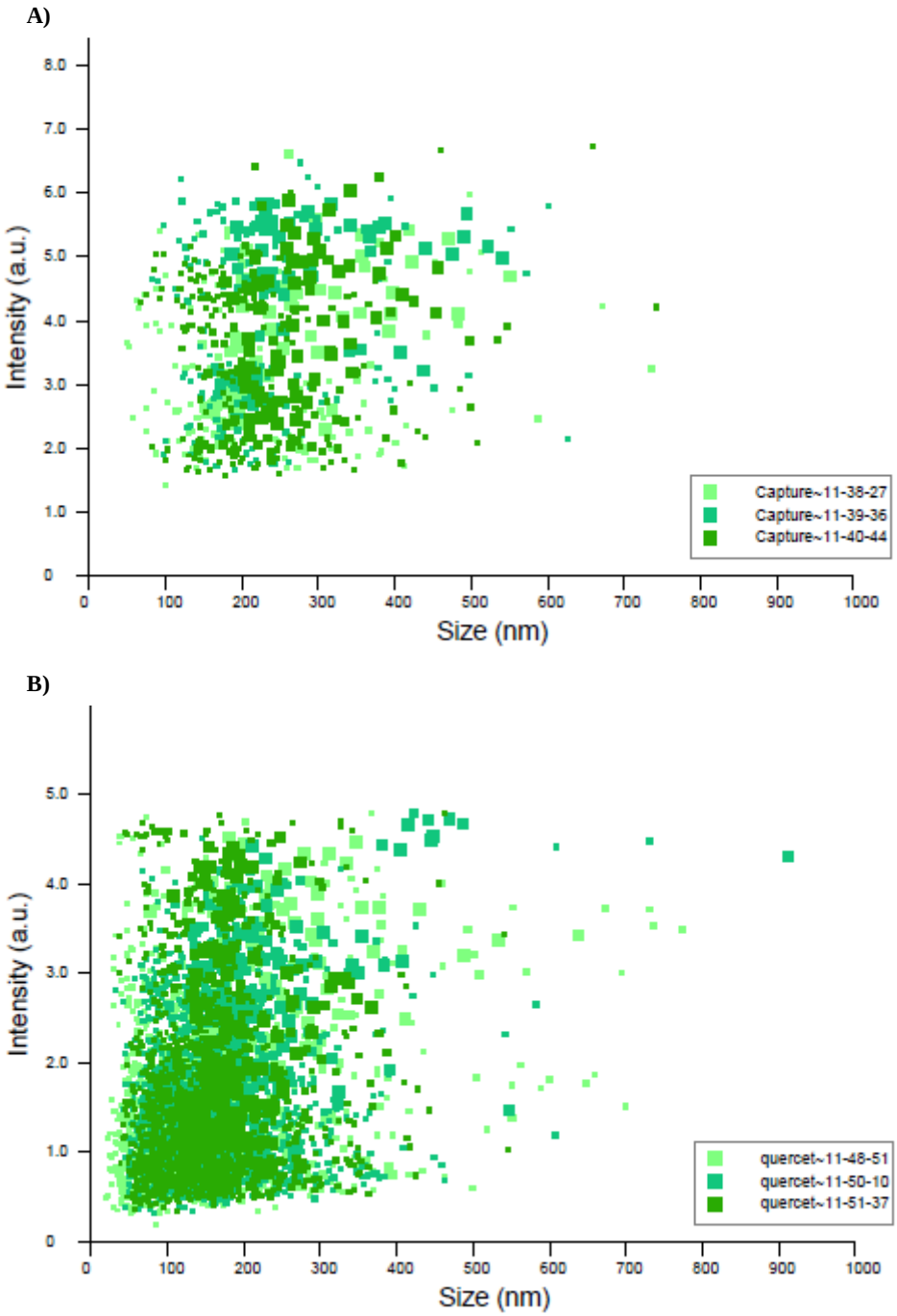

Figure 4.6: size distribution of (A) empty and (B) quercetin-loaded nanoliposomes obtained with nanoparticles tracking analysis.

The nanoparticles tracking analysis confirmed all the data concerning the liposome size obtained by DLS. The presence of multilayers around each liposomes in the presented video frame (Figure 4.5) does not to be misled. In fact, these layers are not real ones but they are produced as a consequence of the light diffraction after the contact with the liposome surface during the analysis. Figure 4.6 shows the size

distribution for empty (A) and quercetin-loaded (B) liposomes. The majority of the particles is located around 200 nm.

4.3.5. Stability of size and ζ-potential

Long-term storage stability studies were carried out at three different temperatures over a period of 60 days measuring the particle size and the zeta potential. We choose three different temperatures: 4°C for potential food and pharmaceutical preparations that are, for example, thermosensitive, 20°C for the potential storage of food or pharmaceutical formulation at room temperature, and 37°C to reproduce physiological conditions of our body. No differences ($p < 0.05$) between the two samples (empty and quercetin-loaded) and among the studied temperatures in terms of size and zeta-potential were noticed as shown in Figure 4.7 (A, B. and C) and Figure 4.8 (A, B, and C). Liposomes were stable at each studied temperature, keeping constant their size and their surface charge.

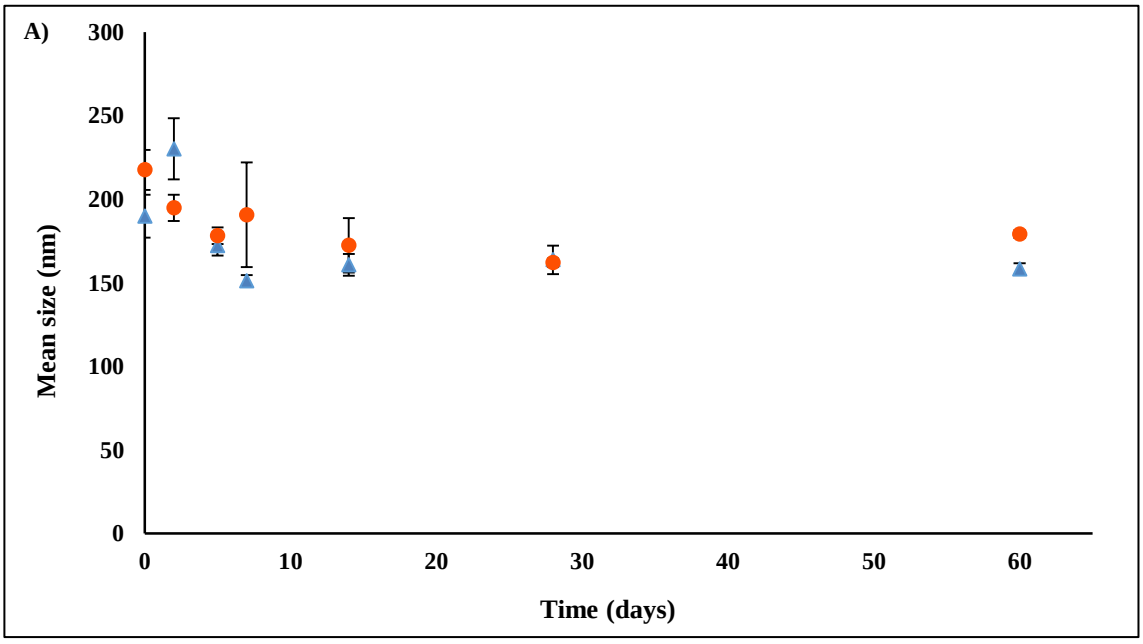

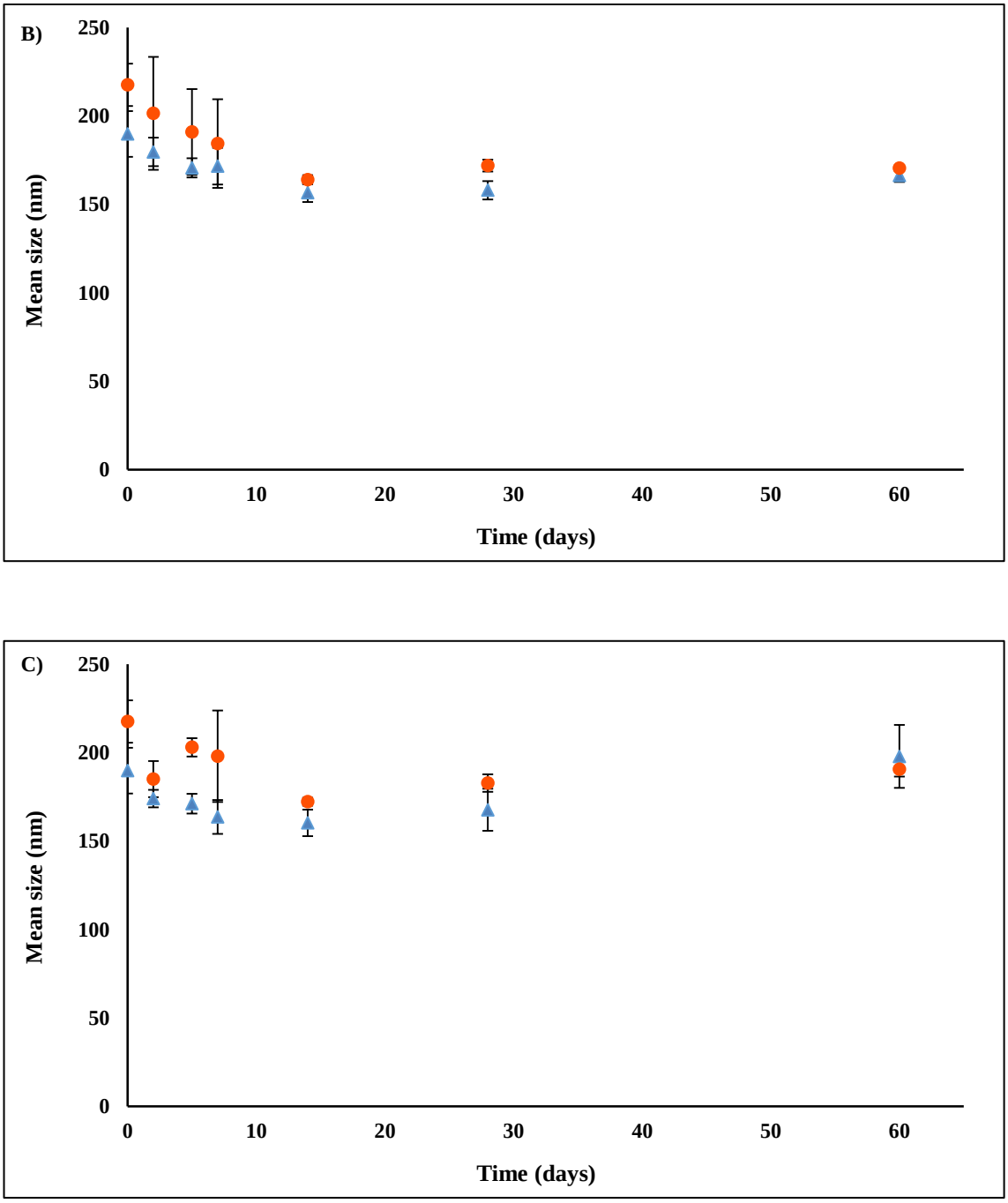

Figure 4.7: size stability of control (●) and quercetin-loaded (▲) nanoliposomes at (A) 4, (B) 20, and (C) 37°C.

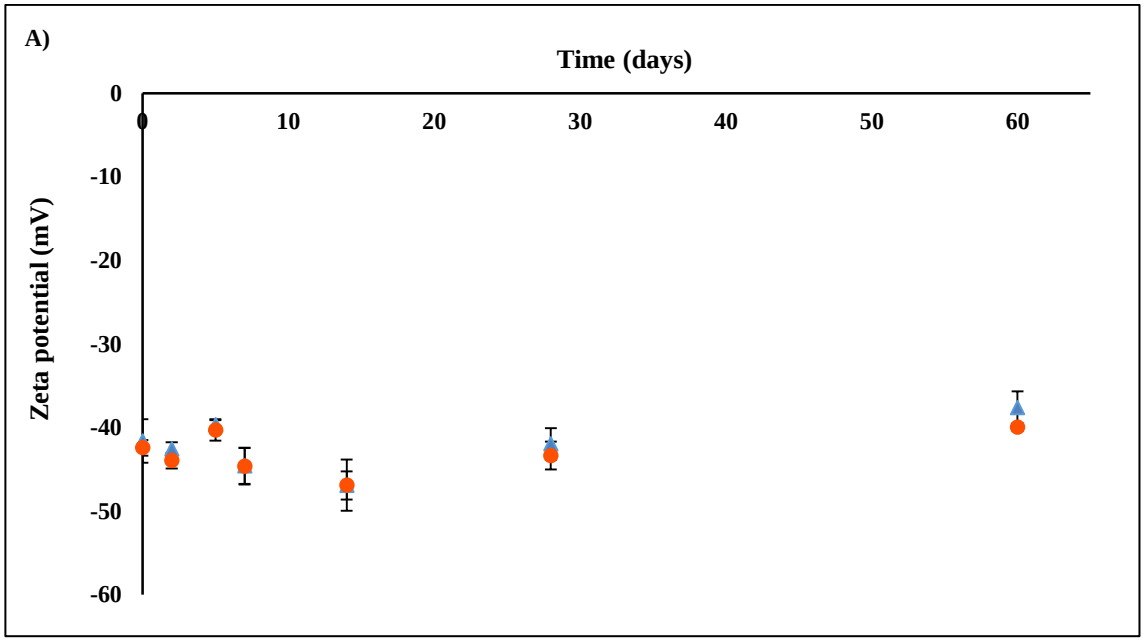
A)
Time (days)
Zeta potential (mV)
0
10
20
30
40
50
60
0
-10
-20
-30
-40
-50
-60

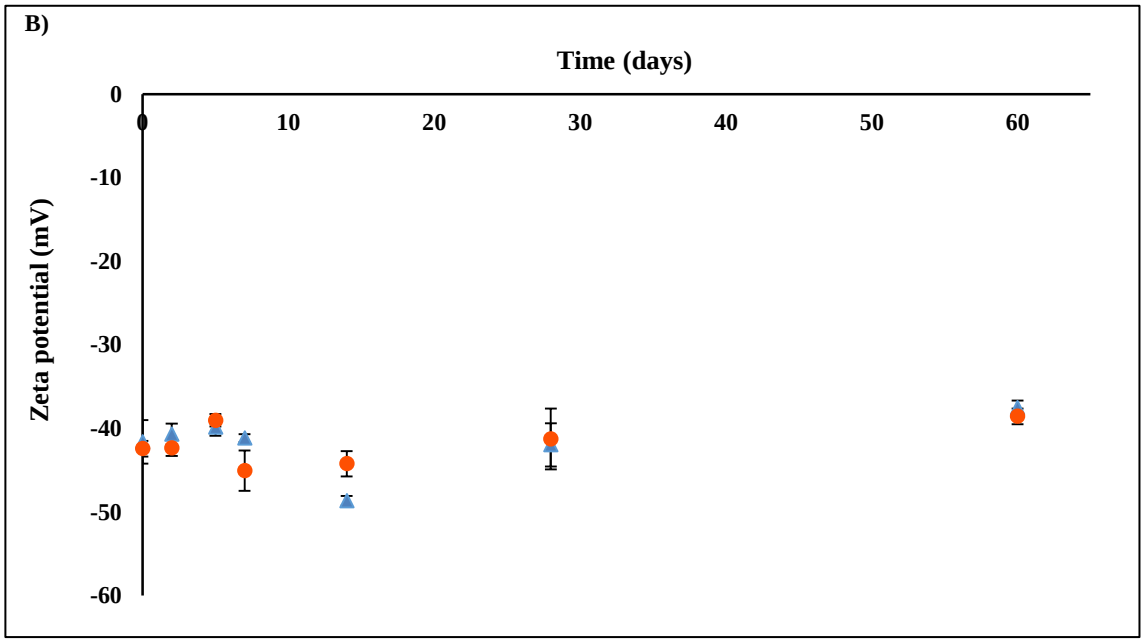
B)
Time (days)
Zeta potential (mV)
0
10
20
30
40
50
60
0
-10
-20
-30
-40
-50
-60

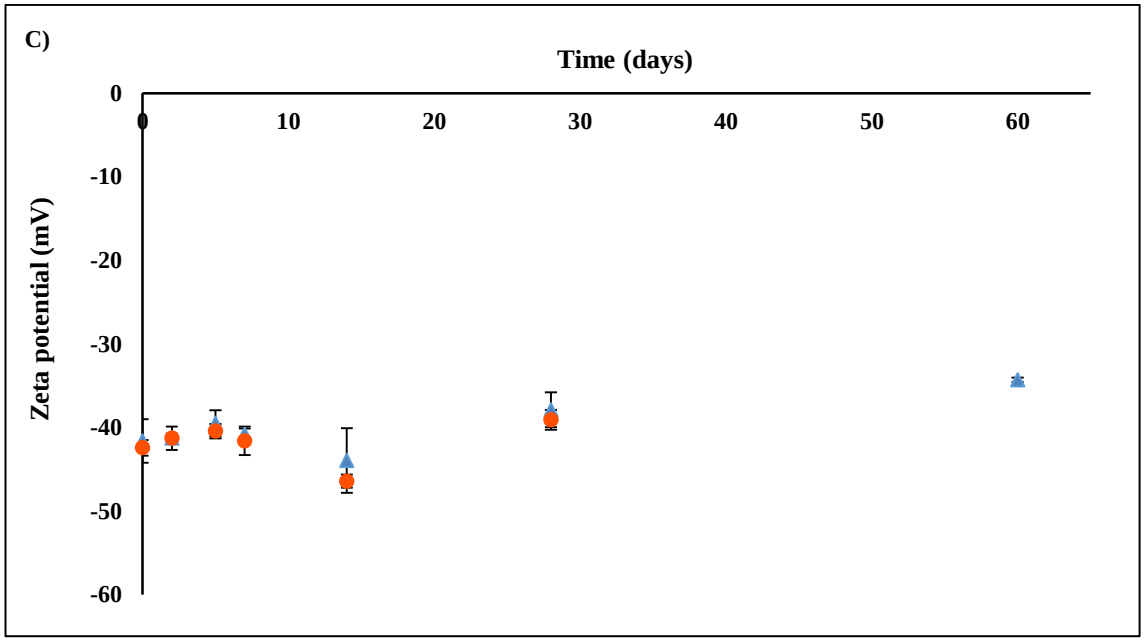

Figure 4.8: zeta potential stability of control (●) and quercetin-loaded (▲) nanoliposomes at (A) 4, (B) 20, and (C) 37°C.

4.3.6. Entrapment efficiency

Quercetin is recognized as one of the most promising natural therapeutic agent in the vascular medicine due to its anti-inflammatory and antioxidant activities. Despite of its positive effects on human health, it suffers from some limitations such as light and oxygen sensitivity, low solubility in water and low bioavailability (Jangde & Singh, 2014). For this reasons, it was decided to encapsulate it in liposomes. With the aim of studying the effect of quercetin loading on its molecular integrity, HPLC analysis were done before and after the encapsulation step. The chromatogram of quercetin showed that the retention time of this molecule was 14.6 min. Quercetin after breakage of the nanoliposomes showed a very similar HPLC profile (data not shown). The entrapment efficiency of quercetin in nanoliposomes were calculated using the equation 4.2 and it was 28.84 ± 4.79 %. This value was not as high as we expected because of the low solubility of quercetin in water. In fact, during the sonication process, a huge amount of that compound precipitated in form of insoluble crystals before being encapsulated.

4.3.7. *In vitro* release of quercetin from nanoliposomes

The *in vitro* release behaviour of quercetin-loaded nanoliposomes was studied over a period of 14 days in PBS and the cumulative release curves are reported in Figure 4.9. By way of example, the release curves

reported below refer to one of the protocols described in Section 4.2.10. In details the same protocol described in Aditya et al. (2002) were applied with some modifications. As well as in the case of stability study, these experiments were performed at three different temperatures to cover all the range of the possible application of liposomes in food and pharmaceutical sectors. The release of drugs from nanosystems depends on different factors, like physicochemical properties of the entrapped drug and of the encapsulating agent, the chemical properties of the solvent used during the release studies, the size of the nanoparticles, the temperature kept constant during the experiments, the use of stabilizers during the synthesis of the nanoparticles, and the presence of nanostructured layers that cover the particles (e.g. chitosan, dextran sulfate, poly-L-arginine etc.) (Bala et al., 2006). The three different curves showed an exponential release of quercetin that didn't reach a steady-state after 14 days at 20 and 37°C. At 4°C the exponential behaviour of the release of quercetin was less remarkable and the release was pretty poor at each interval. In 14 days, for all the studied temperature, it was not possible to obtain a complete release (100 %) of quercetin from nanoliposomes. This fact could be explained considering that the solubility of quercetin in aqueous solution (in this case PBS) is extremely low. The cumulative release curves showed significant differences at the three different studied temperature. Only after 60 minutes, the quantity of released quercetin was similar for the different temperatures. In details, working at 4°C, the final amount of quercetin was 66.86 and 69.33 % lower in comparison with released quercetin at 20 and 37°C, respectively. In general, at 4°C, for each point, the quantity of released quercetin was significantly slower in comparison with the values obtained at the same time, keeping the nanoliposomes at 20 and 37°C. In contrast to what is reported by Jangde & Singh (2014), in this case it was not registered a burst release that generally, in the case of liposome, is due to molecules adsorbed onto their surfaces. This step was overcome washing the nanoliposome suspension many times before starting the releasing experiments. In conclusion, the release of quercetin from nanoliposomes did not show a burst release, but rather a sustained release during time, indicating that these nanoparticles could potentially find application as a good drug delivery system.

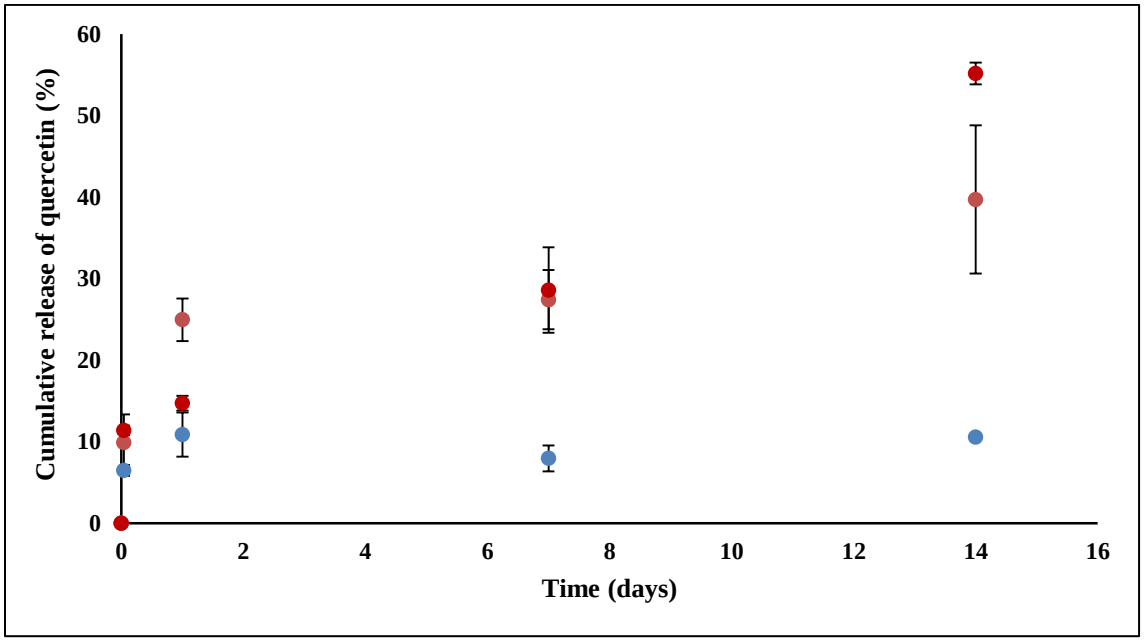

Figure 4.9: cumulative release of quercetin from nanoliposomes at 4 (—), 20 (—), and 37°C (—).

4.3.8. Rheological studies

Steady-state shear viscosity

To evaluate if the loading of quercetin in nanoliposomes was able to induce changes in the properties of the liquid formulation, rheological studies were carried out. The possibility to control the rheological behaviour of liposome dispersions is considered of great importance under an industrial point of view. In fact, the rheological properties of such dispersion depend on the interaction between vesicles and vesicle deformability. Taking into account that the rheological behaviour of liposomal suspension is related to microstructural changes, a thorough knowledge of the changes in microstructure under shear could provide significant opportunities of enhancing the process of liposome dispersions (Hasan et al., 2016). Steady-shear viscosity, shear stress and oscillatory rheometry to study mechanical stability of liposomal samples, were performed. The flow curves of empty and quercetin-loaded liposomes are reported in Figure 4.10.

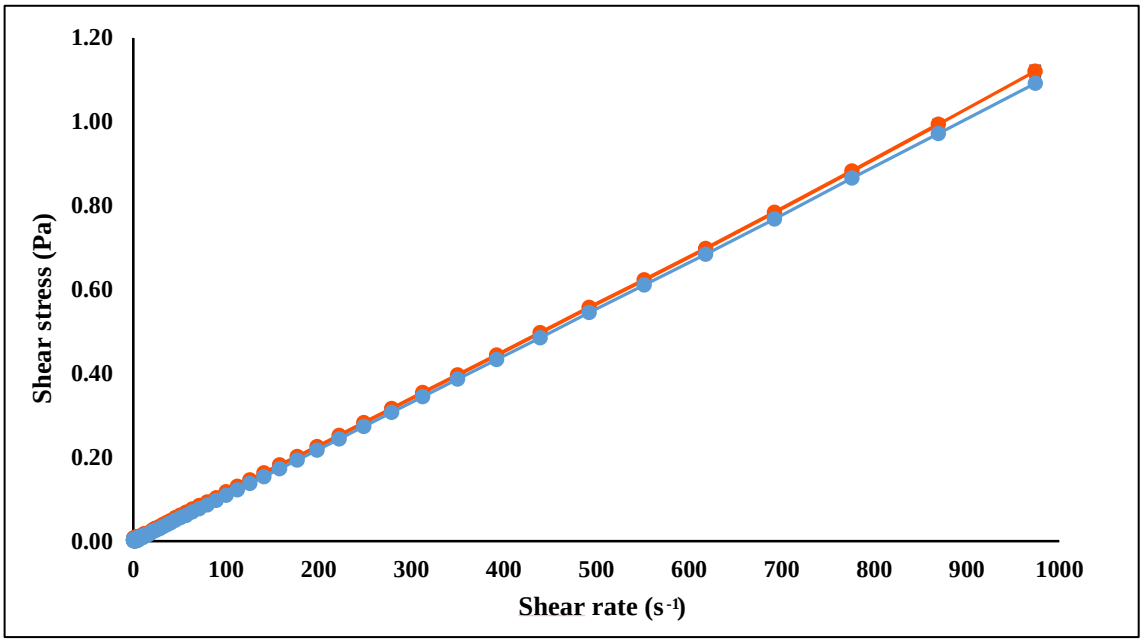

Figure 4.10: flow curves of empty ( ) and quercetin-loaded liposomes ( ).

The solid lines of flow curves represent fits to the power law model:

$$\partial = k\gamma^n \qquad \text{(Equation 4.4)}$$

where ∂ is the shear stress;

k is the consistency index;

γ is the shear rate;

n is the flow behaviour index.

Representing a general measurement of viscosity, the k index is useful in the case of comparative purposes and it is numerically equal to the viscosity at 1 s^{-1}. The plastic viscosity and the yield stress of the two samples were determined plotting the flow curves of the square root of shear stress against the square root of shear rate (Figure 4.11).

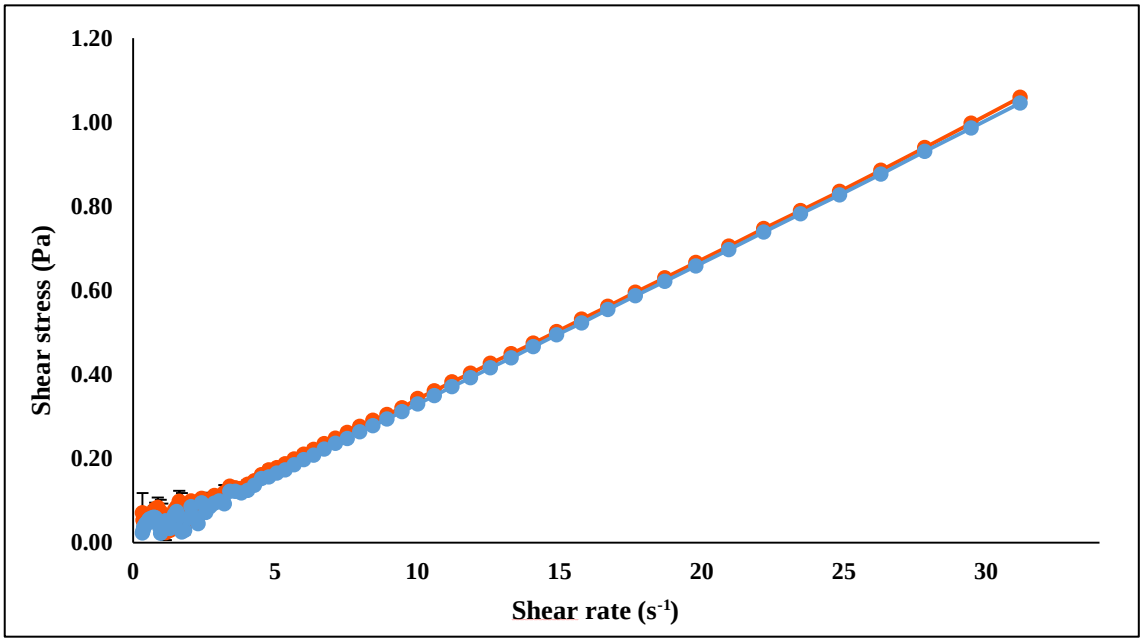

Figure 4.11: Casson plots of the square root of the shear stress versus the square root of the shear rate for empty (—) and quercetin-loaded liposomes (—).

Table 4.4: rheological properties according to the power law model for empty and quercetin-loaded liposomes.

Sample	*k* (Pa s)	*n*	R^2
Empty liposomes	0.00010 ± 0.0005	1.016 ± 0.051	0.9986
Quercetin-loaded liposomes	0.0014 ± 0.0003	0.973 ± 0.036	0.9996

The Casson model is a structure-based model:

$$(\partial)^{0.5} = K_{0c} + K_c(\gamma)^{0.5} \quad \text{(Equation 4.5)}$$

where the square of the intercept is the Casson yield stress, $\partial_{0c} = (K_{0c})^2$, and the square of the slope is Casson plastic viscosity, $\eta_{Casson} = (K_c)^2$ (Equation 4.6)

The above mentioned equations were used to fit the experimental data of the two different samples. The rheological parameters are reported in Table 4.5.

Table 4.5: rheological properties according to the Casson model for empty and quercetin-loaded liposomes.

Sample	Plastic viscosity (mPa s)	Yield stress (mPA)	R^2
Empty liposome	1.07 ± 0.05	0.08 ± 0.01	0.9967
Quercetin-loaded liposome	1.05 ± 0.02	0.07 ± 0.01	0.9937

Both liposome suspensions showed a nearly Newtonian flow behaviour (n approximately equal to 1). With the aim of studying the time-dependent flow behaviour of the liposomal dispersion, the shear stress was augmented from 10^{-3} to 0.5 Pa and then decreased in the same stress range. For the quercetin-loaded liposomes the plot (Figure 4.12) shows a thixotropic behaviour.

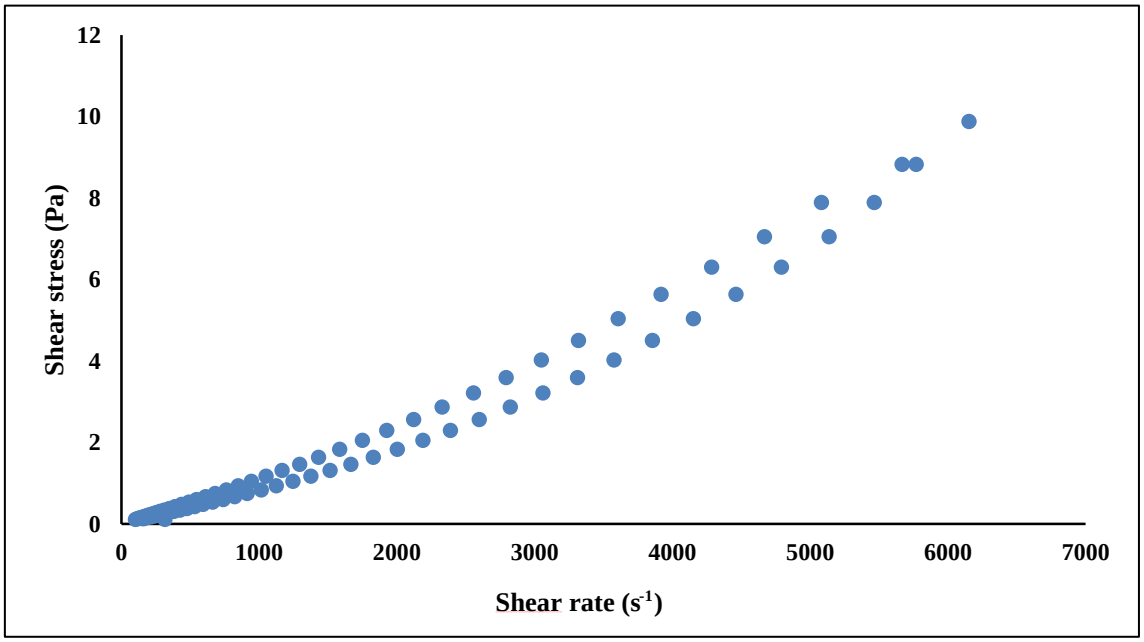

Figure 4.12: curves obtained with quercetin-loaded nanoliposomes increasing and decreasing in the shear stress in the same shear stress range.

Oscillatory rheometry

Oscillatory rheology experiments were performed to evaluate the mechanical stability of the liposomal samples at a fixed strain within the linear viscoelastic region. The mechanical properties of the solutions are reported in Figure 4.13. The encapsulation of quercetin did not negatively influenced the general mechanical properties of liposome solution. Lipid vesicles interactions, such as electrostatic repulsion, long range entropic repulsion, and van der Waals attraction mediated the mechanical stability of liposomal suspension (Hasan et al., 2016; Jangde & Singh, 2016).

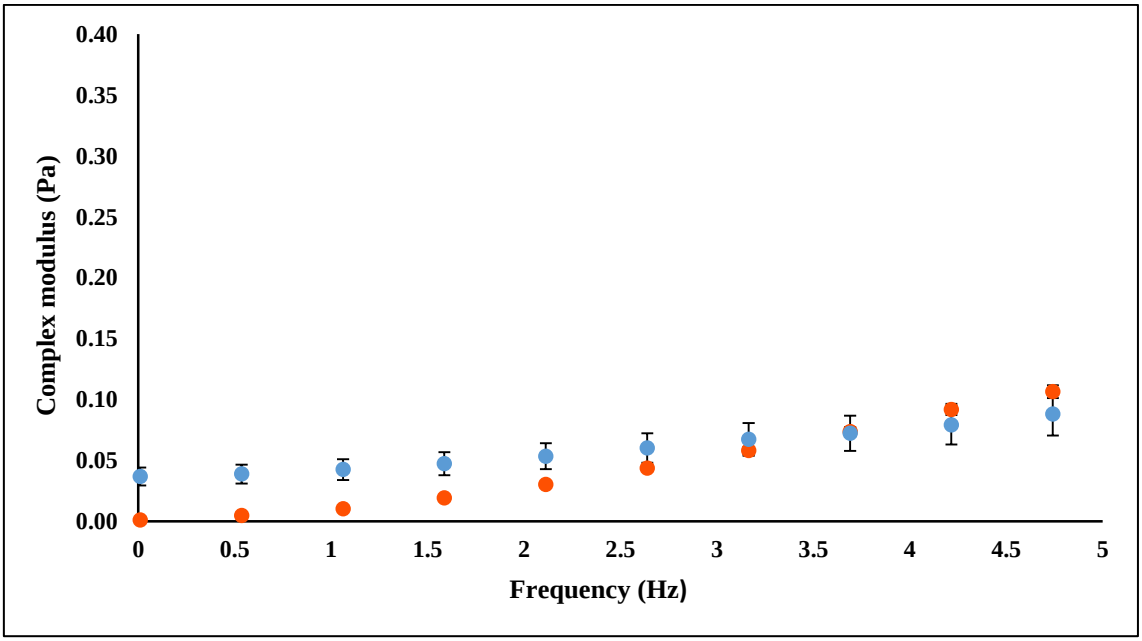

Figure 4.13: frequency sweep test of empty ( ) and quercetin-loaded liposomes ( ).

4.3.9. *In vitro* cytotoxicity assay

The effects of empty and quercetin-loaded nanoliposomes on hMSC and fibroblast were evaluated through MTS assay. The viability of treated cells with different concentrations of free quercetin (Q) (1, 10, 25 and 50 μM) or of liposomes (6.87 and 13.8 μg/mL and 0.33 and 0.67 mg/mL, both empty liposome, EL, and quercetin-loaded liposome, QL) as well as untreated cells (control, CTL) was studied for 1, 3, and 7 days. Figure 4.14 shows the results expressed as a percentage value with respect to the control. Working with hMSC (Figure 4.14, A), with the two lowest concentrations of quercetin-loaded liposomes there was no any significant differences with the control. However, the presence of quercetin-loaded liposomes at the concentration of 0.33 and 0.67 mg/mL induced a partial toxicity on hMSC. In the case of cells treated with free quercetin, it is noticeable that at the concentration of 25 and 50 μM there was cytotoxicity after 7 days of incubation. These results have not to be addressed to a cytotoxicity of quercetin, but rather to the presence of ethanol as solvent. In fact, treating the cells with the same volume of ethanol used for preparing the solution of quercetin at 25 and 50 μM, the same cytotoxic effect was reported.

Human fibroblast resulted to be more sensitive to the liposomes, to quercetin itself, and to ethanol (Figure 4.14 B). Fibroblasts showed cytotoxicity to quercetin in a dose-dependent manner. These results are in line with those published by Pawlikowska-Pawlega & Gawron (1995). In fact, these authors found that mouse fibroblasts showed a partial growth inhibition when they were cultivated with 10 μg/mL of quercetin. In our case, even the lowest concentration was higher. It was not possible to discern at the highest

concentration of quercetin used, if the cellular toxicity derived from the volume of ethanol employed or from quercetin itself. It was not important to define if the responsible of this cellular behaviour was quercetin or ethanol because quercetin was toxic even at lower concentration. Treating the fibroblasts with liposomes, it was noticed a partial cytotoxicity with empty liposomes at a concentration equal to 0.33 mg/mL and a significant cytotoxicity working with 0.66 mg/mL. In the case of quercetin-loaded liposomes, the cytotoxicity at these two concentrations was more marked. In the case of QL, the presence of a high concentration of non-well tolerated liposomal particles and a contemporary release of quercetin from them, could induced an enhanced cellular alterations. Even working with fibroblast, it was confirmed that the highest volumes of ethanol used during the experiments were not biocompatible.

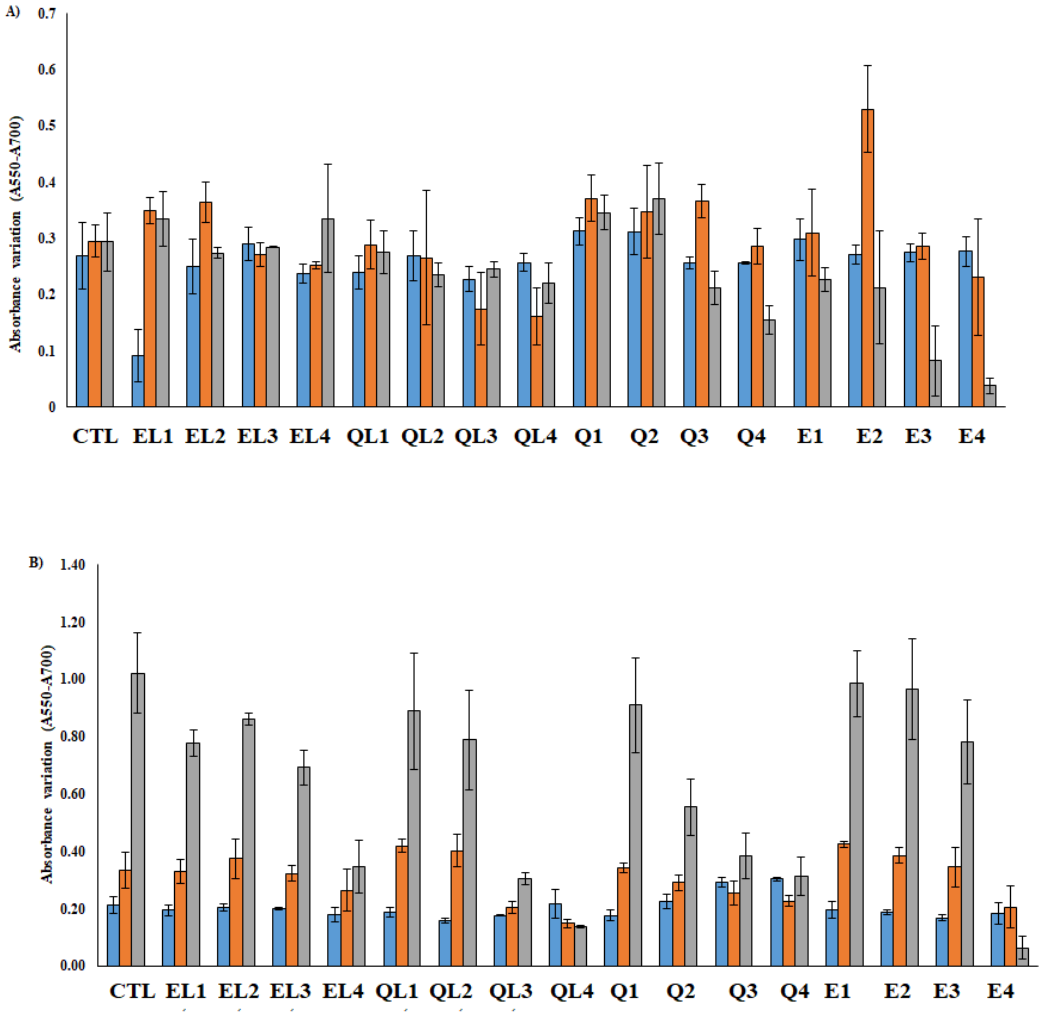

Figure 4.14: cell viability of free quercetin, empty and quercetin-loaded nanoliposomes at different concentrations on (A) hMSC and (B) human fibroblast. CTL: control, EL: empty liposomes, QL: quercetin-loaded liposomes, Q: quercetin, E: ethanol ■ day 1, ■ day 2, ■ day 3. EL1: 6.87 µg/mL, EL2: 13.8 µg/mL, EL3: 0.33 mg/mL, EL4: 0.67 mg/mL, QL1: 6.87 µg/mL, QL2: 13.8 µg/mL, QL3: 0.33 mg/mL, QL4: 0.67 mg/mL, Q1: 1 µM, Q2: 10 µM, Q3: 25 µM, Q4: 50 µM, E1, E2, E3, E4: same volume of ethanol of Q1, Q2, Q3, and Q4

4.3.10. Conclusions

In this part of the work, BSA-loaded and quercetin-loaded nanoliposomes (QL) were successfully synthetized starting from rapeseed lecithin, using a sonication process. Liposomes were characterized under a physicochemical point of view, showing a mean diameter of around two hundred nanometres and a negative surface charge. BSA-loaded liposomes had a good entrapment efficiency, 47.31 ± 2.37 %, working with 0.5 mg/mL of BSA in the loading solution, whereas in the case of QL it was 28.84 ± 4.79 %. Stability studies revealed that this kind of particles are very stable in a wide range of temperatures for 60 days, in term of size and ζ-potential. The release of quercetin was sustained during time, allowing a long-term release of this antioxidant. Rheological studies demonstrated that liposome suspension can be considered as a Newtonian fluid, showing a thixotropic behaviour. All the tested concentrations of QL were well-tolerated by hMSC. In the case of fibroblasts, the highest tested concentration (0.33 and 0.67 mg/mL of QL) revealed to be not biocompatible. Taking into account all these data, it will be necessary to characterize more BSA-loaded nanoliposomes to understand if their properties (stability over time, BSA release, rheological properties, and cell viability) will be as good as or better than those presented by QL. On the other hand, QL represent a good candidate system to be further studied and engineered with antibodies to obtain a valid antioxidant delivery system.

5. OVERALL CONCLUSIONS

In the first part of this Ph.D. thesis, several free or encapsulated bioactive compounds were used to functionalize small diameter vascular prostheses (2 and 5 mm in diameter) with the aim of fabricating a new innovative tool to be employed in vascular tissue engineering. A coating of gelatin was necessary to reduce the excessive permeability of the scaffolds. Overall, the coating with gelatin, the presence of free quercetin, of $CaCO_3$ nanoparticles encapsulating proteins and of free rapeseed and salmon lecithin did not negatively influenced the morphological, physico-chemical, mechanical, and biological properties of the scaffolds. All these data, taken together, will allow us in the next future to synthetize a multiscale model of scaffold, combining all the functionalizating agents all together, in which each component will play a particular role:

- PCL:PGS: they are the two biodegradable polymers using during the electrospinning process. They will ensure the biodegradability of the electrospun scaffold;
- gelatin: its role it to reduce the blood permeability of the prostheses and to increase their biocompatibility and hemocompatibility;
- quercetin: it will be able to act as anti-inflammatory agent in the post-surgical period;
- $CaCO_3$ nanoparticles: if they will be loaded with chemoattractant proteins, growth or differentiation factors, they will be able to recruit cells from the blood, induce their growth and, in some cases, their trans-differentiation;
- rapeseed and salmon lecithin: their role will consist of preventing oxidative processes at the level of the prostheses.

Overall, it is possible to do a comparison of all the studied coating and functionalizating agents during the Ph.D. research activity, taking into consideration Table 5.1.

Table 5.1: main results of the studied coated/functionalized scaffolds.

Type of sample	Results
PPS	- morphological studies: promising; - physico-chemical studies: promising; - permeability: not promising; - mechanical studies: promising; - suturability: promising; - biocompatibility studies: promising; - hemocompatiblity studies: promising.
GCSS	- morphological studies: promising; - physico-chemical studies: promising; - permeability: promising; - mechanical studies on dry samples: not promising; - mechanical studies on wet samples: promising; - *in vivo* suturability: promising; - biocompatibility studies: promising; - hemocompatiblity studies: promising.
QS and QGCS	- morphological studies: promising; - physico-chemical studies: promising; - permeability: promising (only in the case of QGCS); - mechanical studies on dry samples: promising (only in the case of QS); - mechanical studies on wet samples: promising; - biocompatibility studies: promising; - *in vivo* anti-inflammatory activity: promising.
NS	- morphological studies: promising; - physico-chemical studies: promising; - mechanical studies: promising; - biocompatibility studies: promising;

	- hemocompatibility studies: promising.
RLS and SLS	- morphological studies: promising; - physico-chemical studies: to be completed; - mechanical studies: to be done; - biocompatibility studies: promising; - hemocompatibility studies: to be done.

Concerning the future perspectives of this first part, they include:

- study of the mechanical properties of the fabricated scaffolds in more details performing other tests;
- multi-functionalization of the PCL:PGS scaffolds with different bioactive molecules at the same time;
- set up of a controlled-flow bioreactor;
- *in vivo* experimentation.

In the second part of this thesis, different techniques were investigated for the nanoencapsulation of proteins and polyphenols, in order to make possible the development of new drug delivery systems. These bioactive compounds were encapsulated with the aim of modulating their solubility, their stability, and their release. In conclusion, it is possible to compare the two encapsulation systems studied during the Ph.D. research activity, $CaCO_3$ particles and rapeseed lecithin nanoliposomes, referring to Table 5.2.

Table 5.2: main results and future perspectives of the studied encapsulation techniques.

Nanodelivery system	Main results	Future perspectives
$CaCO_3$ particles	- nanometric dimensions; - potential release control with LbL; - biocompatibility working with 160 μg/mL; - possibility to attach antibodies on their surface; - no inflammatory response; - hemocompatibility; - cellular up-take	- increase of entrapment efficiency; - stability studies - studies of rheological properties
Liposomes	- nanometric dimensions; - good entrapment efficiency; - stability during storage;	- immobilization of antibodies on the surface - improving of biocompatibility

- sustained release without LbL;
- good rheological properties
- biocompatibility working with 13.8 μg/mL
- studies of inflammatory response
- hemocompatibility
- cellular-uptake

References

Aditya, N. P., Chimote, G., Gunalan, K., Banerjee, R., Patankar, S., Madhusudhan, B. (2012). Curcuminoids-loaded liposomes in combination with arteether protects against *Plasmodium berghei* infection in mice. Experimental Parasitology, 131 (3), 292–299. https://doi.org/10.1016/j.exppara.2012.04.010

Alpes, H., Allmann, K., Plattner, H., Reichert, J., Rick, R., Schulz, S. (1986). Formation of large unilamellar vesicles using alkyl maltoside detergents. Biochimica et Biophysica Acta (BBA) - Biomembranes, 862 (2), 294–302. https://doi.org/10.1016/0005-2736(86)90231-2

Ambler, G. K., Radwan, R., Hayes, P. D., Twine, C. P. (2014). Atherectomy for peripheral arterial disease. Cochrane Database of Systematic Reviews, (3). https://doi.org/10.1002/14651858.CD006680.pub2

An, Z., Kavanoor, K., Choy, M. L., Kaufman, L. J. (2009). Polyelectrolyte microcapsule interactions with cells in two- and three-dimensional culture. Colloids and Surfaces B: Biointerfaces, 70 (1), 114–123. https://doi.org/10.1016/j.colsurfb.2008.12.022

Angelova, N., Yordanov, G. (2017). Entrapment of β-FeO(OH) nanoparticles in human serum albumin: Preparation, characterization and hemocompatibility. Colloids and Surfaces A: Physicochemical and Engineering Aspects, 516 (5) 317–324. https://doi.org/10.1016/j.colsurfa.2016.12.048

Arab Tehrany, E., Kahn, C. J. F., Baravian, C., Maherani, B., Belhaj, N., Wang, X., Linder, M. (2012). Elaboration and characterization of nanoliposome made of soya; rapeseed and salmon lecithins: Application to cell culture. Colloids and Surfaces B: Biointerfaces, 95, 75–81. https://doi.org/10.1016/j.colsurfb.2012.02.024

Ariga, K., Lvov, Y. M., Kawakami, K., Ji, Q., Hill, J. P. (2011). Layer-by-layer self-assembled shells for drug delivery. Advanced Drug Delivery Reviews, 63 (9), 762–771. https://doi.org/10.1016/j.addr.2011.03.016

Badylak, S. F. (2007). The extracellular matrix as a biologic scaffold material. Biomaterials, 28 (25), 3587–3593. https://doi.org/10.1016/j.biomaterials.2007.04.043

Baguneid, M. S., Seifalian, A. M., Salacinski, H. J., Murray, D., Hamilton, G., Walker, M. G. (2006). Tissue engineering of blood vessels. British Journal of Surgery, 93 (3), 282–290. https://doi.org/10.1002/bjs.5256

Bala, I., Bhardwaj, V., Hariharan, S., Kharade, S. V., Roy, N., Kumar, M. N. V. R. (2006). Sustained release nanoparticulate formulation containing antioxidant-ellagic acid as potential prophylaxis system for oral administration. Journal of Drug Targeting, 14 (1), 27–34. https://doi.org/10.1080/10611860600565987

Bale, S. S., Kwon, S. J., Shah, D. A., Banerjee, A., Dordick, J. S., Kane, R. S. (2010). Nanoparticle-mediated cytoplasmic delivery of proteins to target cellular machinery. ACS Nano, 4 (3), 1493–1500. https://doi.org/10.1021/nn901586e

Balguid, A., Mol, A., van Marion, M. H., Bank, R. A., Bouten, C. V. C., Baaijens, F. P. T. (2009). Tailoring fiber diameter in electrospun poly(ε-caprolactone) scaffolds for optimal cellular infiltration in cardiovascular tissue engineering. Tissue Engineering Part A, 15 (2), 437–444. https://doi.org/10.1089/ten.tea.2007.0294

Bangham, A. D., Standish, M. M., Watkins, J. C. (1965). Diffusion of univalent ions across the lamellae of swollen phospholipids. Journal of Molecular Biology, 13 (1), 238-227. https://doi.org/10.1016/S0022-2836(65)80093-6

Barenholzt, Y., Amselem, S., Lichtenberg, D. (1979). A new method for preparation of phospholipid vesicles (liposomes) - french press. FEBS Letters, 99 (1), 210–214. https://doi.org/10.1016/0014-5793(79)80281-1

Beachley, V., Wen, X. (2009). Effect of electrospinning parameters on the nanofiber diameter and length. Materials Science and Engineering C, 29 (3), 663–668. https://doi.org/10.1016/j.msec.2008.10.037

Bender, E. A., Adorne, M. D., Colomé, L. M., Abdalla, D. S. P., Guterres, S. S., Pohlmann, A. R. (2012). Hemocompatibility of poly(ε-caprolactone) lipid-core nanocapsules stabilized with polysorbate 80-lecithin and uncoated or coated with chitosan. International Journal of Pharmaceutics, 426 (1–2), 271-279. https://doi.org/10.1016/j.ijpharm.2012.01.051

Benedet, J. A., Umeda, H., Shibamoto, T. (2007). Antioxidant activity of flavonoids isolated from young green barley leaves toward biological lipid samples. Journal of Agricultural and Food Chemistry, 55 (14), 5499–5504. https://doi.org/10.1021/jf070543t

Bhatt, L. K., Addepalli, V. (2010). Attenuation of diabetic retinopathy by enhanced inhibition of MMP-2 and MMP-9 using aspirin and minocycline in streptozotocin-diabetic rats. American Journal of Translational Research, 2 (2), 181–189.

Biradar, S., Ravichandran, P., Gopikrishnan, R., Goornavar, V., Hall, J. C. Ramesh, V., Baluchamy, S., Jeffers, R. B., Ramesh, G. T. (2011). Calcium carbonate nanoparticles: synthesis,characterization and biocompatibility. Journal of Nanoscience and Nanotechnology, 11, (8), 6868-6874. https://doi.org/10.1166/jnn.2011.4251

Boots, A. W., Haenen, G. R. M. M., Bast, A. (2008). Health effects of quercetin: From antioxidant to nutraceutical. European Journal of Pharmacology, 585 (2–3), 325–337. https://doi.org/10.1016/j.ejphar.2008.03.008

Bosworth, L., Downes, S. (2009). Biocompatible three-dimensional scaffolds for tendon tissue engineering using electrospinning, in Di Silvio L., editor, Cellular response to biomaterials, chapter 1.CRC Press.

Bouarab, L., Maherani, B., Kheirolomoom, A., Hasan, M., Aliakbarian, B., Linder, M., Arab-Tehrany, E. (2014). Influence of lecithin-lipid composition on physico-chemical properties of nanoliposomes loaded with a hydrophobic molecule. Colloids and Surfaces B: Biointerfaces, 115, 197–204. https://doi.org/10.1016/j.colsurfb.2013.11.034

Boyjoo, Y., Pareek, V. K., Liu, J. (2014). Synthesis of micro and nano-sized calcium carbonate particles and their applications. Journal of Materials Chemistry A, 2 (35), 14270–14288. https://doi.org/10.1039/C4TA02070G

Burdick, J. A., Padera, R. F., Huang, J. V., Anseth, K. S. (2002). An investigation of the cytotoxicity and histocompatibility of in situ forming lactic acid based orthopedic biomaterials. Journal of Biomedical Materials Research, 63 (5), 484–491. https://doi.org/10.1002/jbm.10298

Buruaga, L., Gonzalez, A., Iruin, J. J. (2009). Electrospinning of poly (2-ethyl-2-oxazoline). Journal of Materials Science, 44 (12), 3186–3191. https://doi.org/10.1007/s10853-009-3424-9

Buruaga, L., Gonzalez, A., Iruin, J. J. (2009). Electrospinning of poly (2-ethyl-2-oxazoline). Journal of Materials Science, 44 (12), 3186–3191. https://doi.org/10.1007/s10853-009-3424-9

Calder, P. C. (2006). n-3 polyunsaturated fatty acids, inflammation, and inflammatory diseases. The American Journal of Clinical Nutrition, 83 (6), 1505S–1519S. https://doi.org/16841861

Camilleri, J. P., Phat, V. N., Bruneval, P. (1985). Surface healing and histological maturation of patent polytetrafluoroethylene grafts implanted in patients for up to 60 months. Archives of Pathology & Laboratory Medicine, 109 (9), 833-837. PMID: 3927869

Campbell, C. D., Goldfarb, D., Roe, R. (1975). A small arterial substitute: expanded microporous polytetrafluoroethylene: patency versus porosity. Annals of Surgery, 182 (2), 138–43. https://doi.org/10.1097/00000658-197508000-00010

Cardiovascular implants – Tubular vascular prostheses. Association for the Advancement of Medical Instrumentation, ANSI/AAMI/ISO 7198:1998/2001/(R) 2004.

Chakraborty, S., Stalin, S., Das, N., Thakur Choudhury, S., Ghosh, S., Swarnakar, S. (2012). The use of nano-quercetin to arrest mitochondrial damage and MMP-9 upregulation during prevention of gastric inflammation induced by ethanol in rat. Biomaterials, 33 (10), 2991–3001. https://doi.org/10.1016/j.biomaterials.2011.12.037

Chang, H., Yeh, M. K. (2012). Clinical development of liposome-based drug : formulation , characterization , and therapeutic efficacy. International Journal of Nanomedicine, 7, 49–60. https://doi.org/10.2147/IJN.S26766

Chansiri, G., Lyons, R. T., Patel, M. V., Hem, S. L. (1999). Effect of surface charge on the stability of oil/water emulsions during steam sterilization. Journal of Pharmaceutical Sciences, 88 (4), 454-458. https://doi.org/10.1021/js980293i

Cho, K., Wang, X., Nie, S., Chen, Z., Shin, D. M. (2008). Therapeutic nanoparticles for drug delivery in cancer. Clinical Cancer Research, 14 (5), 1310–1316. https://doi.org/10.1158/1078-0432.CCR-07-1441

Colas, J. C., Shi, W., Rao, V. S. N. M., Omri, A., Mozafari, M. R., Singh, H. (2007). Microscopical investigations of nisin-loaded nanoliposomes prepared by Mozafari method and their bacterial targeting. Micron, 38 (8), 841–847. https://doi.org/10.1016/j.micron.2007.06.013

Colletier, J. P., Chaize, B., Winterhalter, M., Fournier, D. (2002). Protein encapsulation in liposomes: Efficiency depends on interactions between protein and phospholipid bilayer. BMC Biotechnology, 2, 1–8. https://doi.org/10.1186/1472-6750-2-9

Coonrod, D., Brick, M.A., Byrne, P.F., DeBonte, L., Chen, Z. (2008). Inheritance of long chain fatty acid content in rapeseed (*Brassica napus* L.). Euphytica, 164 (2), 583-592. https://doi.org/10.1007/s10681-008-9781-7

Crespo, I., García-Mediavilla, M. V., Gutiérrez, B., Sánchez-Campos, S., Tuñón, M. J., González-Gallego, J. (2008). A comparison of the effects of kaempferol and quercetin on cytokine-induced pro-inflammatory status of cultured human endothelial cells, British Journal of Nutrition, 100 (5), 968-976. https://doi.org/10.1017/S0007114508966083

Cui, W., Li, X., Zhu, X., Yu, G., Zhou, S., Weng, J. (2006). Investigation of drug release and matrix degradation of electrospun poly (DL-lactide) fibers with paracetanol inoculation. Biomacromolecules, 7, 1623–1629. https://doi.org/10.1021/bm060057z

Cui, W., Zhou, Y., Chang, J. (2010). Electrospun nanofibrous materials for tissue engineering and drug delivery. Science and Technology of Advanced Materials, 11 (1), 14108. https://doi.org/10.1088/1468-6996/11/1/014108

Dash, S., Murthy, P. N., Nath, L., Chowdhury, P. (2010). Kinetic modeling on drug release from controlled drug delivery systems. Acta Poloniae Pharmaceutica, 67 (3), 217–23. https://doi.org/10.1016/S0928-0987(01)00095-

1

De Clercq, E. (2013). Antiviral drug development - Success and failure: A personal perspective with a Japanese connection. Antiviral Chemistry and Chemotherapy, 23 (2), 45–55. https://doi.org/10.3851/IMP2396

De Cock, L. J., De Koker, S., De Geest, B. G., Grooten, J., Vervaet, C., Remon, J. P., Antipina, M. N. (2010). Polymeric multilayer capsules in drug delivery. Angewandte Chemie - International Edition, 49 (39), 6954–6973. https://doi.org/10.1002/anie.200906266

De Geest, B. G., Vandenbroucke, R. E., Guenther, A. M., Sukhorukov, G. B., Hennink, W. E., Sanders, N. N., Demeester, J., De Smedt, S. C. (2006). Intracellularly degradable polyelectrolyte microcapsules. Advanced Materials, 18 (8), 1005–1009. https://doi.org/10.1002/adma.200502128

De Koker, S., De Geest, B. G., Singh, S. K., De Rycke, R., Naessens, T., Van Kooyk, Y., Demeester J., De Smedt, S. C., Grooten, J. (2009). Polyelectrolyte microcapsules as antigen delivery vehicles to dendritic cells: Uptake, processing, and cross-presentation of encapsulated antigens. Angewandte Chemie - International Edition, 48 (45), 8485–8489. https://doi.org/10.1002/anie.200903769

Deitzel, J., Kleinmeyer, J., Harris, D., Beck Tan, N. (2001). The effect of processing variables on the morphology of electrospun nanofibers and textiles. Polymer, 42 (1), 261–272. https://doi.org/10.1016/S0032-3861(00)00250-0

Del Gaudio, C., Bianco, A., Folin, M., Baiguera, S., Grigioni, M. (2009). Structural characterization and cell response evaluation of electrospun PCL membranes: Micrometric versus submicrometric fibers. Journal of Biomedical Materials Research - Part A, 89 (4), 1028–1039. https://doi.org/10.1002/jbm.a.32048

Dvir, T., Timko, B. P., Kohane, D. S., Langer, R. (2011). Nanotechnological strategies for engineering complex tissues. Nature Nanotechnology, 6 (1), 13–22. https://doi.org/10.1038/nnano.2010.246

Eghbal, N., Choudhary, R. (2018). Complex coacervation: Encapsulation and controlled release of active agents in food systems. LWT - Food Science and Technology, 90, 254–264. https://doi.org/10.1016/j.lwt.2017.12.036

Elahi, M., Guan, G., Wang, L. (2014). Hemocompatibility of surface modified silk fibroin materials: A review. Reviews on Advanced Materials Science, 38 (2), 148–159.

Fang, Z., Bhandari, B. (2010). Encapsulation of polyphenols - A review. Trends in Food Science and Technology, 21 (10), 510–523. https://doi.org/10.1016/j.tifs.2010.08.003

Farra, R., Sheppard, N. F., McCabe, L., Neer, R. M., Anderson, J. M., Santini, J. T., Cima, M. J., Langer, R. (2012). First-in-human testing of a wirelessly controlled drug delivery microchip first-in-human testing of a wirelessly controlled drug delivery microchip, 4 (122). https://doi.org/10.1126/scitranslmed.3003276

Fathi, M., Mozafari, M. R., Mohebbi, M. (2012). Nanoencapsulation of food ingredients using lipid based delivery systems. Trends in Food Science and Technology, 23 (1), 13–27. https://doi.org/10.1016/j.tifs.2011.08.003

Ferrari, P. F., Aliakbarian, B., Lagazzo, A., Tamayol, A., Palombo, D., Perego, P. (2017). Tailored electrospun small-diameter graft for vascular prosthesis. International Journal of Polymeric Materials and Polymeric Biomaterials, 66 (12), 635–643. https://doi.org/10.1080/00914037.2016.1252361

Ferrari, P. F., Aliakbarian, B., Zattera, E., Pastorino, L., Palombo, D., Perego, P. (2017). Engineered $CaCO_3$

nanoparticles with targeting activity: A simple approach for a vascular intended drug delivery system. Canadian Journal of Chemical Engineering, 95 (9), 1683–1689. https://doi.org/10.1002/cjce.22871

Fleckenstein, P., Werner, H.H. (1988). Vessel and prosthesis impregnated with diisocyanate crosslinked gelatin. Patent number: 4784659.

Formichi, M. J., Guidoin, R. G., Jausseran, J. M., Awad, J. A., Johnston, K. W., Eng, M. W. K. P., Courbier, R., Marois, M., Rouleau, C., Batt, M., Girard, J. F., Gosselin, C. (1988). Expanded PTFE prosthesis as arterial substitute in humans: Late pathological findings in 73 excised grafts. Annals of Vascular Surgery, 2 (1), 14-27. https://doi.org/10.1016/S0890-5096(06)60773-5

Fuchs, J. R., Nasseri, B. A., Vacanti, J. P. (2001). Tissue Engineering: A 21st Century Solution to Surgical Reconstruction. The Annals of Thoracic Surgery, 72, 577–591.

Fujihara, K., Kotaki, M., Ramakrishna, S. (2005). Guided bone regeneration membrane made of polycaprolactone/calcium carbonate composite nano-fibers. Biomaterials, 26 (19), 4139–4147. https://doi.org/10.1016/j.biomaterials.2004.09.014

Gabay, C. (2006). Interleukin-6 and chronic inflammation. Arthritis Research & Therapy, 8 (2), 1-6. https://doi.org/10.1186/ar1917

Ge, Y., Wang, J., Shi, Z., Yin, J. (2012). Gelatin-assisted fabrication of water-dispersible graphene and its inorganic analogues. Journal of Materials Chemistry, 22 (34), 17619. https://doi.org/10.1039/c2jm33173j

Georgetti, S. R., Casagrande, R., Souza, C. R. F., Oliveira, W. P., Fonseca, M. J. V. (2008). Spray drying of the soybean extract: Effects on chemical properties and antioxidant activity. LWT - Food Science and Technology, 41 (8), 1521–1527. https://doi.org/10.1016/j.lwt.2007.09.001

Ghasemi-Mobarakeh, L., Prabhakaran, M. P., Morshed, M., Nasr-Esfahani, M. H., Ramakrishna, S. (2008). Electrospun poly(ε-caprolactone)/gelatin nanofibrous scaffolds for nerve tissue engineering. Biomaterials, 29 (34), 4532–4539. https://doi.org/10.1016/j.biomaterials.2008.08.007

Gomathi, K., Gopinath, D., Ahmed, M. R., Jayakumar, R. (2003). Quercetin incorporated collagen matrices for dermal wound healing processes in rat. Biomaterials, 24 (16), 2767–2772. https://doi.org/10.1016/S0142-9612(03)00059-0

Gomez-Guillen, M. C., Gimenez, B., Lopez-Caballero, M. E., Montero, M. P. (2011). Functional and bioactive properties of collagen and gelatin from alternative sources: A review. Food Hydrocolloids, 25 (8), 1813–1827. https://doi.org/10.1016/j.foodhyd.2011.02.007

Grazia Calvagno, M., Celia, C., Paolino, D., Cosco, D., Iannone, M., Castelli, F., Doldo, P., Fresta, M. (2007). Effects of lipid composition and preparation conditions on physical-chemical properties, technological parameters and *in vitro* biological activity of gemcitabine-loaded liposomes. Current Drug Delivery, 4, 89–101. https://doi.org/10.2174/156720107779314749

Gui, L., Muto, A., Chan, S. A., Breuer, C. K., Niklason, L. E. (2009). Development of decellularized human umbilical arteries as small-diameter vascular grafts. Tissue Engineering Part A, 15 (9), 2665–2676. https://doi.org/10.1089/ten.tea.2008.0526

Guidon, R., Chakfé, N., Maurel, S. (1993). Expanded polytetrafluoroethylene arterial prosthesis in humans:

Histopathological study of 298 surgically excised grafts. Biomaterials, 14 (9), 678-693. https://doi.org/10.1016/0142-9612(93)90067-C

Gunatillake, P. A., Adhikari, R. (2003). Biodegradable synthetic polymers for tissue engineering. European Cells and Materials, 5, 1-16. https://doi.org/10.22203/eCM.v005a01

Habibi, N., Pastorino, L., Soumetz, F. C., Sbrana, F., Raiteri, R., Ruggiero, C. (2011). Nanoengineered polymeric S-layers based capsules with targeting activity. Colloids and Surfaces B: Biointerfaces, 88 (1), 366–372. https://doi.org/10.1016/j.colsurfb.2011.07.015

Harborne, J. B., Baxter, H. (1999). The handbook of natural flavonoids, John Wiley, Chichester, vii-xiii.

Hasan, M., Belhaj, N., Benachour, H., Barberi-Heyob, M., Kahn, C. J. F., Jabbari, E., Linder, M., Arab-Tehrany, E. (2014). Liposome encapsulation of curcumin: Physico-chemical characterizations and effects on MCF7 cancer cell proliferation. International Journal of Pharmaceutics, 461 (1–2), 519–528. https://doi.org/10.1016/j.ijpharm.2013.12.007

Hasan, M., Ben Messaoud, G., Michaux, F., Tamayol, A., Kahn, C. J. F., Belhaj, N., Linder, M., Arab-Tehrany, E. (2016). Chitosan-coated liposomes encapsulating curcumin: study of lipid–polysaccharide interactions and nanovesicle behavior. Royal Society of Chemistry Advances, 6 (51), 45290–45304. https://doi.org/10.1039/c6ra05574e

He, X. W., Liu, T., Chen, Y. X., Cheng, D. J., Li, X. R., Xiao, Y., Feng, Y. L. (2008). Calcium carbonate nanoparticle delivering vascular endothelial growth factor-C siRNA effectively inhibits lymphangiogenesis and growth of gastric cancer in vivo. Cancer Gene Therapy, 15, 193–202. https://doi.org/10.1038/sj.cgt.7701122

Hollister, S. J. (2005). Porous scaffold design for tissue engineering. Nature Materials, 4 (7), 518–524. https://doi.org/10.1038/nmat1421

Hu, J. J., Chao, W. C., Lee, P. Y., Huang, C. H. (2012). Construction and characterization of an electrospun tubular scaffold for small-diameter tissue-engineered vascular grafts: A scaffold membrane approach. Biomedical Materials, 13, 140-155. https://doi.org/10.1016/j.jmbbm.2012.04.013

Huang, S. C., Naka, K., Chujo, Y. (2007). A carbonate controlled-addition method for amorphous calcium carbonate spheres stabilized by poly(acrylic acid)s. Langmuir, 23 (24), 12086–12095. https://doi.org/10.1021/la701972n

Hutmacher, D. W. (2000). Scaffolds in tissue engineering bone and cartilage. Biomaterials, 21 (24), 2529–2543. https://doi.org/10.1016/S0142-9612(00)00121-6

Imai, Y., Nose, Y. (1972). A new method for evalution of antithrombogenicity of materials. Journal of Biomedical Materials Research Part A, 6 (3), 165-172. https://doi.org/10.1002/jbm.820060305

Isenberg, B. C., Williams, C., Tranquillo, R. T. (2006). Endothelialization and flow conditioning of fibrin-based media-equivalents. Annals of Biomedical Engineering, 34 (6), 971–985. https://doi.org/10.1007/s10439-006-9101-0

Jangde, R., Singh, D. (2014). Compatibility studies of quercetin with pharmaceutical excipients used in the development of novel formulation. Research Journal of Pharmacy and Technology, 7 (10), 1101-1105.

Jangde, R., Singh, D. (2016). Preparation and optimization of quercetin-loaded liposomes for wound healing, using

response surface methodology. Artificial Cells, Nanomedicine, and Biotechnology, 44(2), 635–641. https://doi.org/10.3109/21691401.2014.975238

Jenkins, M. J., Harrison, K. L. (2008). The effect of crystalline morphology on the degradation of polycaprolactone in a solution of phosphate buffer and lipase. Polymers for Advanced Technologies, 19 (12), 1901-1906. https://doi.org/10.1002/pat.1227

Johnston, A. P. R., Cortez, C., Angelatos, A. S., Caruso, F. (2006). Layer-by-layer engineered capsules and their applications. Current Opinion in Colloid and Interface Science, 11(4), 203–209. https://doi.org/10.1016/j.cocis.2006.05.001

Kadri, R., Ben Messaoud, G., Tamayol, A., Aliakbarian, B., Zhang, H. Y., Hasan, M., Sánchez-González, L., Arab-Tehrany, E. (2016). Preparation and characterization of nanofunctionalized alginate/methacrylated gelatin hybrid hydrogels. RSC Advances, 6(33), 27879–27884. https://doi.org/10.1039/C6RA03699F

Kaempfe, P., Lauth, V. R., Halfer, T., Treccani, L., Maas, M., Rezwan, K. (2013). Micromolding of calcium carbonate using a bio-inspired, coacervation-mediated process. Journal of the American Ceramic Society, 96 (3), 736–742. https://doi.org/10.1111/jace.12194

Kamphuis, M. M. J., Johnston, A. P. R., Such, G. K., Dam, H. H., Evans, R. A., Scott, A. M., Nice, E. C., Heath, J. K., Caruso, F. (2010). Targeting of cancer cells using click-functionalized polymer capsules. Journal of the American Chemical Society, 132, 15881–15883. https://doi.org/10.1021/ja106405c

Kannisto, K., Murtomäki, L., Viitala, T. (2011). An impedance QCM study on the partitioning of bioactive compounds in supported phospholipid bilayers. Colloids and Surfaces B: Biointerfaces, 86 (2), 298–304. https://doi.org/10.1016/j.colsurfb.2011.04.012

Khalfoun, B., Thibault, F., Watier, H., Bardos, P., Lebranchu, Y. (1997). Docosahexaenoic and eicosapentaenoic acids inhibit *in vitro* human endothelial cell production of interleukin-6. Advances in Experimental Medicine and Biology, 400B, 589-597. PMID: 9547608

Kharaziha, M., Nikkhah, M., Shin, S. R., Annabi, N., Masoumi, N., Gaharwar, A. K., Camci-Unala, G., Khademhosseini, A. (2013). PGS:Gelatin nanofibrous scaffolds with tunable mechanical and structural properties for engineering cardiac tissues. Biomaterials, 34 (27), 6355–6366. https://doi.org/10.1016/j.biomaterials.2013.04.045

Kim, S. E., Heo, D. N., Lee, J. B., Kim, J. R., Park, S. H., Jeon, S. H., Kwon, I. K. (2009). Electrospun gelatin/polyurethane blended nanofibers for wound healing. Biomedical Materials, 4, 1-11. https://doi:10.1088/1748-6041/4/4/044106

Kisel, M. A., Kulik, L. N., Tsybovsky, I. S., Vlasov, A. P., Vorob'yov, M. S., Kholodova, E. A., Zabarovskaya, Z. V. (2001). Liposomes with phosphatidylethanol as a carrier for oral delivery of insulin: Studies in the rat. International Journal of Pharmaceutics, 216 (1–2), 105–114. https://doi.org/10.1016/S0378-5173(01)00579-8

Kobuchi, H., Roy, S., Sen, C. K., Nguyen, H. G., Packer, L. (1999). Quercetin inhibits inducible ICAM-1 expression in human endothelial cells through the JNK pathway. American Journal of Physiology - Cell Physiology, 277 (3), C403–C411.

Konig, G., McAllister, T. N., Dusserre, N., Garrido, S. A., Iyican, C., Marini, A., Fiorillo, A., Avila, H.,

Wystrychowski, W., Zagalski, K., Maruszewski, M., Linthurst Jones, A., Cierpka, L., de la Fuente, L. M., L'Heureux, N. (2009). Mechanical properties of completely autologous human tissue engineered blood vessels compared to human saphenous vein and mammary artery. Biomaterials, 30 (8), 1542–1550. https://doi.org/10.1016/j.biomaterials.2008.11.011

Kurapati, R., Raichur, A. M. (2013). Composite cyclodextrin–calcium carbonate porous microparticles and modified multilayer capsules: novel carriers for encapsulation of hydrophobic drugs. Journal of Materials Chemistry B, 1 (25), 3175. https://doi.org/10.1039/c3tb20192a

Lamprecht, A., Ubrich, N., Hombreiro Pérez, M., Lehr, C.M., Hoffman, M., Maincent, P. (2000). Influences of process parameters on nanoparticle preparation performed by a double emulsion pressure homogenization technique. International Journal of Pharmaceutics, 196 (2), 177–182. https://doi.org/10.1016/S0378-5173(99)00422-6

Langer, R. (1998). Drug delivery and targeting. Nature 392, 5-10. PMID:9579855

Langer, R., Vacanti, J.P. (1993). Tissue Engineering. Science, 260, 920-926.

Lanza, R. P., Langer, R., Vacanti, J. P. (2000) Principle of Tissue Engineering, 2nd edition. Academic press.

Lauth, V., Maas, M., Rezwan, K. (2014). Coacervate-directed synthesis of $CaCO_3$ microcarriers for pH-responsive delivery of biomolecules. Journal of Materials Chemistry B, 2 (44), 7725–7731. https://doi.org/10.1039/C4TB01213E

Lawrence, B. J., Madihally, S. V. (2008). Cell colonization in degradable 3D porous matrices. Cell Adhesion & Migration, 2 (1), 9–16. https://doi.org/10.4161/cam.2.1.5884

Lee, K. Y., Mooney, D. J. (2001). Hydrogels for tissue engineering. Chemical Reviews, 101 (7), 1869–1879. https://doi.org/10.1021/cr000108x

Lee, Y. H., Lee, J. H., An, I. G., Kim, C., Lee, D. S., Lee, Y. K., Nam, J. D. (2005). Electrospun dual-porosity structure and biodegradation morphology of Montmorillonite reinforced PLLA nanocomposite scaffolds. Biomaterials, 26 (16), 3165–3172. https://doi.org/10.1016/j.biomaterials.2004.08.018

Lee, Y., Kwon, J., Khang, G., Lee, D. (2012). Reduction of inflammatory responses and enhancement of extracellular matrix formation by vanillin-incorporated poly(lactic- co -glycolic acid) scaffolds. Tissue Engineering Part A, 18 (19–20), 1967–1978. https://doi.org/10.1089/ten.tea.2012.0001

Leopoldini, M., Russo, N., Toscano, M. (2011). The molecular basis of working mechanism of natural polyphenolic antioxidants. Food Chemistry, 125 (2), 288–306. https://doi.org/10.1016/j.foodchem.2010.08.012

Lingaiah, S., Shivakumar, K. N., Sadler, R., Sharpe, M. (2007). Electrospinning of nanofabrics. Center for Composite Materials Research.

Liu H., Wang, S., Qi, N. (2012). Controllable structure, properties, and degradation of the electrospun PLGA/PLA-blended nanofibrous scaffolds. Journal of Applied Polymer Science, 125, E468–E476. https://doi:10.1002/app.36757

Liu, Q., Boyd, B. J. (2013). Liposomes in biosensors. The Analyst, 138 (2), 391–409. https://doi.org/10.1039/C2AN36140J

Liu, X., Gao, C., Shen, J., Möhwald, H. (2005). Multilayer microcapsules as anti-cancer drug delivery vehicle:

Deposition, sustained release, and in vitro bioactivity. Macromolecular Bioscience, 5 (12), 1209–1219. https://doi.org/10.1002/mabi.200500176

Loh, Q. L., Choong, C. (2013). Three-dimensional scaffolds for tissue engineering applications: role of porosity and pore size. Tissue Engineering Part B: Reviews, 19 (6), 485–502. https://doi.org/10.1089/ten.teb.2012.0437

Lovelyn, C., Attama, A. A. (2011). Current state of nanoemulsions in drug delivery. Journal of Biomaterials and Nanobiotechnology, 2 (5), 626–639. https://doi.org/10.4236/jbnb.2011.225075

Madhavan, K., Elliott, W. H., Bonani, W., Monnet, E., Tan, W. (2013). Mechanical and biocompatible characterizations of a readily available multilayer vascular graft. Journal of Biomedical Materials Research Part B: Applied Biomaterials, 101 (4), 506–519. https://doi:10.1002/jbm.b.32851

Mady, M. M., Darwish, M. M., Khalil, S., Khalil, W. M. (2009). Biophysical studies on chitosan-coated liposomes. European Biophysics Journal, 38 (8), 1127–1133. https://doi.org/10.1007/s00249-009-0524-z

Maherani, B., Arab-Tehrany, E., Kheirolomoom, A., Cleymand, F., Linder, M. (2012). Influence of lipid composition on physicochemical properties of nanoliposomes encapsulating natural dipeptide antioxidant L-carnosine. Food Chemistry, 134 (2), 632–640. https://doi.org/10.1016/j.foodchem.2012.02.098

Mayer, A., Vadon, M., Rinner, B., Novak, A., Wintersteiger, R., Fröhlich, E. (2009). The role of nanoparticle size in hemocompatibility. Toxicology, 258 (2–3), 139-147. https://doi.org/10.1016/j.tox.2009.01.015

McKay, T. B., Lyon, D., Sarker-Nag, A., Priyadarsini, S., Asara, J. M., Karamichos, D. (2015). Quercetin attenuates lactate production and extracellular matrix secretion in keratoconus. Scientific Reports, 5. https://doi.org/10.1038/srep09003

Meng, Z. X., Zheng, W., Li, L., Zheng, Y. F. (2010). Fabrication and characterization of three-dimensional nanofiber membrance of PCL-MWCNTs by electrospinning. Materials Science and Engineering C, 30 (7), 1014–1021. https://doi.org/10.1016/j.msec.2010.05.003

Mine, Y., Noishiki, Y., Mitsui, H., Nakai, M., Oshima, Y., Sano, S. (2010). Suture retention strength of expanded Polytetrafluoroethylene (ePTFE) graft. Acta Medica Okayama, 64 (2), 121-128

Moore, K. J., Tabas, I. (2011). Macrophages in the pathogenesis of atherosclerosis. Cell, 145 (3), 341–355. https://doi.org/10.1016/j.cell.2011.04.005

Mora-Huertas, C. E., Fessi, H., Elaissari, A. (2010). Polymer-based nanocapsules for drug delivery. International Journal of Pharmaceutics, 385 (1–2), 113–142. https://doi.org/10.1016/j.ijpharm.2009.10.018

Motlagh, D., Yang, J., Lui, K. Y., Webb, A. R., Ameer, G. A. (2006). Hemocompatibility evaluation of poly(glycerol-sebacate) *in vitro* for vascular tissue engineering. Biomaterials, 27 (24), 4315–4324. https://doi.org/10.1016/j.biomaterials.2006.04.010

Mozafari, M. R., Johnson, C., Hatziantoniou, S., Demetzos, C. (2008). Nanoliposomes and their applications in food nanotechnology. Journal of Liposome Research, 18 (4), 309–327. https://doi.org/10.1080/08982100802465941

Munin, A., Edwards-Lévy, F. (2011). Encapsulation of natural polyphenolic compounds; a review. Pharmaceutics (Vol. 3). https://doi.org/10.3390/pharmaceutics3040793

Murakami, A., Ashida, H., Terao, J. (2008). Multitargeted cancer prevention by quercetin. Cancer Letters, 269 (2),

315–325. https://doi.org/10.1016/j.canlet.2008.03.046

Nagaraja, A. T., Pradhan, S., McShane, M. J. (2014). Poly (vinylsulfonic acid) assisted synthesis of aqueous solution stable vaterite calcium carbonate nanoparticles. Journal of Colloid and Interface Science, 418, 366–372. https://doi.org/10.1016/j.jcis.2013.12.008

Navas Díaz, A., Ramos Peinado, M. C., Torijas Minguez, M. C. (1998). Sol-gel horseradish peroxidase biosensor for hydrogen peroxide detection by chemiluminescence. Analytica Chimica Acta, 363 (2–3), 221–227. https://doi.org/10.1016/S0003-2670(98)00080-4

Ndesendo V. M. K., Pillay, V., Choonara, Y. E., Du Toit, L. C., Meyer, L. C. R., Buchmann, E., Kumar, P., Khan, R.A. (2011). *In vivo* evaluation of the release of zidovudine and polystyrene sulfonate from a dual intravaginal bioadhesive polymeric device in the pig model. Journal of Pharmaceutical Sciences, 100 (4), 1416-1435. https://doi.org/10.1002/jps.22365

Nerem, R. M., Seliktar, D. (2001). Vascular Tissue Engineering. Annual Review of Biomedical Engineering, 3 (1), 225–243. https://doi.org/10.1146/annurev.bioeng.3.1.225

Nicolas, J., Mura, S., Brambilla, D., Mackiewicz, N., Couvreur, P. (2013). Design, functionalization strategies and biomedical applications of targeted biodegradable/biocompatible polymer-based nanocarriers for drug delivery. Chemical Society Reviews, 42 (3), 1147–1235. https://doi.org/10.1039/C2CS35265F

Nilsen-Nygaard, J., Strand, S. P., Vårum, K. M., Draget, K. I., Nordgård, C. T. (2015). Chitosan: Gels and interfacial properties. Polymers, 7 (3), 552–579. https://doi.org/10.3390/polym7030552

Nuti, S. (2010). Tissue engineered vascular grafts: The bright future of heart health. Yale Scientific Magazine.

Onder, E., Sarier, N., Cimen, E. (2007). Encapsulation of phase change materials by complex coacervation to improve thermal performances of woven fabrics. Thermochimica Acta, 467 (1–2), 63–72. https://doi.org/10.1016/j.tca.2007.11.007

Osathanon, T., Chanjavanakul, H., Phunphimp, Kongdecha, P., Clayhan, P., Huynh, N. C. N. (2017). Regeneration membrane polycaprolactone-based biomaterials for guided tissue regeneration membrane. Periodontitis - A Useful Reference Successful, 171–188. https://doi.org/10.5772/intechopen.69153

Otake, K., Shimomura, T., Goto, T., Imura, T., Furuya, T., Yoda, S., Takebayashi, Y., Sakai, H., Abe, M. (2006). Preparation of liposomes using an improved supercritical reverse phase evaporation method. Langmuir, 22(6), 2543–2550. https://doi.org/10.1021/la051654u

Paini, M., Aliakbarian, B., Casazza, A. A., Perego, P., Ruggiero, C., Pastorino, L. (2015 A). Chitosan/dextran multilayer microcapsules for polyphenol co-delivery. Materials Science and Engineering C, 46, 374–380. https://doi.org/10.1016/j.msec.2014.10.047

Paini, M., Casazza, A.A., Aliakbarian, B., Perego, P., Binello, A., Cravotto, G. (2016). Influence of ethanol/water ratio in ultrasound and high-pressure/high-temperature phenolic compound extraction from agri-food waste. International Journal of Food Science & Technology, 51 (2), 349–358. https://doi.org/10.1111/ijfs.12956

Paini, M., Daly, S. R., Aliakbarian, B., Fathi, A., Tehrany, E. A., Perego, P., Dehghani, F., Valtchev, P. (2015 B). An efficient liposome based method for antioxidants encapsulation. Colloids and Surfaces B: Biointerfaces, 136, 1067–1072. https://doi.org/10.1016/j.colsurfb.2015.10.038

Pal, K., Pal S. (2006). Development of porous hydroxyapatite scaffolds. Materials and Manufacturing Processes, 21, (3), 325–328. https://doi.org/10.1080/10426910500464826

Pan, H. C., Jiang, Q., Yu, Y., Mei, J. P., Cui, Y. K., Zhao, W. J. (2015). Quercetin promotes cell apoptosis and inhibits the expression of MMP-9 and fibronectin via the AKT and ERK signalling pathways in human glioma cells. Neurochemistry International, 80, 60–71. https://doi.org/10.1016/j.neuint.2014.12.001

Papadimitriou, S., Bikiaris, D. (2009). Novel self-assembled core-shell nanoparticles based on crystalline amorphous moieties of aliphatic copolyesters for efficient controlled drug release. Journal of Controlled Release, 138(2), 177–184. https://doi.org/10.1016/j.jconrel.2009.05.013

Park, M. K., Deng, S., Advincula, R. C. (2005). Sustained release control via photo-cross-linking of polyelectrolyte layer-by-layer hollow capsules. Langmuir, 21(12), 5272–5277. https://doi.org/10.1021/la047008x

Pastorino, L., Erokhina, S., Soumetz, F. C., Bianchini, P., Konovalov, O., Diaspro, A., Ruggiero, C., Erokhin, V. (2011). Collagen containing microcapsules: Smart containers for disease controlled therapy. Journal of Colloid and Interface Science, 357(1), 56–62. https://doi.org/10.1016/j.jcis.2011.02.010

Patil, Y. P., Jadhav, S. (2014). Novel methods for liposome preparation. Chemistry and Physics of Lipids, 177, 8–18. https://doi.org/10.1016/j.chemphyslip.2013.10.011

Pawlikowska-Pawlega, B., Gawron, A. (1995). Effect of quercetin on the growth of mouse fibroblast cells in vitro. Polish Journal of Pharmacology, 47 (6), 531-535. PMID: 8868376

Petrov, A. I., Volodkin, D. V, Sukhorukov, G. B. (2005). Protein calcium- carbonate coprecipitation – a tool for protein encapsulation Abstract, 85.

Pham, Q. P., Sharma, U., Mikos, A. G. (2006). Electrospun poly (ε-caprolactone) microfiber and multilayer nanofiber/microfiber scaffolds: Characterization of scaffolds and measurement of cellular infiltration. Biomacromolecules, 7 (10), 2796–2805. https://doi.org/10.1021/bm060680j

Pulieri, E., Chiono, V., Ciardelli, G., Vozzi, G., Ahluwalia, A., Domenici, C., Vozzi, F., Giusti, P. (2008). Chitosan/ gelatin blends for biomedical applications. Journal of Biomedical Materials Research Part A, 86A (2), 311–322. https://doi.org/10.1002/jbm.a.31492

Pupo, E., Padrón, A., Santana, E., Sotolongo, J., Quintana, D., Dueñas, S., Duarte, C., de la Rosa, M. C., Hardy, E. (2005). Preparation of plasmid DNA-containing liposomes using a high-pressure homogenization-extrusion technique. Journal of Controlled Release, 104 (2), 379–396. https://doi.org/10.1016/j.jconrel.2005.02.001

Rai, R., Tallawi, M., Grigore, A., Boccaccini, A. R. (2012). Synthesis, properties and biomedical applications of poly(glycerol sebacate) (PGS): A review. Progress in Polymer Science, 37 (8), 1051–1078. https://doi.org/10.1016/j.progpolymsci.2012.02.001

Rampino, A., Borgogna, M., Blasi, P., Bellich, B., Cesàro, A. (2013). Chitosan nanoparticles: Preparation, size evolution and stability. International Journal of Pharmaceutics, 455 (1–2), 219–228. https://doi.org/10.1016/j.ijpharm.2013.07.034

Ranelletti, F. O., Maggiano, N., Serra, F. G., Ricci, R., Larocca, L. M., Lanza, P., Scambia, G., Fattorossi, A., Capelli, A., Piantelli, M. (2000). Quercetin inhibits p21-RAS expression in human colon cancer cell lines and in primary colorectal tumors. International Journal of Cancer. Journal International Du Cancer, 85 (3), 438–445.

https://doi.org/10.1002/(SICI)1097-0215(20000201)85:3<438::AID-IJC22>3.0.CO;2-F

Ravi, S., Chaikof, E. (2010). Biomaterials for vascular tissue engineering. Regenerative Medicine, Biomaterials, 5 (1), 1–21. https://doi.org/10.2217/rme.09.77.

Rice-Evans, C. A., Miller, N. J., Paganga, G. (1996). Structure-antioxidant activity relationships of flavonoids and phenolic acids. Free Radical Biology and Medicine, 20 (7), 933–956. https://doi.org/10.1016/0891-5849(95)02227-9

Russo, M., Spagnuolo, C., Tedesco, I., Bilotto, S., Russo, G. L. (2012). The flavonoid quercetin in disease prevention and therapy: Facts and fancies. Biochemical Pharmacology, 83 (1), 6–15. https://doi.org/10.1016/j.bcp.2011.08.010

Salehi, S., Bahners, T., Gutmann, J. S., Gao, S. L., Mäder, E., Fuchsluger, T. A. (2014). Characterization of structural, mechanical and nano-mechanical properties of electrospun PGS/PCL fibers. RSC Advances, 4 (33), 16951–16957. https://doi.org/10.1039/C4RA01237B

Salehi, S., Fathi, M., Javanmard, S. H., Bahners, T., Gutmann, J. S., Ergün, S., Steuhl, K. P., Fuchsluger, T. A. (2014). Generation of PGS/PCL blend nanofibrous scaffolds mimicking corneal stroma structure. Macromolecular Materials and Engineering, 299 (4), 455–469. https://doi.org/10.1002/mame.201300187

Sant, S., Hwang, C. M., Lee, S. H., Khademhosseini, A. J. (2011). Hybrid PGS–PCL microfibrous scaffolds with improved mechanical and biological properties. Journal of Tissue Engineering and Regenerative Medicine, 5 (4), 1–14. https://doi:10.1002/term.313

Sant, S., Iyer, D., Gaharwar, A. K., Patel, A., Khademhosseini, A. (2013). Effect of biodegradation and de novo matrix synthesis on the mechanical properties of valvular interstitial cell-seeded polyglycerol sebacate-polycaprolactone scaffolds. Acta Biomaterialia, 9 (4), 5963–5973. https://doi.org/10.1016/j.actbio.2012.11.014

Sauerbrey, G. (1959). Verwendung von Schwingquarzen zur Wägung dünner Schichten und zur Mikrowägung. Zeitschrift Für Physik, 155 (2), 206–222. https://doi.org/10.1007/BF01337937

Sauvage, L. R., Berger, K. E., Wood, S. J., Yates, S. G., Smith, J. C., Mansfield, P. B. (1974). Interspecies healing of porous arterial prosthesis. Archives of Surgery, 109 (5), 698-705. https://doi.org/10.1001/archsurg.1974.01360050092020

Schubert, M. A., Müller-Goymann, C. C. (2003). Solvent injection as a new approach for manufacturing lipid nanoparticles – evaluation of the method and process parameters. European Journal of Pharmaceutics and Biopharmaceutics, 55, (1), 125-131. https://doi.org/10.1016/S0939-6411(02)00130-3

Scoditti, E., Calabriso, N., Massaro, M., Pellegrino, M., Storelli, C., Martines, G., De Caterina, R., Carluccio, M. A. (2012). Mediterranean diet polyphenols reduce inflammatory angiogenesis through MMP-9 and COX-2 inhibition in human vascular endothelial cells: A potentially protective mechanism in atherosclerotic vascular disease and cancer. Archives of Biochemistry and Biophysics, 527 (2), 81–89. https://doi.org/10.1016/j.abb.2012.05.003

Serizawa, T., Yamaguchi, M., Akashi, M. (2002). Enzymatic hydrolysis of a layer-by-layer assembly prepared from chitosan and dextran sulfate. Macromolecules, 35 (23), 8656–8658. https://doi.org/10.1021/ma012153s

Shen, X., Liu, J., Feng, X., Zhao, Y., Chen, L. (2015). Preliminary investigation on hemocompatibility of

poly(vinylidene fluoride) membrane grafted with acryloylmorpholine via ATRP. Journal of Biomedical Materials Research - Part A, 103 (2), 683–692. https://doi.org/10.1002/jbm.a.35213

Shen, Y.H., Shoichet, M.S., Radisic M. (2008). Vascular endothelial growth factor immobilized in collagen scaffold promotes penetration and proliferation of endothelial cells. Acta Biomaterialia, 4 (3), 477–489. https://doi.org/10.1016/j.actbio.2007.12.011

Singh Baghel, S., Shrivastava, N., Singh Baghel, R., Agrawal, P., Rajput, S. (2012). A review of quercetin: antioxidant and anticancer properties. World journal of pharmacy and pharmaceutical sciences, 1 (1), 146-160.

Singh, D. K., Ray, A. R. (2000). Biomedical applications of chitin, chitosan, and their derivatives. Journal of Macromolecular Science, Part C: Polymer Reviews, 40 (1), 69–83. https://doi.org/10.1081/MC-100100579

Skotak, M., Ragusa, J., Gonzalez, D., Subramanian, A. (2011). Improved cellular infiltration into nanofibrous electrospun cross-linked gelatin scaffolds templated with micrometer-sized polyethylene glycol fibers. Biomedical Materials, 6 (5). https://doi.org/10.1088/1748-6041/6/5/055012

Sood, S., Jain, K., Gowthamarajan, K. (2014). Optimization of curcumin nanoemulsion for intranasal delivery using design of experiment and its toxicity assessment. Colloids and Surfaces B: Biointerfaces, 113 (1), 330-337. https://doi.org/10.1016/j.colsurfb.2013.09.030

Soppimath, K.S., Aminabhavi, T.M., Kulkarni, A.R., Rudzinski, W.E. (2001). Biodegradable polymeric nanoparticles as drug delivery devices. Journal of Controlled Release, 70, 1–20. https://doi.org/10.1016/S0168-3659(00)00339-4

Sterner, K., Busch, R., Petersen, S. (2015). Polymers in cardiology. In Pucci, F. editor, Advanced polymers in medicine. Springer.

Sukhorukov, G. B., Volodkin, D. V., Günther, A. M., Petrov, A. I., Shenoy, D. B., Möhwald, H. (2004). Porous calcium carbonate microparticles as templates for encapsulation of bioactive compounds. Journal of Materials Chemistry, 14 (14), 2073–2081. https://doi.org/10.1039/B402617A

Sun, H., Mei, L., Song, C., Cui, X., Wang, P. (2006). The *in vivo* degradation, absorption and excretion of PCL-based implant. Biomaterials, 27 (9), 1735–1740. https://doi.org/10.1016/j.biomaterials.2005.09.019

Takezawa, T. (2003). A strategy for the development of tissue engineering scaffolds that regulate cell behavior. Biomaterials, 24 (13), 2267–2275. https://doi.org/10.1016/S0142-9612(03)00038-3

Tamayol, A., Akbari, M., Annabi, N., Paul, A., Khademhosseini, A., Juncker, D. (2013). Fiber-based tissue engineering: progress, challenges, and opportunities. Biotechnology Advances, 31 (5), 669–687. https://doi:10.1016/j.biotechadv.2012.11.007

Tatterton, M., Wilshaw, S. P., Ingham, E., Homer-Vanniasinkam, S. (2012). The use of antithrombotic therapies in reducing synthetic small-diameter vascular graft thrombosis. Vascular and Endovascular Surgery, 46 (3), 212–222. https://doi.org/10.1177/1538574411433299

Teebken, O.E., Bader, A., Steinhoff, G., Haverich, A. (2000). Tissue engineering of vascular grafts: human cell seeding of decellularised porcine matrix. European Journal of Vascular and Endovascular Surgery, 19 (4), 381–386. https://doi:10.1053/ejvs.1999.1004

Thasneem, Y.M., Sajeesh, S., Sharma, C.P. (2011). Effect of thiol functionalization on the hemo-compatibility of PLGA nanoparticles. Journal of Biomedical Materials Research Part A, 99A (4), 607–617. https://doi.org/10.1002/jbm.a.33220

Tong, Z., Sant, S., Khademhosseini, A., Jia, X. (2011). Controlling the fibroblastic differentiation of mesenchymal stem cells via the combination of fibrous scaffolds and connective tissue growth factor. Tissue Engineering Part A, 17(21–22), 2773–2785. https://doi.org/10.1089/ten.tea.2011.0219

Tribolo, S., Lodi, F., Connor, C., Suri, S., Wilson, V. G., Taylor, M. A., Needs P. W., Kroon, P. A., Hughes, D. A. (2008). Comparative effects of quercetin and its predominant human metabolites on adhesion molecule expression in activated human vascular endothelial cells. Atherosclerosis, 197 (1), 50–56. https://doi.org/10.1016/j.atherosclerosis.2007.07.040

Trudel, J., Massia, S. P. (2002). Assessment of the cytotoxicity of photocrosslinked dextran and hyaluronan-based hydrogels to vascular smooth muscle cells. Biomaterials, 23 (16), 3299–3307. https://doi.org/10.1016/S0142-9612(02)00009-1

Tsao, R. (2010). Chemistry and biochemistry of dietary polyphenols. Nutrients, 2 (12), 1231–1246. https://doi.org/10.3390/nu2121231

tubular scaffold for small-diameter tissue-engineered vascular grafts: A scaffold membrane approach. Journal of the Mechanical Behavior of Biomedical Materials, 13, 140-155. https://doi.org/10.1016/j.jmbbm.2012.04.013

Uhrich, K. E., Cannizzaro, S. M., Langer, R. S., Shakesheff, K. M. (1999). Polymeric Systems for Controlled Drug Release. Chemical Reviews, 99 (11), 3181–3198. https://doi.org/10.1021/cr940351u

Van Dijk, C., Driessen, A. J. M., Recourt, K. (2000). The uncoupling efficiency and affinity of flavonoids for vesicles. Biochemical Pharmacology, 60(11), 1593–1600. https://doi.org/10.1016/S0006-2952(00)00488-3

Venugopal, J., Low, S., Tar Choon, A., Ramakrishna, S. (2008). Interaction of cells and nanofiber scaffolds in tissue engineering. Journal of Biomedical Materials Research Part B: Applied Biomaterials, 84B, 34–48. https://doi.org/10.1002/jbm.b.30841

Voinova, M. V., Rodahl, M., Jonson, M., Kasemo, B. (1998). Viscoelastic acoustic response of layered polymer films at fluid-solid interfaces: Continuum mechanics approach. https://doi.org/10.1238/Physica.Regular.059a00391

Voinova, M.V., Rodahl, M., Jonson, M., Kasemo, B., (1999). Viscoelastic acoustic response of layered polymer films at fluid-solid interfaces: Continuum mechanics approach. Physica Scripta, 59 (5), 391-396. https://doi.org/10.1238//Physica.Regular.059a00391

Wang, C. Q., Wu, J. L., Zhuo, R.-X., Cheng, S. X. (2014). Protamine sulfate–calcium carbonate–plasmid DNA ternary nanoparticles for efficient gene delivery. Mol. BioSyst. Mol. BioSyst, 672 (10), 672–678. https://doi.org/10.1039/c3mb70502a

Wang, J., Chen, J. S., Zong, J. Y., Zhao, D., Li, F., Zhuo, R. X., Cheng, S. X. (2010). Calcium carbonate/carboxymethyl chitosan hybrid microspheres and nanospheres for drug delivery. Journal of Physical Chemistry C, 114 (44), 18940–18945. https://doi.org/10.1021/jp105906p

Wang, L., Sondi, I., Matijević, E. (1999). Preparation of uniform needle-like aragonite particles by homogeneous precipitation. Journal of Colloid and Interface Science, 218 (2), 545–553. https://doi.org/10.1006/jcis.1999.6463

Wang, M. O., Etheridge, J. M., Thompson, J. A., Vorwald, C. E., Dean, D., Fisher, J. P. (2013). Evaluation of the in vitro cytotoxicity of cross-linked biomaterials. Biomacromolecules, 14 (5), 1321–1329. https://doi.org/10.1021/bm301962f

Wang, S., Zhang, Y., Yin, G., Wang, H., Dong, Z. (2009). Electrospun polylactide/silk fibroin–gelatin composite tubular scaffolds for small-diameter tissue engineering blood vessels. Journal of Applied Polymer Science, 113, 2675–2682. https://doi:10.1002/app.30346

Wang, Y., Ameer, G. A., Sheppard, B. J., Langer, R. (2002). A tough biodegradable elastomer. Nature Biotechnology, 20 (6), 602–606. https://doi.org/10.1038/nbt0602-602

Wang, Y., Cui, F.Z., Jiao, Y.P., Hu, K., Fan, D.D. (2008). Modification of bone graft by blending with lecithin to improve hydrophilicity and biocompatibility. Biomedical Materials, 3 (1), 1-6. https://doi.org/10.1088/1748-6041/3/1/015012

Wattel, A., Kamel, S., Prouillet, C., Petit, J. P., Lorget, F., Offord, E., Brazier, M. (2004). Flavonoid quercetin decreases osteoclastic differentiation induced by RANKL via a mechanism involving NFκB and AP-1. Journal of Cellular Biochemistry, 92 (2), 285–295. https://doi.org/10.1002/jcb.20071

Wenninger, J. A., Canterbery R. C., McEwan, G. N. (2000). International cosmetic ingredient dictionary and handbook. 8th ed., 652, 783-785. Washington. DC: CTFA.

Williams, D.F. (1986). Biomaterials ESf. Definitions in biomaterials: proceedings of a consensus conference of the European Society for Biomaterials. Chester, England, March 3-5, Elsevier.

Wippermann, J., Schumann, D., Klemm, D., Kosmehl, H., Salehi-Gelani, S., Wahlers, T. (2009). Preliminary results of small arterial substitute performed with a new cylindrical biomaterial composed of bacterial cellulose. European Journal of Vascular and Endovascular Surgery, 37 (5), 592-596. https://doi.org/10.1016/j.ejvs.2009.01.007

Wong, S. Y., Moskowitz, J. S., Veselinovic, J., Rosario, R. A., Timachova, K., Blaisse, M. R., Fuller, R. C., Klibanov, A. M., Hammond, P. T. (2010). Dual functional polyelectrolyte multilayer coatings for implants : permanent microbicidal base with controlled release of therapeutic agents, Journal of the American Chemical Society, 132 (50), 17840–17848. https://doi.org/10.1021/ja106288c

Wood, K. C., Boedicker, J. Q., Lynn, D. M., Hammond, P. T. (2005). Tunable drug release from hydrolytically degradable layer-by-layer thin films. Langmuir, 21 (4), 1603–1609. https://doi.org/10.1021/la0476480

Wu, P., Grainger, D. W. (2006). Drug/device combinations for local drug therapies and infection prophylaxis. Biomaterials, 27 (11), 2450–2467. https://doi.org/10.1016/j.biomaterials.2005.11.031

Xiang, Y., Lua S., Jiang, S.P. (2012). Layer-by-layer self-assembly in the development of electrochemical energy conversion and storage devices from fuel cells to supercapacitors. Chemical Society Reviews, 41, 7291–7321. https://doi.org/10.1039/C2CS35048C

Young, S., Wong, M., Tabata, Y., Mikos, A. G. (2005). Gelatin as a delivery vehicle for the controlled release of bioactive molecules. Journal of Controlled Release, 109 (1–3), 256–274. https://doi.org/10.1016/j.jconrel.2005.09.023

Zandi, M., Mirzadeh, H., Mayer, C. (2007). Early stages of gelation in gelatin solution detected by dynamic oscillating

rheology and nuclear magnetic spectroscopy. European Polymer Journal, 43 (4), 1480–1486. https://doi.org/10.1016/j.eurpolymj.2007.01.011

Zhang, C., Jin, J., Zhao, J., Jiang, W., Yin, J. (2013). Functionalized polypropylene non-woven fabric membrane with bovine serum albumin and its hemocompatibility enhancement. Colloids and Surfaces B: Biointerfaces, 102, 45–52. https://doi.org/10.1016/j.colsurfb.2012.08.007

Zhang, M., Wang, K., Wang, Z., Xing, B., Zhao, Q., Kong, D. (2012). Journal of Materials Science: Materials in Medicine, 23 (11), 2639–2648. https://doi.org/10.1007/s10856-012-4721-4

Zhang, Y., Ouyang, H., Chwee, T. L., Ramakrishna, S., Huang, Z. M. (2005). Electrospinning of gelatin fibers and gelatin/PCL composite fibrous scaffolds. Journal of Biomedical Materials Research - Part B Applied Biomaterials, 72(1), 156–165. https://doi.org/10.1002/jbm.b.30128

Zhou, J., Romero, G., Rojas, E., Ma, L., Moya, S., Gao, C. (2010). Layer by layer chitosan/alginate coatings on poly(lactide-co-glycolide) nanoparticles for antifouling protection and Folic acid binding to achieve selective cell targeting. Journal of Colloid and Interface Science, 345 (2), 241–247. https://doi.org/10.1016/j.jcis.2010.02.004

Zilberman, M., Kraitzer, A., Grinberg, O., Elsner, J. (2010). Drug-eluting medical implants. In: Schäfer-Korting M, editor. Drug Delivery: Springer Berlin Heidelberg, p. 299-341.

Zweers, M. L. T., Grijpma, D. W., Engbers, G. H. M., Feijen, J. (2003). The preparation of monodisperse biodegradable polyester nanoparticles with a controlled size. Journal of Biomedical Materials Research, 66B (2), 559–566. https://doi.org/10.1002/jbm.b.10046

Appendix

1. Papers concerning the Ph.D. thesis published in International Journal

2. Awards

3. Papers published in International Journal

4. Papers published in National Journal

5. Oral communications in International Congress

6. Oral communications in National Congress

7. Contribution to International Scientific Meeting concerning the Ph.D. thesis

8. Contribution to International Scientific Meeting

9. Summer Schools

10. Research periods abroad

1. Papers concerning the Ph.D. thesis published in International Journal

1. A

INTERNATIONAL JOURNAL OF POLYMERIC MATERIALS AND POLYMERIC BIOMATERIALS
2017, VOL. 66, NO. 12, 635–643
http://dx.doi.org/10.1080/00914037.2016.1252361

Taylor & Francis
Taylor & Francis Group

Tailored electrospun small-diameter graft for vascular prosthesis

Pier Francesco Ferrari[a,b], Bahar Aliakbarian[a,b], Alberto Lagazzo[a], Ali Tamayol[c], Domenico Palombo[b,d] and Patrizia Perego[a,b]

[a]Department of Civil, Chemical and Environmental Engineering, University of Genoa, Genoa, Italy; [b]Research Center for Biologically Inspired Engineering in Vascular Medicine and Longevity, Genoa, Italy; [c]Harvard-MIT Division of Health Sciences and Technology, Massachusetts Institute of Technology, Cambridge, MA, USA; [d]Vascular and Endovascular Surgery Unit, Research Laboratory of Experimental and Clinical Vascular Biology, University of Genoa and IRCCS San Martino Hospital, Genoa, Italy

ABSTRACT

There is an unmet need for engineering small vascular graft that can be anastomosed without inducing thrombosis. The objective of this work is to fabricate tubular graft with 2 mm of diameter with biomimetic mechanical and biological properties. Poly(ε-caprolactone) and poly(glycerol sebacate) blends with different concentrations and ratios are used to fabricate fibrous grafts using electrospinning process. Porous and degradable scaffolds with enhanced mechanical properties and comparable suture retention to the native human artery are fabricated. Scaffold–blood interaction revealed good anticoagulation properties. The fabricated constructs can serve as biocompatible and hemocompatible vascular graft with enhanced mechanical properties.

ARTICLE HISTORY
Received 4 June 2016
Accepted 10 October 2016

KEYWORDS
Electrospun graft; hemocompatibility; poly(glycerol sebacate):poly (ε-caprolactone) (PGS–PCL); vascular prosthesis

GRAPHICAL ABSTRACT

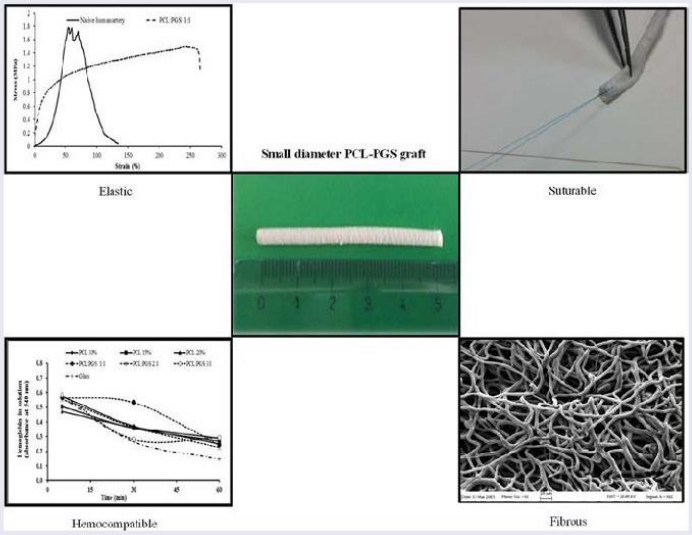

1. Introduction

Cardiovascular diseases including ischemic heart diseases and peripheral vascular diseases are among the leading causes of disability and morbidity [1]. These disorders can be caused by occlusion or stenosis of small-diameter vessels. Current treatment strategies include the use of stents which are not permanent solutions or the use of auto or allografts. The limited availability of suitable autogenous and allograft veins for complete coronary revascularization and the frequency of occlusion with small-diameter prosthesis have attracted several

CONTACT Bahar Aliakbarian bahar.aliakbarian@unige.it Department of Civil, Chemical and Environmental Engineering, University of Genoa, Via Opera Pia 15, Genoa 16145, Italy.
Color versions of one or more of the figures in the article can be found online at www.tandfonline.com/gpom.
P. F. Ferrari and B. Aliakbarian equally contributed to this work.

1. B

Engineered $CaCO_3$ Nanoparticles with Targeting Activity: A Simple Approach for a Vascular Intended Drug Delivery System

Pier Francesco Ferrari,[1]* Bahar Aliakbarian,[1,2] Elena Zattera,[3] Laura Pastorino,[3] Domenico Palombo[2,4] and Patrizia Perego[1,2]

1. *Department of Civil, Chemical and Environmental Engineering (DICCA), University of Genoa, Genoa, Italy*
2. *Research Center for Biologically Inspired Engineering in Vascular Medicine and Longevity (BELONG), University of Genoa, Genoa, Italy*
3. *Department of Informatics, Bioengineering, Robotics and Systems Engineering (DIBRIS), University of Genoa, Genoa, Italy*
4. *Vascular and Endovascular Surgery Unit, Research Laboratory of Experimental and Clinical Vascular Biology, University of Genoa and IRCCS San Martino Hospital, Genoa, Italy*

During the last decade, great attention has been paid to drug delivery systems that are able to induce a site-specific and tunable release of biomolecules, attenuating the drawbacks of common therapy. The encapsulation of bioactive compounds, such as proteins and drugs, offers the advantage of enhancing the pharmacokinetics and bioavaliability of the entrapped molecules. The encapsulating technique and coating agents are chosen on the basis of the desired functionality of the final product, release kinetics, and fabrication costs. Calcium carbonate ($CaCO_3$) is considered an ideal substrate to fabricate particles at the nanoscale level. In this work, $CaCO_3$ nanoparticles were synthesized through a two-step protocol which comprised complex coacervation and mineralization, and they were loaded with bovine serum albumin (BSA) as a model protein. The synthesized nanoparticles were then functionalized with the layer-by-layer (LbL) electrostatic self-assembling technique using chitosan as a polycation and dextran sulphate as a polyanion. The multilayered architecture that covers $CaCO_3$ nanoparticles prevented a burst release of BSA, resulting in 77.34 ± 1.22 % of the released protein, after 72 h of incubation. A horseradish peroxidase-linked IgG was immobilized at the outer particle layer and its presence was detected via chemiluminescence. Multilayered and non-multilayered nanoparticles were biocompatible until 7 days using EA. hy926 endothelial cells. Here, we report a cost-effective protocol to obtain protein-loaded $CaCO_3$ nanoparticles (diameter < 155 nm) using a coacervate-based synthesis system. Furthermore, with a very simple technique these nanoparticles were functionalized with antibodies, developing immuno-nanoparticles to apply in the drug delivery field.

Keywords: calcium carbonate, immuno-nanoparticles, layer-by-layer, drug delivery

INTRODUCTION

Drug delivery is described as the possibility to administer pharmacologically active compounds with the intention of minimizing unexpected side effects due to their non-specific distribution in the whole body.[1] Several systems to nano-encapsulate bioactive molecules have been proposed in the literature over the last years, such as polymeric particles,[2,3] nanoliposomes,[4] nanoemulsion,[5] and mineralization-based nanoparticles.[6] Among them, calcium carbonate ($CaCO_3$) nanoparticles are considered one of the best tools for drug delivery nanosystems because of their cost-effectiveness,[7] low cell cytotoxicity,[8] the potentiality to tailor the particle size,[9] the capability to load a wide range of molecules,[10] and to show stimuli responsive properties. For these reasons, $CaCO_3$ nanocarriers represent one of the most studied drug vehicles used to encapsulate proteins,[11] anti-inflammatory drugs,[12] antigens,[13] and genes.[14] One of the most common approaches to confine biological compounds in $CaCO_3$ particles is complex coacervation. In general, coacervation is defined as liquid/liquid phase separation of colloids into a two-phase system. Simple coacervation consists of a partial desolvation of biomolecules[15] while complex coacervation presumes that at least one component is a charged colloid (e.g. poly (acrylic) acid) (PAANa) that interacts with oppositely charged ions (e.g. Ca^{2+}).[16] When using complex coacervation of PAANa and Ca^{2+} ions, the formation of droplets that continuously sequester water from the polymer solution is induced. This entrapping method shows many advantages, such as good encapsulation efficiency, the possibility of encapsulating different drugs together, and the conjugation of biomolecules for targeting purposes. Conversely, its major drawback is represented by the high instability of the obtained constructs. With the aim of stabilizing the coacervate droplets, the addition of sodium carbonate (Na_2CO_3) leads to the mineralization of the complexes into particles consisting of PAANa and $CaCO_3$.

Nowadays, another aim of new drug therapy protocols is to control the release of drugs at the therapeutically optimal dose regimen directly into the tissue/organ where they are needed. For this purpose, $CaCO_3$ nanoparticles have been considered a good template for the electrostatic self-assembling layer-by-layer (LbL) technique. Versatility, possibility to be easily controlled at a nanoscale level, and low costs allow to fabricate innovative nanoparticles for intelligent drug delivery.[17] The LbL technique has attracted the attention of many researchers because of the

* *Author to whom correspondence may be addressed.*
E-mail address: pier.francesco.ferrari@edu.unige.it
Can. J. Chem. Eng. 95:1683–1689, 2017

DOI 10.1002/cjce.22871
Published online 29 May 2017 in Wiley Online Library (wileyonlinelibrary.com).

1. C

CHEMICAL ENGINEERING TRANSACTIONS
VOL. 57, 2017
A publication of AIDIC
The Italian Association of Chemical Engineering
Online at www.aidic.it/cet
Guest Editors: Sauro Pierucci, Jiří Jaromír Klemeš, Laura Piazza, Serafim Bakalis

ISBN 978-88-95608- 48-8; **ISSN** 2283-9216

Small Diameter Vascular Grafts Coated with Gelatin

Pier Francesco Ferrari*[a], Bahar Aliakbarian[a,b], Domenico Palombo[b,c], Patrizia Perego[a,b]

[a] Department of Civil, Chemical and Environmental Engineering, University of Genoa, Genoa, Italy
[b] Research Center of Biologically Inspired Engineering in Vascular Medicine and Longevity, Genoa, Italy
[c] Vascular and Endovascular Surgery Unit, Research Laboratory of Experimental and Clinical Vascular Biology, University of Genoa and IRCCS San Martino Hospital, Genoa, Italy
pier.francesco.ferrari@edu.unige.it

In the field of tissue engineering, there is an increased demand for small diameter vascular grafts to treat peripheral vascular pathologies and ischemic heart diseases. The limited availability of suitable autogenous veins and the drawbacks related to the use of synthetic materials, such as polyethylene terephthalate (Dacron®) and expanded polytetrafluoroethylene (ePTFE), especially when they are used as substitutes for small diameter vessels, have attracted several investigators turning their attention toward the fabrication of alternative biocompatible grafts. In this study, small diameter tubular grafts (2 mm), made of poly (ε-caprolactone) (PCL) and poly (glycerol sebacate) (PGS) at a ratio of 1:1 (v/v) were obtained by electrospinning. With the aim to reduce water permeability, their surface was modified by dynamic coating of gelatin at 37 °C for 1 h, followed by UV-irradiation. Thickness, fiber diameters, porosity, mass loss, fluid uptake, water permeability, gelatin release, mechanical properties, cytotoxicity, and hemocompatibility of gelatin-coated electrospun scaffolds (GCS) were studied and compared with uncoated scaffolds (UCS). Scanning electron microscopy (SEM) images showed that the gelatin surface modification did not affect the 3D structure and pore interconnectivity of the scaffolds. A significant decrease in the water permeability was noticed when gelatin was used as coating agent. The results of this study highlighted the importance of a very low cost surface treatment with gelatin to improve the properties of PCL:PGS electrospun grafts. In conclusion, these gelatin-coated prostheses could be considered as a good candidate for vascular replacement in tissue engineering.

1. Introduction

The majority of vascular diseases are characterized by thickening of arterial wall with subsequent decrease in the arterial lumen (Boland et al., 2004). Once blood flow is compromised, vascular bypass is often the only solution to restore blood flow to tissues distal to the stenosis or occlusion site. The success of artificial vascular substitutes with diameter larger than 6 mm, realized in materials such as polyethylene terephthalate (Dacron®) or expanded polytetrafluoroethylene (ePTFE) is now consolidated (Greenwald and Berry, 2000). Although the introduction of these synthetic materials has been considered as a definitive solution, many drawbacks, especially when they are used as substitutes for small diameter vessels (< 5-6 mm), are noticed (Teebken and Haverich, 2002). One of their most important limitations is the absence of endothelization after implantation leading to thrombosis and intimal hyperplasia (De Visscher et al., 2012), post-surgical infections and reocclusion. The development of engineered blood vessel substitutes has driven much of the research in the tissue engineering field over the past 30 years. Different approaches were introduced to obtain high performing blood vessel replacements, such as hydrogel scaffolds (Liu and Chan-Park, 2009), cell-seeded biodegradable synthetic polymers (Pawlowski et al, 2004), self-assembling methodologies (Stegemann et al., 2007), decellularized bioprostheses (Schaner et al., 2004), electrospun constructs (Gaharwar et al., 2015), and bioprinted scaffolds (Norotte et al., 2009). The ideal vascular prosthesis could be biodegradable, acting as a structural framework, in order to reproduce a native artery, like vessel (Nojiri et al., 1995). It should hopefully exhibit resistance to thrombosis, infections, aneurysmal dilatation and ectopic calcification showing good suture retention, ease of handling, flexibility with kink resistance, predictable degradation kinetic, bio- and

2. Awards

2. A

66th ESCVS
International Congress of the European Society for CardioVascular and Endovascular Surgery

in conjunction with

LIVE 2017
Leading Innovative Vascular Education

May 11-14, 2017 Makedonia Palace Hotel Thessaloniki-Greece

Best Oral Presentation Award

This is to certify that the study entitled

An innovative drug delivery system for atherosclerosis

[1]Pier Francesco Ferrari, [1,2]Bahar Aliakbarian, [3]Paola Bagnato, [2,3]Domenico Palombo, [1,2]Patrizia Perego

[1]*Department of Civil, Chemical and Environmental Engineering, University of Genoa, Genoa, Italy*
[2]*Research Center of Biologically Inspired Engineering in Vascular Medicine and Longevity, Genoa, Italy*
[3]*Vascular and Endovascular Surgery Unit, Research Laboratory of Experimental and Clinical Vascular Biology, University of Genoa and IRCCS San Martino Hospital, Genoa, Italy*

which was presented as **Oral Presentation** during the scientific programme of the **66th ESCVS in conjunction with LIVE 2017** has been awarded the

YOUNG VASCULAR AWARD SESSION

Professor Lazar Davidovic
President of the ESCVS 2016-18

Professor Athanasios Giannoukas
Chair of the Local Organizing Committee

3. Papers published in International Journal

3. A

Casazza AA**, Ferrari PF**, Aliakbarian B, Converti A, Perego P, 2015. Effect of UV radiation or titanium dioxide on polyphenol and lipid contents of *Arthrospira* (*Spirulina*) *platensis*. Algal Research 12: 308-315.

3. B

Barisione C, Garibaldi S, Furfaro AL, Nitti M, Palmieri D, Passalacqua M, Garuti A, Verzola D, Parodi A, Ameri P, Altieri P, Fabbi P**, Ferrari PF**, Brunelli C, Arsenescu V, Balbi M, Palombo D, Ghigliotti G, 2016. Moderate increase of indoxyl sulfate promotes monocytes transition into profibrotic macrophages. PLoS ONE 11: 1-17.

3. C

da Silva MF, Casazza AA, **Ferrari PF**, Perego P, Bezerra RP, Converti A, Figueiredo Porto AL, 2016. A new bioenergetic and thermodynamic approach to batch photoautotrophic growth of *Arthrospira* (*Spirulina*) *platensis* in different photobioreactors and under different light conditions. Bioresource Technology 207: 220-228.

3. D

Vergani L, Vecchione G, Baldini F, Voci A, **Ferrari PF**, Aliakbarian B, Casazza AA, Perego P, 2016. Antioxidant and hepatoprotective potentials of phenolic compounds from olive pomace. Chemical Engineering Transactions 49: 475-480.

3. E

Casazza AA, **Ferrari PF**, Aliakbarian B, Comotto M, Perego P, 2016. Microalgae growth using winery wastewater for energetic and environmental purposes. Chemical Engineering Transactions 49: 565-570.

3. F

da Silva MF, Casazza AA, **Ferrari PF**, Aliakbarian B, Converti A, Pedrosa Bezerra R, Figueiredo Porto AL, Perego P, 2017. Recovery of phenolic compounds of food concern from *Arthrospira platensis* by green extraction techniques. Algal Research 25: 391:401.

3. G

Vergani L, Vecchione G, Baldini F, Grasselli E, Voci A, Portincasa P, Ferrari PF, Aliakbarian B, Casazza AA, Perego P, 2017. Polyphenolic extract attenuates fatty acid-induced steatosis and oxidative stress in hepatic and endothelial cells. European Journal of Nutrition (in press).

4. Papers published in National Journal

4. A

Casazza AA, **Ferrari PF**, Aliakbarian B, Pettinato M, Novelli F, Converti A, Perego P, 2016. Recupero di antiossidanti da *Arthrospira platensis*: estrazione di polifenoli mediante alte pressioni e temperature e successiva purificazione. Atti di convegno GRICU 2016.

5. Oral communications in International Congress (the speaker is underlined):

5. A

Aliakbarian B, **Ferrari PF**, Perego P, Palombo D. Effect of electrospinning parameters on mechanical properties of engineered small diameter vascular grafts. The Journal of Cardiovascular Surgery, abstract book, Vol. 56 – Suppl. 1 to n° 2, 94. ESCVS 2015, Istanbul, Turkey.

5. B

Aliakbarian B, **Ferrari PF**, Perego P, Palombo D. Functionalizing small diameter vascular grafts with gelatin. The Journal of Cardiovascular Surgery, abstract book, Vol. 57 – Suppl. 2 to n° 2, 73. ESCVS 2016, Belgrade, Serbia.

5. C

Vergani L, Vecchione G, Baldini F, Voci A, **Ferrari PF**, Aliakbarian B, Casazza AA, Perego P. Antioxidant and hepatoprotective potentials of phenolic compounds from olive pomace, International Congress on Industrial Biotechnology (IBIC) 2016, Bologna, Italy.

5. D

Aliakbarian B, **Ferrari PF**, Bagnato P, Palombo D, Perego P. Engineered small diameter vascular grafts with anti-inflammatory properties. The Journal of Cardiovascular Surgery, abstract book, Vol. 58 – Suppl. 2 to n° 3, 14. ESCVS 2017, Thessaloniki, Greece.

5. E

Ferrari PF, Aliakbarian B, Bagnato P, Palombo D, Perego P. An innovative drug delivery system for atherosclerosis. The Journal of Cardiovascular Surgery, abstract book, Vol. 58 - Suppl. 2 to n° 3, 6. ESCVS 2017, Thessaloniki, Greece. This presentation was awarded a “Best Oral Presentation” in the “Young Vascular Award Session”.

6. Oral communications in National Congress (the speaker is underlined):

6. A

Ferrari PF, Aliakbarian B, Zattera E, Pastorino L, Palombo D, Perego P. Engineered $CaCO_3$ nanoparticles with targeting activity, GRICU MEETING 2016, Anacapri, Italy.

6. B

Casazza AA, **Ferrari PF**, Converti A, Perego P. Crescita di *Chlorella vulgaris* in fotobioreattore elicoidale impiegando acque reflue da vinificazione. FITEMI 2017, Palermo, Italy.

7. Contribution to International Scientific Meeting concerning the Ph.D. thesis

7. A Summer School on Biomaterials and Regenerative Medicine 2016, 04-09 July, Riva del Garda, Italy

Functionalization of PCL:PGS electrospun scaffold with protein-loaded nanoparticles

DICCA

Pier Francesco Ferrari[a*], Bahar Aliakbarian[a], Laura Pastorino[b], Domenico Palombo[c] and Patrizia Perego[a]

[a] Department of Civil, Chemical and Environmental Engineering (DICCA), University of Genoa, Via Opera Pia 15, 16145 Genoa, Italy
[b] Department of Informatics, Bioengineering, Robotics and Systems Engineering (DIBRIS), University of Genoa, Via Opera Pia 13, 16145 Genoa, Italy
[c] Vascular and Endovascular Surgery Unit, Research Laboratory of Experimental and Clinical Vascular Biology (DISC), University of Genoa and IRCCS San Martino Hospital, Largo Rosanna Benzi, 16132 Genoa, Italy

*pier.francesco.ferrari@edu.unige.it

Introduction

Cardiovascular diseases are mainly caused by the occlusion or stenosis of small diameter vessels. Current treatment strategies include the use of synthetic materials such as Dacron and expanded polytetrafluoroethylene (ePTFE) which do not represent a definitive solution (Drilling et al., 2008). An ideal vascular substitute is not only a good substrate for cell attachment and proliferation but should be able to actively guide cells during the regeneration process, realising growth factors and chemoattractant proteins. Today electrospinning is considered a high versatile technique to produce fibrous scaffold for the purpose of mimicking the extracellular matrix microenvironment (Bhardwaj and Kundu, 2010). The encapsulation of proteins into small particles leads to a controlled release of them after the prosthesis implant. The aim of this work was to functionalize an electropsun poly(ε-caprolactone) (PCL) and poly(glycerol sebacate) (PGS) blended scaffold, using calcium carbonate ($CaCO_3$) nanoparticles loaded with bovine serum albumin (BSA), as a model protein.

Materials and Methods

$CaCO_3$ nanoparticles were synthesized via combination of the complex coacervation between poly(acrylic acid) sodium salt (PAANa) and BSA, and mineralization by the addition of sodium carbonate (Na_2CO_3) (Lauth at al., 2014). PCL and PGS solutions (20 % w/v) were both prepared in a mixture of chloroform:ethanol (9:1) and then mixed at a final volume ratio of 1:1 (Sant et al., 2013). An equivalent of 0.1 % (wt) of $CaCO_3$ nanoparticles was added to the spinning solution (a scheme of BSA-loaded nanoparticles and of nano-functionalized scaffold is represented in Fig. 1A, B; an image of the tubular graft is reported in Fig. 1C). Electrospinning was performed using a steel cylindrical collector (2 mm of diameter) with a rotation and translation speed of 500 rpm and 600 mm min^{-1}, respectively, at a flow rate of 2.20 mL h^{-1} and under a driving voltage of 17.0 kV. Physicochemical properties (morphology, degradation rate and BSA release), mechanical behaviour, biocompatibility, using EAhy926 human endothelial cells, and hemocompatibility of the nano-functionalized scaffold were assessed.

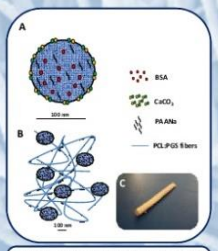

Figure 1. Schematic representation of BSA-loaded nanoparticles (A) and nanoparticles embedded in PCL:PGS fibers (B). Electrospun functionalized tubular scaffold (C).

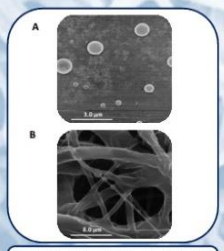

Figure 2. SEM images of BSA-loaded nanoparticles (A) and nano-functionalized scaffold (B).

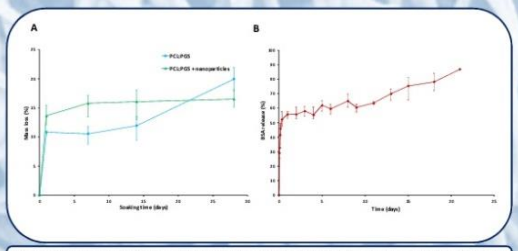

Figure 3. Mass loss in function of time of PCL:PGS with and without nanoparticles (A) and BSA-release profile from scaffold (B).

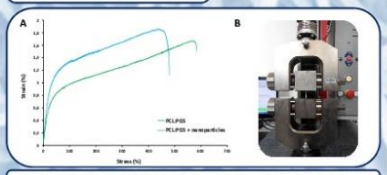

Figure 4. Stress-strain curves of PCL:PGS with and without nanoparticles (A) and set-up for mechanical tests (B).

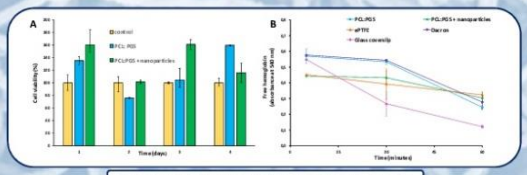

Figure 5. Cell viability by MTS assay (A) and blood clotting profile (B).

Results and Discussion

SEM analysis (Fig. 2B) of electrospun scaffold showed randomly oriented fibers with 2.44 ± 0.03 μm diameter. The polymer creep and weakening during time referrig to degradation behaviour of the electrospun constructs was taken into consideration. In our scaffold a notable weight loss was noticed after the first weeks of soaking, both in the samples with nanoparticles and in those without. The mass loss was more evident for the nano-functionalized scaffold (appoximatevely 13 and 16 % at 1 and 7 days, respectively) while it was stabilized after 14 days (Fig. 3A). The amount of protein released in 21 days amounted at 86 % of the total encapsulated protein (Fig. 3B). The values of Young's modulus and elongation percentage of scaffold with and without nanoparticles were statistically different (7.61 ± 0.92 and 4.91 ± 1.37 MPa, 218.48 ± 27.72 and 576.99 ± 132.5, respectively) (Fig. 4). Any difference between the growth of cells with or without electropsun scaffold was not noticed (Fig. 5A). The presence of nanoparticles, after 30 minutes, induced a reduction of free hemoglobin content in comparison with PCL:PGS and Dacron, but this value was still comparable to ePTFE (Fig. 5B).

Conclusions

Our results show that in all the measurements performed, the scaffolds with nanoparticles have properties comparable with those of the scaffold without particles, suggesting that the addition of the nanoparticles does not degrade the performance of PCL:PGS constructs. Overall, our results highlight that the nanoparticles we have produced, can be embedded inside the fibers during the electrospinning process, opening to the possibility of a gradually release of proteins directly where they are needed.

References

Bhardwaj N., Kundu S.C., 2010, Biotechnology Advances, 28, 325-347.
Drilling S., Gaumer J., Lannutti J., 2009, Journal of Biomedical Materials Research Part A, 88 A, 923-934.
Lauth V., Maas M., Rezwan., 2014, Journal of Material Chemistry B, 2, 7725-7731.
Sant S., Iyer D., Gaharwar A.K., Patel A., Khademhosseini A., 2013, Acta Biomaterialia 9, 5963-5973.

7. B 13th International Conference on Chemical and Process Engineering, 28-31 May 2017, Milan, Italy

Small Diameter Vascular Grafts Coated with Gelatin

IcheaP13

DICCA

Pier Francesco Ferrari*[a], Bahar Aliakbarian[a,b], Domenico Palombo[b,c], Patrizia Perego[a,b]

a Department of Civil, Chemical and Environmental Engineering, University of Genoa, Genoa, Italy
b Research Center of Biologically Inspired Engineering in Vascular Medicine and Longevity, Genoa, Italy
c Vascular and Endovascular Surgery Unit, Research Laboratory of Experimental and Clinical Vascular Biology, University of Genoa and IRCCS San Martino Hospital, Genoa, Italy
*pier.francesco.ferrari@edu.unige.it

Introduction

The majority of vascular diseases are characterized by thickening of arterial wall with subsequent decrease in the arterial lumen (Boland et al., 2004). Once blood flow is compromised, vascular bypass is often the only solution to restore blood flow to tissues distal to the stenosis or occlusion site. The success of artificial vascular substitutes with diameter larger than 6 mm, realized in materials such as polyethylene terephthalate (Dacron®) or expanded polytetrafluoroethylene (ePTFE) is now consolidated (Greenwald and Berry, 2000). The development of engineered blood vessel substitutes has driven much of the research in the tissue engineering field over the past 30 years. The ideal vascular prosthesis could be biodegradable, acting as a structural framework, in order to reproduce a native artery, like vessel (Nojiri et al., 1995). It should hopefully exhibit resistance to thrombosis, infections, aneurysmal dilatation and ectopic calcification showing good suture retention, ease of handling, flexibility with kink resistance, predictable degradation kinetic, bio- and hemocompatibility. In this work, PCL:PGS electrospun scaffolds were coated with gelatin in order to decrease their water permeability.

Materials and Methods

PCL and PGS solutions (20 % w/v) were both prepared in a mixture of chloroform:ethanol (9:1) and then mixed at a final volume ratio of 1:1 (Sant et al., 2013). Electrospinning was performed using a steel cylindrical collector (2 mm of diameter) with a rotation and translation speed of 500 rpm and 600 mm min^{-1}, respectively, at a flow rate of 2.20 mL h^{-1} and under a driving voltage of 17.0 kV. In order to obtain surface coated scaffolds, they were completely immersed in a gelatin solution (67 mg mL^{-1}, w/v) and maintained under mechanical agitation for 1 h at 37 ± 2°C. After that, gelatin-coated scaffolds were placed under an UV lamp for 1 h to allow gelatin cross-linking. Gelatin-coated scaffolds (GCS) and uncoated scaffold (UCS) were studied in terms of thickness, fiber diameters, porosity, degradation, fluid uptake, water permeability, gelatin release profile, mechanical properties, cell viability, using EAhy926 human endothelial cells and hemocompatibility.

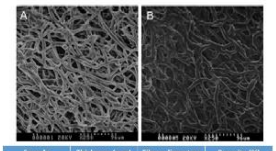

Sample	Thickness (mm)	Fibers diameters (μm)	Porosity (%)
PCL:PGS 1:1	0.46 ± 0.11[a]	5.29 ± 1.31[a]	68.19 ± 0.02[a]
PCL:PGS 1:1 + gelatin	0.43 ± 0.11[a]	5.50 ± 1.34[a]	43.49±10.85[b]

Figure 1. SEM images of external (A) and internal (B) surfaces of GCS.
Table 1. Thickness, fiber diameters and porosity of GCS and UCS

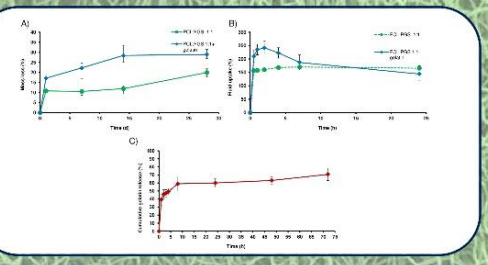

Figure 2. Mass loss (A), fluid uptake (B) of GCS and UCS and cumulative release of gelatin (C) from GCS.

Sample	Young's modulus (MPa)	Tensile strength (MPa)	Elongation (%)
PCL:PGS (1:1) (dry)	6.21 ± 2.13[a]	2.35 ± 0.75[a]	482.34 ± 193.64[a]
PCL:PGS (1:1) + gelatin (dry)	62.02 ± 8.81[b]	4.00 ± 1.21[a]	12.79 ± 4.44[b]
PCL:PGS (1:1) (wet)	8.05 ± 0.86[a]	2.89 ± 0.81[a]	516.66 ± 63.13[a]
PCL:PGS (1:1) + gelatin (wet)	8.63 ± 2.02[a]	3.27 ± 1.44[a]	327.56 ± 74.36[a]

Table 2. Mechanical properties of GCS and UCS
Figure 3. Set-up for mechanical tests (B).

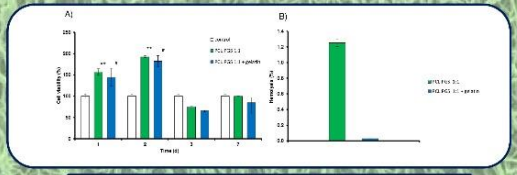

Figure 4. Cell viability (A) of GCS and UCS by MTS assay and hemolysis percentage (B).

Results and Discussion

Figure 1 shows the SEM micrographs of gelatin coated external (A) and internal (B) surfaces of scaffolds. Fibers appeared randomly distributed and they were bead-free. In the case of GCS, porosity was significantly lower (43.49 ± 10.85 %) in respect of UCS (68.19 ± 0.02 %) (Table 1). As can be seen from Figure 2 A, mass loss was more evident with GCS. In fact, during the first period of degradation, also gelatin is released from the scaffolds, lowering their weights. The presence of gelatin caused an increase of fluid uptake during the first hours (Figure 2 B). Gelatin induced a peak of fluid uptake after 2 h (248 %) and after 24 h this parameter decreased (144 %) as a consequence of a concomitant gelatin release. As shown in Figure 2 C, the majority of gelatin (58.96 %) is released within the 8 h and the total amount of released gelatin was 70.64 % after 72 h. Water permeability was greatly decreased by gelatin surface modification. In fact, in the case of UCS, first water drops were already registered at 0.2 atm, while working with GCS there was not water leakage until 0.7 atm was reached. Considering Young's modulus, statistically significant differences ($p < 0.05$) were reported only in the case of dry GCS that presented a modulus approximately nine times higher in respect with UCS (Table 2). This hardening property was overcome immersing GCS in a NaCl solution (0.9 %, w/v). Surprisingly, all the tested samples showed a comparable tensile strength without any relevant differences ($p < 0.05$). Wet samples were considered nearer than dry samples to the final application of the prostheses, and therefore, taken together, all these data suggested that the coating of PCL:PGS scaffolds with gelatin did not modify the mechanical properties of native scaffolds. No statistically significant differences ($p < 0.05$) were evidenced between the cells grown on a tissue culture plate as control and the cells grown in presence of GCS and UCS after a week (Figure 4 A). Figure 4 B shows that GCS diminished dramatically the hemolysis percentage, probably because of the gelatin coating, also reducing the porosity of the scaffolds.

Conclusions

Fibrous, degradable, porous, bio- and hemocompatible scaffolds of PCL:PGS 1:1 showed good mechanical properties. Oppositely, these scaffolds exhibited an excessive water permeability even at low pressure. In order to overcome this limitation, our scaffolds were coated with gelatin. Gelatin presence did not influence degradation rate and fluid uptake of the studied PCL:PGS blended polymer. Furthermore, the surface modification with gelatin did not alter thickness, fiber diameters, mechanical properties, when they are wet, biocompatibility, and hemocompatibility of PCL:PGS scaffolds, reducing the water permeability. These gelatin coated electrospun scaffolds could be used to be surgically implanted in animal model as arterial graft.

8. Contribution to International Scientific Meeting

8. A

Casazza AA, **Ferrari PF**, Aliakbarian B, Comotto M, Perego P. Microalgae growth using winery wastewater for energetic and environmental purposes. International Congress on Industrial Biotechnology (IBIC) 2016, Bologna, Italy.

8. B

Casazza AA, **Ferrari PF**, Aliakbarian B, Pettinato M, Novelli F, Converti A, Perego P. Recupero di antiossidanti da *Arthrospira platensis*: estrazione di polifenoli mediante alte pressioni e temperature e successiva purificazione. GRICU MEETING 2016, Anacapri, Italy.

8. C

Aliakbarian B, **Ferrari PF**, Perego P. An innovative methodology to fabricate antioxidant active packaging. Food Innova 2017, Cesena, Italy.

8. D

da Silva MF, **Ferrari PF**, Casazza AA, Aliakbarian B, Converti A, Bezerra RP, Figueiredo Porto AL, Perego P. Use of non-conventional extraction techniques for the recovery of polyphenols from *Arthrospira* (*Spirulina*) *platensis*. FITEMI 2017, Palermo, Italy.

9. Summer Schools:

9. A

Summer school on Biomaterials and Regenerative Medicine 2015, 06-08 July 2015, Riva del Garda, Italy;

9. B

GRICU PhD National School 2015: "Biological and bioprocess engineering", 07-11 September 2015, Padova, Italy;

9. C

Summer school on Biomaterials and Regenerative Medicine 2016, 04-09 July 2016, Riva del Garda, Italy;

9. D

GRICU Meeting and PhD National School 2016, 12-16 September 2016, Anacapri, Italy.

10. Research periods abroad

10. A

Laboratoire d'Ingénierie des Biomolécules (LIBio), École Nationale Supérieure d'Agronomie et des Industries Alimentaires (ENSAIA), University of Nancy, France

Supervisor: Prof. Elmira Arab-Tehrany

Topic: physicochemical and biological characterization of scaffolds functionalized with quercetin and encapsulation of quercetin and bovine serum albumin in nanoliposomes

Period: from 30th May 2017 to 30th October 2017